

Slope stability analysis and landslide susceptibility assessment on the SE foot slopes of Mt Cameroon



Che Vivian Bih

2011

Promoter: Prof. Dr. Patric Jacobs

Co-Promoters: Prof. Dr. Emmanuel Suh, Prof. Dr. Matthieu Kervyn, Prof. Dr. Philippe Trefois

*Thesis submitted in fulfilment of the requirements for
the degree of Doctor of Science, Geology*



Slope stability analysis and landslide susceptibility assessment on the SE foot slopes of Mt Cameroon

Analyse van de hellingstabiliteit en beoordeling van de aardverschuivingsgevoeligheid van de hellingen op de zuidoostelijke voet van Mt Cameroon

by

Vivian Bih Che

2011

PhD Review Committee

Prof. Dr. Emmanuel Suh (UBuea) (Co-Promoter)
Prof. Dr. Matthieu Kervyn (VUB) (Co-Promoter)
Prof. Dr. Philippe Trefois (RMCA) (Co-Promoter)
Prof. Dr. Morgan De Dapper (UGent)

Other Jury Members

Prof. Dr. Jacques Verniers (UGent, Chair)
Prof. Dr. Patric Jacobs (UGent, Secretary) (Promoter)
Prof. Dr. Veerle Vanacker (UCL)
Prof. Dr. Eric Van Ranst (UGent)
Dr. Gerald Ernst (UGent)
Dr. Jan Moeyersons (RMCA)

Cover picture: N view of the 2009 slide at Moliwe.



This study was financed by the ‘Vlaamse Interuniversitaire Raad – Universitaire OntwikkelingsSamenwerking’ (VLIR-UOS; Flemish Interuniversity Council – University Development Cooperation) as an ‘Own Initiative’ project (ZEIN2006PR325-9070), entitled ‘Capacity building in geohazard monitoring in volcanically active areas of South-West Cameroon’.

Written at

Department of Geology and Soil Sciences
Ghent University
Krijgslaan 281/S8
B-9000 Ghent, Belgium

ISBN _____

Acknowledgements

This thesis is a product of four years of interaction and cooperation with a very wide range of dynamic and non-compromising set of individuals without whom this work would not have come to completion. For this reason, I would like to dedicate this work to all those who stood by me throughout this period and to thank them for being there for me.

I would first like to thank my promoter, Prof. Patric Jacobs for his relentless efforts to make my stay at Ghent University constructive and for constant help and support. Sincere gratitude to my co-promoter Prof. Philippe Trefois for constructive criticism, you have been very instrumental in the realisation of this work. I owe lots of gratitude to my co-promoter, Prof Matthieu Kervyn de Meerendré, for his friendship, constructive criticism and ideas that have been very crucial for this work. In addition, his dedication, tireless effort, energy and the countless hours he spent on correcting previous versions of this work are truly enormous. Indeed, I say thank you.

I would like to acknowledge Dr. Gerald Ernst and Prof. Cheo Emmanuel Suh who initiated this project that gave me the opportunity to work in a multicultural and multidisciplinary environment. Their encouragement and willingness to read this work were gratifying. Their constant advice and mentorship are unforgettable. I must say it is thanks to you that I did not give up. I truly appreciate your integrity. Prof Suh can you remember what you said, “Vivian, life is never white or black, it is always gray. Keep up and do not loose heart, we are here for you. Do not forget to ask if you need anything”. These words will forever remain on my mind. They have become a driving force that keep me going when all seem dark or cloudy. I would like to thank Prof. Samuel Ayonghe because interaction with him motivated in me the spirit of independence, determination and self-reliance.

Prof. Eric Van Ranst and Prof. Marlina Elburg are acknowledged for welcoming me in their laboratories and assisting with XRD and ICPOES analyses and interpretation of obtained results. Dr. Karen Fontijn assisted enormously in carrying out the chemical analysis, and spent several hours editing the entire document. I would say the output would have been mediocre without her contributions. Her soft-spoken nature was also a source of inspiration. Prof. Jean-Claude Verbrugge and Prof. Christian Schroeder of the Laboratoire de Mécanique des Sols, Université Libre de Bruxelles, are appreciated for giving me a chance to do geotechnical

Acknowledgements

characterization of the soils in their laboratory. The technical expertise of the laboratory technicians Nicolas Canute and Willy are also appreciated.

I am also thankful to the staff of IRAD Ekona, particularly Mr. Njib and Dr. George Mafany who acted as facilitators so that I got access to some aerial photographs and the soil map. Thanks to all those who dedicated their time to collect rainfall data, particularly Brother Reine and Letarus Yuh of the St Martin de Porres brotherhood in Muntengene and Mr. Sule of St. Paul's College, Bonjongo. The staffs of the CDC meteorological centre and Dr Aka Festus are acknowledged for providing rainfall data.

I wish to thank the Lord Mayor of the Limbe I council, Mr Matute, for his cooperation and interest in this work. Many thanks to the local population of the Limbe area for providing information on the location of landslide scars and for constructive discussion about pre-failure conditions.

Interactions and stimulating discussions with Dr. Beatrice Fonge, Dr. George Chuyong, Dr. Aaron Tenning, Dr. Mary-Ann del Marmol, Dr. Mathias Mih, Dr. Athanasius Nkwatoh, Dra Mabel Wantim and other project team members was very exciting. Contributions and collaboration from Miss Charlotte F. Enjoh, Mr Peter N. Nchia, and Mr Albert N. Fon have been amazing. Thanks to my friends Mr. Tangko Noel, Dr. Germaine Mboudo and Ms Confidence Mosoh for their constant support and encouragement particularly in moments when I was really down. Friends who participated during field expeditions in particular Dieudonne Tamfu, Ebai, and Miro Yena are heartily acknowledged.

Assistance from Kurt Blom, Marc Faure, Nina Smeyers and Nancy Terryn who facilitated my integration at the UGent Department of the Geology and Soil Science is greatly appreciated.

Finally, my deepest thanks go to my parents, my brothers and sisters, for their love, help, care understanding and support throughout my life and above all, thanks to the Almighty God for strength, good health and the spirit of endurance.

This research was funded by the Vlaamse Interuniversitaire Raad (VLIR), as part of a broader project on Geohazards affecting the SW region of Cameroon, between the University of Buea and Ghent University, entitled 'Capacity building in geohazard monitoring in volcanically active areas of South-West Cameroon'.

Table of Content

Acknowledgements.....	iii
Table of Content.....	v
List of Figures.....	viii
List of Tables	xi
List of Abbreviation	xiii
Introduction.....	1
1.1 Landslide problems in Cameroon.....	5
1.2 Objectives and overview	6
1.3 Rationale.....	7
1.4 Structure of the thesis.....	7
Chapter One	9
Description of study area	9
1.1 Location of the Limbe area	9
1.2 General physiographic characteristics of the Limbe area	12
1.3 Climate of the Limbe area	16
1.4 Geology of the study area.....	18
Chapter Two.....	21
Inventory, mapping and description of geometric parameters of landslide scars	21
2.1 Introduction	21
2.2 Importance of landslide inventory	22
2.3 Landslide mapping method	25
2.4 Equipment used	27
2.5 Results from field observations	28
2.5.1 Description of landslide scars.....	28
2.5.2 Statistical analysis of geometric parameters	34
2.6 Slide description	41
2.6.1 Mabeta slides	41
2.6.2 Bonjo slide.....	44
2.6.3 Makuka debris slide	47
2.6.4 Debris slide at Unity Quarters	49
2.6.5 Earth slide at Moliwe	51
2.6.6 Earth slide at Kie Village (Ngeme).....	52
2.7 Internal morphology of the landslide scars	54
2.8 Landslide triggering factors.....	55

2.9	Discussion	60
2.9.1	Causal factors	62
2.9.2	Triggering factors	62
2.10	Conclusion.....	64
Chapter Three		65
Geotechnical characteristics of landslide prone soils.....		65
3.1	Introduction	65
3.2	Equipment, sample preparation and analysis	68
3.3	Methods used in the determination of index and physical properties.....	68
3.3.1	Colour of soils	68
3.3.2	Determination of natural moisture content.....	70
3.3.3	Loss on ignition (LOI)	70
3.3.4	Determination of Atterberg’s Limits	70
3.3.5	Grain size distribution.....	72
3.3.6	Determination of bulk density (γ).....	73
3.3.7	Determination of particle specific gravity (Gs).....	73
3.3.8	Consolidated undrained triaxial test.....	74
3.4	Result of geotechnical characterization	76
3.4.1	Description of geotechnical profiles	78
3.4.1.1	Profile 1 Bonjo	78
3.4.1.2	Profiles 2, 3 and 4, Mabeta New Layout	80
3.4.1.3	Profiles 5 and 6, Makuka	83
3.5	Textural classification and its significance	86
3.6	Shear strength parameters and their significance	91
3.7	Sliding mechanism.....	96
3.7.1	Fracture permeability mechanism model	96
3.7.2	Human induced, rain triggered mechanism.....	98
3.8	Discussion	100
3.9	Conclusion.....	103
Chapter Four.....		105
Mineralogy, chemistry and element distribution in landslide prone-soils		105
4.1	Introduction	105
4.2	Mineralogical characterisation	105
4.3	Chemical characterisation	108
4.4	Results	111

4.4.1	X-ray diffraction	111
4.4.2	Element distribution patterns.....	122
4.5	Discussion	128
4.5.1	Diffraction patterns	128
4.5.2	Variations in element distribution.....	131
4.5.3	Weathering indices.....	134
4.5.4	Mass Balance Evaluations.....	134
4.6	Conclusion.....	135
Chapter Five.....		137
Landslide susceptibility mapping (modelling)		137
5.1	Introduction	137
5.1	Methods of landslide susceptibility assessments.....	138
5.1.1	Raw data.....	141
5.1.2	Landslide mapping and generation of seed cells	144
5.1.3	Data processing and generation of factor maps.....	144
5.2	Landslide susceptibility evaluation.....	157
5.3	Landslide risk assessment	158
5.3.1	Relationship between factors and seed cells.	160
5.3.2	Selection of suitable factor combinations	170
5.4	Limitation of the model.....	176
5.5	Risk assessment	176
5.6	Discussion	180
5.7	Conclusions	183
Conclusions and perspectives		184
References.....		192
Appendix		212

List of Figures

Fig. 1. 1.	Location of the study area.	10
Fig. 1. 2.	Panoramic view of the study area with numerous degraded asymmetric pyroclastic cones.	12
Fig. 1. 3.	Geological map of the study area.	13
Fig. 1. 4.	Soil map of the study area modified from physiographic maps for soil investigations by Hasselo (1961).	14
Fig. 1. 5.	Hydrologic map of the Limbe area superimposed on a shaded relief.	15
Fig. 1. 6.	Spatial distribution of mean monthly precipitation in the study area.	17
Fig. 1. 7.	Geologic map of Mount Cameroon,	19
Fig. 2. 1.	Landslide related deaths and cumulative death toll for landslides recorded in Cameroon in the last 3 decades.	22
Fig. 2. 2.	Sketch of plan view of 2009 debris slide at Moliwe indicating where and how various parameters were measured in the field.	27
Fig. 2. 3.	Catalogue of equipment used in the field.	28
Fig. 2. 4.	Distribution of landslide scars.	29
Fig. 2. 5.	Proportion of various landslide types observed within the study area,	30
Fig. 2. 6.	Field photographic view of some landslide scars within the study area.	31
Fig. 2. 7.	Characteristic field view of the head scarp of some observed scars.	32
Fig. 2. 8.	Contact between soils and saprolite and the characteristics observed at the head scarp.	32
Fig. 2. 9.	Sketch of observed slides:	33
Fig. 2. 10.	Distribution of geometric parameters.	35
Fig. 2. 11.	Distribution of the areas and volumes of 50 individual landslides triggered by rainfall in the Limbe area.	37
Fig. 2. 12.	Distribution of landslide zones within the Limbe area.	40
Fig. 2. 13.	Material making up the slide scarp at Mabeta.	42
Fig. 2. 14.	Internal morphology of the Mabeta slide.	43
Fig. 2. 15.	Close view of anarchical construction at Mabeta.	44
Fig. 2. 16.	21st July 2005 landslide at Bonjo.	45
Fig. 2. 17.	Field view of 2008 reactivation of the Bonjo slide.	46
Fig. 2. 18.	Profile of Bonjo slide exposed by road construction in 2009. Pale yellowish soil occurs on purplish saprolite.	47
Fig. 2. 19.	Field view of translational slide at Makuka with scarp height, outline of slide indicated by dotted lines and direction of movement indicated by white arrows.	48
Fig. 2. 20.	June 29th, 2009 slide at Unity quarters, looking west.	50
Fig. 2. 21.	Typical land use patterns observed at Unity Quarter.	50
Fig. 2. 22.	Photograph; transverse and plan view of the 2009 Moliwe landslide	51
Fig. 2. 23.	Photograph of the August 6th, 2009 rotational slide at Kie Village.	52
Fig. 2. 24.	Typical landslide damage at Kie village.	53
Fig. 2. 25.	Spheroidal or onion skin weathering at head scarp.	54
Fig. 2. 26.	30-day cumulative rainfall and daily totals at recorded the closest station for five recorded landslide events in Limbe.	58
Fig. 2. 27.	Period of 3- days antecedent rainfall recorded within the study area.	59

List of figures

Fig. 3. 1	Location of sampling pits dug into 3 landslides scars analysed in detail during this study.	66
Fig. 3. 2.	View of geometric configuration of Pit 1 dug into a slides scar at Bonjo.	67
Fig. 3. 3.	Collecting block samples for laboratory analysis from the wall of a pit sunk at Bonjo.....	67
Fig. 3. 4.	Catalogue of the laboratory equipment used for sample analysis	69
Fig. 3. 5.	Procedure involved in sample preparation and analysis in a triaxial cell.....	75
Fig. 3. 6.	Photograph mosaic and sketch of the Bonjo soil profile with associated index properties measured in the laboratory	79
Fig. 3. 7.	Grain size distribution for samples P1S01, P1S02 and P1S03 from Pit 1 at Bonjo.....	79
Fig. 3. 8.	Grain size distribution of samples from Pits 2, 3 and 4 at Mabeta.	81
Fig. 3. 9.	Cross sectional view of the Mabeta slide showing the nature of associated soil profiles.	82
Fig. 3. 10.	Sketch of Makuka slide showing the location of sampling pits. Diagram not drawn to scale....	83
Fig. 3. 11.	Geotechnical profile of Pit 5 at Makuka.....	84
Fig. 3. 12.	Profile of Pit 6 at Makuka with associated index properties.....	85
Fig. 3. 13.	Grain size distribution curve for samples collected at Makuka Pits 5 and 6.....	86
Fig. 3. 14.	Textural classification of samples using the USDA textural triangle.....	87
Fig. 3. 15.	USCS classification of samples based on Casagrande's (1948) plasticity chart.....	88
Fig. 3. 16.	Relationship between clay content and Atterberg's limits of the soils	88
Fig. 3. 17.	Modified activity chart, i.e. a plot of the plasticity index against the amount of clay size particle.	89
Fig. 3. 18.	Activity coefficient calculated for soil samples analysed in this study: a) plots of AC versus clay fraction..	90
Fig. 3. 19.	Plasticity index against liquid limit on a plasticity chart.	91
Fig. 3. 20.	Relative undrained shear strength measured with a Torvane meter.	92
Fig. 3. 21.	Probability distribution curve for the factor of safety adapted from Popescu.	93
Fig. 3. 22.	Variation in calculated factor of safety with slope gradient for a completely dry soil and fully saturated soil assuming.....	94
Fig. 3. 23.	Calculated factor of safety on variable slope with variable thickness of the sliding layer.....	95
Fig. 3. 24.	Calculated factor of safety for weathered lava flow deposits on variable slope with variable thickness of the sliding layer.	95
Fig. 3. 25.	Sketch of the steps and processes involved in the proposed fracture permeability sliding mechanism.....	98
Fig. 3. 26.	Sketch of the human induced, rain-triggered landslide mechanism observed in Limbe, particularly on pyroclastic cones.....	99
Fig. 4. 1.	X-ray diffraction patterns of oriented clay fractions of soils from the 2005 landslide at Bonjo	114
Fig. 4. 2.	X-ray diffraction patterns of random soil powders of the 2005 landslide at Bonjo:.....	115
Fig. 4. 3.	a) Picture of the head scarp. X-ray diffraction patterns of oriented clay fractions of slide 22 at Bonjo after Mg ²⁺ saturation and glycolation:	116
Fig. 4. 4.	X-ray diffraction patterns of Mg saturated and glycolated oriented clay fractions of soils from Mabeta New Layout.....	117
Fig. 4. 5.	X-ray diffraction patterns for sample powders from a pyroclastic cone at Mabeta New Layout:.....	118
Fig. 4. 6.	Diffraction patterns of bulk sample powders from Pit 6 at Makuka.....	120

List of figures

Fig. 4. 7.	Photomicrographs of the sand fraction of soils derived from the weathering of pyroclastic material from the landslide scar at Mabeta.	121
Fig. 4. 8.	Photomicrographs of the sand fraction of soils developed on weathered lava flows	122
Fig. 4. 9.	Element distribution patterns.....	124
Fig. 4. 10.	Total Alkali – Silica (TAS) diagram after Le Bas et al. (1986).	125
Fig. 4. 11.	Parent normalised element patterns of soils and saprolites from landslide scars in Limbe.....	126
Fig. 4. 12.	Si-Al-Fe ternary diagram by Hill et al. (2000) for the parent rocks and soil samples.	128
Fig. 5. 1.	False colour composite of: a) band 532 of 1986 image and b) band 542b of 2000 image.....	145
Fig. 5. 2.	Schematic illustration of the steps involved in the creation of factor maps and in the susceptibility evaluation procedure used in this study.....	146
Fig. 5. 3.	Geological map of the study area.....	148
Fig. 5. 4.	Land use map of Limbe and its environment, manually digitised from a 2000 Landsat image.	150
Fig. 5. 5.	Slope map of the study area generated from a 20 m DEM showing the location of observed landslide scars.....	151
Fig. 5. 6.	Slope orientation map of the study area showing the location of observed landslide scars.	152
Fig. 5. 7.	Stream density map (search radius 600 m) of streams identified in the Limbe area..	153
Fig. 5. 8.	Proximity to faults and major fractures digitised from the geological map of Mt Cameroon... ..	155
Fig. 5. 9.	MAP of the study area obtained by the inverse distance interpolation technique.	156
Fig. 5. 10.	Time series changes in the outline of built-up areas on the SE foot slope of MC	159
Fig. 5. 11.	Spatial distribution of important facilities within the study area.....	160
Fig. 5. 12.	Distribution of the various rock types, proportion of seed cells they contain and associated normalized weighted values (Infoval) for the factor layer.....	161
Fig. 5.13.	Distribution of the various soil types, proportion of seed cells they contain and associated normalized values (Infoval) for the factor layer.....	163
Fig. 5. 14.	Summary of land use factor class distribution, proportion of seed cells they contain and associated normalized values for the land cover type.....	164
Fig. 5. 15.	Distribution of slope gradient factor classes associated seed cells and associated Infoval.	165
Fig. 5. 16.	Distribution of slope orientation factor classes, associated seed cells and Infoval.....	166
Fig. 5. 17.	Distribution of proximity to stream factor classes, associated seed cells and Infoval.	166
Fig. 5. 18.	Distribution of stream density factor classes, associated seed cells and associated Infoval for the factor stream density used in landslide susceptibility assessment in the Limbe area.	167
Fig. 5. 19.	Distribution of factor classes for factor distance to road, associated seed cells and associated Infoval	168
Fig. 5. 20.	Distribution of proximity to lineament factor classes, associated seed cells, and associated Infoval	169
Fig. 5. 21.	Distribution of MAP factor classes associated seed cells and Infoval.....	169
Fig. 5. 22.	Prediction performance (success rate curve) of grouping of multiple factor combinations	173
Fig. 5. 23.	Landslide susceptibility map of Limbe, using the six-factor combination	175
Fig. 5. 24.	Specific objects at risk superimposed on the susceptibility map.....	178
Fig. 5. 25.	Spatial distribution of the outline of built-up areas.....	179
Fig. A. 1.	Stress envelopes and Mohr circles of reconstructed samples.....	215

List of Tables

Table 1. 1.	Mean monthly and annual precipitation (mm) summary from 12 rain gauges manage by the Cameroon development Cooperation.	16
Table 1. 2.	Stations with 8-16 years of daily rainfall indicating the maximum 24 hours rainfall and the maximum number of rainy days /years..	18
Table 2. 1	Some recorded landslides in Cameroon	24
Table 2. 2.	Descriptive statistics of geometric parameters of landslide scars (depletion zones) observed in and around Limbe.	34
Table 2. 3.	Size classification for landslides (Fell, 1994).	36
Table 2. 4.	Pearson correlation coefficient matrix for geometric parameters.....	38
Table 2. 5.	Observed landslides with corresponding rainfall values recorded in 24 hours at the gauge nearest to the slide location.....	57
Table 3. 1.	Index and geotechnical properties of soils from landslide scars in the study area derived from laboratory analysis.	77
Table 3. 2.	Shear strength parameters and permeability values of reconstructed soil samples	91
Table 4. 1.	Description of samples used for XRD analysis:	106
Table 4. 2.	Mineralogical composition of bulk samples and oriented clay fractions.....	112
Table 4. 3.	WR major and trace element composition of fresh rocks and soil samples from the Limbe area, SE foot-slope of MC.	123
Table 4. 4.	Pearson’s correlation matrix for major and trace element analysed in this study.....	133
Table 5. 1.	Raw data, associated list of parameters (factors) observed to control landslide activities and factor classes used in landslide susceptibility assessment on the SE foot slopes of Mt Cameroon.	142
Table 5. 2.	Properties of Landsat TM images.	143
Table 5. 3.	Properties of Landsat ETM+ images.....	143
Table 5. 4.	Properties of ASTER images.....	143
Table 5. 5.	Summarised inventory of objects at risk.	158
Table 5. 6.	Distribution of the various rock types, proportion of seed cells they contain and associated normalized values (Infoval) for the factor layer.....	162
Table 5. 7.	Factor grouping, associated proportion of pixels in the high and very high susceptibility classes, percentage of training and test seed cells	172
Table 5. 8.	Training and validation results for landslide susceptibility in Limbe for three scenarios analysed in this study..	174
Table 5. 9.	Proportion of built-up areas in various landslide susceptibility categories on the SE foot slope of MC. Totals given in square kilometers.....	177
Table 5. 10.	Distribution of individual objects at risk, objects are located in the high and very high susceptibility classes of the susceptibility map	177
Table A. 2.	Year during which landslides were recorded with associated damage involved at each site. ...	213
Table A. 3.	Parameters and components used and derived from the triaxial cell test for samples from the pyroclastic cones.....	214

List of tables

Table A. 4.	Parameters and components used and derived from the triaxial cell test for samples from lava flows.....	214
Table A. 5.	Percentage retained fraction from dry sieving and sedimentation analysis	216
Table A. 6.	Proportion of pixels within the study area, seed cells, landslide density and Infoval for the factor soil type.	220
Table A. 7.	Proportion of pixel within the study area, seed cell, landslide density and Infoval for the factor land use.	220
Table A. 8.	Proportion of pixels within the study area, seed cells, landslide density and Infoval for the factor slope gradient.....	220
Table A. 9.	Proportion of pixels within the study area, seed cells, landslide density and Infoval for the factor slope orientation.....	220
Table A. 10.	Proportion of pixels within the study area, seed cells, landslide density and Infoval for the factor proximity to stream/river.....	221
Table A. 11.	Proportion of pixels within the study area, seed cells, landslide density, and Infoval for the factor stream density.	221
Table A. 12.	Proportion of pixels within the study area, seed cells, landslide density and Infoval for the factor proximity to roads.	221
Table A. 13.	Proportion of pixel within the study area, seed cell, landslide density and Infoval for the factor proximity to fault and major lineament.	221
Table A. 14.	Proportion of pixels within the study area, seed cells, landslide density and Infoval for the factor MAP.....	222

List of Abbreviation

Ac	Activity coefficient
ASTER	Advance Space Borne Thermal Emission and Reflection radiometer
Ca	Approximately
C	Cohesion
CDC	Cameroon Development Cooperation
DEM	Digital Elevation Model
DN	Digital Number
e	Void ratio
ETM	Enhanced Thematic Mapper
Fs	Factor of safety
Gs	Particle specific gravity
GIS	Geographic Information System
GLCF	Global Land Cover Facility
GRINP	Management of Natural Risks and Civil Protection
H	High
ICPOES	Inductively Coupled Plasma Optical Emission Spectroscopy
Infoval	information value
kPa	Kilo pascal
LI	Liquidity Index
LL	Liquid Limit
LOI	Loss on ignition
Ma	Million years
MC	Mount Cameroon
Mc	Natural moisture content
MH	Inorganic silt of high plasticity
MI	Inorganic silt of medium plasticity
n	Porosity
PI	Plasticity Index
PL	Plastic Limit
SC	Susceptibility class
TAS	Total Alkali-Silica
TM	Thematic Mapper
USCS	Unified Soil Classification System
USDA	United State Department of Agriculture
VLIR	Vlaamse Interuniversitaire Raad (Flemish Interuniversity Council)
VH	Very high
WR	Whole Rock
XRD	X-Ray Diffraction
γ	Bulk density

List of abbreviations

Introduction

Landslides are a recognized and well-studied geomorphologic phenomenon due to the major role they play in the development of hill slopes in mountainous regions, and their socio-economic consequences (Sidle *et al.*, 1985; Ahmad *et al.*, 1999). Despite this, the causes and mechanisms of slope failures remain poorly understood. A number of methods have been used in their analysis ranging from systematic field observations and/or interpretation of aerial photographs and other remote sensing data, to both simple and sophisticated field, experimental and numerical modelling of initiation and sliding mechanisms (Casadei *et al.*, 2003; Fernandez Merodo *et al.*, 2004; Jaiswal & Van Westen, 2009, Che *et al.*, 2011).

Milestone studies of landslides are provided by Varnes (1978); Cruden & Varnes (1996); Carrara *et al.* (1999); Guzzetti *et al.* (2003) and Davies *et al.* (2005). Notwithstanding, present state of knowledge in understanding, forecasting and controlling hazards associated with slope movements is still a difficult task. It necessitates multidimensional and multidisciplinary research and interactions to understand the dynamics of landslide processes. This entails integrating qualitative and quantitative data generated from distinct disciplines such as civil engineering, geology, geochemistry, geomorphology, geophysics, geotechnics, hydrology, hydrogeology, etc. Landslide analysis can be performed at numerous spatio-temporal scales depending on the objectives of the study (Aleotti & Chowdhury, 1999; van Westen *et al.*, 2006). Accordingly, the methods and tools used in landslide analysis are quite varied. They range from empirical and statistical techniques applied in predicting slopes failure susceptibility at regional scale (Dai & Lee, 2002; Süzen & Doyuran, 2004; Duman *et al.*, 2005; Knapen *et al.*, 2006; Claessens *et al.*, 2007; Buh, 2009) to process-based approaches (limit-equilibrium methods, numerical deformation methods) applied at a more local scale. Other researchers have focused on evaluating the run out behaviour of slides defining what has been termed ‘the angle of reach’ or ‘angle of apparent cohesion’ defined by the ratio of height drop to horizontal distance reached by a given landslide (Corominas, 1996). Most of these studies are based on slide descriptions from papers, reports and on the interpretation of aerial photographs rather than on first-hand field studies (Wen *et al.*, 2004). In this study, landslide

occurrences on the SE lower slopes of Mount Cameroon are analysed based on extensive field characterization and a combination of geological, chemical and engineering perspectives.

A landslide may be defined as a downward and outward movement of slope forming material (vegetation, soil, rock or debris) from a higher point to a lower one under the influence of gravity (Varnes, 1987; Hutchinson, 1988; Cruden 1991; Terzaghi *et al.*, 1996; Cruden & Varnes, 1996). After movement, scars are left behind on the landscape and can be used to identify areas that have been affected by failure. In plan view, slide scars are bounded by an acute, concave-down slope head scarp, strike-slip faults along its flanks and a concave uphill toe (Martel, 2004). Several classification systems have been used to categorize landslides with each method having some particular usefulness or applicability related to the recognition, avoidance, control, or correlation of the hazard. Fell (1994) introduced a classification scheme based on volume. Leroueil (1996) introduced another, based on slope movement stages where slides are classified to be in a pre-failure, failure, post failure or reactivation stages. This scheme is particularly relevant in the evaluation of future events. Terzaghi *et al.* (1996) proposed another scheme based on the location of the slip plane's intersection with the slope surface. They discriminated base and slope failure for which the down slope intersection of the slip plane with the surface is found above or below the slope base, respectively.

The most widely accepted and used classification scheme is the one developed by Varnes (1978) and modified by Cruden & Varnes (1996). This classification is based on the material type involved in the movement, the type of movement and the sliding mechanism. Based on this classification, slide material can be categorized as earth (material in which 80% or more is less than 2 mm), debris (20 to 80% of material is greater than 2 mm and the remainder less than 2 mm) or rock (hard firm mass that was intact and in place before movement). Movement may proceed through falling (material moving through free air), sliding (movement along a more or less defined plane) and flowing (where the material moves *en masse* in a fluid, plastic or viscous state) or may exhibit a combination of two or more types of movement and are then termed complex slides (Varnes, 1978; Crozier, 1986; Hutchinson, 1988; Dikau *et al.*, 1996; Terzaghi, 1996). Slides can further be classified as translational, rotational and/or complex. Rotational slides have a curve (spoon shaped) slip surface, show backward rotation of trees

within the debris and generally result in slope reversal. Translational slides on the other hand are characterized by a planar slip surface, show forward rotation of object within the debris, with no slope reversal. Complex slides define slides with multiple failure characteristics (Dikau *et al.*, 1996).

These movements could either be slow, i.e. moving a few millimetres per year, or fast, i.e. about 3 m/s or more. Slides may also be described as shallow or deep-seated failures. Deep-seated slides are slides that are > 5 m in depth, i.e. the sliding surface lies well below the maximum rooting system of plants, while shallow slides are < 5 m or occur within the maximum rooting system of plants (Dikau *et al.*, 1996).). Although lots of efforts have been made in defining an exhaustive landslide classification scheme, it is not always easy to assign a slide into a particular category because a single slide may involve more than one mechanism and more than one type of material.

The range of landslide phenomena is extremely large, making them one of the most diverse and complex natural hazards (Guzzetti, 2005). The area and volume of landslides span many orders of magnitude ranging from small slides only a few m² wide to extremely large submarine slides that cover several hundreds of km², capable of triggering other hazards such as tsunamis and floods (Guzzetti *et al.*, 2005). The extraordinary wide spectrum of landslide phenomena makes it very difficult to define a single methodology for the identification and mapping of landslides for risk assessment and susceptibility evaluations. Variation in the slope movement types reflect the diversity of conditions that cause slopes to become unstable as well as the processes that trigger them.

Sliding can occur as swarms or as individual slides on natural slopes after intense heavy rains, earthquakes, or snow melting. The majority of landslides occurring in the humid tropics are initiated in uninhabited areas or are not reported or recorded unless human casualties or a large amount of property damage is involved. Hence, monitoring and hazard mitigation is often hampered because landslide inventory is incomplete and the timing of landslide occurrence is not known exactly. In addition, the causal factors and the processes involved are not known or are not properly understood.

Natural hazards such as earthquakes, tropical cyclones, volcanic eruptions, and tsunamis can trigger the occurrence of landslides. Likewise, landslides may enhance floods, and generate tsunamis. Because of this interaction, landslides are considered the second most significant natural hazard amongst those identified by the United Nations Development Programme (UNDP, 1999). However, they differ from other hazards because they need both causal and triggering factors to occur (Ayalew *et al.*, 2005). They are commonly triggered by melt water, heavy rains and/or earthquake activities (Guzzetti *et al.*, 2005) though others may occur without any particular trigger. On steep unchannelled slopes, cycles of colluvium accumulation punctuated by periodic discharge due to landsliding have been observed. In area with a homogenous vegetation canopy, as soils progressively thicken, effective root strength diminishes and eventually renders the site much more susceptible to failure during intense storms.

Economic losses and casualties due to landslides are greater than commonly recognized. Yearly property loss due to landslides is larger than that caused by any other natural hazard, including earthquakes, floods and windstorms (Schuster & Fleming, 1986; Alexander, 1989; Schuster, 1995; Glade, 1998), probably because most of the damage associated with the aforementioned natural hazards is caused by landslides that usually accompany them. Their consequences are even greater within developing countries than in the developed world, where societal and economic problems are often so large and serious that little attention is paid to the prevention or mitigation of the negative effects of natural hazards in general, and of landslides in particular. Landslides in the developing world account for about 95 % of all landslide related fatalities worldwide (Hansen, 1984). In these countries, the limited available resources are invested primarily to improve health and education or to promote the economy, and little remains available to mitigate the catastrophic effects of natural hazards, including slope failures (Guzzetti *et al.*, 2007). In addition, poverty, lack of equipment and technology to identify potentially threatened areas, reduce the capability of these countries to identify, mitigate and rapidly recover after these catastrophic events.

Furthermore, poverty, destitution and demographic pressure have forced more people to live in areas prone to landslides thereby increasing risk and exacerbating the effects of disasters

(Rosenfeld, 1994; Alexander, 1995; Guzzetti *et al.*, 1999; Annan, 2000). Moeyersons *et al.* (2004) noted that new immigrants around Bukavu (Democratic Republic of Congo) built their houses in landslide scars, lobes and other dangerous areas thereby exposing a larger number of persons to hazards. Brabb (1991) noted that landslides are a worldwide problem but are more manageable and predictable than other hazards such as earthquakes, volcanic eruptions, and storms. However, only a few countries have taken advantage of this knowledge to reduce landslide hazards. Landslides are thus likely to become more important to decision makers in the future as more people concentrate in urban areas causing settlement to expand into less stable or marginal slopes, like in the SW Region of Cameroon. It is in response to this problem that this work was designed, with the objective of providing knowledge that can lead to the reduction of landslide-related death and economic losses associated with landslide events on the SE foot slopes of Mount Cameroon.

1.1 Landslide problems in Cameroon

In Cameroon, landslides have been reported mainly in the Bamboutos (Zogning *et al.*, 2007, Ayonghe & Ntasin, 2008), Limbe, Bafaka and in the Northwest Region of the Country (Lambi & Ngwana, 1991; Lambi *et al.*, 2002; Ayonghe *et al.*, 1999, 2002, 2004; Ngole *et al.*, 2007, Thierry *et al.*, 2008). Despite their frequent occurrence and dramatic impact for local communities, no systematic data on this geomorphic process has yet been collected for the Limbe area.

In the broader NW, W and SW Regions of Cameroon, crater lake outgassing has caused two major disasters in the 1980s and remains a concern that is being tackled at Lake Nyos and Lake Monoun so that small landslides are arguably the most common and recurrent geohazard in these regions where ~6 million people live. Landslides in this region have considerable social and economic consequences (Lambi *et al.*, 2002, Ayonghe *et al.*, 2004; Ayangi, 2004 unpublished report; Ayonghe & Ntasin, 2008). They result in the destruction of farmland, subsistent and industrial cash and food crops, disrupt transportation means, cause immediate damage to infrastructure and probably contribute to soil and biodiversity loss even though this has not been monitored in the affected areas.

At Mt Cameroon (MC), though volcanic and low intensity earth tremors, lava flows and toxic ash falls (Thierry *et al.*, 2008) all pose threats as eruptions historically recurred every 10-20 years on average (Suh *et al.* 2003), recurrent small scale landslides have been the main cause of fatalities and destruction of local community livelihood. Hence, small landslides can be rated as the most significant and recurrent hazard. Despite these threats, MC remains an active volcano, which has not been studied in detail. Most published work on the MC region has focused on its seismicity (Ateba & Ntepe, 1997; Ubangoh *et al.*, 1998), petrology, eruptive behaviour and general volcanology (Fitton, 1983; Suh *et al.*, 2003, 2010; Rankenbury *et al.*, 2005; Ngwa *et al.*, 2010). Only a few reports dealt with landslides as geohazards in the Limbe area (e.g. Lambi, 1990; Lambi & Ngwana, 1991, Lambi *et al.*, 2002; Ayonghe *et al.*, 2004; Zogning *et al.*, 2007; Ngole *et al.*, 2007; Thierry *et al.*, 2008; Buh, 2009). Most of these publications focus on the 2001 landslide swarm and floods around Limbe during which 23 persons were killed, farmland destroyed, and about 2800 people rendered homeless (Ayonghe *et al.*, 2004; Ayangi, 2004; Tytgat, 2008; Thierry *et al.*, 2008). Some of these articles focus on evaluating damage caused by landslides (Ayonghe *et al.*, 2004) and others, in assessing some of the factors responsible for failure (Lambi & Ngwana, 1991; Zogning *et al.*, 2007; Ngole *et al.*, 2007; Buh, 2009). Most of these slides appear to be enhanced by anthropogenic activities. Very little has been published on the geometric characteristics, magnitude or frequency/size relationships of the landslides, geotechnical characteristics of the landslide prone soils or landslide susceptibility evaluations, although researchers in other parts of the world have focused on these aspects (e.g. Hovius *et al.*, 1997; Malamud *et al.*, 2004; Dahl *et al.*, 2010).

1.2 Objectives and overview

The overall objective of this project is to produce a landslide susceptibility map for the Limbe area and to understand the mechanism and controlling factors of landslides. The specific objectives include:

- Identification, mapping, classification and measurement of the geometric characteristics of past landslides (landslide inventory map);

- Assessment of the geotechnical characteristics of landslide prone soils to evaluate their contribution in sliding,
- Identification of possible pre-disposing, triggering and sustaining factors for subsequent landslide susceptibility evaluation
- Construction of a landslide susceptibility map for the area that can be used in make informed decision for future investment and development to minimise risk and losses than can result from future slides.

1.3 Rationale

This work was carried out as part of a broader project on geohazards affecting the SW Region of Cameroon, in the format of a development cooperation agreement between the University of Buea (Cameroon) and Ghent University (Belgium-Flanders), and sponsored by the ‘Vlaamse Interuniversitaire Raad – Universitaire OntwikkelingsSamenwerking’ (VLIR-UOS; Flemish Interuniversity Council – University Development Cooperation) as an ‘Own Initiative’ project (ZEIN2006PR325-9070), entitled ‘Capacity building in geohazard monitoring in volcanically active areas of South-West Cameroon’.

1.4 Structure of the thesis

Chapter 1 focuses on the location, physiographic setting and climatic characteristics of the study area **Chapter 2** is dedicated to the systematic documentation and geometric characterisation of landslide scars observed within the study area. It includes methods applied during fieldwork and the identification of possible causal and triggering factors of landslides. From measured geometric characteristics, the area of the depletion zone, the volume of generated debris and the frequency/size relationship of the landslides scars are determined. Results indicate that landslides in this area are predominantly translational slides of limited volumes. Detail field observation were required because there are no aerial photographic coverage for this region coupled with the fact that landslides in this area are small and could not be identified on satellite image.

Chapter 3 focuses on the characterisation of landslide prone soils with emphasis on the determination of the index and geotechnical properties of soils from landslides, the calculation of the factor of safety and modelling of sliding mechanisms. Other studies have shown that ground condition (weak strength, fabric sensitivity, degree of weathering and fracturing are influential parameters and we wanted to evaluate if this was the case in our study area.

Chapter 4 involves mineralogical characterisation and geochemical element distribution patterns. Attention is focused on assessing the impact of clay mineralogy on the occurrence of slides. Weathering processes are evaluated and the degree of weathering that has taken place determined through weathering indices and the assessment of element distributions within the weathering profiles.

In **chapter 5**, a data driven bivariate landslide susceptibility model is presented. A brief literature review of landslide susceptibility assessment principles and methods is made, then the datasets used in this study and the corresponding thematic maps generated from them are introduced. The methodology used to assess susceptibility is based on seed cells generated from a landslide inventory map. The seed cells are used to constrain the weights of each potential explanatory factor. The model is tested and the best set of explanatory factors is validated using an independent dataset. The landslide susceptibility map is then interpreted in terms of risks by looking at the distribution of settlements and key infrastructures located in zones of high and very high landslide susceptibility.

Finally, the **conclusion and perspectives** are presented, highlighting the practical relevance of the findings of this thesis to mitigate shallow translational landslide hazard in the study area and in other tropical regions and the need for the development of new research and application projects.

Chapter One

Description of study area

1.1 Location of the Limbe area

The study area is situated on the SE lower slopes of the active Mt Cameroon (MC) volcano located in the Fako Division of the SW Region of Cameroon. It lies between latitudes 3°55' and 4°13' N and longitudes 9°12' and 9°23' E (Fig. 1.1), covering a total area of 361 km². It is flanked to the SW and S by the Atlantic Ocean and to the SE by the Mabeta Creek.

Major settlements in this area include the towns of Limbe and Bonadikombo (Mile Four) nested in flat areas located between the ridges of the Mabeta massif and the towns of Buea and Mutengene located on the foot hills of MC. Settlement in this area dates back to the pre-colonial era and since then, the population has increased tremendously to over 174000 people (84223 in the Limbe area and 90088 in the Buea Municipality; data from the Bureau Central des Recensements et des Etudes de Population, (2010). Most of these inhabitants are low-income earners engaged in extensive and subsistence agricultural activities, petty trading, fishing and hunting. The main crop types produced by indigenous subsistence farmers include maize, cassava, banana, yams, cocoyams, sweet potatoes and cocoa, but also widespread agro-industrial complexes of banana (*Musa acuminata*), rubber (*Hevea brasiliensis*), and oil palms (*Elaeis guineensis*) occur..

As the population grows, so does urbanisation of steep meta-stable slopes on weathered pyroclastic cones and flood plains. This has already led to an increase in the recurrence of landslides and flooding problems within the region. Recent constructions have witnessed a boom in the use of reinforced concrete and cement blocks though wooded structure- locally called "carabot"- are also abundant. Construction projects usually do not take in to account building codes put in-place by the Ministry of Town Planning and Housing, thereby enhancing slope stability problems. Field evidence shows the presence of natural slope instability problems; however, instability induced by humans following deforestation, land development and construction programs, are becoming increasingly evident.

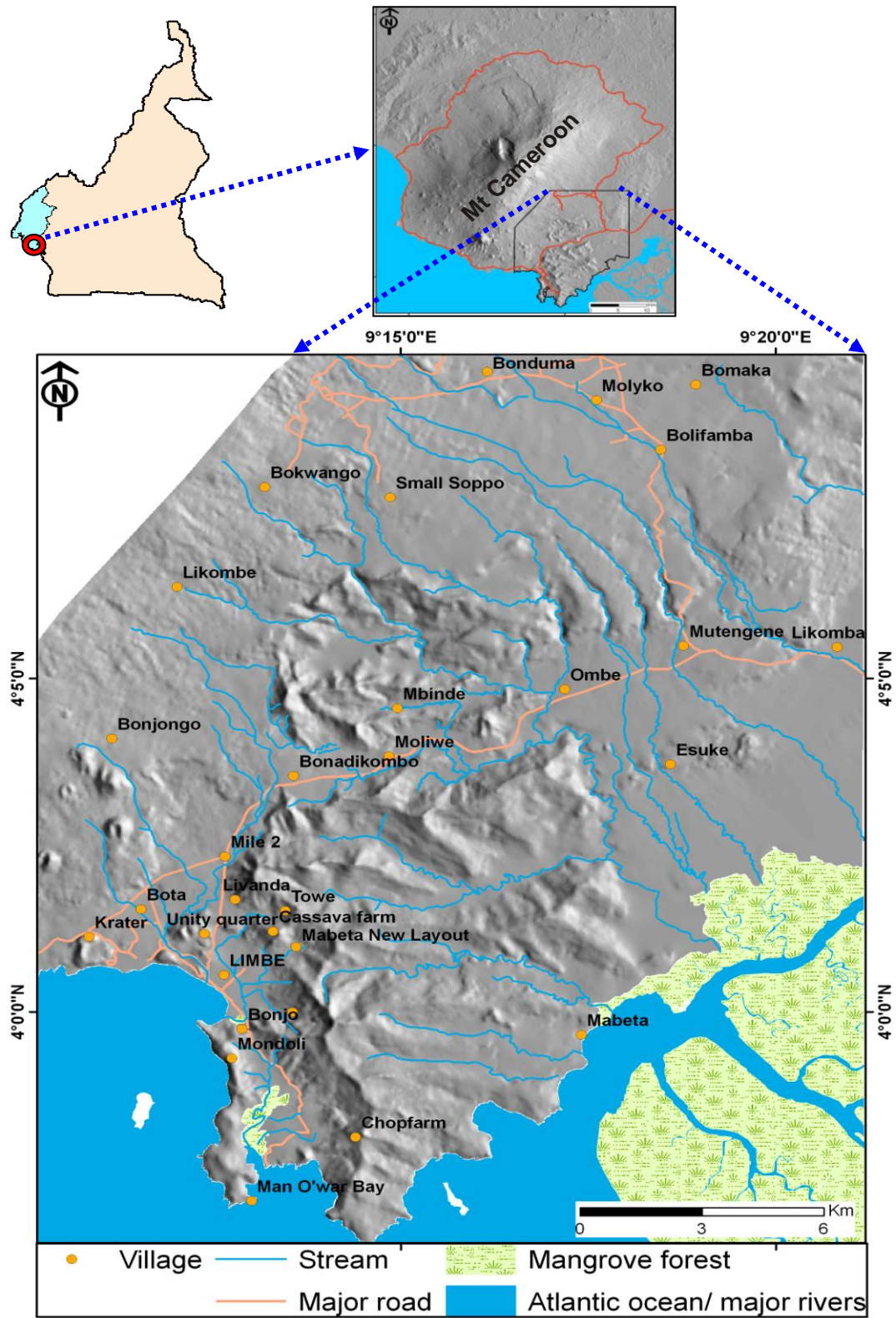


Fig. 1. 1. Location of the study area. Inset shows map of Cameroon with the SW region (in green) indicating where Mt Cameroon is situated.

Geomorphologically, the area is characterized by two different types of volcanic terrains that generate thick, weathered, soil columns which might remain meta-stable for long periods of time in the absence of external factors (such as human intervention through widespread excavation and rapid deforestation). These include:

- 1) Gently sloping lower slopes of MC made up of mudflow deposits and multiple lava flow deposits, punctuated by tens of ~50 – 300 m high, ~20-40° steep Strombolian volcanic cones particularly to the W of the study area (Fig. 1.1). The cones extend from the elevated summit of MC to the lower foothills in both the NE and SW direction (Suh *et al.*, 2003; Bonne, 2006; Bonne *et al.*, 2008). This corresponds to material of the third volcanic phase defined by Hasselo (1961). This corresponds to initial MC lava flow deposited over Miocene (10 - 20 Ma) sediment (Dumort, 1968).
- 2) Volcanic terrain composed of E – W trending ridges separated by asymmetric valleys of the Limbe-Mabeta massif (Fig. 1.1) bounded to the east by the Ombe 170° trending structure (Mathieu *et al.*, 2011). These ridges are made up of weathered volcanic flows thought to correspond to an early stage of growth of the active volcano during the Palaeogene and Pliocene (10 - 60 Ma) over Cretaceous soft sediments. They constitute material of the first volcanic phase according to Hasselo (1961).

These two areas have been described as the ‘young’ and ‘old’ volcanic landscape of Tertiary and Quaternary age by Hasselo (1961). The ridges and low elevation cones are covered by several meters thick of soils formed from prolonged and protracted intense weathering. On the ground, the terrain is characterized by a series of mounds and depressions, the low-lying areas between the ridges being occupied by human settlements (Fig. 1.2) which are gradually invading steeper slope due to growing population densities.

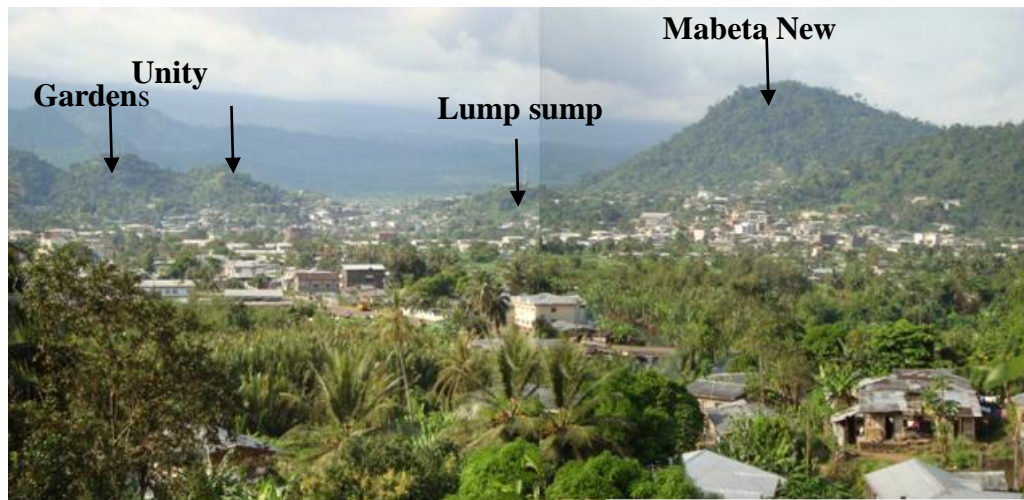


Fig. 1. 2. Panoramic view of the study area with numerous degraded asymmetric pyroclastic cones. Note the extension of building onto the steep slopes on the fragile cones.

1.2 General physiographic characteristics of the Limbe area

The major rock types in this area are Tertiary to Recent alkali basaltic lava flow deposits, pyroclastic deposits commonly occurring as cones of diverse shapes (circular, elliptical and asymmetric) and sizes, mudflow (lahar) deposits and alluvial deposits confined within stream channels and flood plains (Fig. 1.3). Due to limitation in the number of out crops within the study area, position of lithologic boundary are poorly defined. Pyroclastic deposits include volcanic bombs and vesiculated scoria (or cinders) and tephra. Tephra particles range from ash (< 2 mm) through lapilli (2 - 64 mm) to blocks and bombs (> 64 mm). These either lay exposed at the surface or are covered by dark brown, reddish brown and/or pale yellowish brown sticky, clayey soils derived from the weathering of these materials. Soil thicknesses range from a few centimetres to over 10 m, particularly on the old volcanic terrain of the Mabeta massif. i

Soil investigations within the study area indicate the presence of loamy soils developed on lahar deposits at elevations above 650 m above sea level (a.s.l.) whereas very clayey soils occur below 450 m a.s.l. forming a chrono-toposequence (Van Ranst *et al.*, 1990). Intense agriculture, vegetation and soil development within the study area actually conceal the nature of the parent material on which the soils have been developed, but it is likely that the soil can

act as a fingerprint to the source parent material. A 1/100,000 scale map of MC produced by Hasselo in 1961 exists and has been used to extract the soil map of the study area (Fig. 1.4).

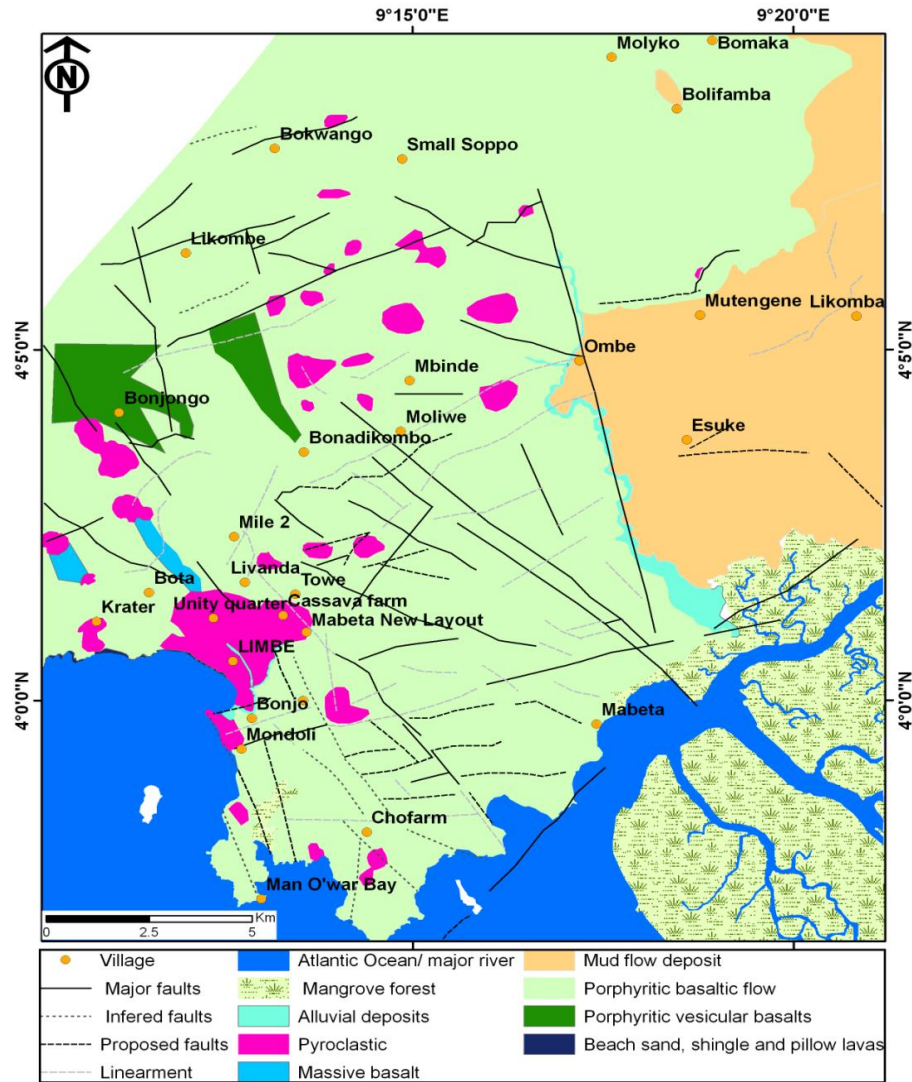


Fig. 1. 3. Geological map of the study area. Note the presence of lahar deposits to the E and pyroclastic cones (dotted) to the N and W section of the study area.

According to Hasselo's classification, there are basically seven soil types, namely old volcanic soils, ash, lava, lithosol, valley clay soils, rocky soils and fragipan. Old volcanic clay soils are moderately deep soils developed on basalts of the first volcanic phase (Mabeta massif). Ash soils are derived from soils on lava flows washed away by lahars. Lithosols are shallow soils developed on hard rock such as basalts. Stony soils are less than 60 cm thick, characterised by undulating broken surfaces and correspond to gravelly and stony soils developed on "young

lava flows”. Ash, lava and lithosols developed from lava of the third volcanic phase. Valley clay soils, fragipan and stony soils are young transported soils containing volcanic parent material.

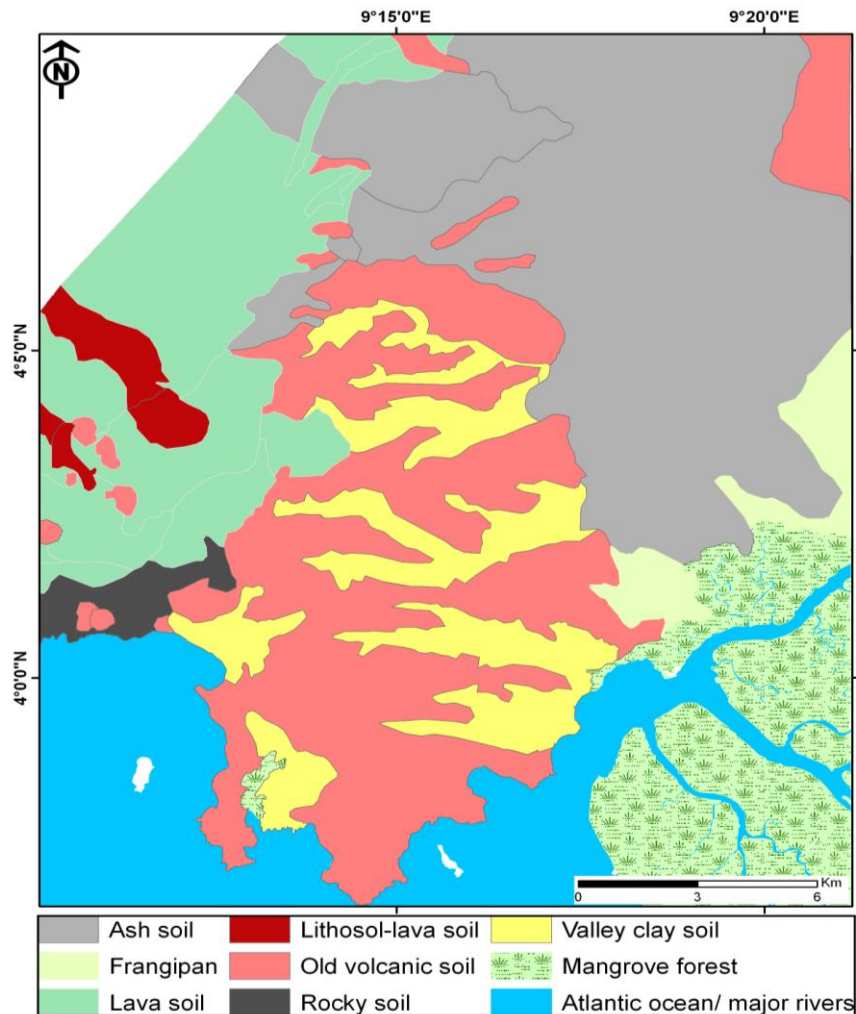


Fig. 1. 4. Soil map of the study area modified from physiographic maps for soil investigations by Hasselo (1961).

Hillsides are drained by numerous small ephemeral streams (most of which flow only during the rainy season) and a few perennial streams (whose discharge seasonally varies dramatically, emphasizing the contribution of surface runoff in sculpturing the landscape). The streams provide the area with a characteristic parallel to dendritic drainage pattern (Fig. 1.5).

Observations from water wells in the Limbe area indicate that the regional ground water level lies within the saprolite or at the saprolite – bedrock interface located at a depth of ~3 – 15 m. The coastal areas to the E of the study area are covered by mangrove forest, the central, north

and Southern parts by low land forest, while the W and E sections are occupied by peasant farmland, and by palm, rubber and banana industrial plantations. Here, the forest is luxuriant, immense with an interrupted canopy of leaves and thick undergrowth.

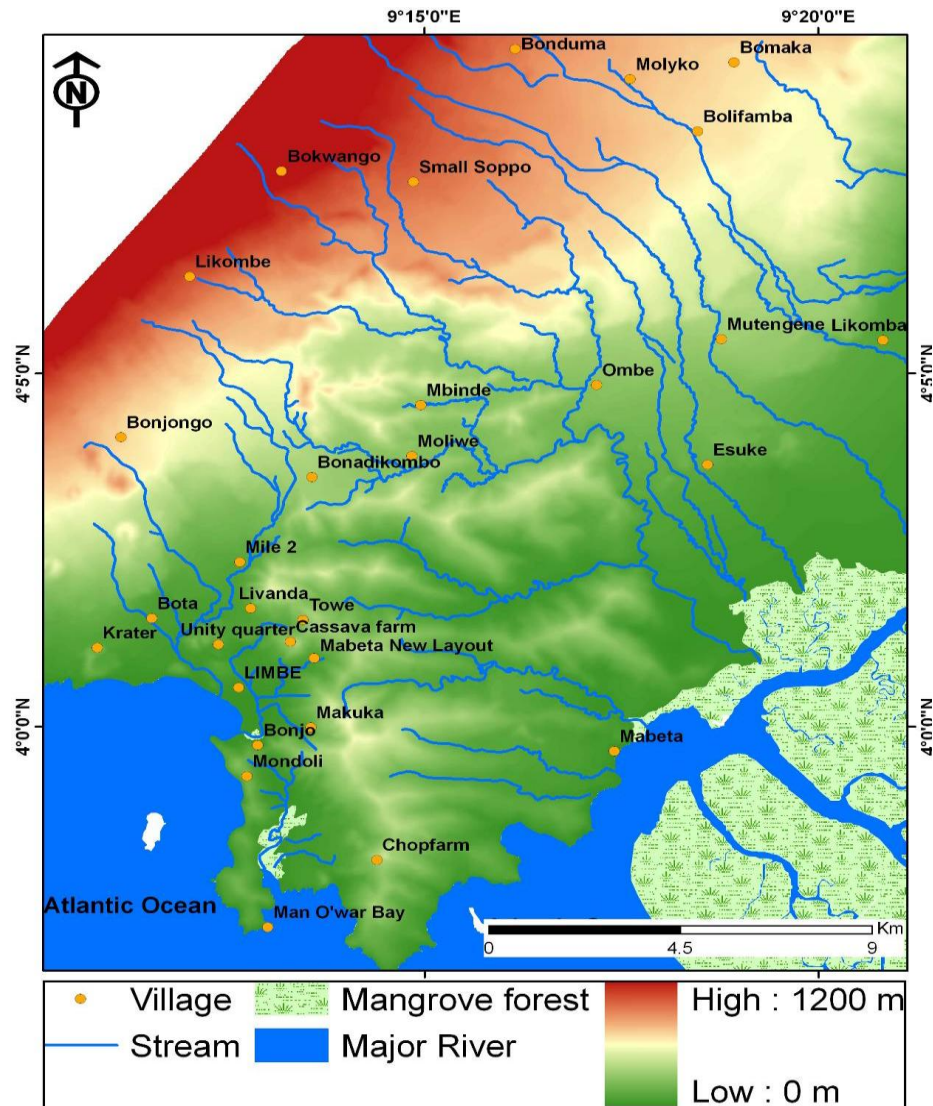


Fig. 1. 5. Hydrologic map of the Limbe area superimposed on a shaded relief. Note the parallel to dendritic drainage pattern that characterises the study area. Elevation ranges from 0 m to 1200 m a.s.l.

At the time this study was carried out, ~36 % of the study area was covered by banana, rubber and palm plantations, ~58 % by secondary/low land forest and other indigenous subsistence farm land, and < 1 % by mangrove forest. MC is home to some rare and endangered plant and animal species such as the *Prunus africana*, red eyed monkeys, drills, elephants, chimpanzees,

birds and is the life wire of the Cameroonian economy as it hosts the only national oil refinery, several palm, rubber, banana and tea plantations, a number of hospitals, schools, churches, and the lone anglo-saxon university centre (the University of Buea), in the country.

1.3 Climate of the Limbe area

The Limbe area is characterized by a Tropical Monsoon Climate. It is marked by two distinct seasons: a four-month dry season that begins in November and ends mid-March, and an eight-month long rainy season that runs from mid-March to November. These seasonal variations are a result of the migration of the Inter Tropical Convergence Zone formed by the convergence of the Monsoon and Harmattan winds. The Monsoon or Southeast Trade Winds generated from the St-Helen high pressure zone or anticyclone are warm and moist, and move from the Atlantic into the interior of the country in a NE direction bringing rain, whereas the Harmattan or Northeast Trade Winds are cold and dry, and are generated from above the Sahara, blowing in a SW direction resulting in a dry season. The rainy or wet season is characterized by highly localized rainfall events with the number of rainy days and rainfall quantity decreasing as one moves away from the coast inland (data from the Cameroon Development Cooperation Meteorological Centre). Precipitation occurs in the form of rain and dew with very rare occasions of hailstones that accompany severe rainstorms. Mean annual precipitation from 12 rain stations in the area is provided in Table 1.

STATION	LAT	LONG	Jan	Feb	Mar	Apr	May	Jun	Jul	Aug	Sept	Oct	Nov	Dec	Mean annual
Bimbia	439030	525348	89	77	158	187	296	635	752	849	560	352	183	45	4182
Bota	445065	521348	16	30	134	140	228	523	860	741	459	214	89	32	3465
Ekona	465779	537707	6	23	84	174	178	211	368	453	300	245	68	9	2119
Esuke	449019	534375	12	31	104	157	208	341	620	536	263	199	93	11	2575
Krater	444678	519795	15	62	164	239	325	722	985	901	476	311	120	38	4357
Likomba	452258	538481	13	24	96	157	212	293	554	499	253	215	97	7	2421
Mabeta Camp	441484	532214	14	58	179	218	328	597	996	939	459	316	161	63	4326
Mokundange	444677	511655	53	97	172	206	337	757	990	1093	720	301	151	51	4926
Moliwe	449347	527934	14	31	36	65	65	173	364	555	122	89	40	31	1583
Molyko	459328	533079	10	22	82	133	170	210	408	389	278	203	89	20	2016
Tole	455050	527260	14	21	85	145	169	283	551	567	329	209	71	10	2455
Saxenhof	452721	523602	7	17	101	148	181	312	772	692	346	207	68	20	2871
Mean			22	41	116	164	225	421	685	684	380	238	102	28	3108
Sd			24	26	44	46	82	212	242	221	161	71	43	18	1102

Table 1. 1. Mean monthly and annual precipitation (mm) summary from 12 rain gauges managed by the Cameroon development Cooperation. Note maximum rainfall in the months of July and August.

The rainy season begins in March and ends in November with peak rainfall recorded between June and September. June and July are characterised by intense and short-lived rainfall whereas August and September experience less intense but more prolonged rainfalls. Monthly rainfall frequently exceeds 500 mm and sometimes attains 1000 mm in June, July and August. These months coincide with periods of reported landslide events. Figure 1.6 shows the monthly distribution of rainfall within the study area based on 20 to 34 years of monthly rainfall data (from 1974 to 2009) from 12 rain stations (10 located within the study area and 2 out of the study area) operated by the Cameroon Development Cooperation (CDC).

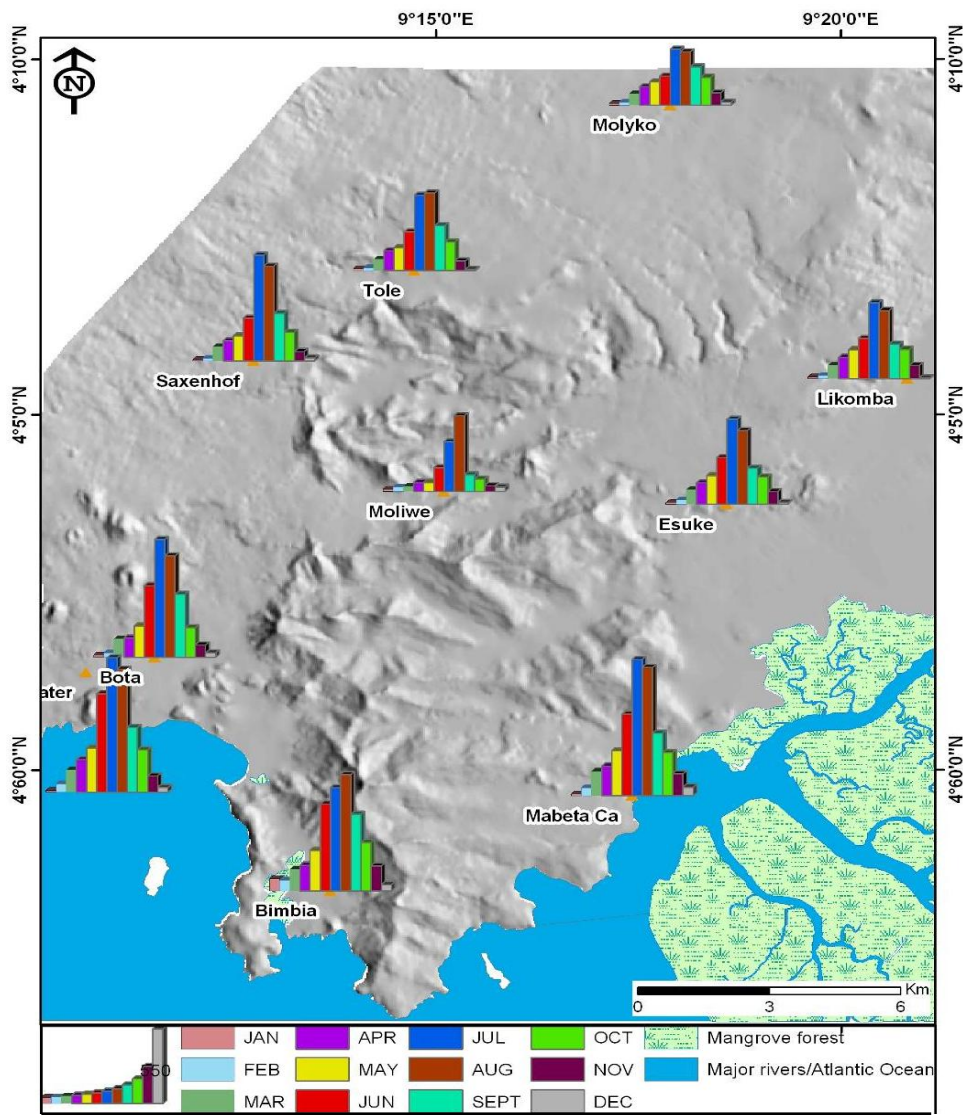


Fig. 1. 6. Spatial distribution of mean monthly precipitation in the study area. Note similarity in the pattern with maximum rainfall in July and August and minimum values in December and January. Data from the two station located out of the study area are excluded

From the figure, it is observed that monthly rainfall decreases with increasing distance from the coast. However, monthly data from all the stations show a similar annual distribution pattern with maximum values recorded either in the month of July or August. These months coincide with the occurrence of recorded landslides. December and January are the driest months. Of the 12 station available within the study area, only four namely: Mokundange, Krater, Moliwe and Esuke Benuoe provide daily rainfall records as shown on Table 1.2.

Station	Recording interval	Duration in years	MAP (mm)	SD	Max daily (mm)	Max number of rainy days/year
Esuke	1999-2009	11	2496	587	271	159
Krater	2001-2009	8	3609	1344	400	154
Moliwe	2000-2009	9	2630	1774	300	146
Mokundange	1994-2009	16	4732	967	447	197

Table 1. 2. Stations with 8-16 years of daily rainfall indicating the maximum 24 hours rainfall and the maximum number of rainy days /years. All values given in the table are calculated based on the number of years for which daily rainfall is available. Note significant differences in MAP here and those presented in Table 1.1 calculated over longer periods of time.

The most intensive one-day rainfall recorded in the last 14 years at the above-mentioned stations is included in Table 2. These maxima have a 17-, 13-, 12-, and 11-years return period, respectively, assuming Gumbel Extreme Value Distribution. From the rainfall records, it is evident that daily rainfall intensity and duration vary enormously throughout the region.

Relative humidity in this area is generally above 85 % (CDC Meteorological Centre). Mist and clouds are very abundant within the study area, particularly during the rainy season. Mean annual temperatures range from 21.0 to 30 °C, and show minimal variation with seasons.

1.4 Geology of the study area

Mount Cameroon (MC) is an unusually steep lava dominated, elliptical volcano that covers a total area of about 1400 km². It is 35 km wide and 60 km long and lies at the continent-ocean boundary of a 1600 km long chain of volcanic centres called the Cameroon Volcanic Line (Rakenbury *et al.*, 2005; Fig. 1.7).

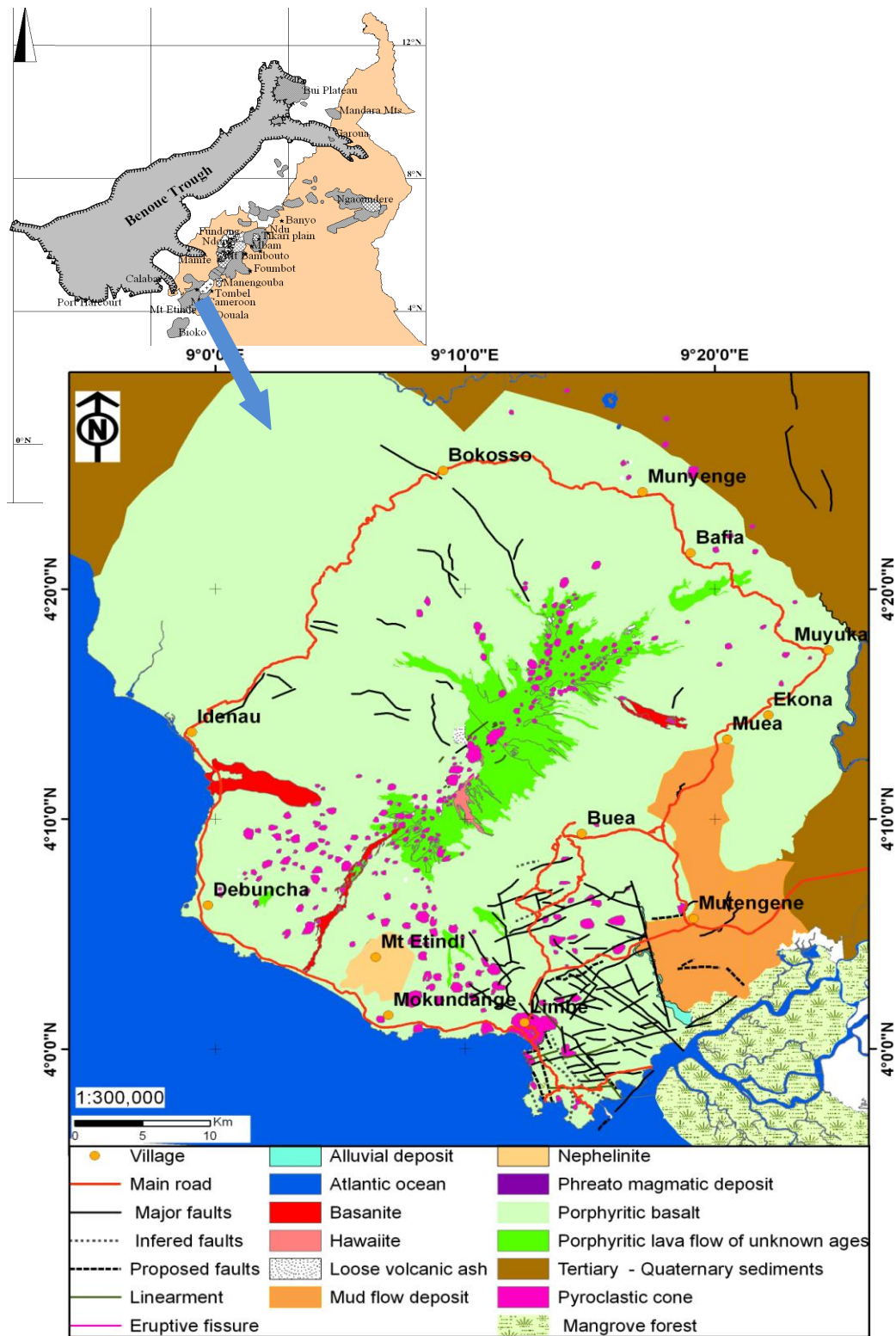


Fig. 1. 7. Geologic map of Mount Cameroon, modified from Endeley *et al.* (2001) and Thierry *et al.* (2008) with field checks. Inset is the map of the Cameroon Volcanic Line, modified after Marzoli *et al.* (2000) and Rankenbury *et al.* (2005).

Volcanic rocks from MC are mainly of alkaline affinity and include basalt, basanite, hawaiite, ankaramite, mugearite and picrite lavas characterised by high concentrations of high field strength elements (Suh *et al.*, 2008).

Hundreds of pyroclastic cones occur on the flanks and summit regions (Suh *et al.*, 2003; Bonne, 2006; Njome *et al.*, 2008). These cones are mostly concentrated along the volcano's long axis while the lower flanks are covered with lahar deposits probably derived from sector collapses of the volcano initiated by intense rains. Typical eruptive behaviour ranges from effusive eruptions producing lava flows to moderately explosive eruptions (Hawaiian to Strombolian-style) resulting in the formation of pyroclastic cones (Suh *et al.*, 2003; Njome *et al.*, 2008).

Chapter Two

Inventory, mapping and description of geometric parameters of landslide scars

2.1 Introduction

Landslides activities represent one of the principal geomorphologic processes through which hill slopes evolve (Ahmad *et al.*, 1999) and have long been overlooked and/or underestimated as important natural disturbing agents that modify the terrain, ecosystem and the environment at large (Geertsema & Pojar, 2007). The effects of slope movements range from negligible to catastrophic levels. However, the consequence of landslides could be minimized if people are vigilant, watch and report abnormal occurrences around their vicinity and look out for some evidence of slope movements such as the presence of cracks, bent trees, tilted pole and fences, earth moving away from foundations and why not avoid areas that are prone to sliding.

Within the last three decades, a number of mass movement events occurred in Cameroon with ca 99 % of these slides occurring along the Cameroon Volcanic Line. Analysis of recorded landslide events reveal a total death toll of 142 persons within this time span (Table 2.1) suggesting an average of 4.3 deaths per year assuming a Poisson distribution, and enormous damage to crops, farmland, and other human infrastructure such as roads, bridges, and houses. The death toll resulting from landslide activities in Cameroon appears to be on the rise (Fig. 2.1) probably because of demographic pressure and territory mismanagement or because of the increasing awareness about natural hazard, resulting in major hazards being reported. It is therefore obvious to question the cause of the observed increase and attempt to evaluate the degree of vulnerability associated with this increase.

Though landslides are an important geohazard affecting the lives of individuals in Cameroon, particularly in the NW, SW and W Regions, literature coverage of landslides in Cameroon is scarce and mostly limited to short reports from the formal Ministry of Mines, Water and Energy, (Ayonghe *et al.*, 1999). Some information is also made available by news paper reports which simply make mention of where the slide occurred and number of casualties, from eye witness reports and approximately 10 published articles (Lambi 1989, 2004; Lambi & Ngwana 1991; Lambi *et al.*, 2002; Ayonghe *et al.*, 1999, 2002, 2004; Ngole *et al.*, 2007;

Zogning *et al.* 2007; Ayonghe & Ntasin, 2008) that provide descriptive analysis of the causal factors, statistical analysis of rainfall events that triggered some of these slides. Landslide susceptibility assessment for the Limbe area has been attempted by Thierry *et al.* (2008) and Buh (2009). Table 2.1 below presents an inventory of some recorded landslide activities in Cameroon from 1976 to 2010. It is worth noting that this is not an exhaustive list as most slides occur in sparsely populated area and are not reported or recorded unless significant human and/or material casualties are involved.

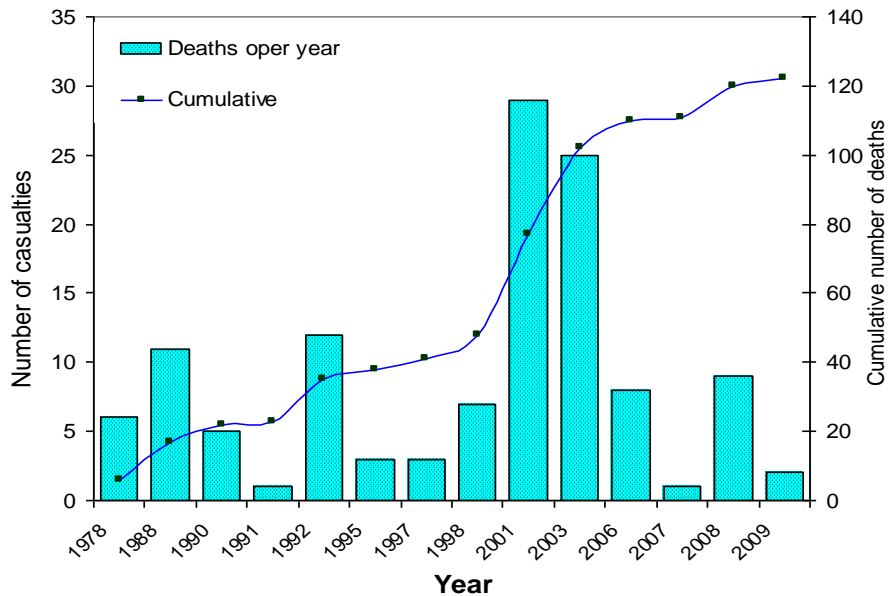


Fig. 2. 1. Landslide related deaths (bar graph, left scale) and cumulative death toll (line graph, right scale) of landslides recorded in Cameroon in the last 3 decades.

2.2 Importance of landslide inventory

Landslide inventory and the generation of inventory maps is a fundamental part of any landslide study. The information shown on them can be used to investigate landslide spatio-temporal abundance and estimate exceedence probability (Crovilli, 2000). They can also be used to obtain statistics of landslide size and volume (Malamud *et al.*, 2004). Landslide inventory are used to estimate the frequency of occurrence and determine areas that are likely to be affected by future slides (Susceptibility evaluation). In addition, frequency/size distributions have been used to estimate the severity of landslide events and to determine the contribution of landslides to erosion.

Month and year	Locality	Causalities and damage	Rock type	Possible triggering factors	Number of slides
June- October 1976*	Akum, Mile 8.	Destroyed the Bamenda Bafoussam highway that had just been constructed; traffic halted for several hours.	Weathered trachytic and basaltic rocks	Human intervention , rainfall and earth tremor	
August 1978*	Dschang	6 deaths			
Late August 1982*	Kongbou , along the Mbouda-Santa highway		Weathered trachytic and basaltic rocks		
Mid September 1982*	Santa, close to the former custom Frontier post			Earth tremor with intensity of about 3-4 on the Richter scale	
December 1986*	Mount Mbankolo and Akok Bikanda	No casualties	Metamorphic rocks		
June 1988*	Bakombo, Melong (CVL)	11 deaths, a lot of damage to property farmland and houses destroyed	Volcanic rocks		
September-October 1989*	Cassava Farm, Limbe (CVL)	houses destroyed, farmland lost and lot of property destroyed	Weathered scoriaceous material, volcanic rocks	Human intervention and Rainfall	
August 1990*	Oyomabang, Yaoundé	5 deaths, damage to property	Metamorphic rocks		
July 1991*	Mt Cameroon, Limbe	1 death, a house damaged	Pyroclastics on volcanic cone	Human intervention, terracing on slope and precipitation	One
September 1992*	Santa, Pinyin Bamenda Highlands	12 deaths, damage to property	Volcanic rocks		
5th September 1995*	Bafaka Balue Ndain Division, Rumpi Hills	3 deaths, farmland and property destroyed	Volcanic and sedimentary rocks	3 days of continuous rainfall, and an earthquake of magnitude about ~4 on the Richter scale	57 landslides, 1 rockfall and mudflow.
September 1997*	Sho, Belo subdivision	2 deaths, highway, farmland and property destroyed	Volcanic rocks	Heavy rainfall	
September 1997*	Guoata (Dschang)	1 death and damage to farmland	Weathered granite	Precipitation	
July 1998*	Baingo, Belo subdivision	5 deaths, damage to 3 houses and farmland	Weathered rhyolites	Precipitation and earth tremor	One slide
September 1998*	Anjin, Belo	2 deaths and loss of farmland	Weathered volcanic rocks	Precipitation	

27 th June 2001*	Limbe	23 deaths, 2400 displaced, farmland and property destroyed	Weathered basaltic blocks	Precipitation	Several landslide swarms
September 2001*	Ron (Nwa)	6 deaths and damage to farmland	Weathered volcanics and migmatites	Precipitation	
July 2003 *	Wabane , West Region	25 deaths and property valued at US \$ 803,773.6			Slide swarms
21 th July 2005 **	Bonjo	No deaths but destruction of farmland	Weathered basaltic material	Precipitation	Several Landslides
2006 *	Station Bamenda	4 deaths, one house completely destroyed	Rhyolites	Precipitation	One landslide
5 am, 14 th July 2006 **	Mini coquette, Bonduma, Buea	4 deaths and one house destroyed	Lahar deposits	Precipitation	One landslide
June 12 2007**	Abangoh, Bamenda	3 deaths, 1injured and subsequently died in hospital			
20 th October 2007*	Kekem	1 death, 1 injured, 16 families displaced, farmland and Bafoussam Douala road destroyed	Weathered rhyolite	Precipitation	One slide
July – August 2008*	Bonjo, Mondoli, Makuka Limbe	No major destruction	Weathered porphyritic basalts, pyroclastics	Precipitation	4, all reactivations of older slides
August and early September 2008*	Garoua	9 deaths, livestock and houses destroyed by floods and landslides 27 communities affected		Precipitation	
1 and 3 am, 29 th June 2009**	Unity Quarter and Moliwe	2 deaths, damage to 3 buildings	Weathered loose pyroclastic material	Precipitation	3 and 2 respectively
4:30, 4 th August 2009**	Below Governor's office Station, Bamenda	Bamenda high way completely blocked	Weathered rhyolitic material	Precipitation	One slide
4 th August 2009	Sisia Quarter	1 death, 2 seriously injured	Weathered Gneisses	Precipitation	One slide
7 th August 2009	Anindoh, mile 3, Bamenda	Collapse of bridge on Major national high way			
2pm, 6 th August 2009**	Kie Village, Limbe	Bota-Mukundange road completely blocked, water tank partially buried, fence broken.	Soil on pyroclastic material	Precipitation	1 car owner injured and car partially destroyed
7-8 of August 2009**	Mile 3 station	Bamenda- Bafoussam highway completely cut off for over two weeks	Weathered rhyolite	Precipitation	subsidence
July 2010	Likomba	No major damage	Lahar deposits	Precipitation	One slide
12-13 September 2010**	Zekeng-fondom	Damage to cocoa and palm farms, road and foot path linking the 3 villages blocked	Weathered volcanic	Precipitation	Multiple slides

Table 2. 1 Some recorded landslides in Cameroon from 1988 to 2010 updated after Ayonghe *et al.* (1996), and Zogning *et al.* (2007), field surveys carried out from 2008 to 2010, and from news reports. Note that landslide record is incomplete. * Slides reported by previous landslide studies, ** reported by this study.

Landslide inventory maps can also be used to evaluate the number of historical landslides that have been erased by erosion, human activities, and vegetation cover (Malamud *et al.*, 2004).

Landslide inventory can be obtained by analyzing historical catalogues of landslide events from reports, newspaper articles and other published literature, interpretation of multi-temporal aerial photos and satellite images, intensive field mapping or a combination of the aforementioned methods. In this study, all documented slides were observed and described in the field due to the lack of recent and regular aerial photography surveying in the region. Assuming that landslide occurrences are independent random point events in time, a Poisson model was adopted to investigate the occurrence of landslides within the study area. According to this model, the probability of experiencing X slides during time t is given by

$$P(X : \lambda) = \frac{e^{-\lambda} \lambda^x}{X!}, X = 0,1,2,3,\dots$$

where P = the probability,

X = is time

λ = the estimated mean number of slides per year.

From the above equation, and considering the 10 year period from 2001 to 2010 with well documented landslide records, a total of 56 landslide sites were identified (43 produced in 2001 and 13 others from 2002-2010). This results in a mean of 5.1 slides per year for the study area and a 3.1 % probability that 1 slide would occur each year. From equation 1, and assuming that landslide recurrence will remain the same, the exceedence probability (probability of experiencing one slide or more) is given by

$$P(X(t) \geq 1) = 1 - P\{(X(t) = 0)\} = 1 - e^{-\lambda t} = 1 - e^{-t/x}$$

For the Limbe area, this results in a 96.3 % probability of at least one slide occurrence per year within the area.

2.3 Landslide mapping method

This study involves detailed field observations and mapping of the geometric configuration of landslide scars produced between the year 2001 and 2010. Because vegetation recovery rates within the study area are rather high such that scars are completely covered within five years

after failure, only landslide scars observed in the field are accounted for in this study. Field mapping, reports and interviews with local inhabitants who witnessed the landslide events or their impacts provided insights into the factors responsible for landslide occurrence within the study area. Several field visits and ground reconnaissance surveys were made to locate slide scars and systematically measure their morphological characteristics. Landslide scars were recognized in the field by sharp changes in vegetation type, the presence of bare crescent (acute slope) shaped scarps, sharp depressions in the landscape as well as the presence of displaced material at the foot of the scar (jumbled-up mixture of subsoil and topsoil). Recognition was aided by published reports and by inquiries made to the local population, particularly farmers and hunters. During field, mapping the traverse mapping technique was adopted due to inaccessibility and the rugged nature of the terrain. Hence, the inventory is incomplete particularly for densely vegetated areas. Traverses were made by car and on foot. Geographic coordinates of all scars were obtained at the left margin, centre and right margin of the crown and toe of the slide with a Garmin Etrex GPS receiver using a common reference system (Universal Transverse Mercator (UTM) Zone 32 N, WGS84 datum). Measurements of the geometric parameters (width of rupture (W_r), length of rupture (L_r) and scarp height (h) (Fig. 2.2) were made with a graduated surveyor's tape. From these parameters, the area of the rupture zone (A) and the volume (V_l) of displaced material were estimated using the follow standard formulae:

$$A = L_r \times W_r \text{ (Guthrie \& Evans, 2004a)}$$

$$V_l = \frac{1}{6} \times \Pi \times L_r \times W_r \times h \text{ (Cruden \& Varnes, 1996)}$$

The latter equation assumes that each slide has an elliptical shape, which appears to be a reasonable first-order approximation based on detailed field observations. Worthy of note is the fact that L_r is difficult to measure because the outline of the rupture surface around the foot is usually buried under displaced material. Hence L_r was extrapolated from the outline of the main scarp and slide flanks with the elevation along the extrapolation line taken as the elevation at the foot. Slide run-out distance was measured for all fresh slides and ignored in cases where the slide trail had either been completely re-colonized by vegetation or converted into farmland. From these, the total surface area covered by the rupture zone and the accumulation zone was calculated. Slope gradient before failure was estimated by measuring the gradient of slopes adjacent to the slide with a Silva compass/clinometer.

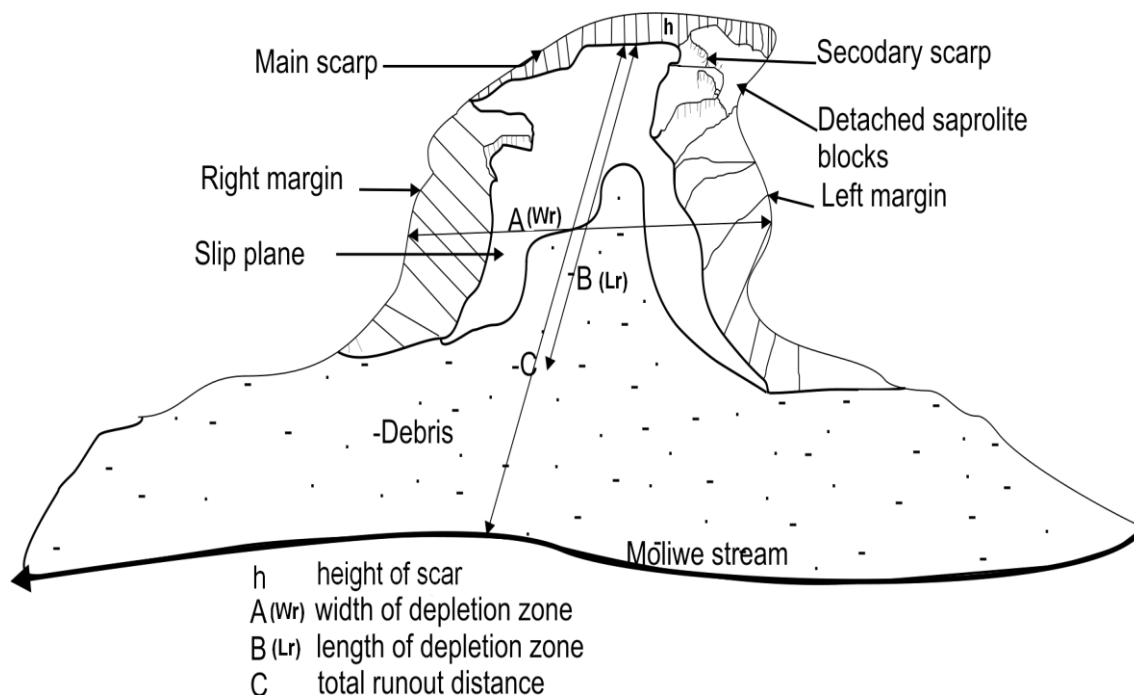


Fig. 2. 2. Sketch of plan view of 2009 debris slide at Moliwe indicating where and how various parameters were measured in the field. Nomenclature after Cruden & Varnes (1996), Dikau *et al.* (1996) and Knapen *et al.* (2006).

The aspect (slope orientation, which refers to the direction of movement or the direction the failure plane faces), was obtained with the aid of a compass.

The mode of movement was determined following the procedure proposed by Davies *et al.* (2005). Rotational and translational movements are distinguished based on the presence of perched ponds at the head of the slide or backward rotation of displaced objects and vegetation. The McCalpin (1994) age classification system was used. This provides a qualitative description of the state of activity and age of the slide rather than providing absolute ages. Furthermore, vegetation type, land use patterns, presence of streams/rivers, effective soil thickness, rock type and other factors believed to be responsible for sliding at each location were noted and later used to construct factor maps for susceptibility assessment (Chapter 5). Land use and land cover characteristics such as vegetation type, limits of built-up areas, farmland, forest, etc., was noted and used in the validation of data obtained from satellite images.

2.4 Equipment used

Figure 2.3 represents a catalogue of some of the equipment used in the field.



Fig. 2. 3. Catalogue of equipment used in the field; a) Silva compass clinometer for orientation and inclination measurements; b) Permanent bold marker used in the labelling of samples; c) Hand lens; d) Torvanometer used to measure in situ relative shear strength of the soils; e) geologic hammer; f) Measuring tape; g) Etrex Garmin GPS receiver.

2.5 Results from field observations

2.5.1 Description of landslide scars

A total of 63 slides, 53 recent (i.e. slides with well-defined margins, head scarp, with no or partially developed drainage channels) and 10 older landslide (i.e. slides where margins and head scarp have been degraded) scars were observed. These slides together produced a total volume of $\sim 10^5 \text{ m}^3$ of debris from a total area of $\sim 0.1 \text{ km}^2$, which is $\sim 0.03 \%$ of the study area. The width of the depletion zone (W_r) ranges from 3.0 -79.0 with a mean of $22 \text{ m} \pm 17 \text{ m}$, and length (L_r) from 1-110 m (mean $25 \pm 23 \text{ m}$). Individual aerial extent and volume ranges from a few m^2 to $9.3 \times 10^3 \text{ m}^2$ and 2.5 m^3 to $5 \times 10^4 \text{ m}^3$, respectively. Measured widths are approximately equal to the length of the rupture zone for rotational slides whereas the width is smaller than the length for the translational slides observed in this study.

Most of the studied slides initiated at mid slope rather than at the shoulder or top of the slope. 51 % of the observed slides are associated with road cuts, and built-up areas whereas 49 % occur in areas where there has been minimal excavation and/or close to stream channels. Figure 2.4 shows the distribution of landslides in combination with land use patterns. It was also observed that most of the slides occurred on slopes with a gradient between 25 and 40°. Slides occurring on slopes above 40° are associated with artificial slopes created by excavation works (Fig. 2.4b).

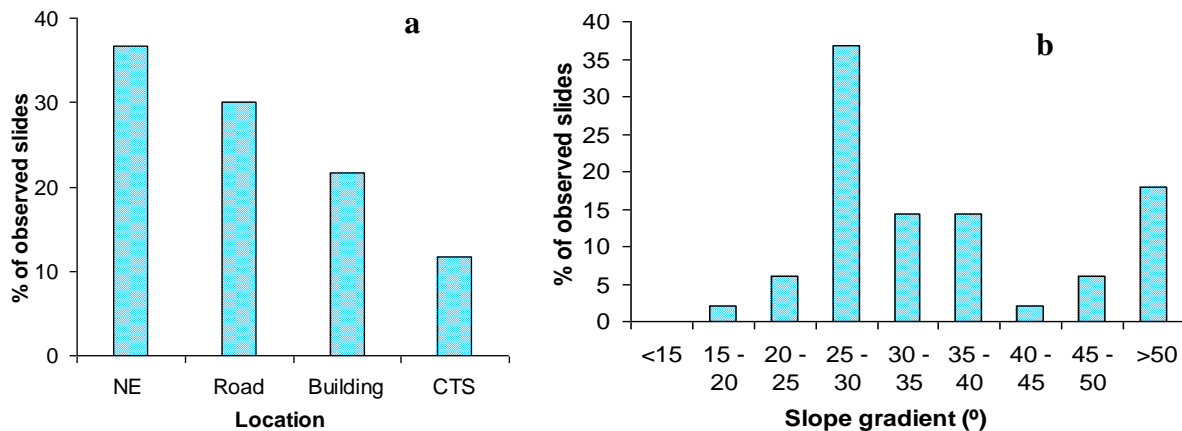


Fig. 2. 4. Distribution of landslide scars: a) based on characteristics close to the initiation site. NE represents natural environment with no excavation works. CTS: close to stream channels; b) in relation to slope gradient measure at the initiation zone.

Landslide height, measured as elevation difference between the crown and the toe of the slide (drop in height of the depletion zone) ranges from 1 - 81 m with a mean of 18 ± 16 m. The accumulation zone of 87 % of the observed slides is covered by vegetation, converted into farmland or portions of it had been washed away by streams. Hence the actual run-out distance could not be measured in these cases. Estimated values of run-out distance generally underestimate the total mass or volume of material that moved down slope and the total area affected by slide debris.

According to the landslide classification scheme of Cruden & Varnes (1996), most of the slides observed in this study are shallow translational (96 %) earth and debris slides while rotational, complex slides and rock fall make up 2 % each (Fig 2.5).

Two slides initiated as shallow translational slides and then transformed into mudflows with debris thickness above 2.5 m, probably as a result of excess water supplied by intense rain and the entrainment of surface runoff into the slide debris. From the classification scheme of

Terzaghi *et al.* (1996), which is based on the location where the slip surface intersects the slope, all the slides are classified as slope failures because the slip surface intersects the slope above its base (foot).

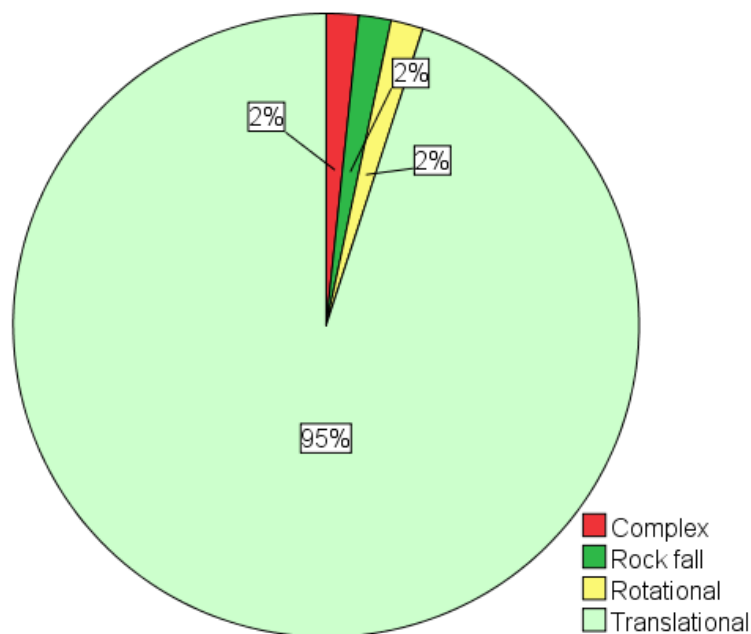


Fig. 2. 5. Proportion of various landslide types observed within the study area, based on the classification scheme of Cruden & Varnes (1996).

A catalogue of some of the observed slides is presented below (Fig. 2.6). The slides generally have well defined crescent shaped head scarps with near vertical head walls and margins similar to the map view of slides described by Martel *et al.* (2004). They are made up of dark red, reddish brown and yellowish soils overlying gray or purple mottled saprolite (Fig. 2.7). In some cases, the head scarp is composed of a mixture of soils and rock fragments that are a few centimetres to over 1 m in diameter with completely weathered surfaces and fresh interiors (Fig. 2.8). This observation emphasises the influence of jointing in the weathering of the parent rocks. These are dark, porphyritic rocks with abundant large dark (black), greenish, and a few white minerals as phenocrysts probably (pyroxene, olivine, and plagioclase).

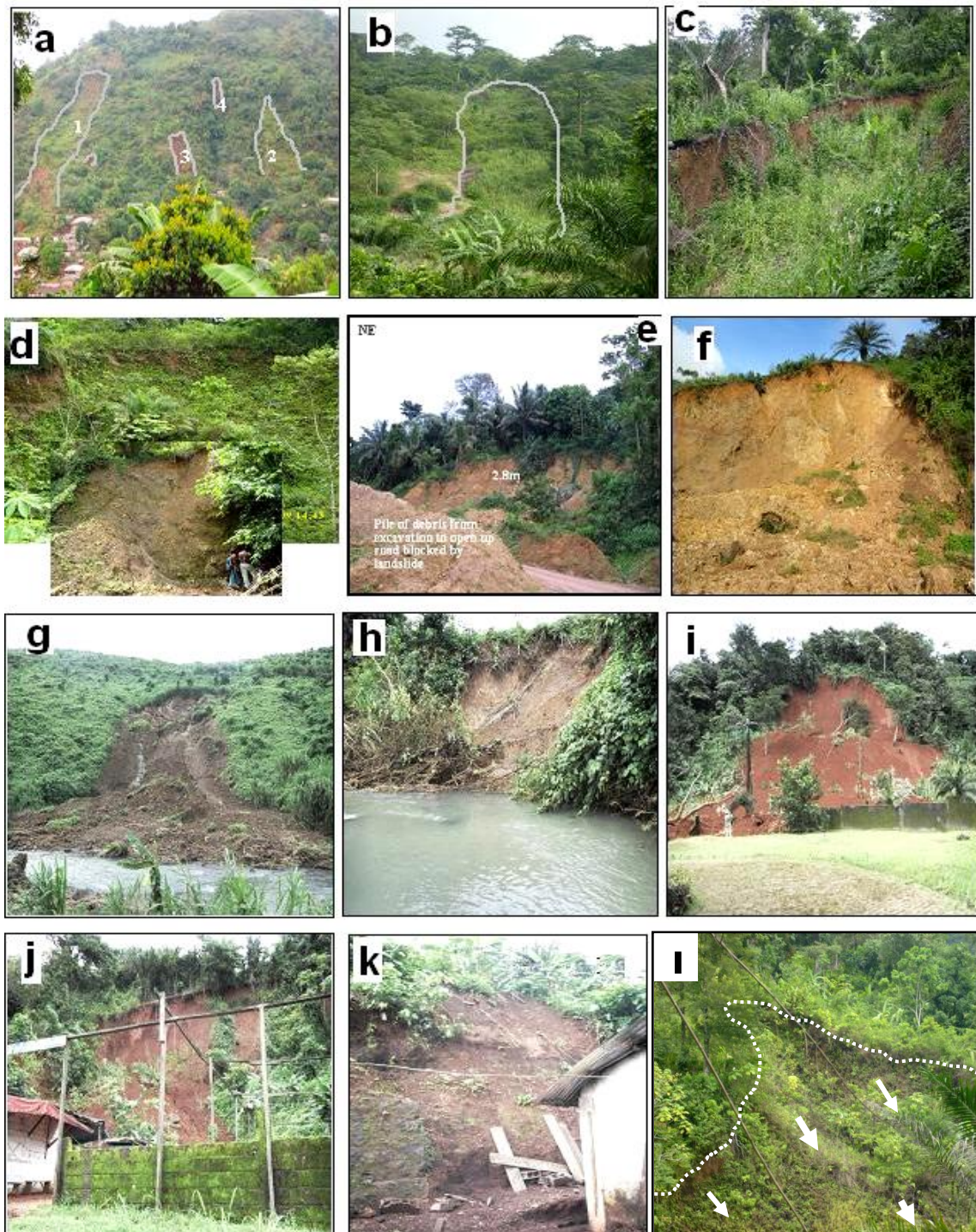


Fig. 2. 6. Field photographic view of some landslide scars within the study area: a) 2001 landslides on pyroclastic cones at Mabeta New Layout; b) translational slide at Makuka; c) Close up view of slide of slide B at Makuka; d) translational slide at the banks of a stream at Makuka, reactivated in August 2008; e) 2005 rotational slide at Bonjo (Courtesy of Nele Tytgat, field observations in 2006); f) earth slides at a road cut in Bonjo initiated from excavation works; g) and h) June 29-30th 2009 translational slides at Moliwe; i) August 2009 rotational slide at Kie Village; j) reactivation of translational slide at Kie with retrogressive characteristics; k) translational slide at Unity Quarter; l) translational slide at Makuka Limbe. White arrows indicate the direction while broken line marks slide margin.

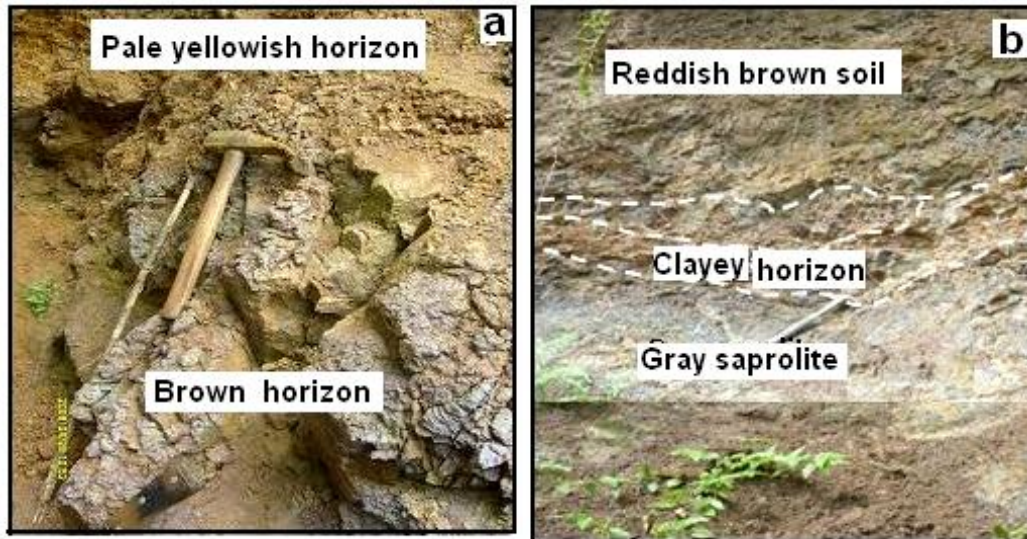


Fig. 2. 7. Characteristic field view of the head scarp of some observed scars: a) slide 22 at Bonjo and b) slide 6 at Makuka. Note the change in texture and colour of the overlying soil and the underlying saprolite.



Fig. 2. 8. Contact between soils and saprolite and the characteristics observed at the head scarp: a) reddish brown soils and underlying gray saprolites at slide 8 Makuka; b) jointed basaltic blocks at head scarp of a rotational slide at Bonjo sandwiched by pale yellow clayey soils.

The crown and areas close to the main scarp are commonly marked by the presence of acute, open tension cracks that are between 30 cm and 100 cm wide and were observed at or close to the head scarps of most of the slides.

According to Terzaghi *et al.* (1996), slope failure in cohesive material is generally preceded by the formation of tension cracks behind the upper edge of the slope. Pinnacles, representing aborted slide material were also observed in some areas. Longitudinal sections through the different slide types are shown below (Fig. 2.9).

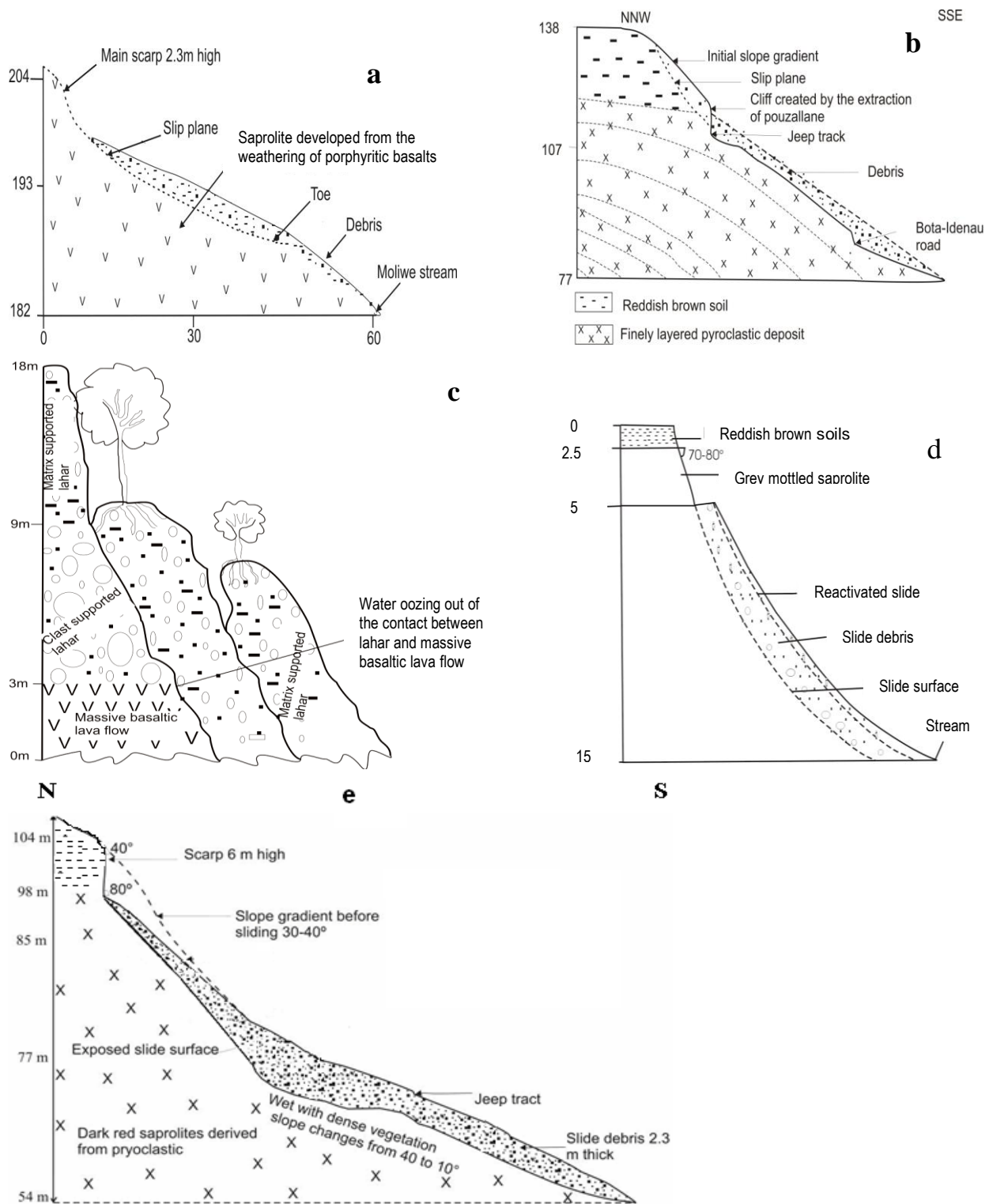


Fig. 2. 9. Sketch of observed slides: a) shallow translational slide at Moliwe; b) rotational earth slide at Kie; c) rock slide along the banks of the Ombe river. Note the presence of mature vertical trees at the top of the slip mass indicating block movement with minimal rotation; d) progressive translational slide at Makuka on steep slope with a very short run out distance. Sliding plane lies at the contact between lateritic soils and saprolite; e) Shallow translational slide developed on a degraded pyroclastic cone at Mabeta New Layout.

2.5.2 Statistical analysis of geometric parameters

The geometric properties of the slides were statistically analyzed in SPSS 16.0 to obtain trends and patterns exhibited by the data set. A summary of the descriptive statistical parameters are shown in Table 2.2.

Geometric parameter	N	Minimum	Maximum	Mean	Std. Deviation	Skewness	Kurtosis
Height of scarp (m)	60	1	10	3	2	1.2	1.1
Width of rupture (m)	60	3	85	22	17	1.9	4.1
Length of rupture (m)	53	1	110	25	23	2.0	4.9
Initial slope (°)	49	20	70	38	15	1.1	.31
Elevation (m)	63	13	716	157	124	2.6	8.7
Area (m ²)	53	3	9350	7.6 x 10 ²	1391	4.8	28.5
Volume (m ³)	53	5	48976	2.1 x 10 ³	6802	6.6	45.6

Table 2. 2. Descriptive statistics of geometric parameters of landslide scars (depletion zones) observed in and around Limbe. N represents the number of samples for which a particular geometric parameter was measured

The geometry of the slide depletion zones vary widely throughout the study area. ~ 96 % of the observed slides were < 50 m wide (Fig. 2.10a). Plots of landslide distribution with elevation above mean sea level indicate that slides are more abundant at low elevation with predominance in the area between 75 and 200 m a.s.l (Fig. 2.10). The height of individual scars ranges from 1 to over 10 m with mean values of 3 ± 2 m (Fig. 2.10d). In addition, these histograms indicate that all measured geometric properties are unimodal and positively skewed except for the height plots that show a bimodal distribution (Fig. 2.10d). Furthermore, the number of landslides decreases with increasing width, depth, length and run-out distance as shown on figures 2.10 a, b c, and d, respectively. A list of the geometric characteristics of all observed slides is given in Appendix 1.

Plots of the proportion of observed slides against slope gradient measured at the head scarp suggest that most of the slides occur on slopes with a gradient between 25 and 38°. No slide was recorded on a slope less than 15°. Further detail regarding the distribution of landslide and the slope gradient in the study area is given in chapter 5 Slides occurring on slopes greater than 38° were mostly on artificial slopes generated by human intervention in the form of excavations for the construction of roads and houses or the extraction of local materials (quarrying). Together all observed slides produced a total volume of $\sim 9.5 \times 10^4$ m³ of debris from the study area.

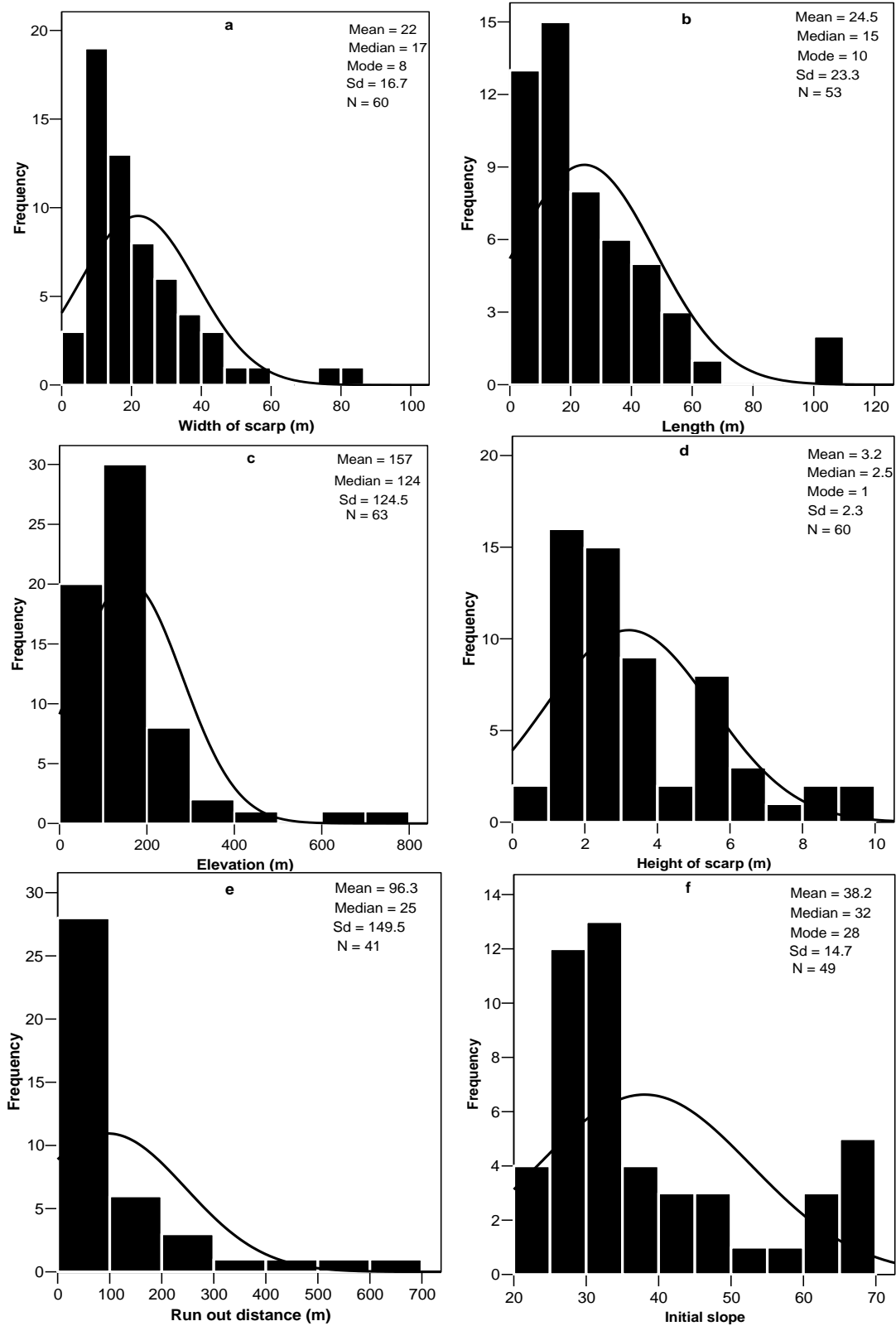


Fig. 2. 10. Distribution of geometric parameters: a) width of depletion zone; b) length of depletion zone; c) elevation at the main scarp in meter above sea level; d) height of the scarp; e) run out distance; f) slope at the point of initiation of main scarp.

According to the classification scheme of Fell (1994, Table 2.3) the landslides in this study can be classified as extremely small, very small, and small slides with volumes that range from a few m^3 to $5 \times 10^4 \text{ m}^3$.

Size class	Magnitude	Size description	Volume (m^3)	Number of observed slides
1	1	Extremely small	<500	30
2	2	Very small	500 – 5000	19
3	3	Small	5000 – 50,000	4
4	4	Medium	50,000 – 250,000	-
5	5	Medium–large	250000 – 1000000	-
6	6	Very large	1,000,000 – 5,000,000	-
7	7	Extremely large	>5,000,000	-

Table 2. 3. Size classification for landslides (Fell, 1994). Volume was not measured for 9 of the recorded slides because of the dense vegetation cover hence all parameters could not be measured.

The largest of the studied slides (Mondoli landslide, 27th June 2001) accounts for ~ 45 % the total volume of displaced material within the study area. Plots of landslide area and volume ranked from the largest to the smallest show some characteristic patterns as observed in Figure 2.11. The ranked order might be interpreted as a proxy for frequency (magnitude) of that landslide size within the study area. These plots on a logarithmic scale display a straight line (Fig. 2.11d), with only the smallest and largest slides offset from this general trend. From the graphs ~75 % of the slides have a surface area < 1000 m^2 and a volume < 1700 m^3 . Only 10 % of the slides have a surface area > 1800 m^2 and a volume > 4000 m^3 . Fluctuations in this linear relationship could be a result of non-exhaustive documentation of the smallest and largest slides, respectively.

The largest Mondoli slide is significantly offset from the frequency-size relationship plot. This is further supported by tests for the presence of outliers, which indicate that 4 of the calculated volumes and 2 areas can be considered outliers. This is an indication that the sliding mechanism of these relatively large landslides is different or that they must be quite infrequent. Deviation from the straight line on the semi logarithmic plot also signifies that the landslide inventory in this study is still incomplete and can be enhanced in the future, bearing in mind accessibility difficulties due to vegetation growth and the absence of aerial photographic coverage of the area.

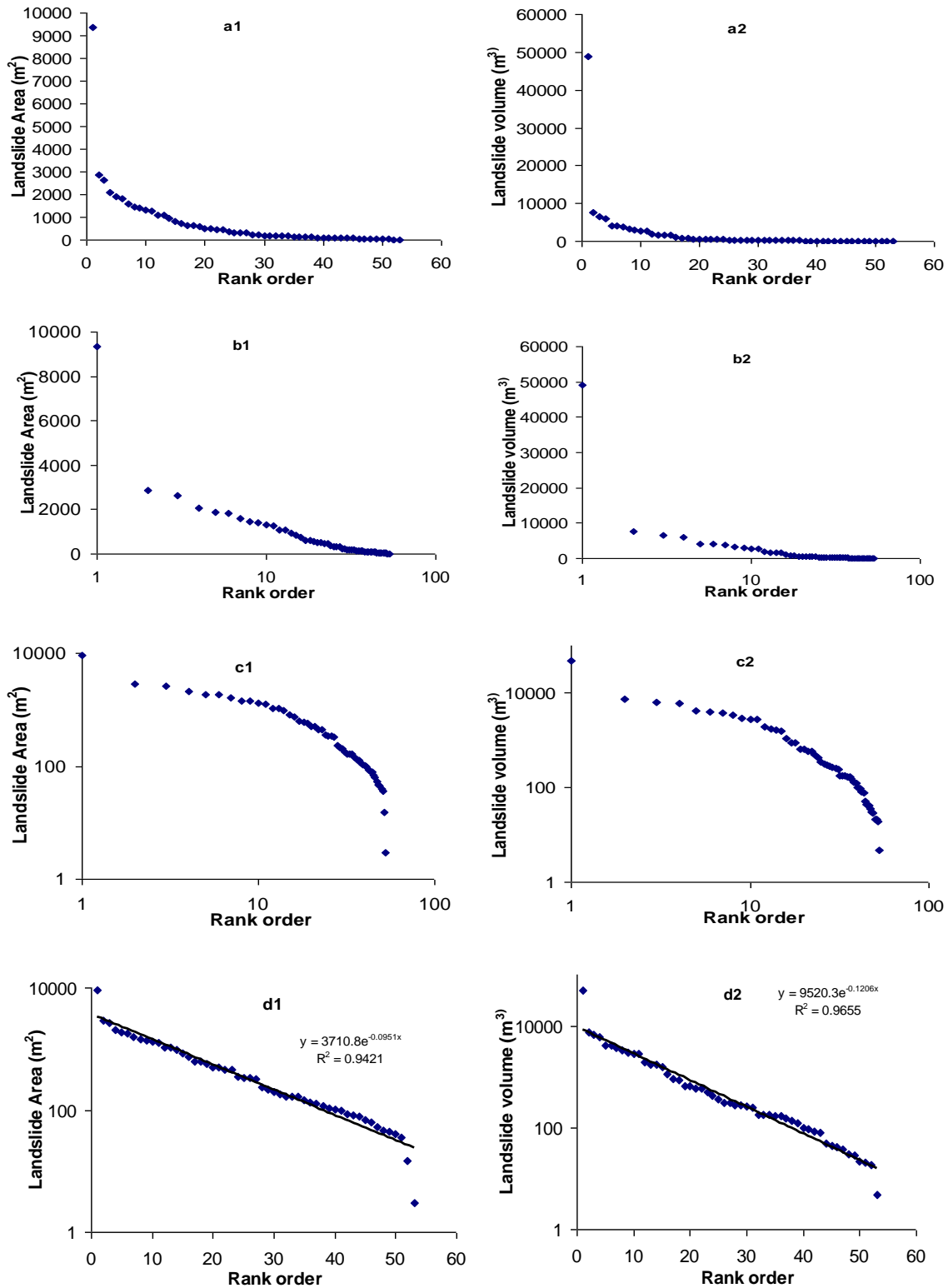


Fig. 2. 11. Distribution of the areas and volumes of 50 individual landslides triggered by rainfall in the Limbe area. In the graphs, x-axes show rank order, from largest to smallest landslide, y-axes show landslide area/volume: a) linear-linear plot; b) linear – log plot; c) log-log plot, d) log–linear scale. Left column represents area plots, right column volume plots.

This semi-logarithmic relationship between the cumulative frequency and the volume of the slide is of great interest to assess the probability of occurrence of slides of a given volume (magnitude) in the future. This relationship is similar to that obtained from geometrical datasets for other landslides (Hovius *et al.*, 1999; Malamud, 2004; Brunetti *et al.*, 2009).

Two tail-t tests for the significance of the correlation between the different geometric parameters (Table 2.4) show the existence of a strong positive correlation between slide volume and area (Pearson's correlation coefficient (r) of 0.96), between length and area ($r = 0.81$), and between slide width and area with ($r = 0.73$). All these correlations are significant at the 99 % confidence interval. These relations advocate that variations in aerial and volumetric dimensions of the depletion zone are generally controlled by the width and length of the failure and to a lesser extent by its depth.

	Elevation (m)	Width of scarp (m)	Height of scarp (m)	Length (m)	Initial slope	Run out distance (m)	Volume (m ³)	Area (m ²)
Elevation (m)	1							
Width of scarp (m)	-.16	1						
Height of scarp (m)	-.311*	.54**	1					
Length (m)	-.04	.55**	.34**	1				
Initial slope	-.10	-.26	-.02	-.44**	1			
Run out distance (m)	-.15	.49**	.47**	.66**	-.25	1		
Volume(m ³)	-.08	.65**	.55**	.66**	-.16	.70**	1	
Area (m ²)	-.08	.73**	.54**	.81**	-.27	.75**	.96**	1

Table 2. 4. Pearson correlation coefficient matrix for geometric parameters. *Correlation is significant at the 0.05 level (2-tailed); **, correlation is significant at the 0.01 level (2-tailed).

This is opposed to landslides on the foot slope of Mt Elgon in Uganda where Knapen *et al.* (2006) showed that variation in volume is mostly controlled by the depth of the shear plane. Secondly, the volume-area correlation suggests that the height of the scarp (depth of failure) does not vary greatly within the region. Run-out distance shows a moderate but significant positive correlation with the volume ($r = 0.67$) implying that the distance over which the material travels is dependent on the volume of generated debris. There is also a moderate correlation between the length of the depletion zone and the run-out distance of the slides suggesting that slides with a long depletion length will also have a longer run-out distance. There is a weak but significant negative correlation between the initial slope angle and the length of the landslide scar with longer scars observed on gentler slopes and shorter lengths on steep slopes. This relationship can

be explained by the idea that as the slope becomes steeper, the distance over which material will move is shorter. A weak but significant negative correlation exists between the width/length ratio and slope gradient (at a 0.05 confidence level). A moderate but significant positive correlation exists between the scar height and the run-out distance as well as the length of the depletion zone.

Plotting the location of observed landslide scars within a Geographic Information System (GIS), we note that landslides are not evenly distributed throughout the study area (Fig. 2.12). Instead, they exhibit some level of clustering with 88 % of the slides occurring on the Limbe Mabeta massif characterised by thick residual soil columns and 12 % on the lower slopes of MC. The slides are also more abundant on pyroclastic cones than on weathered lava flows. Areas that experienced landslides are also characterised by specific land use types, slope gradient, soil colour, and parent material. For this reason, the study area was divided into six landslide zones namely Mabeta, Bonjo, Chopfarm, Makuka, Moliwe and Kie landslide zones. A few isolated cases do not fall within any of these zones.

The Mabeta and Kie landslide zones (Fig. 2.12) are characterized by the presence of pyroclastic deposits, reddish to reddish brown soils and slopes with gradients above 32°. Human activities such as the construction of houses, footpaths and roads are abundantly present. Extensive fieldwork carried out in the Limbe area shows that residual soils are widespread. Red to reddish brown coloured residual soils are mostly located at the top of pyroclastic deposits produced by explosive eruptions of basaltic magmas while pale yellow and dark brown soils develop on lava flows. The unweathered pyroclastic material, typically exploited as aggregates for road construction and repair, are made up of loose mechanically weak particles that are very porous, highly permeable, and stable in the dry and natural state.

Stability comes from the fact that they were formed from the deposition of volcanic ejecta such that the particles are laid down at their angle of repose controlled by the degree of grain-grain chaining between adjacent highly irregular-shaped particles (Riedel *et al.*, 2003).

The Chopfarm, Bonjo, and Makuka landslide zones (Fig 2.12) are located on weathered lava flows, characterized by secondary forest and/or farmland, gentler slopes, and are sparsely inhabited. Excavation activities and other human influences on these slopes are less common

than in the Mabeta zone, with the notable exception of slides in Bonjo, which were directly associated with road cuts and construction works.

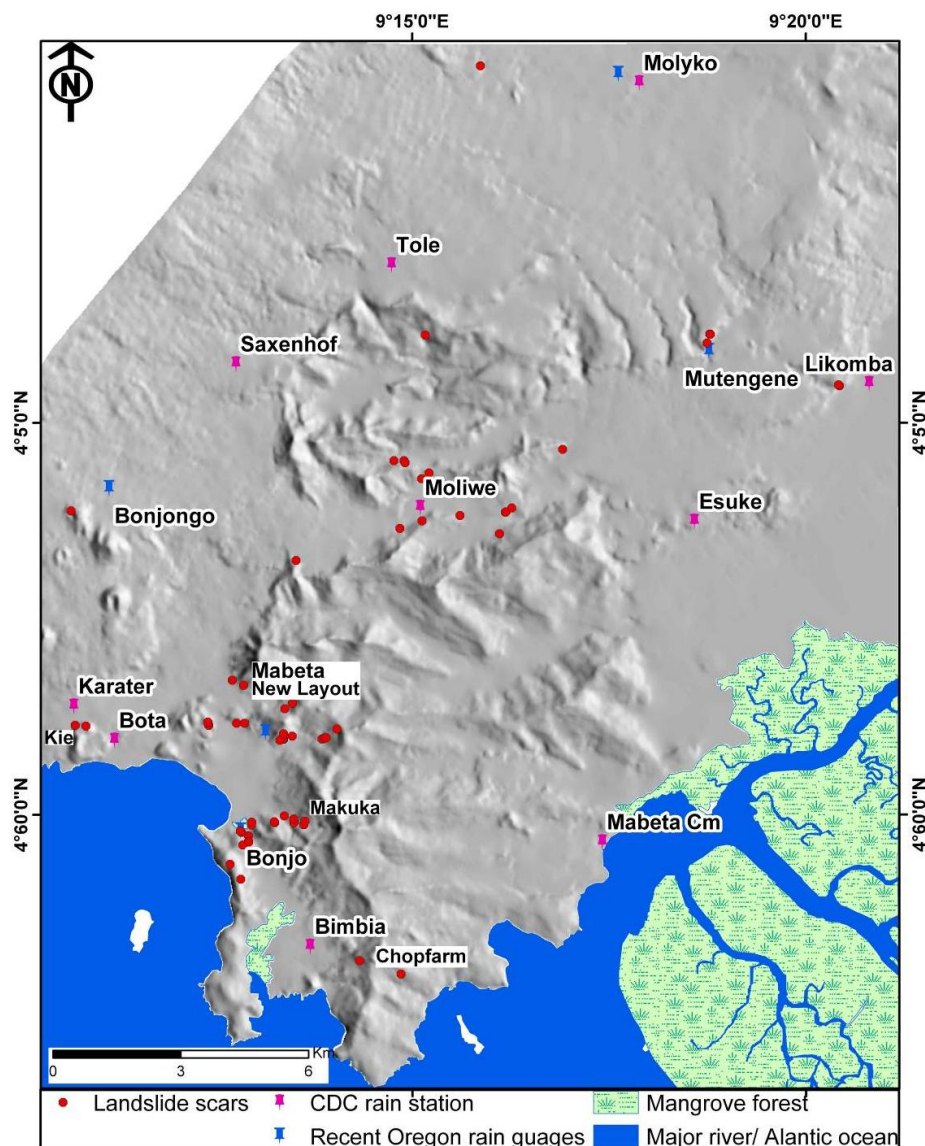


Fig. 2. 12. Distribution of landslide zones within the Limbe area.

The Makuka zone is characterized by secondary forest and farmland, sparsely populated, and has a high stream density with most of the slides terminating along stream channels. Stream undercutting is likely an important factor in slide generation here.

The Moliwe landslide zone (Fig. 2.12) lies within industrial palm plantations grown on pale yellow soils developed from the weathering of basaltic rocks. Slides in this zone occur close to streams, paved and unpaved roads used by CDC tractors and particularly in recently deforested

areas. Individual slides within this zone are relatively small in size with shorter run-out distances compared to those occurring in other zones. Though all the slides within each of these zones have their unique characteristics, only one slide in each of these zones will be described in detail as a type example except for slides within the Chopfarm zone. The latter were all heavily re-vegetated, hence detailed observation and description was not possible. Human, material and economic losses associated with the described slides vary from one place to another and are summarized in Appendix Table A2. Slides in the Chopfarm, Moliwe and Makuka zone commonly result in the destruction of farmland and the environment at large because the areas in which they occur are sparsely inhabited. Slides in the Bonjo zone result in the destruction of buildings, farmland and occasionally block roads.

2.6 Slide description

2.6.1 Mabeta slides

Several first-time (slopes that have never been affected by a landslide) translational landslides (Fig. 2.6) occurred on degraded pyroclastic cones with slope gradients of 30° to 40° in Mabeta New Layout on the afternoon of June 27th, 2001 after severe rains during which 180 mm of rain in 24 hours was recorded at Krater ca. 4 km away. People were buried by the floods and landslides, which destroyed their houses. Together, the flood and the slides at Mabeta destroyed ten houses and killed 23 people (Ayangi, 2004; Ayonghe *et al.*, 2004; Zogning *et al.*, 2007). Although no rainfall intensity data is available, eyewitness accounts attest to prolonged rainfall of high intensity. They also report water oozing out of the ground below the foundations of some houses located down slope and anomalous muddy surface runoff a few hours before sliding. This crucial observation could be used in risk awareness raising for future events and in understanding the processes that led to sliding. According to the local people, landslides in these areas took them by surprise, as is often the case with other natural disasters such as floods. The majority of the respondents did not anticipate the occurrence of landslides. Some of them linked the occurrence of the 2001 slides to supernatural factors and myths.

Wr of individual slides range from 12 to 43 m, Lr from 17 to 58 m and h from 2 to 7 m. The approximate run-out distance of the largest slide located ca. 100 m away from the studied slide is

ca. 350 m (slide 1 on Fig. 2.6a) whereas that of the studied slide is ca. 100 m. Together, these two slides damaged six houses and killed 14 persons either by burial and asphyxiation or as a result of collapsing buildings. Both slides initiated as shallow translational slides and transformed into debris flows due to the entrainment of surface runoff and ground water releases at the slip surface. The run-out distance of these slides were possibly limited by the presence of houses that acted as obstructions decreasing the velocity of movement and the presence of gentler slopes further down slope. Pits dug into the scar of the studied slide suggest that debris thickness is up to 2.3 - 3 m in depth. Boulders account for less than 20 % of the total displaced mass. A longitudinal section through slide 3 (Fig. 2.5a) is presented in Figure 2.8d. The depletion zone has a well-defined scarp (approximately 7 m high) and margins made up of a mixture of mottled dark red (2.5YR3/6) to dark brown (7.5YR3/4) soils/saprolite and weathered vesicular porphyritic basaltic pyroclastic rocks (Fig. 2.13). At the time of observation the slide trail had well-developed drainage corridors separated by longitudinal ridges 30 to 90 cm high and about 1 to 2 m wide, parallel to the slide margin (Fig. 2.14)

The local population in Limbe has increased significantly over the last few decades (from a population of 44,561 in 1987 to 84,223 inhabitants in 2005 implying a annual growth rate of 3.4% for the Limbe municipality (Bureau Centrale des Recensements et des Etudes de Population, 2010).

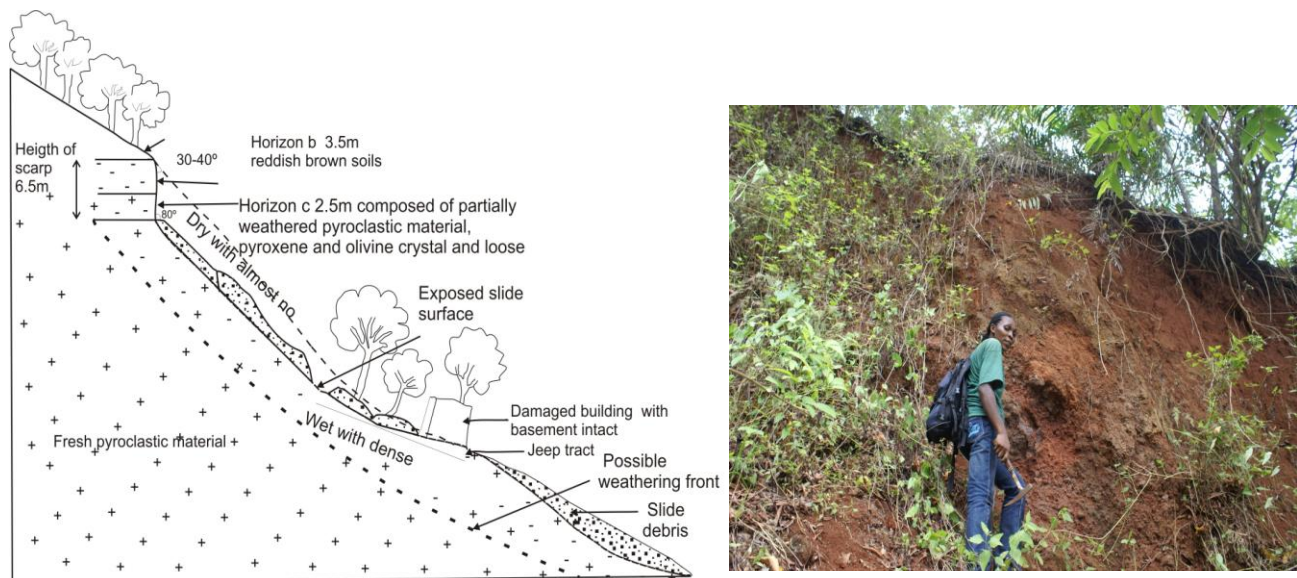


Fig. 2. 13. Material making up the slide scarp at Mabeta. Note the height of the slide margin about 4m high

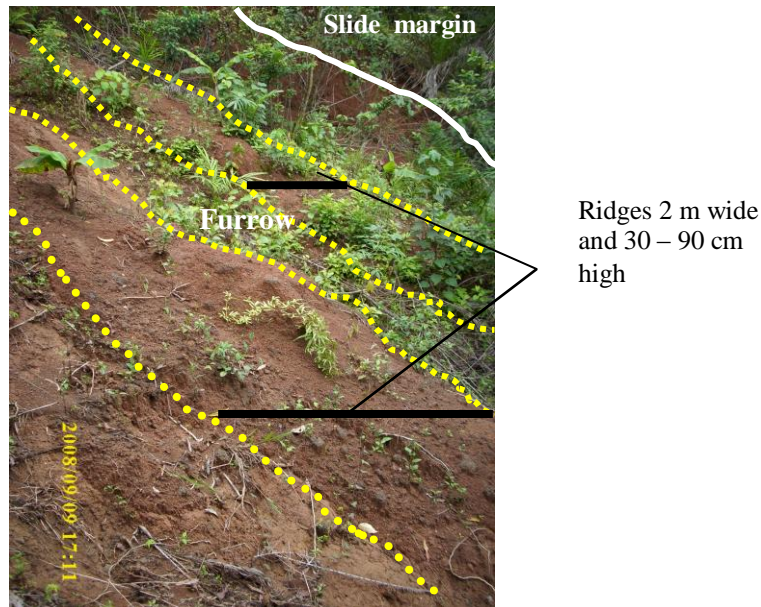


Fig. 2. 14. Internal morphology of the Mabeta slide characterised by the presence of 30- 90 cm high ridges parallel to slide margin and separated by parallel furrows.

In the Mabeta New Layout and Unity Quarter areas, characterized by steep slopes ($> 30^\circ$) and made up of pyroclastic material, construction projects are usually not associated with any formal stabilization measures. Individuals simply cut little terraces in a haphazard manner to provide room for construction (Fig. 2.15). Deforestation for crop cultivation is also a common practice in this area. In the last 20 years individuals have moved further uphill around the Mabeta New Layout to elevations of ca. 120 m a.s.l. to cultivate yams, cassava and maize (Fig. 2.6 a). This has increased the slope length void of vegetation and as such large areas initially covered by primary forest have been stripped of its vegetation and converted into farmland and secondary forest made of fruit trees and wild palms. Considering these observations, it is possible that anarchical construction, excavation of foot slopes, steep slopes and deforestation were the main conditioning factors whereas intense prolonged rainfall for a day or so and associated soil saturation were the main triggers of the 2001 slides at Mabeta.



Fig. 2. 15. Close view of anarchical construction at Mabeta. Note terrace cut into slope to provide space for construction without any stabilization measure put in place. Excavated material piled down slope is a potential threat to down slope located buildings. White arrow indicates near slope created by construction works.

2.6.2 Bonjo slide

On July 21st, 2005, a rotational landslide occurred along a road cut in Bonjo, a small locality within the Limbe Municipality. It blocked the single unpaved road linking the Military Base of Man 'O' War Bay, the Limbe 3 Council area and the town of Limbe (Fig. 2.16) for two days before the debris was excavated and the road reopened. 120 mm of rain in 24 hours was recorded at Krater located ca. 4.5 km away from Bonjo. This slide occurred on a 22° slope and has well-defined scarp and margins. The crown is characterized by the presence of a crescent shaped tension crack, 0.3 to 1 m wide and ca. 1 m deep. The scar is 25 m wide, 24 m long with a scarp height (h) of 2.8 m resulting in an estimated volume of ca. 10^3 m^3 and a total run-out distance of 35 m. Rock clasts range in size from a few mm to over 1 m and make up less than 10 % of the debris material. Prominent phenocrysts observed in the sample are plagioclase feldspar, pyroxene and olivine phenocrysts in a microlite and glass rich groundmass. The phenocrysts make up about 20 % of the rock mass.

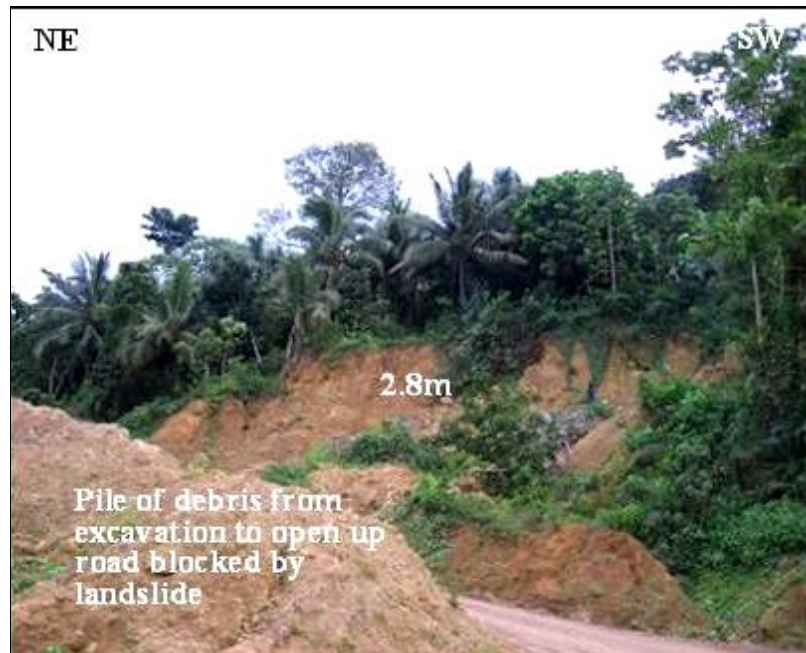


Fig. 2. 16. 21st July 2005 landslide at Bonjo. Slide completely blocked the road to Man 'O' War Bay. Image taken after debris had been cleared to reopen the road. Excavated debris is visible in the foreground (Courtesy of Nele Tytgat, field observations in 2006).

Debris moved from the road itself was piled up on the right side of the road and later remobilized by intense rainfall that followed a few days after the debris was clear off the road, causing significant damage to buildings located tens of meters down-slope such that ca. 80 inhabitants were rendered homeless for ca. 6 months. A key additional finding of crucial relevance for future interventions when clearing a landslide site and for local risk awareness rising is just how hazardous it can be to leave much of a former slide heap by the roadside in the vicinity of down slope located buildings. Inhabitants also reported that some other slides within the Bonjo area are generated by the mobilisation of debris excavated for the construction of foundations.

Between June and August 2008, the NE edge of the slide was reactivated (Fig. 2.17) moving the scarp backward by 5 m giving it a retrogressive character. H increased to 3.2 m and the crown still shows the presence of tension cracks and soil pinnacles. Renewed sliding presents rotational and flow type failure characteristics with a total run-out distance of 24 m.



Fig. 2. 17. Field view of 2008 reactivation of the Bonjo slide; a) slicken slide at the head wall; c) detailed view slide debris; d) view of the 2008 reactivation of the 2005 Bonjo slide a week after slide reactivation. e) View of the July–August 2008 slide (photograph taken in November 2008). Note the backward migration of the head scarp and the degree of re-vegetation of slide debris three months after reactivation.

For this reason, the slide can be characterised as a complex slide according to the classification scheme of Cruden & Varnes (1996). With the paving of the Limbe - Man 'O' War Bay road at the end of 2009, a retaining wall was constructed across the slide. Construction works exposed well developed sections of the soil profile (Fig. 2.18).

From the exposed section, it is observed that rocks that make up the slope are intensely fractured, weathered and show heterogeneous weathering patterns. Thickness of the soil layer around the Bonjo area measures over 10 m and is underlain by purplish saprolites.



Fig. 2. 18. Profile of Bonjo slide exposed by road construction in 2009. Pale yellowish soil occurs on purplish saprolite. Note the presence of fractures, weathering heterogeneity and thickness of soil column.

2.6.3 Makuka debris slide

On the same day, the 27th of June 2001, several slides occurred on slopes in Makuka, a quarter in Limbe. One of these slides is described here in detail. The debris slide occurred on a 26° natural slope developed on weathered basaltic flow within a secondary forest, characterized by the presence of fruit trees located away from built-up areas. The depletion zone or zone of rupture has a width of 55 m, a length of 52 m and a scarp height of 3 m, giving area coverage of $2.8 \times 10^3 \text{ m}^2$ and a volume of $7.6 \times 10^2 \text{ m}^3$. The slide debris is composed of a jumbled mixture of dark porphyritic basaltic rock fragments and clayey soils. These fragments are an admixture of rounded, sub-angular and angular, partially or completely weathered, blocks that range in size from a few mm to over 1 m across. The phenocryst assemblage is made up of shiny black, brownish (pyroxene), greenish (olivine) and whitish minerals (plagioclase) with crystal sizes that range from a few mm to over 2 cm in diameter. The pyroxenes in particular appear to be the most dominant phenocrysts in hand specimen. The scarp and margins are sharp and the eastern margin is characterized by the presence of 3 curved successive concentric tension cracks. The slide terminates along a stream channel flowing on jointed, dense, porphyritic basalts. These joints have diverse orientations, dominantly between N30°–N60° and N120°–N150°E. The orientation of measured fractures is shown in Figure 2.19.

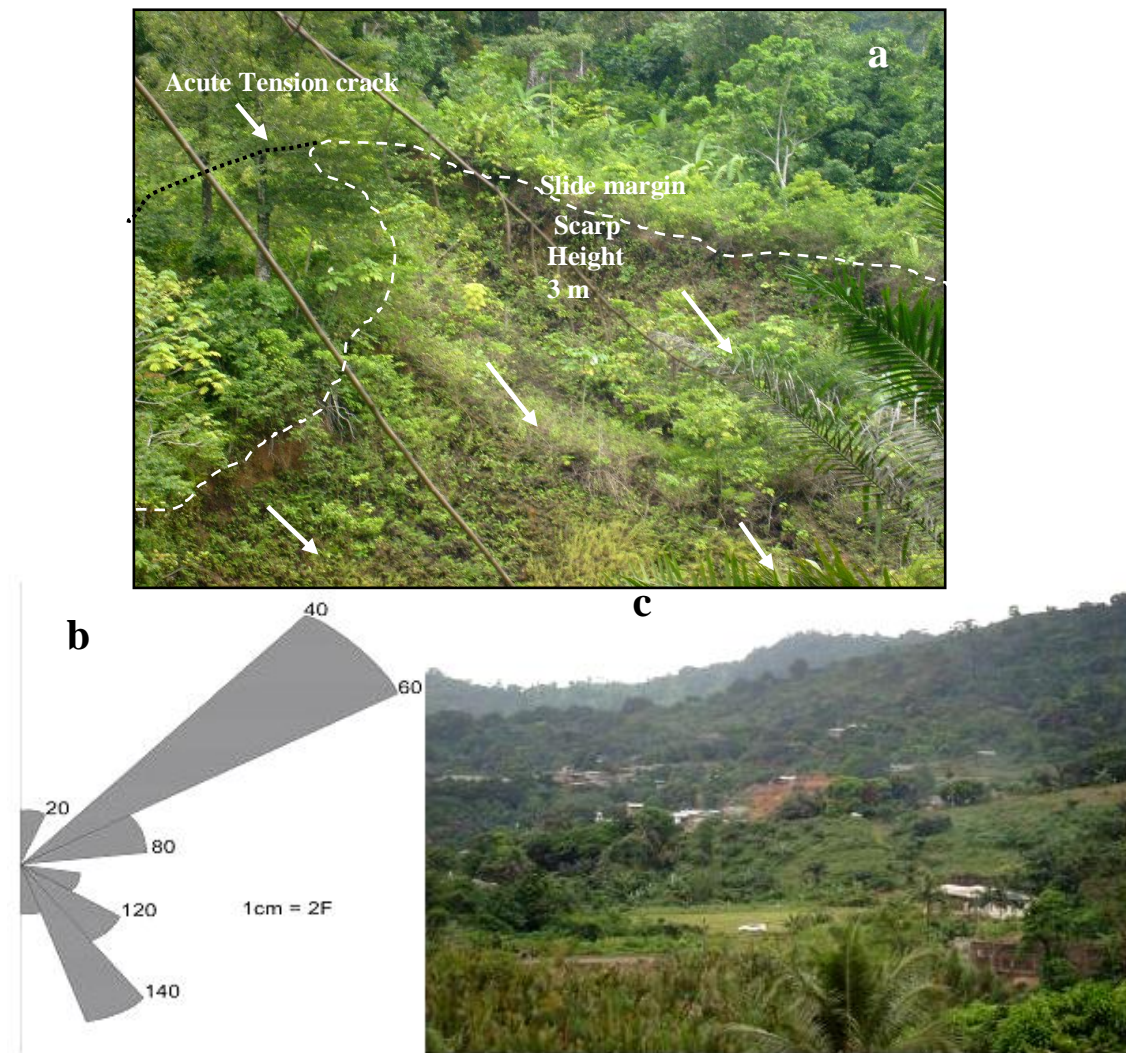


Fig. 2. 19. a) Field view of translational slide at Makuka with scarp height, outline of slide indicated by dotted lines and direction of movement indicated by white arrows. Note difference in stage of vegetation within slide scar and the neighbouring slopes; b) rose diagram for fracture patterns observed and measured in the field. The main fracture pattern is NE-SW; c) characteristic land use pattern in the Makuka area viewed from the Bonjo area west of Makuka.

At the time of observation, debris was still visible within the stream channels although some had been washed away by the stream. The scar was cover with grass and fern plants. Evidence of slope undercutting and material erosion was observed, indicating that stream undercutting played a role in the occurrence of the landslide.

2.6.4 Debris slide at Unity Quarters

On June 29-30th, 2009, three debris slides were reported at Unity quarters, a small locality within the Limbe municipality. All three slides were shallow and translational in nature. Generally, the slides were small with widths ranging from 4 to 9 m, lengths from 7 to 10 m and cumulatively generated debris of 90 m³. One of these slides (Fig. 2.20), though small (9 x 1 x 6 m), caused the collapse of the wall of a house, which killed two children in their sleep and injured their mother. The cost of repairs was evaluated at ca. 4 million FCFA (ca. 6000 Euros, i.e. equivalent to the yearly incomes of about 5 subsistence agric farmers in the area). This illustrates the high human and economic impact of the small-size landslides, especially on less well off and vulnerable people. The local population acknowledges that these slides took them by surprise and cited anarchical construction as the main cause of the failure. The slides occurred on 63 - 64° artificial slopes that range from 5 to over 10 m in height created by the excavation of slope material for construction purposes. These slopes are made up of loose, partially weathered pyroclastic materials with partial or no stabilization measures implemented (Fig 2.20). The debris slides were associated with torrential rains. Eyewitnesses reported that the rains were so heavy that the distress cries of the victims were not heard by neighbours only 10 m away. 400 mm of rain in one day was recorded at Krater located ca. 3 km away. From field observations made two weeks after the event and from eyewitness reports, anarchical construction on steep slopes and slope excavation are possibly the main conditioning factors. Figure 2.21 represents typical land use patterns observed at Unity quarter.



Fig. 2. 20. June 29th, 2009 slide at Unity quarters, looking west. Note the presence of an uncompleted retaining wall west of the scar and steep slope created by material excavation for construction.

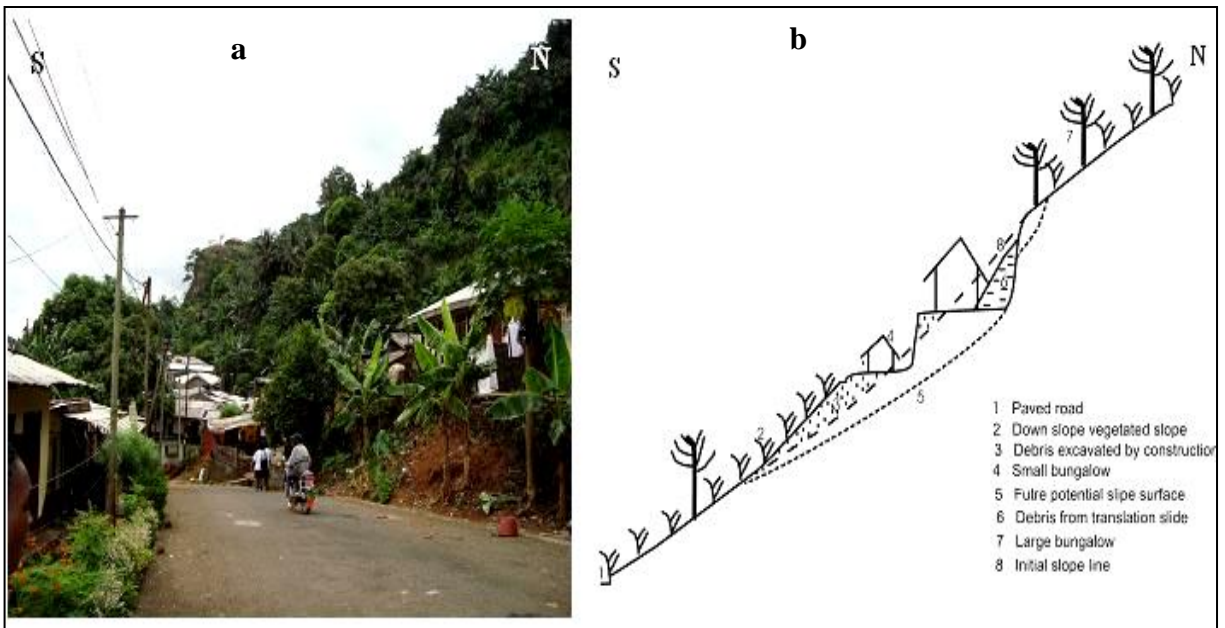


Fig. 2. 21. Typical land use patterns observed at Unity Quarter. Note the steep slope and anarchical construction and irregular terracing; b) sketch of land use patterns, not drawn to scale

2.6.5 Earth slide at Moliwe

Two shallow translational slides on weathered basaltic rocks were reported at Moliwe, ca. 7 km NE of Unity Quarter on the night of June 29-30th, 2009 (Fig. 2.22a).

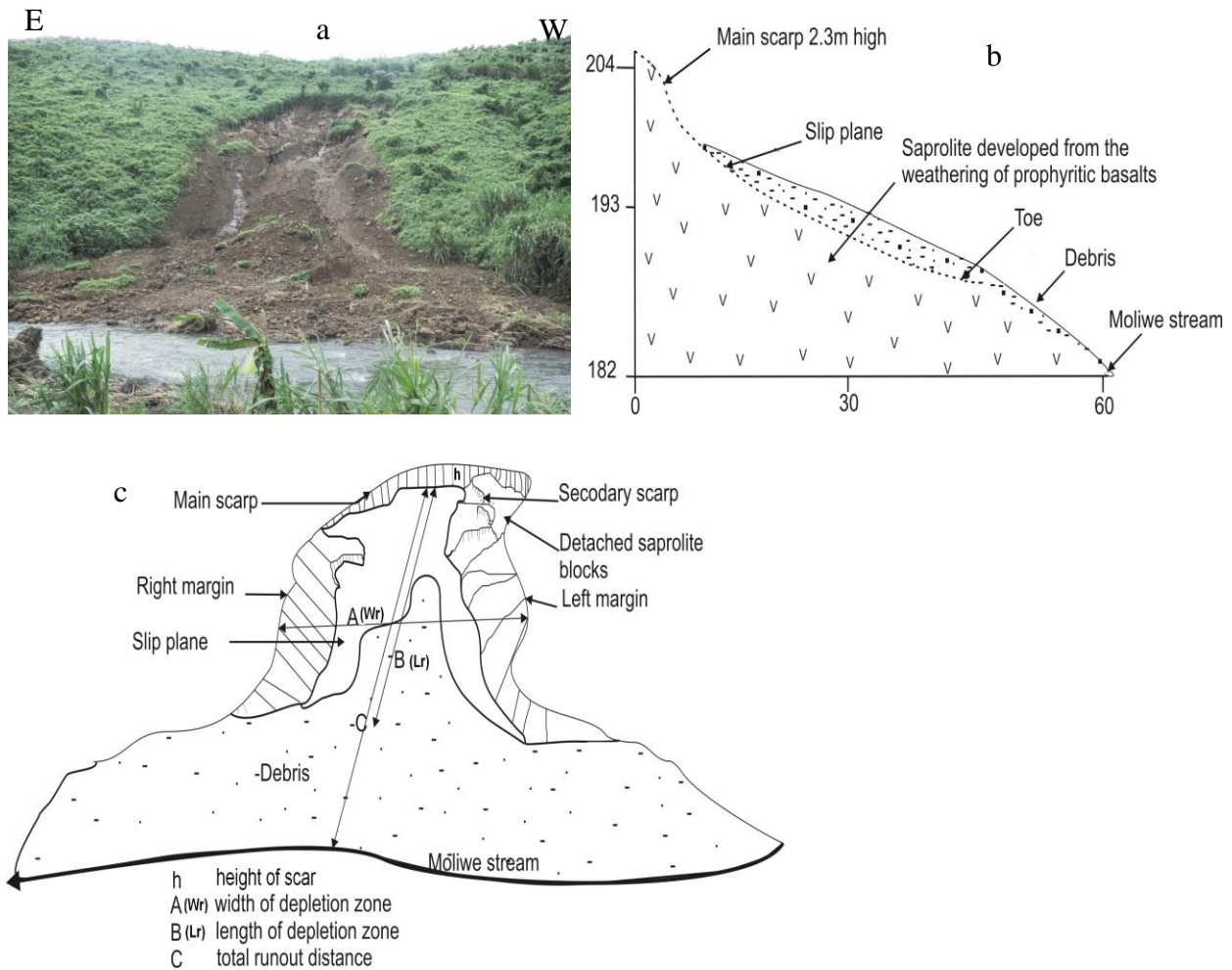


Fig. 2. 22. a) Photograph; b) transverse section and c) plan view of the 2009 Moliwe landslide.

This site was initially occupied by oil palm plantations, which were cut down in April 2009 to prepare the land parcel for replanting of new palms. At the time of observation, the area was covered with climbers (cover crop) only and lacked trees. According to the classification of Cruden & Varnes (1996), the slides are earth slides involving colluvial soil developed from the weathering of basaltic lava flows. The studied slide is 21 m wide and 62 m long, with total run-out of 83 m. The slide was initiated on a 26° slope and has a scarp height of 2.3 m. The failure plane lies along the soil/saprolite boundary. The area of the rupture zone is ca. 1.3×10^3 m²,

whereas the entire slide (rupture and accumulation zone) covered ca. $1.7 \times 10^3 \text{ m}^2$. The estimated volume of material that slid is $1.5 \times 10^3 \text{ m}^3$. The debris formed a wide lobe that terminated in the Moliwe stream (Fig. 2.22a and b). Both earth slides, located ca. 100 m from each other, terminated in the Moliwe stream. Significant evidence of flooding was observed (i.e. bent vegetation and deposited debris indicating that the stream occupied more space than its normal flow channel). Rainfall data from Moliwe show that 64 mm was recorded on the day the landslide occurred and a total of 308 mm of rain fell in the vicinity in the 7 days preceding the event. These slides did not cause any significant damage but illustrate that deforestation and stream undercutting are important predisposing factors for the occurrence of slides.

2.6.6 Earth slide at Kie Village (Ngeme)

At ca. 3 pm on August 6th, 2009, an earth slide occurred at Kie Village (Fig. 2.23).

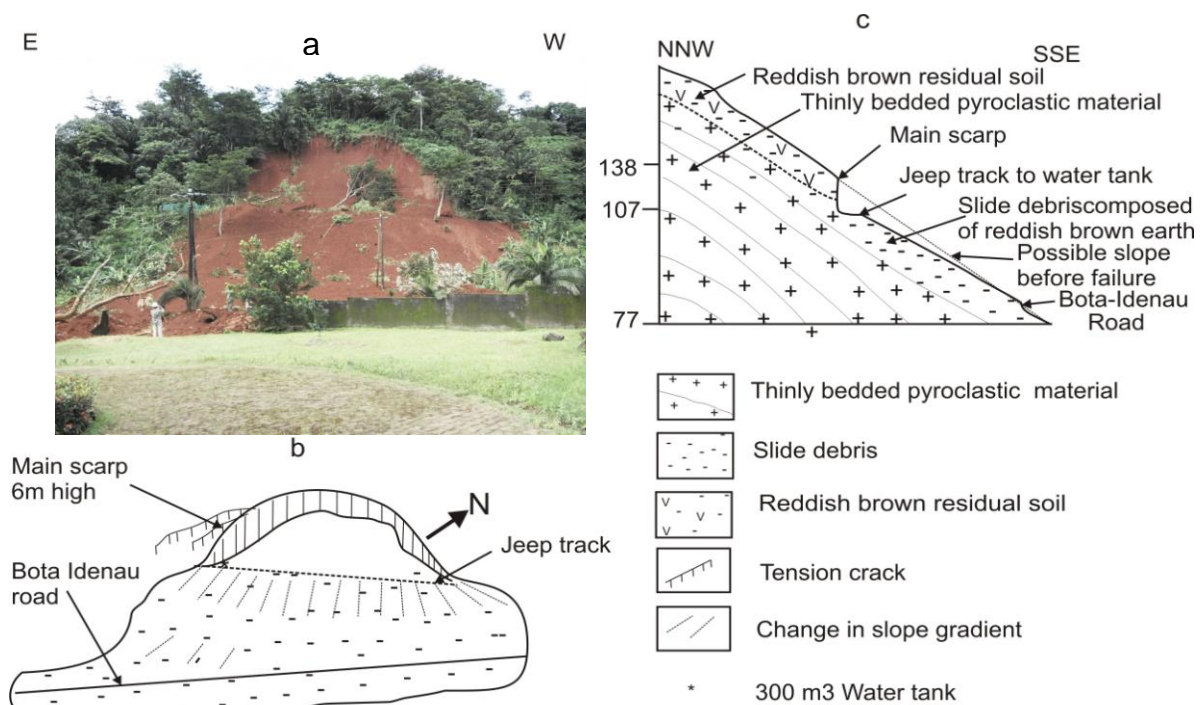


Fig. 2. 23. Photograph of the August 6th, 2009 rotational slide at Kie Village developed within colluvial soils on thinly layered pyroclastic materials; b) plan view; c) longitudinal section through the slide. The slip surface lies at the soil/pyroclastic boundary.

The slide is a rotational earth slide that initiated on a 34° slope. It involves the movement of reddish brown colluvial soils developed from the weathering of thinly bedded pyroclastic material. The thickness of the soil layer observed at the head scar is over 7 m. The head scarp is

characterized by the presence of nearly vertical head walls ca. 6 m high. The slide geometry measures 53 m, 36 m, and 6 m for the depletion zone's width, length, and height, respectively.

Total run-out was 138 m. Approximately $6 \times 10^3 \text{ m}^3$ of soil was moved by the sliding process covering a total area of $7.3 \times 10^3 \text{ m}^2$ with the rupture zone making up $1.9 \times 10^2 \text{ m}^2$ of this total area. The left margin of the scarp shows the presence of acute tension cracks with a 0.5 m displacement of the downthrown block. This slide formed a wide lobe in the SSE direction that blocked the road linking Bota and Idenau, partially buried a 300 m^3 water tank that supplies potable water to local residents, injured one person and partially buried his car (Fig. 2.24), and interrupted electricity supply for about two days.



Fig. 2. 24. Typical landslide damage at Kie village; A, B) house destroyed by debris from the 2009 slide at Kie; C) road blocked and vehicle partially buried by slide debris.

Eyewitnesses reported an increase in the amount of soil washed away by runoff and anomalous muddy runoff at the base of the slope a few hours before sliding, indicating incipient failure prior to the major collapse. They also reported that movement was rapid and came in two batches, the second one occurring ~10 minutes after the first one. During field visits to the site prior to the

collapse, the slope was observed to have been cut to construct a dirt track to the water tank that was partially buried by the slide. In addition, pozzolan (siliceous volcanic ash) excavation was initiated along the dirt track, cut into the pyroclastic cone in April 2009 producing an 8 - 12 m high near-vertical wall. On August 5th and 6th, 2009, ca. 145 and 65 mm of rain, respectively, were recorded at the Krater rain gauge station, located only 400 m away from the slide location. A total of 568 mm of rain was recorded in the 7 days preceding the event. Weathering, slope undercutting to construct a road to the water tank, and the excavation of pozzolan could be the conditioning factors here. The threat possessed by this slide is enormous considering that there are 2 tanks each holding 300 m³ of water within its vicinity. If these had actually broken the water would have mixed with the earth to produce mudflows with more severe consequences.

2.7 Internal morphology of the landslide scars

In most of the observed scars, channel morphometry is shallow and narrow with the depletion/rupture zone either devoid or partially covered by a thin veneer of debris. Nowhere was bedrock exposed. Ridges (approximately 2 m wide and 30 to 90 cm high; Fig. 2.5) were observed within the scars at Makuka, Mondoli and the Mabeta (Fig 2.14) areas probably derived from differential erosion and transportation of debris in the rupture zone by runoff. Furthermore, onion skin weathering was the dominant type of weathering that characterized the scar head and margins with core stones present at the centre of these weathered blocks (Fig. 2.25).



Fig. 2. 25. Spheroidal or onion skin weathering at head scarp. Note the presence of core stone exposed by the 2008 reactivation of the Makuka slide. Blocks are about 5cm in diameter and porphyritic with olivine, pyroxene and plagioclase phenocrysts. The blocks also show a kind of jigsaw fracturing.

2.8 Landslide triggering factors.

Previous research on landslides suggest that melt water, heavy rains and/or earthquake activities are the major triggers of landslides (Guzzetti *et al.*, 2005) though others may occur without any particular trigger. To effectively minimize losses that can result from landslides, it is necessary to understand the triggering factors, their occurrence probability and return periods. These parameters are necessary requirements in the design and implementation of effective early-warning systems.

Considering that the study area lies in a tropical environment and is volcanically active, earthquakes and rainfall are thus the most plausible triggers. Triggers in landslide studies refers to a process or phenomenon that actually initiates failure. The seismicity of this region is monitored by the Unit for Volcanological and Geophysical Research Centre (ARGV) located at Ekona (located out of the study area). According to Ateba *et al.* (2009) normal seismicity in this area is characterised by 1-3 low magnitude events per day that might not even be felt at the epicentre (Aka 2001). Ateba *et al.* (2009) noted an increase in seismic activity between May to mid September following the 2000 eruption. The number of daily event returned to normal after September 2000. According to Aka (2001) in Buh (2009) the month of June 2001 was characterized by 0–8 low-magnitude seismic events/day, and there was no observed increase prior to or after the 27th of June 2001, suggesting that seismicity was not a significance triggering factor of the slide occurrence (Buh 2009). Thus, the importance of seismic activities as a trigger is not evaluated in this study given most of the recorded slides occurred in 2001.

Rainfall has been internationally recognized as one of the major triggering factors of landslides (Glade, 2000). In the Limbe area, the relationship between landslide and rainfall is known from empirical observation during landslide events and eyewitness accounts. However, this relationship has not been quantified to identify the approximate rainfall threshold required initiate failure. Incomplete (or absence of) landslide inventory and inaccuracy in recorded dates and time of slide occurrence make it difficult to quantify rainfall thresholds or sequence that lead to landslides. A threshold refers to the minimum or maximum value of some quantity required for a process to take place or for a state to change (White *et al.*, 1996). Minimum threshold refers to a value below, which a phenomenon will never occur and a maximum refers to that above which the phenomenon must occur. Several attempts have been made (Lumb, 1975; Caine, 1980;

Brand, 1984; Montgomery & Dietrich, 1994; Hengxing *et al.*, 2003; Jakob & Weatherly, 2003; Guzzetti *et al.*, 2007 and other references therein) at various scales to determine the amount of precipitation and its duration required to trigger slope failures. Most of these threshold values are based on empirical or statistical analytical relations between rainfall and landslide initiation. This is probably because the actual relationships existing between rainfall and the occurrence of landslides are poorly understood. Review of literature indicates that there are no standard measurements to characterise rainfall conditions that will or will not trigger slope failure. Reasonably reliable prediction of landslide occurrences based on climatic thresholds has been accomplished in Japan, New Zealand, the United States, Portugal, Italy (Mateos *et al.*, 2007) and in San Francisco Bay (Barb, 1991) where real-time monitoring of rainfall, precipitation forecast and delineated areas susceptible to landslides and debris flows were used to construct an early warning-system. This implies that effective rainfall recording at high temporal resolution and systematic recording of landslide occurrence can be effectively used to predict slope failures and thus minimise human and material losses.

The relationship between landslides and rainfall have generally used mean annual rainfall totals (Glade *et al.*, 2000) and antecedent rainfall. Antecedent rainfall refers to the cumulative amount of rain an area has received within a specific time period. Antecedent rainfall and antecedent soil moisture conditions have been shown to be important in the localisation of rain triggered slides (Campbell, 1975).

To define a possible thresholds, daily rainfall from the four stations described in Table 1.2. and 5 recorded landslide events that resulted in a slide or landslide swarms in different parts of the study area were used (Table 2.5). The effects of a 30 days, 3 days and 24 hrs antecedent rainfall on these 5 rainfall events were evaluated to determine their impacts on the occurrence of landslides.

It is worth noting that the daily rainfall measurement by the CDC is manually operated, thus 24 hours in total represent the 24 hours prior to 9 am on the day of recording. The consequence is that about 62.5 % of the recording time attributed to a given day occurs on the previous day, which introduces a 9 to 15-hours lag when defining rainfall values.

Location of landslide	Date of occurrence	Location of closest rain station	Measured rainfall amount (mm)	Rainfall before slide	No of slides
Mabeta New Layout	27 June 2001	Krater	40	180	43
Bonjo	21 June 2005	Krater	120	60	1
Bonduma	18 June 2006	Esuke	134	79.9	1
Unity Quarter	29-30 June 2009	Krater	81	400	3
Moliwe	29-30 June 2009	Moliwe	55	8.9	2
Krater (Ngeme)	6 -August 2001	Krater	66	145	1

Table 2. 5. Observed landslides with corresponding rainfall values recorded in 24 hours at the gauge nearest to the slide location.

On the other hand, the automatic gauges have an in-built clock that automatically resets and stores data on 24-hours basis. Precipitations in the Limbe area occur in the form of light (< 10 mm/day) to heavy rains (> 50 mm/day) typically associated with spatially localized rainstorms. These storms vary in duration from a few minutes to over four days in a row. On a daily basis, rainstorms produce huge precipitation gradients around MC with significantly different amounts of rainfall recorded in locations located ~ 5 km apart. It is therefore likely that the amount of rain at any location could be higher or lower than that recorded at the closest rain station. Because of these variation, in this study, a 5 km buffer zones was constructed around each slide; the highest daily rainfall recorded from stations located within the 5 km buffer zone or data for the closest rain gauge if located less than 1 km from the observed landslide is used to represent the total rainfall that resulted in sliding.

Figure 2. 26 represents 30 days daily and cumulative rainfall prior to failure.

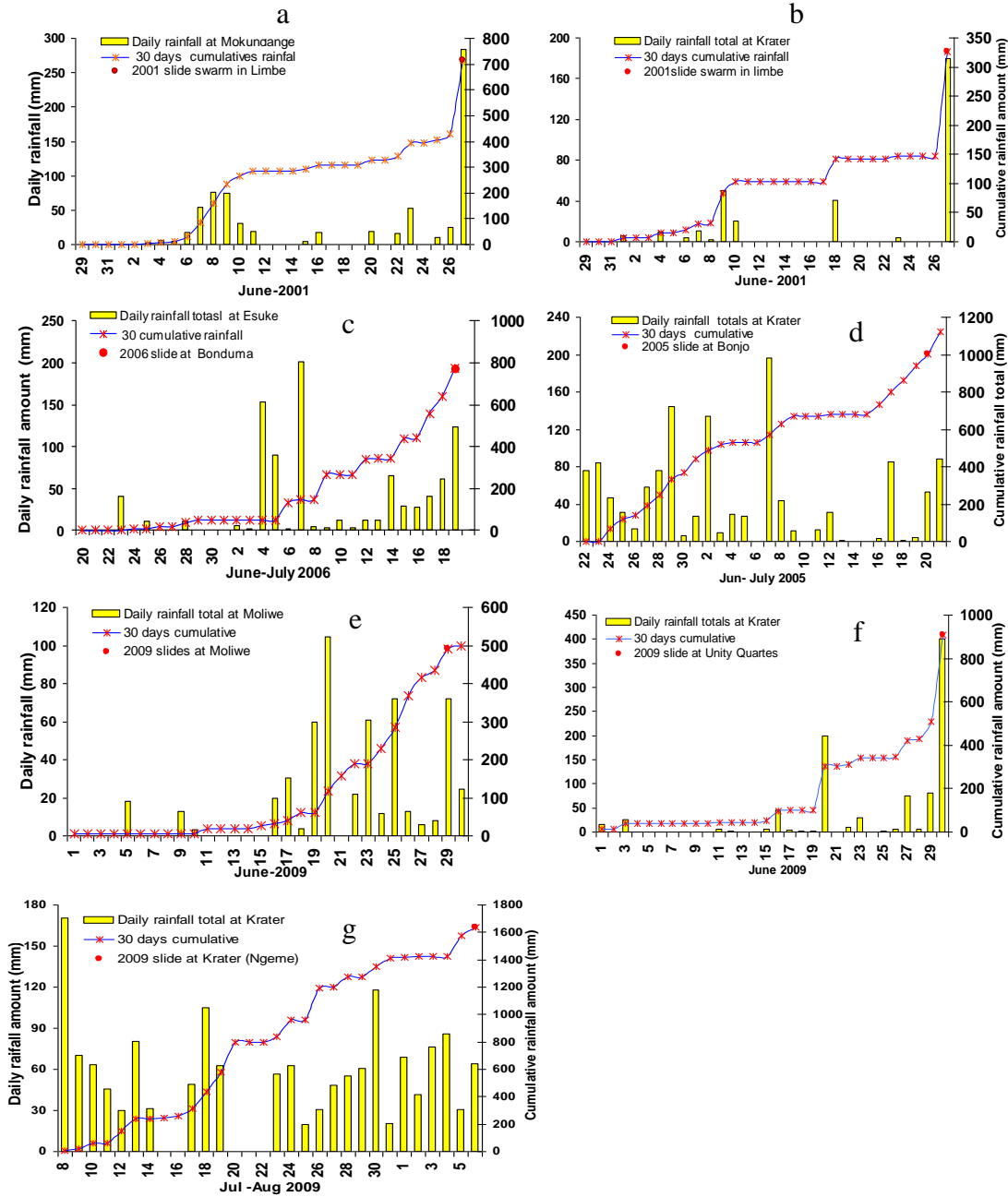


Fig. 2. 26 30-day cumulative rainfall and daily totals at recorded the closest station for five recorded landslide events in Limbe. Red dots represent days with recorded landslides.

The graphs demonstrate that a wide range of 30 days of cumulative rainfall end up in failure suggesting that 30 days cumulative rainfall is not a good predictor of landslide triggering events. With the daily rainfall, some patterns can be identified (Fig. 2. 26). Some of the landslides are associated with extreme rain event (> 110 mm) recorded after 2 - 3 days of very little or no rain

as observed by sharp break on the cumulative curve (Fig. 2.26a, b, d, f). Others occur after prolonged lower intensity rains of ~ 60 mm/day for 5 days in a row (Fig. 2. 26c, e, and g). It is worth noting too that there are days with even higher rainfall amounts that did not trigger landslides or landslides were not recorded. For example, about 170 mm measured at Krater on July 8, 2009, 110 mm at Moliwe on the 20th of June 2009 and 210 mm at Esuke Benoue on July 8, 2006 (Fig 2. 26) but were not associated with slide occurrences.

Using 3-days antecedent rainfall, a threshold of 210 mm can be defined. Figure 2.27 demonstrates that 3-day cumulative rainfall amounts >210 mm are not frequent. Four of the landslides events were triggered after 210 mm of antecedent rain and one with a 3 days cumulative rainfall of less than 100 mm.

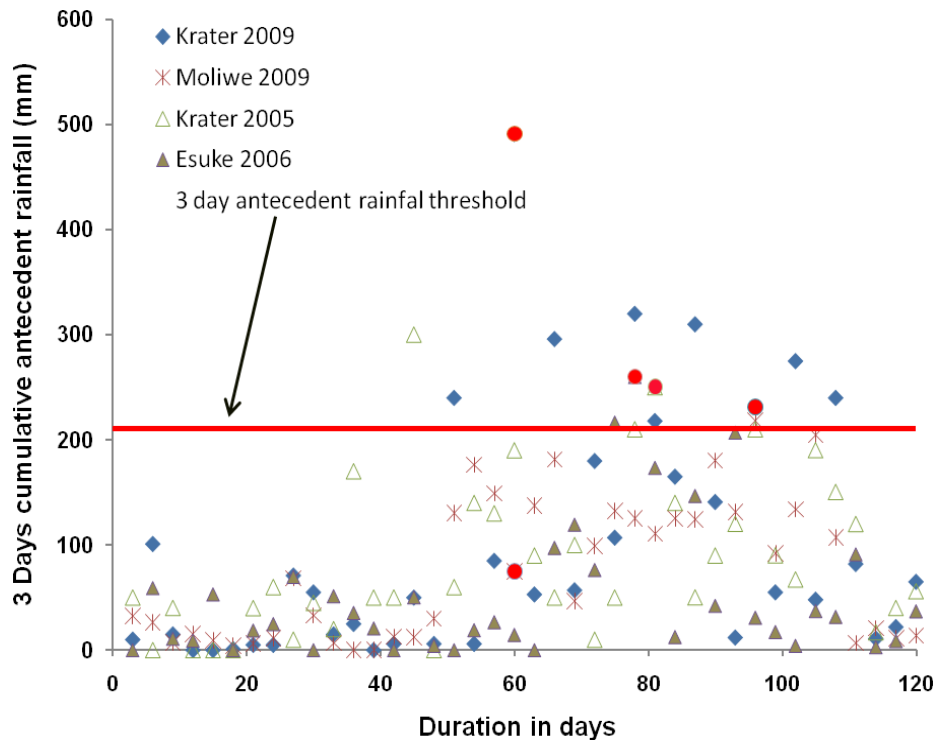


Fig. 2. 27. Period of 3- days antecedent rainfall recorded within the study area for the months of May to August in 2001, 2005, 2006 and 2009 with documented landslide events. Red dots represent landslide occurrences.

The 210 mm interval is therefore proposed as the minimum three day antecedent rainfall threshold for the initiation of some slides. As shown on the graph, periods with 3-day antecedent rainfall higher than the threshold and not associated failure are also observed. Thus, more

analysis with more landslide triggering events and detail rainfall measurements are required to better constrain this value.

2.9 Discussion

The temporal frequency of landslide events can be established from archive inventories (Coe *et al.*, 2000; Guzzetti *et al.*, 2003) and from multi-temporal landslide maps (Guzzetti *et al.*, 2005). This study presents an accurate inventory of slides observed in the study area. It provides data on the location and geometric characteristics of landslides that can be used in the future to update landslide inventory maps from which exceedence and recurrence can be calculated. Landslide statistics indicate that large landslides in the study area are rare. Like other areas in the world like Hongkong, Turkey and Italy, most of the recorded landslides in Limbe are human induced and rain triggered though contributions from natural processes also play an important role.

The geometry of the slide depletion zones vary widely throughout the study area. This result is similar to that observed by Knapen *et al.* (2006) on the foot slopes of Mt Elgon in Uganda. However the volume of generated debris in the Limbe area is dependent on the length and width of the depletion zone rather than on the depth as noted by Knapen *et al.* (2006). There are no standard measuring tools to evaluate the magnitude or impact of individual landslides. Fell (1994) used landslide volume as a measure of magnitude while others use frequency/size distribution (area and volume) (Hovius *et al.*, 1997; Malumad, 2004). In this study, it was noted that the severity/magnitude/nature of landslide related material and economic losses is not proportional to landslide geometry/type, but is closely linked to the location of the slide with respect to human infrastructure. For example a small 9 x 1 x 6 m³ slide at Unity Quarter resulted in the loss of two lives and property damage estimated at ca. 4 million FCFA (ca. 6000 Euros) whereas a 21 x 2.3 x 62 m³ slide at Moliwe resulted in severe local environmental damage but did not lead to any casualty or property damage because these areas are sparsely populated.

Systematic trends are highlighted when landslide volume or area in a data base is plotted on a semi-logarithmic scale, after ranking the slides from the smallest to the largest. This pattern can be used to evaluate the completeness of the landslide inventory. On such a graph, only the smallest and largest slides are offset from this general trend, suggesting a non-exhaustive documentation of the smallest and largest slides or might mean a change in the sliding processes

that produce these types of slides. This semi-logarithmic relationship between the cumulative frequency and the volume of the slide is of great interest because they can be used to assess the probability of occurrence of slides of large volume in the future. A similar relationship is obtained from geometrical datasets for other landslides in New Zealand, Italy, Guatemala and the USA (Hovius *et al.*, 1997; Malamud, 2004; Brunetti *et al.*, 2009).

Slope gradients at which slides developed on pyroclastic material are generally steeper than those on the weathered lava flows, ranging from 32° - 45° on natural slopes, and can go well beyond 63° for slopes with human intervention. Slides on basaltic lava flow deposits initiate at lower slope angles (22° - 36°) except in areas where steep slopes are generated as a result of road and/or building construction. The width and depth of failure does not vary with parent rock type.

The slip surface in most of the slides in this area is not controlled by a saprolite – fresh rock boundary as noted in other studies (Wen *et al.*, 2007), but occurs within the saprolite or at the soil – saprolite boundary. This is probably a result of heterogeneity imposed by weathering as reported by Ngole *et al.* (2007) for the Mabeta area or as a result of the generation of positive pore pressure enhanced by fracture permeability. Larsen & Simmons (1999) noted that high intensity short duration rain results in the occurrence of shallow translational slides with the slip surface located within saprolites or at the soil-saprolite boundary due to the development of excess pore pressure. Deep soils and underlying saprolite result from intense and prolonged weathering governed by voluminous rainfall and high mean annual temperatures of approximately 26 °C.

The Poisson model used to investigate the temporal occurrence of natural hazards allows for determining the probability of future occurrences for different times t (i.e. for a different number of years) based on the statistics of past landslide events assuming that (i) the number of events that occur in disjoint time intervals are independent; (ii) the probability of an event occurring in a very short time is proportional to the length of the time interval; (iii) the probability of more than one event in a short time interval is negligible; (iv) the probability distribution of the number of events is the same for all time intervals of fixed length, and (v) the mean recurrence of events will remain the same in the future as it was observed in the past. These assumptions may not

always hold for landslide events: the interpretation of landslide exceedence probability should be treated with caution when results are derived from a Poisson probability model.

2.9.1 Causal factors

Landslides in the Limbe area are caused by a combination of factors. The presences of steep slopes, anarchical construction, and rock type are observed to be the major causes of failure in this area. In the study area, particularly at Unity Quarter, Bonjo and Mabeta, the construction of houses, roads and foot paths involves the excavation of soil and the creation of small terraces. This removal causes water stagnation on the flattened areas and increased infiltration as well as changes the slope line and the angle of repose of particles located upslope, thereby increasing the amount of stress on these slope materials. The excavated soil in most cases is piled on the down slope end of individual land parcels so that with intense rain, the loose soil rapidly absorbs water, becomes saturated and slides causing damage to down slope located structures. Furthermore, high mean annual precipitation ranging from 2100 to 4600 mm (CDC Meteorological Centre) concentrated in 3 months of an 8 month rainy season, results in high soil moisture contents and soil saturation for long periods of the year and this can be considered as one of the causal factors for landslides.

2.9.2 Triggering factors

Analysis of 20 - 34 years of monthly rainfall data suggest that landslide activities in Limbe are associated with extreme rainfall events. A threshold for the initiation of slides is however difficult to define because of high spatio-temporal variations in intensity and duration of rainfall within the area, and because of the absence of records of the exact date and time for most of the landslides. Hence, the link between landslides and specific rainfall events cannot be precisely defined.

However, most of the slides with known dates suggest that they are associated with rainfall > 110 mm in 24 hours preceded by 2 - 4 days with no or limited rainfall (0 - 4 mm). Other heavy rainfall events, with daily rain amounts > 110 mm and as great as 250 mm particularly preceded by days with more intense rains, are however not associated with landslide events. Lumb (1975) suggested a relationship between the preceding 15 days and 24 h total rainfall and landslide

occurrence. However, Brand *et al.* (1984) argue that in most tropical residual soils, antecedent rainfall is not a controlling factor in slide initiation. Instead, it seems reasonable to assume that the likelihood of landslide occurrence is enhanced subsequent to periods of sustained rainfall. These observations are true for most of the landslides with known dates in the Limbe area. Nevertheless, a successful monitoring of small landslide hazards in the region requires a dense network of rainfall stations continuously recording rainfall intensity and duration. Such information needs to be available in real-time to scientists so as to enable them to define absolute rainfall events capable of triggering landslides.

According to Larsen & Simmons (1999), short-duration/high-intensity rainfalls usually result in the occurrence of shallow landslides caused by excessive pore pressure in shallow soil zone. These slides too tend to have their failure plane in saprolite or at the soil-saprolite boundary, which is typical for most of the 2001 landslides in the Limbe area. Low-intensity/long-duration rainfall instead results in the occurrence of deep seated failure with the slip surface occurring at the saprolite bedrock boundary. It is therefore possible that the 1-day 110-mm and the 3-days 210-mm threshold identified in this study is a proxy for rain triggered landslides in the study area, considering that they are mostly shallow translation slides with the slide surface commonly occurring at the soil-saprolite boundary where saturation and the development of positive pore pressure is possible after high intensity rainfall. However, the data set for landslide events used in this study is rather small to make statistically reasonable conclusion with regards rainfall threshold, thus a wider data set needs to be evaluated.

Buh (2009) analyzes seismic activities as possible triggers for the June 2001 landslides in Limbe and concludes that June 2001 was characterized by 0 - 8 low magnitude events/day. Thus because of the lack of increased seismicity before and/or on the 27th of June 2001, seismicity did not seem to have been a major triggering mechanism. It can thus be concluded that landslide occurrence within the study area is not linked to a single factor but occurs in response to an interplay of several preparatory factors with rainfall as a probable trigger. These results are similar to those reported by Kitutu *et al.* (2009) for the Bududa district, Eastern Uganda.

2.10 Conclusion

From field observations, eyewitness accounts and data interpretation, the following conclusions can be drawn from this field study:

- I. Landslides in Limbe are small to very small translational and/or rotational landslides with a mean width of 24 m. Large landslides ($> 10^4 \text{ m}^3$) are rare and might be triggered by other processes than intense rainfall. Importantly our observations highlight the lack of correlation between landslide size and their impact, which is mostly controlled by the proximity to vulnerable infrastructures and populations.
- II. Landslide occurrence in the Limbe region results from a combination of factors such as the presence of steep slopes, pyroclastic material, thick soil cover, or the proximity to stream channels. Landslides are especially frequent on old pyroclastic cones which have undergone significant weathering.
- III. Intense and prolonged rainfall ($> 110 \text{ mm}$ in 24 hours preceded by 2 - 4 days with no or limited rainfall (0 - 4 mm) act as the major trigger that initiate failure.
- IV. Slide occurrence is exacerbated by human interferences in the form of urban expansion, anarchical construction, slope excavation and deforestation. When deciding on the localization of new development projects, it is essential to pay attention to slope stability issues in order to mitigate potential losses due to landslides. In addition, construction works on steep slopes, especially on deeply weathered pyroclastic cones should be discouraged. If unavoidable, adequate retention walls, drainage paths and slope reinforcement measures should be implemented and maintained to limit damage resulting from sliding.

This study thus provides important new insights and quantitative constraints to be used in deterministic modelling of volume-limited slides. It will also serve as a basis to constrain a landslide susceptibility assessment based on the identified causative factors. It also provides data that can be subsequently used in the development and evaluation of slope instability mechanisms for particular sites considered at risk in the Limbe region of Cameroon, or other areas in a similar context where steep weathered volcanic terrains receive intense and prolonged rainfall in the subtropics worldwide.

Chapter Three

Geotechnical characteristics of landslide prone soils

3.1 Introduction

The occurrence of landslides in any area may be attributed to the geotechnical (Yalcin, 2007), mineralogical and chemical properties of the soils as well as forces acting on these materials. Ground conditions such as weak strength, sensitive fabric, degree of weathering and fracturing can be considered as some of the factors that influence slope stability. Sidle (1985) observed that soil properties such as particle size and pore distribution in the soil matrix can influence slope stability. These properties influence the rate of water movement and the capacity of the soil to retain water. Finer soils tend to hold higher volumes of water under unsaturated conditions than do their coarse textured equivalents (Sidle, 1985). Other soil parameters that contribute in landslide occurrence include the swelling properties of clay and the rate at which water infiltrates into the clay at depth (Inganga & Ucakuwun, 2001). Clays play an important role in slope instability problems because of their plasticity, low permeability, structure, chemistry and mineralogy, moisture dependence of shear strength and above all volume change after water absorption or dehydration.

Thus, after detailed field observations and measurements of the geometric characteristics of the landslide scars, it is necessary to evaluate the properties of these landslide prone soils, in order to understand the sliding mechanisms operating within the study area. Mechanisms of slope movements as defined by Hutchinson (1988) are idealized ways through which slope material might move. Sliding mechanisms depend on geometric, physical and mechanical properties of weathered profiles (particle size, pore pressure, cohesion, effective angle of internal friction, soil thickness, slope angle, bulk density), the transient properties (natural water content, degree of saturation) and the mineralogical composition of the soils. They are also affected by external factors such as human intervention, rainfall and seismic activities. To achieve this, three slide scars were chosen and studied in detail. The choice of these scars was based on accessibility, type and/or mode of failure, observed/reported damage incurred and on the material type involved in the sliding process to cover all slide types observed in the study area.

Figure 3.1 shows the distribution of the pits described in this study.

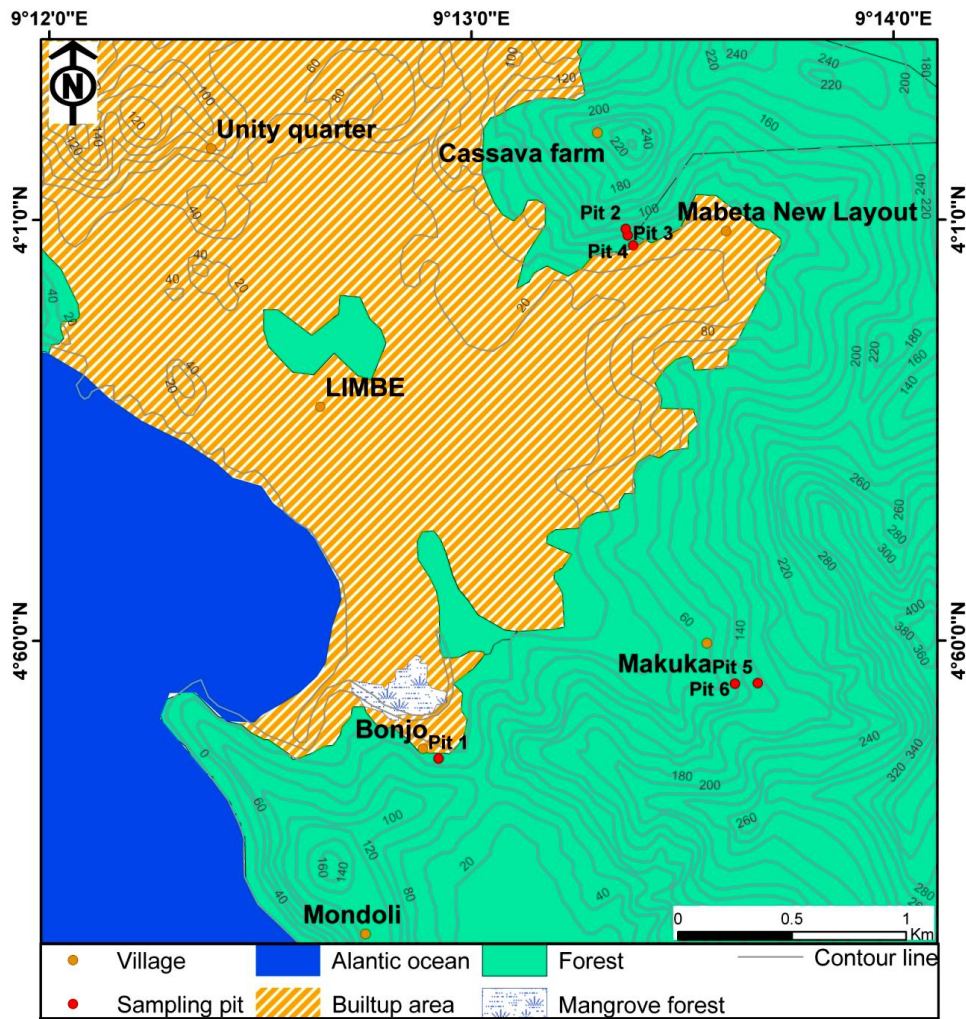


Fig. 3. 1 Location of sampling pits dug into 3 landslide scars analysed in detail during this study.

Six 2.5 to 4 m deep rectangular (1 x 1.5 m) pits (Fig. 3.1) were dug into three landslide scars and their profile described. In situ shear tests were also realised by driving a Torvane meter into the sides of the pit and rotating it until failure. The corresponding torque is read off the vane meter and later converted to shear strength values, providing the in situ apparent cohesion. These undrained field tests were undertaken as a preliminary assessment to determine the degree of vertical and spatial variation in shear strength properties. Measurements were done at 20 cm interval up to a depth of 1.2 m and at intervals of 40 cm after 1.2 m. Figures 3.2a and b show the geometric configuration of Pit 1 and how shear strength was measured with the Torvane meter.



Fig. 3. 2. View of geometric configuration of Pit 1 dug into a slides scar at Bonjo: a) digging pits; b) in situ measurement of relative shear strength with a Torvane meter.

18 block samples (20 x 15 x 10 cm), 3 from each pit, were collected by the channel chipping method (Fig. 3.2) with the exception of Pit 5 (where digging was inhibited by its stony nature and thus only two samples were collected) and Pit 6 (that displayed many more horizons and 4 samples were collected). The samples were wrapped tightly in plastic bags, labelled and transported to the laboratory for the determination of their geotechnical properties, as well as for mineralogical and chemical characterization.



Fig. 3. 3. Collecting block samples for laboratory analysis from the wall of a pit sunk at Bonjo. Note sharp the colour transition on the walls of the pit.

Sample labels contain two parts, e.g. in the sample P1S01, P1 represents the pit number 1 and S01 represents sample number 01. Sampling was done in March of 2009, which marks the end of

the dry season in this area. Thus, measured natural moisture content (measured without any form of drying) provides a genuine or vivid picture of the soil moisture content within the study area. Geotechnical characterization of the soils was done at the “Laboratoire de Mécanique des Sols” in the Department of Building, Architecture and Town Planning of the Université Libre de Bruxelles.

3.2 Equipment, sample preparation and analysis

Some of the equipment used in the laboratory is presented below (Fig. 3.3).

3.3 Methods used in the determination of index and physical properties

The index properties of the soils evaluated in this study include:

- Colour with the aid of a Munsell soil colour classification chart
- Natural moisture content
- Loss on ignition
- Atterberg’s (consistency) limits
- Grain size distribution
- Bulk density
- Particle specific gravity
- Shear strength (cohesion and effective angle of internal friction)
- Permeability

3.3.1 Colour of soils

The colour characteristic of each horizon was obtained from the Munsell Soil Classification Chart. Samples were aerated for 24 hrs. Using a spatula, aggregates of soil samples were mounted on white cardboard paper. The colour was obtained by matching the soil sample with the standard colour on the Munsell chart from which the colour was read off and given in terms of the hue, value and chroma. Results of the colour characterisation are integrated in the next chapter. Soil colour is an important property used in the identification of soils.



Fig. 3. 4. Catalogue of the laboratory equipment used for sample analysis: a) electronic balance used to determine sample bulk density; b) hydrometer; c) sieves and mechanical sieve shaker used for separating particles into different fractions; d) magnetic stirrer; e) 1 litre sample solution in a water bath for measuring the silt and clay fractions within each sample through sedimentometry; f) Casagrande apparatus used in the determination of liquid limits; g) shrinkage dish for linear shrinkage measurements; h) petrologic microscope; i) agate ball mill; j) external view; k) internal view of agate ball mill used for the preparation of sample powders for ICP-OES analysis; l) pressure chamber with pycnometer used for the determination of the specific gravity of the solid particles; m) three automated triaxial cells.

3.3.2 Determination of natural moisture content

Moisture content, affects the weight and the behaviour of soil particularly the clay fraction. The natural moisture content (M_c) was determined according to the procedure described by Van Reeuwijk (1993). About 50 g of sampled material (as collected without any form of drying) is weighed in air (W_b), oven dried at 110 °C for 24 hours and reweighed (W_a). The following equation was used to determine the moisture content in %:

$$M_c = \left(\frac{W_b - W_a}{W_a} \right) \times 100$$

3.3.3 Loss on ignition (LOI)

After the M_c was determined, 10 g of the sample was extracted and heated in a muffle type furnace for 2 hr at 550 °C and the difference in weight before and after firing considered as the LOI. This is also equated to the amount of organic matter present.

3.3.4 Determination of Atterberg's Limits

Atterberg's limits (liquid, plastic and shrinkage limits) are a standard measure of the consistency of fine-grained soils depending on its moisture content. These limits are used to determine the plasticity index, which provides a clue to the type of mass movement (flow or slide) that would characterise a given area. Normally, very dry soils behave like solids; as the moisture content increases, the behaviour of a soil changes from solid to plastic. This transition point is known as the plastic limit (PL; Jackson 1996). If the moisture content increases further, a stage is eventually reached where the soil particles become suspended in water and the soil exhibits viscous behaviour, starting to flow under its own weight.

This transition is referred to as the liquid limit (LL; Summerfield, 1991; Jackson, 1996). These limits are characterised for the < 420 µm size fraction. LL is determined with the aid of a Casagrande's apparatus (Fig. 3.1f). Soil samples are soaked overnight to ensure total saturation. The saturated sample is transferred onto a marble board, mixed thoroughly and allowed to dehydrate with time. In due course, a small fraction of the dehydrating sample is extracted, placed on a brass cup of the Casagrande's apparatus to maximum depth of 13 mm. A groove is

made down into the centre of the soil pad with a standard grooving tool. The cup is repeatedly dropped from a height of 1 cm onto a hard rubber base by turning the crank at a speed of 2 blows per second during which the groove closes up as a result of its impact. The number of blows and the moisture content is recorded and plotted on a semi-logarithmic graph. LL is defined by the moisture content at which the groove closes by 1 cm under the effect of 25 blows.

PL is determined by rolling a ball of soil on a smooth surface into 3 mm thick threads that break into 1 cm long fragments. The fragments are collected and moisture content determined. The moisture content at which this happens represents the plastic limit.

Rosenak (1963) defines the shrinkage limit (SL) as the moisture content at which a soil stops shrinking with further loss of water. To determine the shrinkage limit, three metal shrinkage dishes of known volume (V) (Fig. 3.1g) are greased (so that sample should not stick to the walls) and weighed (M_d), filled with wet soil and compacted by gently tapping on the table to drive off trapped air bubbles. The filled dishes are weighed (M_{dw}) and allowed to air dry for at least 24 hours. This is to prevent the development of cracks or fissures within the sample. The air-dried sample is then oven dried at 110 °C for at least 12 hours, allowed to cool in a desiccator and reweighed (M_s). The soil sample is then immersed in a beaker of known volume filled with Mercury. The mass difference between the Mercury and beaker before and after immersion represent the volume of the sample. The calculated moisture content corresponding to this volume change represents the shrinkage limit.

Though empirically determined, Atterberg's limits are used in soil identification and classification and also allow empirical correlation with other engineering properties that are more difficult or costly to measure. From the PL and LL values, the Plasticity Index (PI; a measure of plasticity or the range of water content at which the soil exhibits plastic behaviour) is calculated. It is defined as the difference between the liquid limit and the plastic limit. It can also be used as a criterion for estimating the liquefaction potential of clayey soils (Lambe & Whitman, 1979).

The natural moisture content, plastic limits and plasticity index and/or grain size data were used to compute the liquidity index (LI) and activity coefficients (AC). The liquidity index, is used for scaling the natural water content of a soil sample to its Atterberg's limits; it is given by

$$LI = \frac{Mc - Pl}{PI} \text{ where } Mc \text{ is the moisture content,}$$

LI = Liquidity index

Pl = Plastic limit

PI = Plasticity index.

LI indicates the behaviour of fine grained soils upon shearing and can be used as a proxy for the undrained shear behaviour of remoulded samples. Negative values suggest that the colluvial soils are unlikely to fail by flow type movement unless a large amount of water is added (Shakoor & Smithmyer, 2005).

The activity coefficient (AC), defined as the plasticity index divided by the percentage of the clay fraction within the sample (Underwood, 1967) was also calculated for all the soil samples (Table 5). From the AC one can predict the dominant clay type present in a soil sample. High activity signifies large volume changes when wetted and large shrinkage when dried while lower values signify small change. Soils with a high AC are chemically very reactive.

3.3.5 Grain size distribution

Grain size influence the moisture content and the rate at which water flows through a soil. Granulometric analysis was done by wet and dry sieving to separate the sand fraction. Sedimentation with a hydrometer (Fig. 3.1b) was used to separate the clay from silt, following the procedure described by Van Reeuwijk (1993). Samples were first dried in a warm room set at 40 °C, disaggregated and sieved to separate fractions greater than 2 mm. 200 to 300 g of the passing fraction was later sieved wet on the 75 µm sieve. The fraction retained on the sieve was then oven dried at 105 °C and sieved through a stack of sieves (1.65 mm; 840, 420, 210, 105, 74 µm) placed on a mechanical shaker (Fig. 3.1c) for 20 minutes. Approximately 0.5 g of the sand size fraction was observed under a petrographic microscope and photomicrographs were made.

5 g of deflocculant (sodium hexametaphosphate) was added to 50 g of the < 75 µm fraction and mixed on a magnetic stirrer (Fig. 3.1d). The sample/deflocculant mixture was allowed to stand for at least 12 hours to ensure complete disaggregation. After this period, samples were agitated for at least 5 minutes to ensure complete dispersal. Samples are then transferred into a 1000 ml measuring cylinder, filled up to the mark with distilled water and placed in a water bath set at 25

°C (Fig. 3.1e). Temperature and hydrometer readings are taken after 0.5, 1, 2, 5, 15, 30, 60, 250, and 1440 minutes to determine the amount of silt and clay fraction within each sample according to Stokes' law. Results obtained are later plotted on a semi-logarithmic graph (grain size chart). The proportions of sand, silt and clay present in each sample were later plotted on a textural triangle to obtain a textural classification of the samples.

3.3.6 Determination of bulk density (γ)

The soil bulk density is a measure of natural soil in situ compaction, and can be used to determine how much air or water can be stored or can migrate through the soil. Bulk density indicates how tight soil particles are packed, hence, can directly or indirectly influence soil stability. To determine the soil bulk density, about 15 g of the field sample clods (samples as collected without any form of drying) was tied with a string and weighed in air, coated with paraffin, reweighed in air, and the soil/paraffin sample immersed in water. The volume of displaced water is measured (Fig. 3.1a) based on Archimedes' principle. The information obtained is then used to calculate the bulk density as shown below. Prior to this, the density of the paraffin and that of water is determined. Sample density was derived from the following equation:

$$\rho_s = \rho_w \left(\frac{W_s}{W_s - W_{spl} + W_{pa} \left(W_{pa} \times \frac{\rho_w}{\rho_a} \right)} \right) \quad (2)$$

where ρ_s = bulk density of sample

ρ_w = density of water

ρ_a = density of paraffin

W_s = weight of sample in air (g)

W_{spl} = weight of sample and paraffin coating in water (g)

W_{pa} = mass of paraffin = weight of paraffin and sample in air (W_{spa}) - W_s

Observed standard deviation in the sample range from 0.01 - 0.18 for the soil samples

3.3.7 Determination of particle specific gravity (G_s)

Particle specific gravity is an important physical property used in volume-weight relationships for soils and rocks (Rosenak, 1963). It is used to determine other important properties such as

void ratio, porosity, and degree of saturation (Yalcin, 2007). The specific gravity is the ratio between the unit weight of a substance and the unit weight of pure water at 4 °C (Cernica, 1995). It was determined with the aid of pycnometers.

Procedure

Approximately 15 g of each soil sample was placed in a pycnometer (density bottle) of known weight and volume. The pycnometer and sample are weighed and demineralised water added and thoroughly mixed with the soil sample before placing it without a stopper in a pressure chamber (Fig. 3.1m) to drive off air bubbles. The pycnometer filled with sample and distilled water is then placed in a water bath set at 25 °C over night to allow for complete saturation. The complete assembly (saturated sample, density bottle, with water) is then reweighed and the temperature of the sample is measured. If it is not equal to 25 °C then, temperature corrected specific gravity (G') will have to be calculated. The pycnometer is then emptied, filled with distilled water and placed in a water bath to the same temperature and weighed. The specific gravity calculated as follows:

$$G_s = \left(\frac{W_2 - W_1}{(W_4 - W_1) - (W_3 - W_2)} \right)$$

where W_1 is the weight of the pycnometer (g)

W_2 = weight of pycnometer and soil (g)

W_3 = weight of pycnometer soil and water (g)

W_4 = weight of pycnometer and water (g)

G_s = particle specific gravity

$$G' = G_s \times \frac{\text{Relative density of water at room temperature}}{\text{Relative density of water at 25}^\circ\text{C}}$$

Observed standard deviation between sample specimens range from 0.006 - 0.04 g/cm³.

3.3.8 Consolidated undrained triaxial test

Shear strength parameters, cohesion and friction angle were determined in the laboratory in an automated triaxial cell (Fig. 3.1m) on reconstructed samples (PS3S08 and PS3S09 for the pyroclastic material and sample P6S19 and P6S20 for lava flows).

Procedure

A mass of dry soil is mixed with distilled water, in order to reconstruct the natural water content and extruder in a metallic cylinder to obtain cylindrical sample specimens (Fig. 3.5) with a length width ratio of 2. Sample mass is calculated to correspond to the sample volume in order to reconstitute the bulk volumic weight. The height and diameter of the sample specimen is measured and then the sample weighed and encased by a rubber membrane. The sample specimen is then placed in the triaxial cell and the cell filled with water.

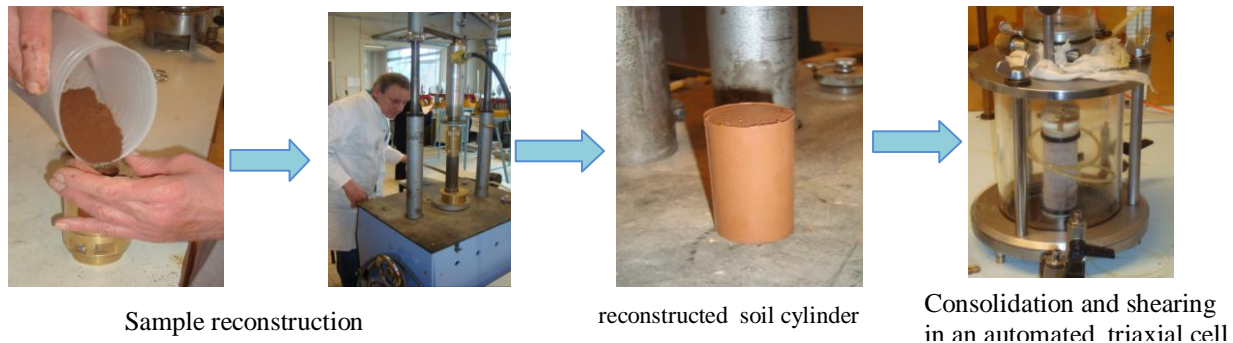


Fig. 3. 5. Procedure involved in sample preparation and analysis in a triaxial cell.

The cell is then gradually subjected to an all round confining pressure and axial load applied ca 10 minute after the application of the chamber pressure. This only changes the normal force acting on the sample whereas the all round pressure remains constant. The sample is compressed at a fixed speed and proving readings of axial stress continuously measured until failure.

The axial stress P/A at failure is read off and the all round pressure (σ_3) is added to obtain the maximum normal stress (σ_1). The unit strain (ϵ) and adjusted instantaneous area (A) are calculated:

$$\text{i.e. } \epsilon = dL/L_0$$

where dL = change in specimen length

L_0 = initial specimen length

The axial load (P) is measured and the principal stress computed as

$$\sigma_1 = \sigma_3 + P/A$$

From the calculated σ_1 , the maximal difference between the principal stresses $\sigma_1 - \sigma_3$ is computed. At least four sets of analysis were made on each sample under different loading

conditions. Using derived σ_1 - σ_3 values, Mohr circles (Appendix 3, Fig. A1) are constructed corresponding to different failure conditions. The tangents of the circles provide the failure envelopes for the soil. The slopes of the tangent represent the angle of internal friction and the intercept characterises the cohesion.

3.4 Result of geotechnical characterization

The natural moisture content, grain size distribution and other index properties measured in this study are presented in Table 3.1. Natural moisture content ranges from 31 to 55 % with a mean value of 43 ± 6 %. It shows an increasing downward trend in Pits 1, 2 and 3, dominated by clay. Plasticity index is 23.6 ± 8 . The plastic and liquid limit range from 31.9 to 61.8 and from 46.7 to 87.3 %, respectively. The average specific gravity is high, ranging from 2.76 to 2.98 g/cm^3 with mean values of 2.86 ± 0.06 g/cm^3 . The average bulk density is 1.95 g/cm^3 which is about half that of the fresh rock samples. Porosity (a measure of the volume of voids in the bulk sample volume) ranges from 24 to 44 % with mean values of 32 ± 5 %. All these data fit with other results obtained from studies on residual soils in tropical climates (Lohnes *et al.*, 1977; Vaughan *et al.*, 1988; Rahman *et al.*, 2010).

S No	Texture	Sand	Silt	Clay	Mc	LOI (%)	PL (%)	LL (%)	PI (%)	Sw (%)	LI	AC	Gs (g/cm ³)	γ_d (g/cm ³)	γ (g/cm ³)	n (%)
P1S 01	Silt loam	15	60	25	38.2		49.9	81.5	31.6		-0.37	1.26	2.90	1.23	1.70	41.30
P1S 02	Silty clay loam	20	45	35	43.7	12.3	50.1	74.3	24.2	26.9	-0.27	0.69	2.84	1.29	1.85	34.75
P1S 03	Clay	22	35	43	44.9	8.9	44.2	71.7	27.4	26.9	0.02	0.64	2.90	1.42	2.06	29.05
P4S 05	Clay loam	34	34	32	37.4	11.3	42.5	73.6	30.9	48.0	-0.16	0.97	2.88	1.35	1.86	35.58
P4S 06	Clay	4	29	68	43.2	13.3	54.1	87.3	33.2	37.6	-0.33	0.49	2.96	1.36	1.95	34.19
P4S 07	Silty clay	4	49	48	50.4	11.7	52.4	79.2	26.8	40.7	-0.07	0.56	2.98	-	2.05	31.35
P3S 08	Clay	2	24	74	39.6	13.1	57.8	81.3	23.5	44.7	-0.78	0.32	2.93	1.38	1.93	34.24
P3S 09	Clay	4	24	73	44.4	15.2	56.3	81.0	24.7	30.0	-0.48	0.34	2.85	1.44	2.08	27.02
P3S 10	Silty clay	3	45	53	46.7	12.1	61.8	80.9	19.1	39.5	-0.80	0.36	2.93	1.32	1.94	33.92
P2S 11	Clay loam	31	41	29	54.8	10.5	46.0	77.3	31.3	30.8	0.28	1.08	2.93	1.39	1.65	44.01
P2S 12	Sandy clay loam	46	26	29	41.5	7.6	40.4	74.8	34.3	30.2	0.03	1.20	2.95	1.34	1.90	35.75
P2S 13	Sandy loam	69	24	8	48.3	7.4	38.8	69.6	30.9	38.2	0.31	4.12	2.94	1.11	2.15	26.58
P5S 14	Clay loam	32	41	27	50.4	9.0	45.0	64.7	19.7	38.8	0.28	0.73	2.88	1.40	2.11	26.79
P5S 15	Silt loam	39	50	11	34.6	8.2	31.9	46.7	14.8	37.4	0.18	1.35	2.83	1.60	2.15	24.02
P6S 17	Silty clay loam	20	45	35	46.4	11.8	38.3	63.6	25.3	28.8	0.3	0.72	2.82	1.34	2.20	24.94
P6S 18	Loam	34	49	17	39.8	8.4	42.4	53.4	11.0	40.7	0.23	0.65	2.88	1.32	1.90	31.28
P6S 19	Silt loam	31	57	13	30.8	7.4	35.2	47.4	12.2	40.6	0.36	0.97	2.76	1.45	1.85	35.84
P6S 20	Silt loam	26	63	11	38.3	7.1	38.9	47.3	8.4	37.4	0.07	0.77	2.93	1.59	1.96	30.44
Minimum		2.3	23.5	7.5	30.8	7.1	31.9	46.7	8.4	26.9	-0.80	0.32	2.76	1.11	1.65	24.02
Maximum		69.0	63.0	74	54.8	15.2	61.8	87.3	34.3	48.0	0.32	4.12	2.98	1.60	2.20	44.01
Mean		24.1	41.0	34.9	42.9	10.0	45.9	69.7	23.9	36.0	-0.14	0.96	2.89	1.37	1.95	32.39
Standard deviation		17.8	12.6	21.1	6.1	2.50	8.31	13.1	8.03	6.3	0.35	0.85	0.06	0.11	0.15	5.42

Table 3. 1. Index and geotechnical properties of soils from landslide scars in the study area as derived from laboratory analysis. Mc: natural moisture content; LOI: Loss on ignition; PL: plastic limit; LL: liquid limit; Sw: shrinkage limit; LI: liquidity; AC: activity coefficient; Gs: particle specific gravity; γ_d : dry density; γ : bulk density; n: porosity.

3.4.1 Description of geotechnical profiles

The above properties are integrated into the soil profiles described for each pit to generate a geotechnical profile. These profiles are described in detail hereafter.

3.4.1.1 Profile 1 Bonjo

The profile at Bonjo was obtained from Pit 1, a 3.5 m deep pit dug into a complex slide at Bonjo, developed on weathered basaltic lava flow deposits. The pit is located ca. 10 m below the main scarp at an elevation of 52 m a.s.l. Within this pit, the soil profile shows 4 distinct horizons (Fig. 3.6). The material is dominantly clay and silt with less than 25 % sand though the sand fraction shows a downward increasing trend. The terms “sand “ and “sandy” will be used here strictly in characterizing the grain size, or granulometry, and not related to the mineralogical composition. The sandy fraction is made of grains of weathered parent rock. The first 20 cm are covered by a dark humus layer. Underneath, a 1 m thick pale yellow mottled plastic clayey loam horizon occurs, with a G_s of 2.83 g/cm³ and a γ of 1.85 g/cm³, interrupted at 80 cm depth by a thin layer of decaying debris, probably representing the top material from the previous slide. At a depth of 1.2 m below the surface, there is an abrupt change in colour from yellow (5Y8/2) to brown (7.5YR5/2) clay with G_s 2.9 g/cm³ and γ 2.06 g/cm³. The material then gradually grades into a light gray (2.5Y7/1) silty saprolite with alternating gray and brown strips. Fragments of unweathered rock found within the slide debris suggest that the parent rock is dark coloured porphyritic basalt characterized by plagioclase, pyroxene and olivine phenocrysts and which has a γ of 2.93 g/cm³. Within this profile, the moisture content, proportion of sand and clay increases with depth, whereas the specific gravity, plasticity index and plastic limit show more irregular patterns as seen in Table 3.1 and Figure 3.6. The porosity is also observed to decrease downward in the profile. It is worth noting that the sand fraction is characterised by the presence of yellowish concretions (probably iron oxides) that were not analysed in this study.

The grain size distribution for Pit 1 is shown in Figure 3.7. Grain size analysis data from which this and other graphs were obtained, are given in Appendix 4. These soils are dominated by the silt fraction while the sand fraction is characterised by the presence of yellowish brown concretions.

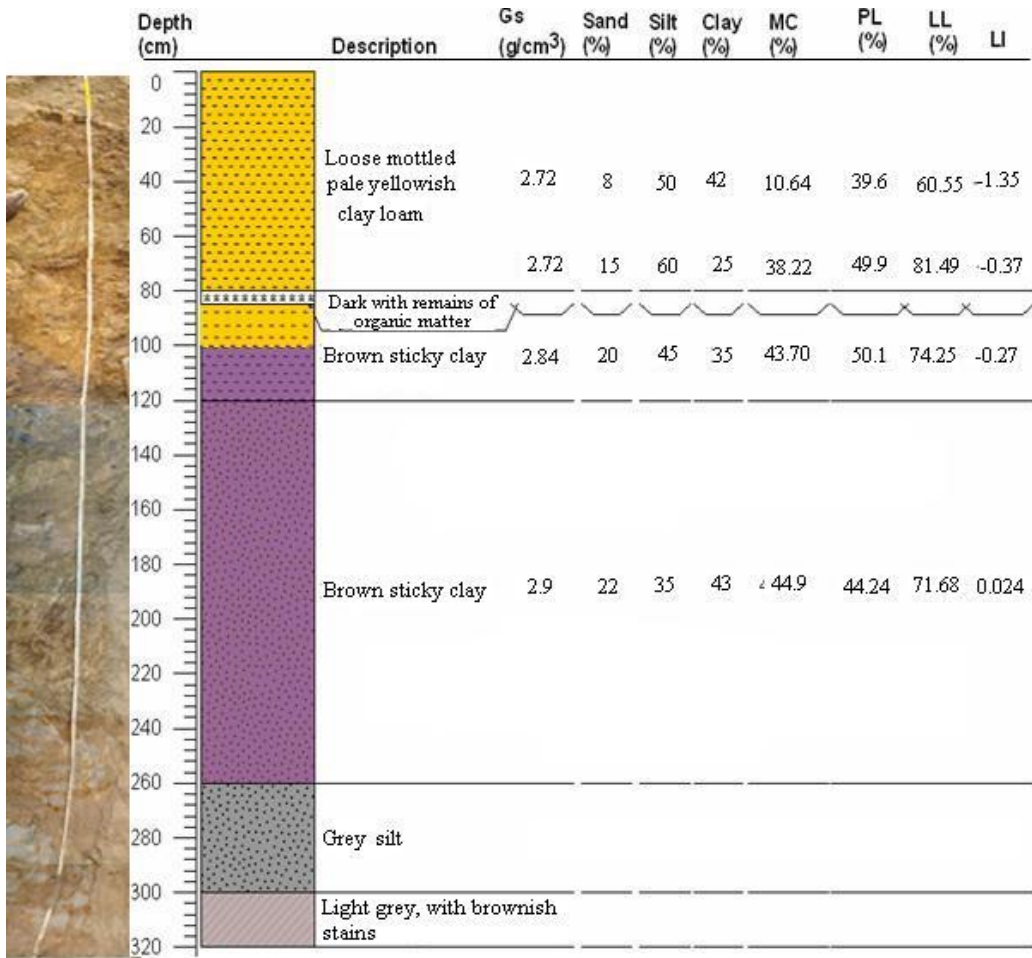


Fig. 3. 6. Photograph mosaic and sketch of the Bonjo soil profile with associated index properties measured in the laboratory. Note significant and abrupt colour changes downward in the profile.

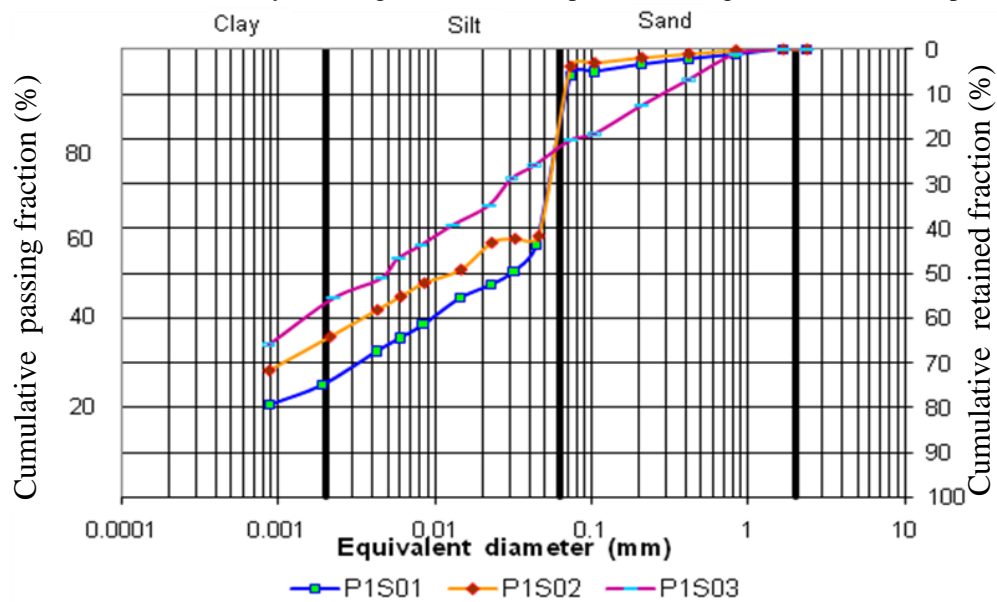


Fig. 3. 7. Grain size distribution for samples P1S01, P1S02 and P1S03 from Pit 1 at Bonjo. Note the dominance of the silt fraction. Sand fraction is made up of yellowish brown concretions.

3.4.1.2 Profiles 2, 3 and 4, Mabeta New Layout

Pits 2, 3 and 4 were dug into one of the several slides at Mabeta (Fig. 2.5d). The profiles show no sharp colour differences but exhibit significant differences in terms of texture and humidity down the profiles.

Profile 2 (Fig. 3.8b) describes the section of a 3.8 m deep pit dug into a 30 - 40° slope on a degraded pyroclastic cone at Mabeta. It is located 30 m below the main scarp at an elevation of 89 m a.s.l. The first 70 cm are characterised by loose reddish brown clayey loam soil with G_s 2.93 g/cm³ and γ 2.15 g/cm³, probably representing loose debris from the previous slide. This depth corresponds to the maximum rooting system of plants within the slide at this point. Underlying to this horizon down to a depth of 2.8 m below the ground surface, a moist mottled sandy clay loam horizon occurs with G_s 2.95 g/cm³, γ_d 1.34 g/cm³ and γ 1.90 g/cm³. Below 2.8 m, the profile is wet (saturated), and characterised by loose sandy loam soils with visible olivine and pyroxene crystals together with completely weathered rock blocks. This section has a G_s of 2.94 g/m³, γ_d 1.34 g/cm³ and γ 1.65 g/cm³. The parent rock is a spongy dark brown porphyritic rock with a density of 2.29 g/cm³. Measured index properties indicate that the amounts of silt and clay, and the values for PL and LL decrease down the profile while the sand fraction, natural moisture content and porosity increase down the profile. Material from this pit represents intact material that was not involved in previous slides.

Profile 3 (Fig 3.8c) describes a 3.2 m deep pit dug at an elevation of 73 m a.s.l. and lies 30 m down slope from Pit 2 where there exists an abrupt change in slope gradient from 33 to 10°, probably representing the accumulation zone or as a result of human intervention on this slope. This zone is heavily vegetated as compared to the location of Pit 2 with only sparse vegetation. The area of Pit 3 also appears damp at the surface and throughout the profile. However the moisture content was several orders lower than observed at the bottom of Pit 2, suggesting the presence of a permeability boundary or barrier. From 0 to 2 m, corresponding to the maximum rooting system depth, the soil has a clayey texture, and is moist, mottled, (reddish brown with white patches) and maintains the same colour throughout the profile. Below the maximum rooting depth no rock fragment, gravel and sand sized particles occur. In this profile, the moisture content increases downward while the grain size distribution shows only minor

variations. Measured index properties show irregular patterns, hence it is concluded that the pit represents debris that was mobilized by sliding and accumulated at the foot of the slope.

Profile 4 (Fig. 3.8d) is 2.4 m deep and lies at 53 m a.s.l. close to the toe of the landslide. It is composed entirely of loose, reddish brown clayey soils, representing debris mobilized during the 2001 landslide events. This conclusion is drawn from the fact that the bottom of the pit is marked by the presence of a floor layer made up of Portland cement, indicative of former human activity, which was buried under the debris. This observation implies that the thickness of the debris at this location was at least 2.4 m. Measured index properties also do not show any visible trends. This can be accounted for by the fact that the soils are a jumbled mixture of material moved down the slope by sliding.

Characteristic grain size distribution patterns of these soils are presented in Figure 3.9. It is observed that soils from Pit 4 located at the base of the slope, are dominated by the clay fraction. As one moves upslope, the sand concentrations increase with peak values recorded in Pit 2. This is an indication that the veneer of soil initially present on the slope has been moved down the slope to expose a new surface to the agents of weathering. In addition, the sand fraction increases with depth suggesting the presence of a more permeable layer underneath a less permeable clayey horizon.

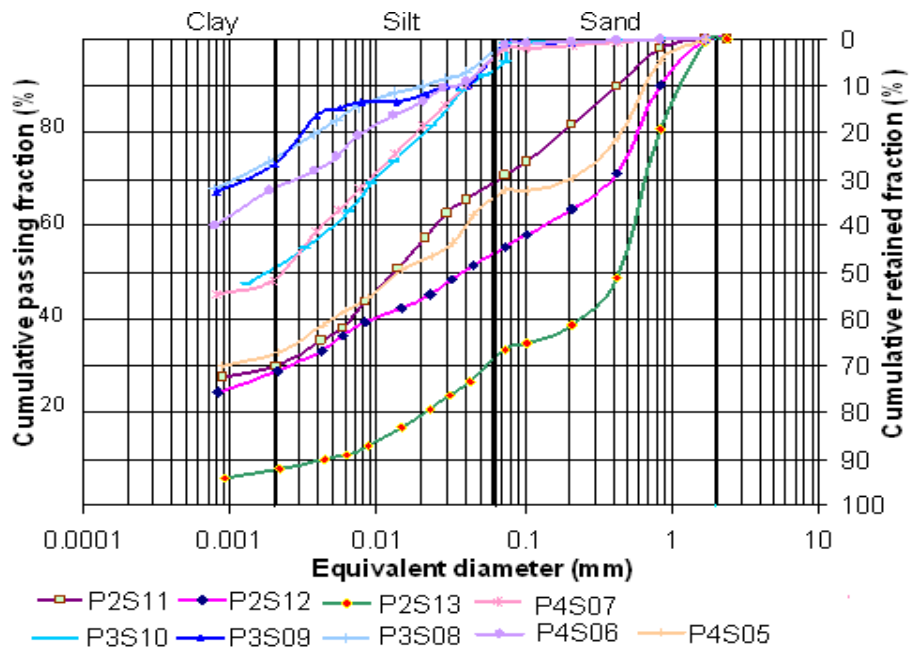


Fig. 3. 8. Grain size distribution of samples from Pits 2, 3 and 4 at Mabeta. Note the dominance of the silt fraction and a progressive increase in the sand fraction with depth in Pit 2.

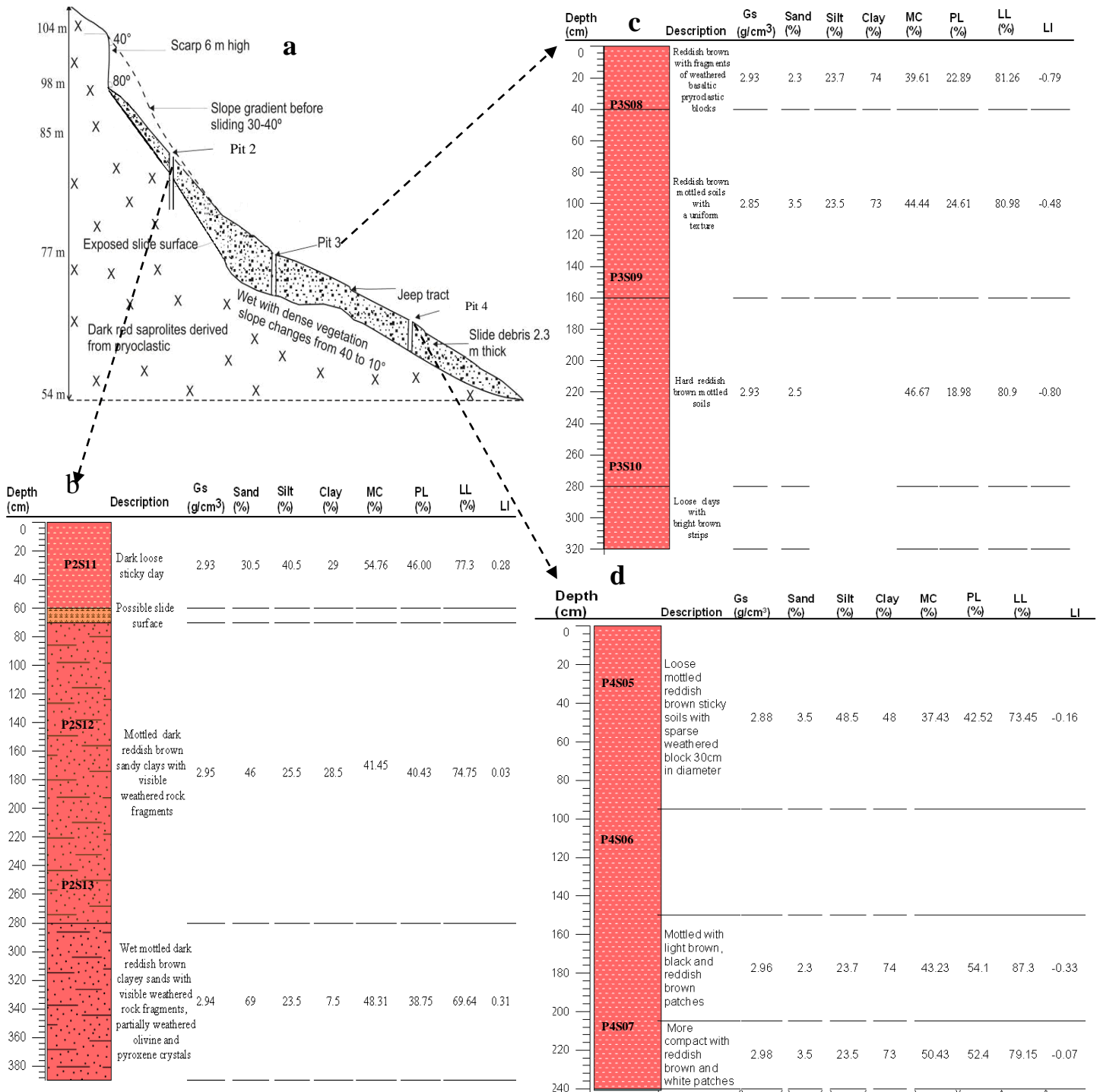


Fig. 3. 9. Cross sectional view of the Mabeta slide showing the nature of associated soil profiles: a) longitudinal section; b) profile described from Pit 2; c) profile of Pit 3; d) profile of Pit 4.

3.4.1.3 Profiles 5 and 6, Makuka

Profiles 5 and 6 are described from Pits 5 and 6 dug in a translational slide at Makuka (Figure 3.10).

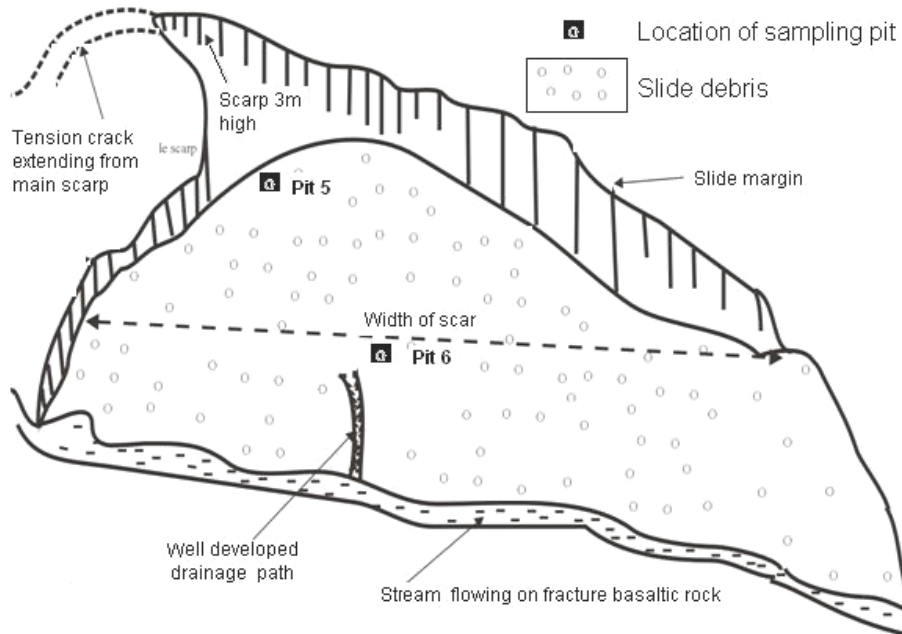


Fig. 3. 10. Sketch of Makuka slide showing the location of sampling pits. Diagram not drawn to scale.

These soils are principally silt dominated though large boulders were observed within slide debris. Profile 5 (Fig. 3.11) is only 2.4 m deep because the bottom was too stony and digging was impossible. It is located 10 m away from the main scarp. From 0 to 20 cm the profile is characterized by a dark humus layer below which lies a 30 cm thick purplish to gray clayey layer. At depths greater than 50 cm, yellowish brown soils which are wet, sticky, and silty with rounded basaltic blocks showing characteristic onion-skin weathering. Onion-skin weathering (exfoliation) is initiated by the presence of dense fractures that favour differential weathering commonly observed in the study area. The blocks range in diameter from a few mm to over 40 cm. However, within the slide debris, blocks of more than 1 m were observed. The index properties of the two horizons observed are shown on Figure 3.11.

Profile 6 describes a 4 m deep pit that shows remarkable variations in colour, texture and composition with depth (Fig. 3.12). It is located about 30 m down slope from Pit 5 (Fig. 3.10).

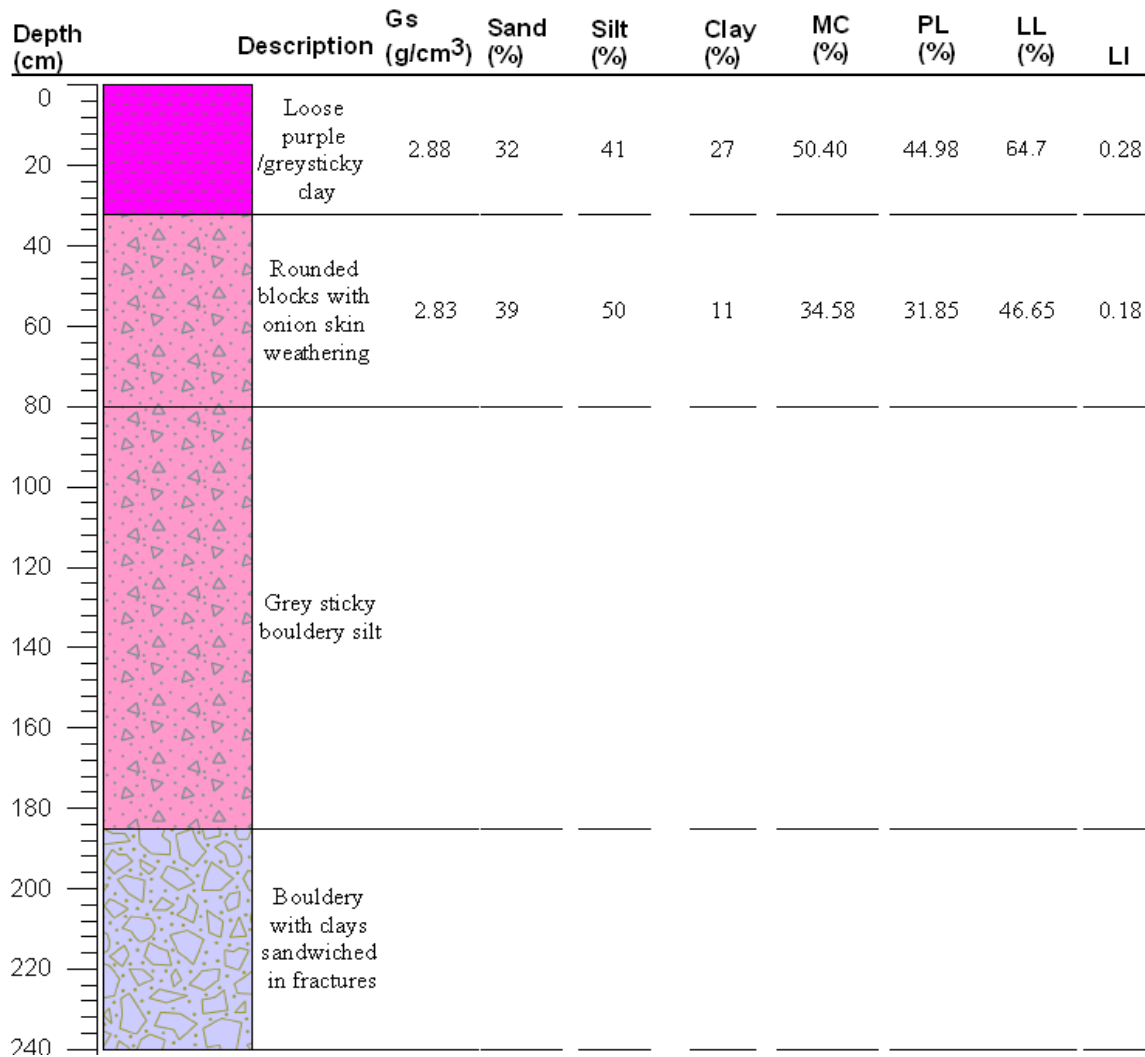


Fig. 3. 11. Geotechnical profile of Pit 5 at Makuka.

The profile is topped by 30 cm thick loose purplish horizon probably representing a humus layer underlain by a 50 cm thick light olive brown clayey layer with G_s 2.82 g/cm³, γ_d 1.34 g/cm³ and γ 1.96 g/cm³. Underneath, a 70 cm thick pale olive (5Y6/4) silty horizon occurs with a G_s of 2.89 g/cm³ and γ of 1.85 g/cm³ that slowly transgresses towards a gray (2.5Y6/1) stony and fractured layer with clays sandwiched in between the joints. This material has a G_s of 2.93 g/cm³ and a bulk density of 2.20 g/cm³. The bottom of the pit is made up of a gray (10YR6/1) stony saprolite which still exhibits the textural characteristics of the parent rock. The parent rock is a dark, dense porphyritic basalt with a bulk density of 2.82 g/cm³. Porosity, A_c and Atteberg's limit of these horizons are presented on Table 3.1 and Figure 3.12.

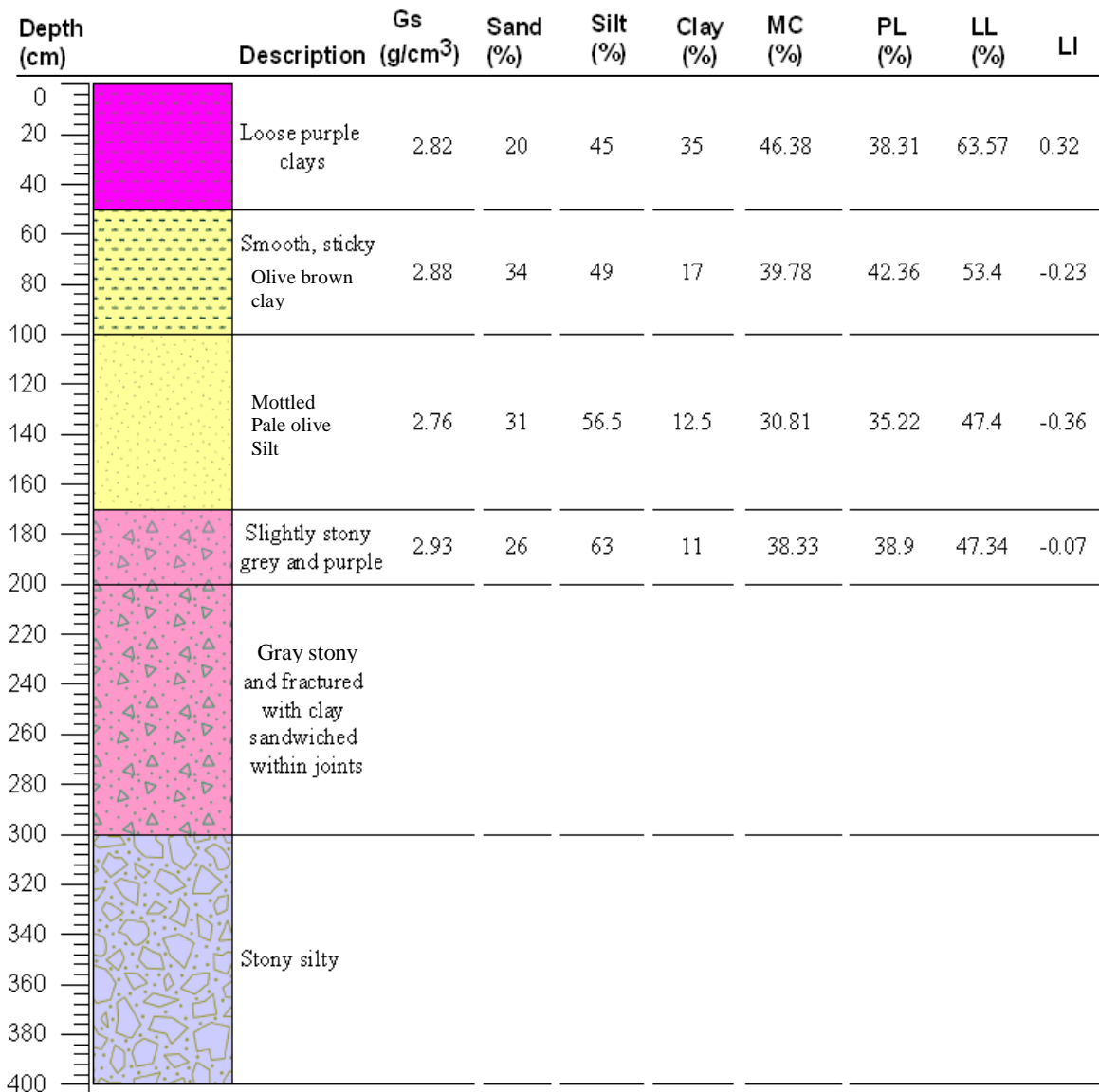


Fig. 3. 12. Profile of Pit 6 at Makuka with associated index properties.

The clay fraction, PL and LL values decrease down the profile, whereas the silt fraction shows an increase. Porosity decreases with depth. However, observed fracturing may enhance surface water infiltration at depth. Profiles 5 and 6 are characterised by low plasticity index values, hence can change rapidly from plastic to viscous behaviour.

Grain size distribution patterns of the soils sampled at Makuka are shown on Figure 3.13. Note the dominance of the silt fraction.

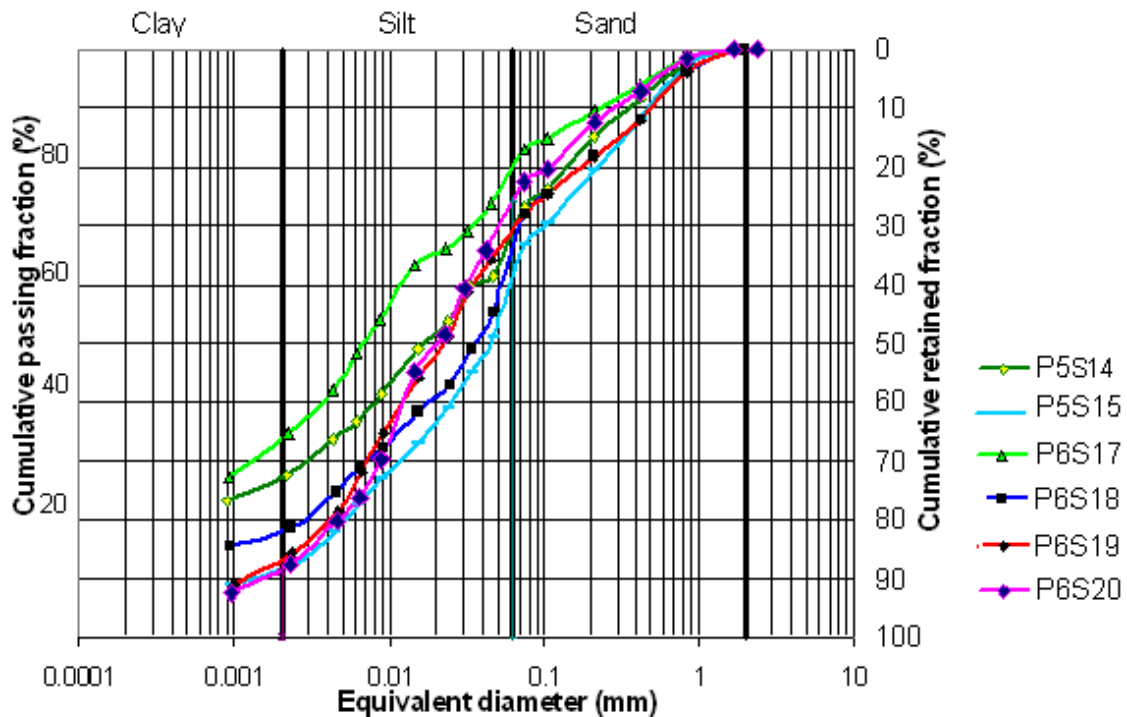


Fig. 3. 13. Grain size distribution curve for samples collected at Makuka Pits 5 and 6. Note the abundance of the silt fraction and low clay and sand concentrations.

3.5 Textural classification and its significance

Grain size distribution plots on the United States Department of Agriculture (USDA) textural triangle indicate that samples P1S03, P2S06, P3S08, P3S09 are clay, P3S07 and P4S10 silty clay, P1S02 and P6S20 silty clay loam, P2S05, P4S13 and P5S14 clay loam, P6S19 loam, P1S01, P5S15, P6S17 and P6S18 silt loam, P4S11 sandy loam and P4S12 sandy clay loam (Fig. 3.14). The soils are silt rich and are thus fine enough to inhibit fast internal water movement and coarse enough to inhibit rapid and fast capillary build up, while simultaneously displaying some cohesion.

Measured plasticity indices (i.e. the water content range over which the soils remain plastic) for most of the samples is medium based on Casagrande's plasticity chart, despite the high clay content and the corresponding high natural moisture content. This suggests that samples can still absorb appreciable moisture before they pass the liquid limit and liquefy. 77 % of the samples analysed in this study have PI values greater than 15. According to Gratchev *et al.* (2006), soils with a PI >15 are non liquefiable.

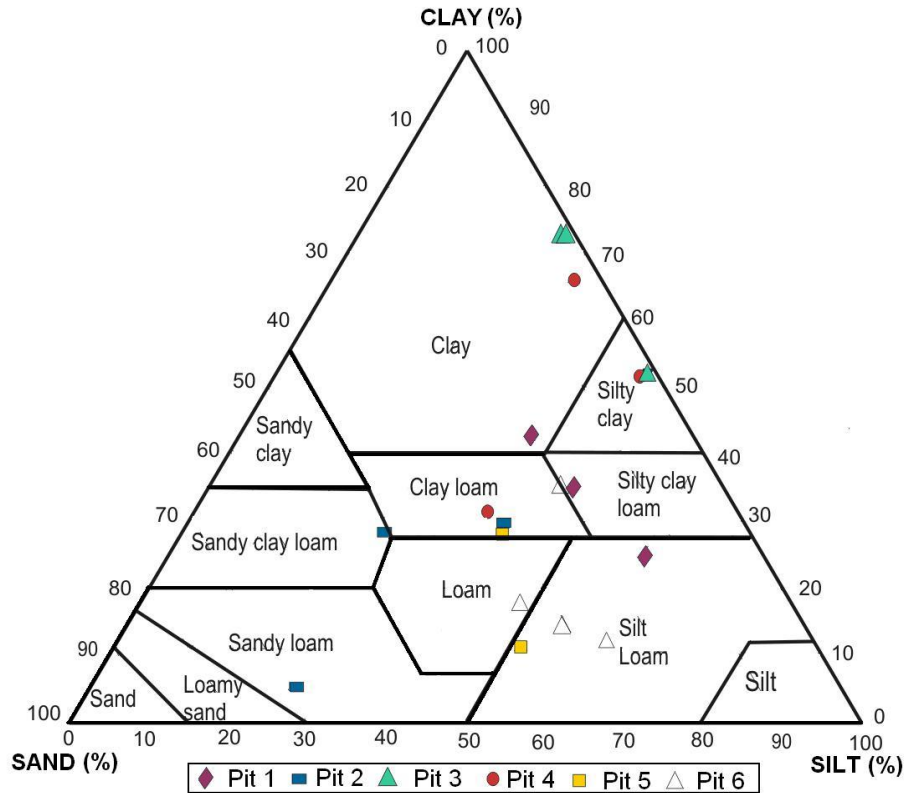


Fig. 3. 14. Textural classification of samples using the USDA textural triangle.

Atterberg's limits were plotted on a Casagrande plasticity chart which is a plot of plasticity index against liquid limit (Fig. 3.15). All the samples plot below the A-line (an empirical boundary that separates inorganic clays from silt and organic soils). Adopting the Unified Soil Classification Scheme (USCS), 77 % of the samples are classified as inorganic silts of high plasticity (MH) and 23 % as inorganic silt of medium plasticity (MI). According to Vaughan (1988) and Rao (1995), tropical residual soils rich in allophane, kaolinite and halloysite are stable and are characterised by excellent geotechnical properties even though they plot below the A-line in the MH field. However, it is worth noting that sedimentary soils that plot in this field tend to have low engineering properties.

Scattered plots of LL, PL and PI against the total clay fraction per sample (Fig. 3.17) show that a slight positive correlation exists between LL and clay fraction, PL and the amount of clay particles present, with R^2 values of 0.57 and 0.67, respectively. A low R^2 value is found for the relationship between PI and the clay fraction present. Similar observations were noted by Croney & Croney (1997).

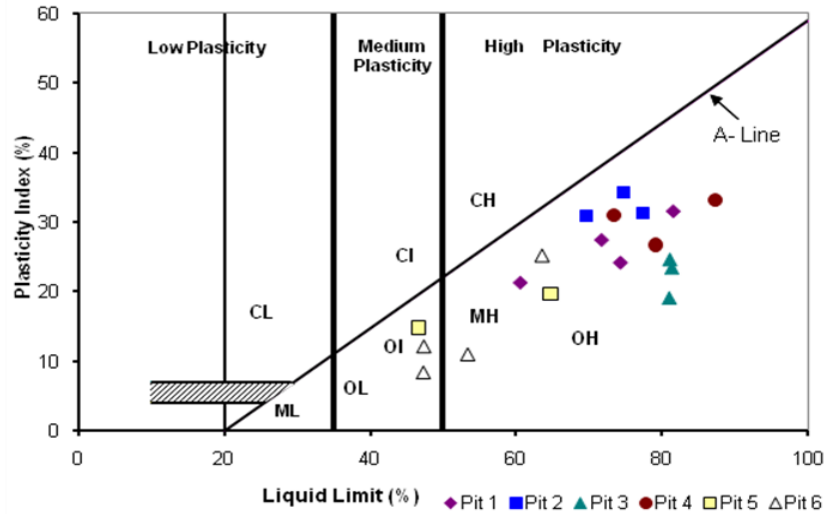


Fig. 3. 15. USCS classification of samples based on Casagrande's (1948) plasticity chart. CL, CI, CH: inorganic clay of low, intermediate and high plasticity, respectively; ML, MI and MH inorganic silt of low, moderate, and high plasticity, OL, OH organic clays of intermediate and high plasticity respectively.

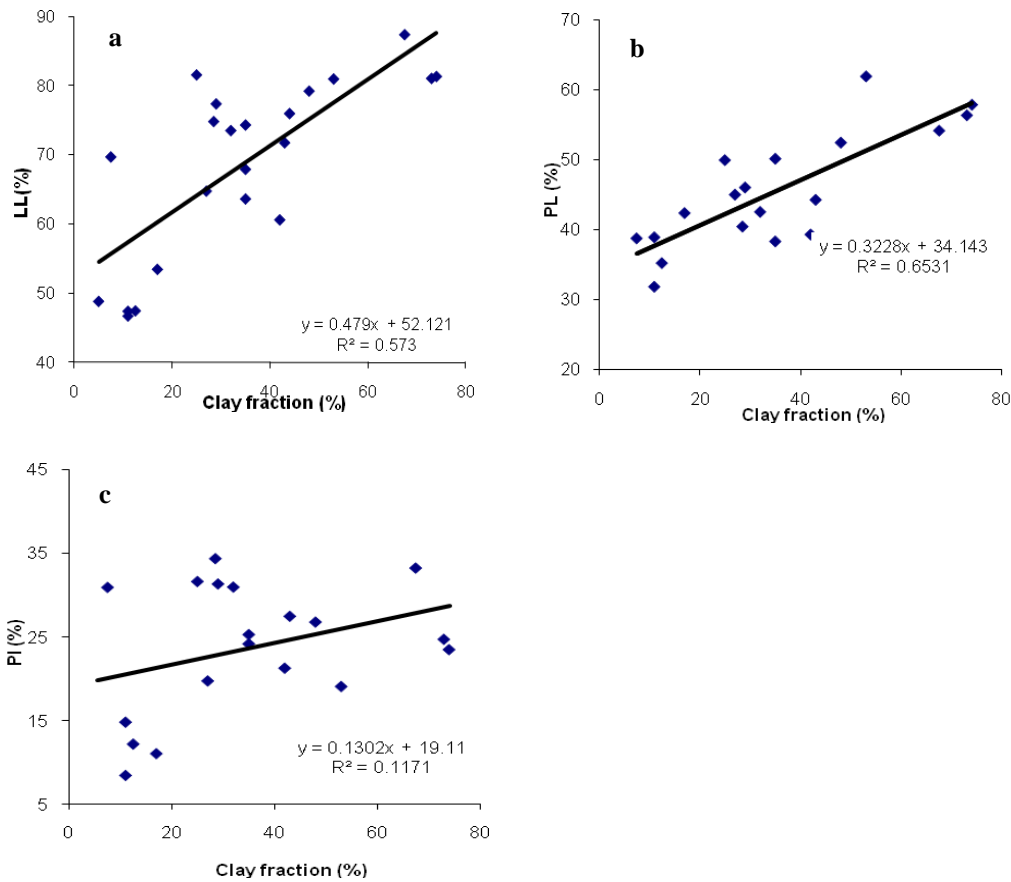


Fig. 3. 16. Relationship between clay content and Atterberg's limits of the soils: a) Liquid Limit (LL); b) Plastic Limit (PL); c) Plasticity Index (PI). Note the positive correlation between PL and LL and the clay fraction and the absence of a clear correlation between PI and clay fraction.

These suggest that the range of water content over which the sample is behaving plastically (between PL and LL) is not dependent on the proportion of clay present but rather on the type (mineralogy) of clay or on the combined effect of all the clay mineral species present within the sample. Contribution from organic matter cannot be ruled out either.

LOI obtained for the soil samples range from 7.4 to 15.2 %. Pits 1, 2, 5 and 6 show a decreasing LOI pattern with depth while Pits 3 and 4 show irregular patterns. The decreasing pattern is associated with decreased weathering intensity whereas the irregular pattern observed in Pit 3 and 4 can be accounted for by the fact that they represent reworked material.

The plasticity index was plotted against the proportion of clay fraction in each sample (%) on the modified activity chart that classifies the swelling – shrinkage potential of the samples (Williams & Donaldson, 1980). The samples show a widely dispersed swelling – shrinkage potential, ranging from low to high with ca. 67 % of the samples in the low and medium (Fig. 3.17) categories. This suggests that the clays present are non-swelling to swelling clays.

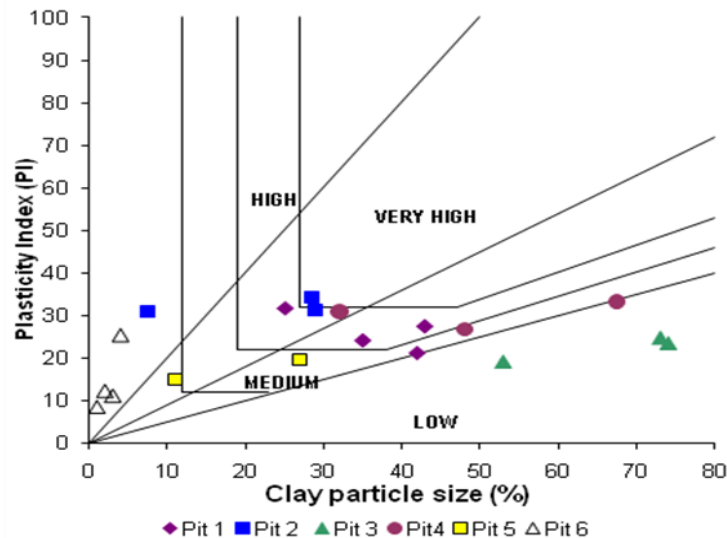


Fig. 3. 17. Modified activity chart, i.e. a plot of the plasticity index against the amount of clay size particle (Williams & Donaldson, 1980), characterising the swelling-shrinkage potential of the samples.

Soils with an activity coefficient between 0.75 and 1.25 are described as normal clays (Skempton, 1953). In this case, it is assumed that the plasticity index is directly proportional to the amount of clay size particles present. When AC is less than 0.75, the material is considered inactive. When AC is greater than 1.25, the material is considered active. Calculated AC values

suggest that 47 % of the samples are normal clays, 41 % inactive clays and 2 % active clays. The activity coefficient can also act as a finger print to the mineralogy of the soils. For sedimentary clays, an AC between 0.4 and 0.5 indicates the presence of muscovite, 0.5 to 0.75 kaolinite, 0.75 - 1.25 illite and > 1.25 smectite. It is observed that calculated AC values for Pit 2 show a downward increasing trend whereas that for the other pits show no clear cut patterns. The downward increasing trend might suggest the presence of poor drainage conditions that might enhance the production of some amount of swelling clays. In addition, all the samples from the pits dug into debris generated from the 2001 slides at Mabeta (Pits 3 and 4) are characterised by relatively low AC values. Pits dug into material that has not yet been mobilized, have AC values greater than 1.25 (Fig. 3.18).

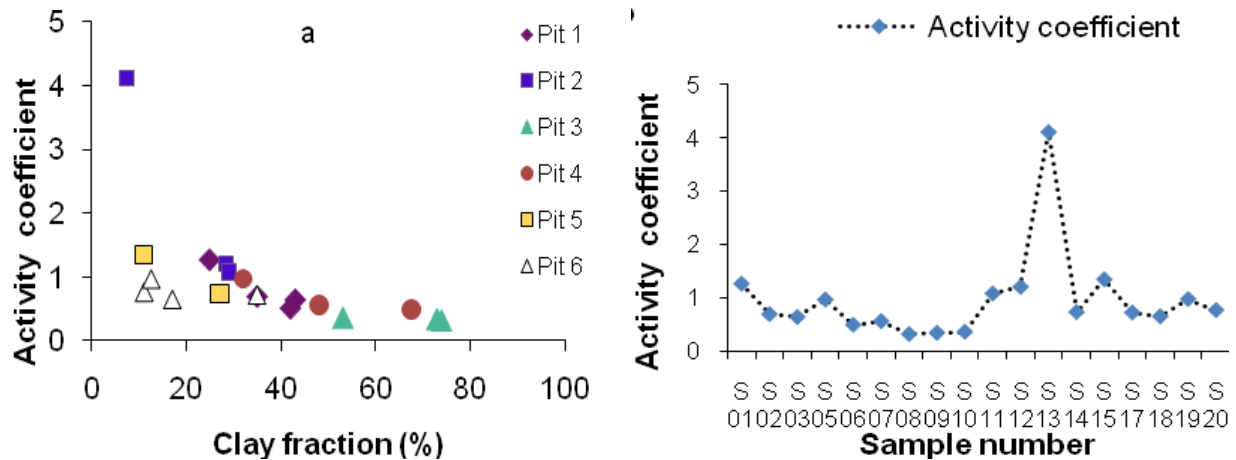


Fig. 3. 18. Activity coefficient calculated for soil samples analysed in this study: a) plots of AC versus clay fraction. Note decreasing activity with increasing clay content; b) activity of sample most AC values are below 1.25.

A very close relationship exists between the position at which Atterberg's limits plot on a plasticity chart and clay mineralogy composition of a soil (Terzaghi *et al.*, 1996; Ohlmacher, 2004). In this study, the Plasticity Index for each sample is plotted on a plasticity chart, which contains montmorillonite, halloysite and allophane fields (Fig. 3.19). These plots indicate that all the samples fall within the field of volcanic ash soil (Andosol) with strong allophane influence. However, mineralogical analysis by X-ray diffraction indicates that the soils are composed of a mixture of swelling and non-swelling clays. Details about the mineralogy of soils samples are given in the next chapter.

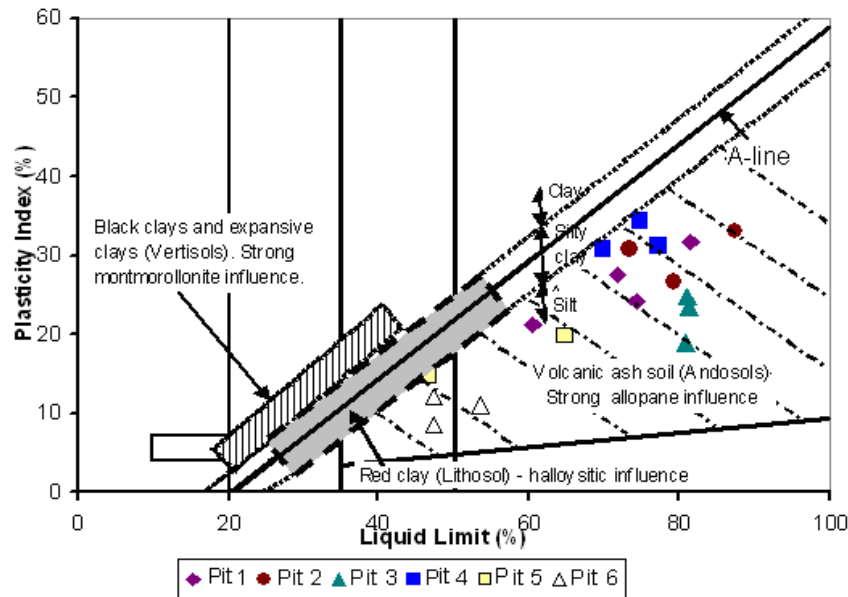


Fig. 3. 19. Plasticity index against liquid limit on a plasticity chart showing the relationship between Atterberg's limits and clay mineralogical composition of the analysed samples.

3.6 Shear strength parameters and their significance

Soil strength parameters (cohesion, residual and effective angle of internal friction) measured in the laboratory from undrained triaxial tests, and permeability measured on two reconstructed samples are given in Table 3.2.

Geotechnical property	Degraded Pyroclastic cone P2S07 and P2S08	Weathered basaltic flow P6S19 and P6S20
Apparent cohesion (kPa) (total stress)	71.0	102.0
Residual frictional angle (°)	22	18.5
Effective angle of internal friction (°)	34.8	34.2
Effective cohesion (kPa)	42.0	67.9
Permeability (m/s)	3.62×10^{-10}	6.90×10^{-10}

Table 3. 2. Shear strength parameters and permeability values of reconstructed soil samples obtained from landslide scars on the SE foot-slopes of MC.

There are significant variations in these properties between soils developed on pyroclastic material and those derived from basaltic lava flows. Woldearegay *et al.* (2006) obtained cohesion values of 5 to 32 kPa and effective frictional angles of 16 to 28° for weathered basalt in Ethiopia. In this case, the cohesion is higher on both types of soils. However, the values fall in the range of values obtained for basaltic parent material by Barton (1973) and Hoek & Bray (1977). In addition, relative undrained shear strength measured in situ with a Torvane meter are similar to

those calculated in the laboratory for the pyroclastic samples but are significantly lower than laboratory results obtained from those in the lava flows. These variations can be explained by the fact that the profile at Makuka was stony and non homogenous whereas Torvane record works well in homogenous clay horizons. Shear strength values are affected by factors such as loading, progressive failure, orientation of the failure plane, pore water migration during testing and the moisture content of the soils while the Torvane meter does not account for any of the above variables. Because of these variations, we use laboratory calculated results for further analysis hereafter.

Relative undrained shear strength values measured in the field are presented on Figure 3.20. It was observed for most of the samples that the shear strength increases progressively to a depth of 8-120 cm. At greater depth, the shear strength shows very irregular patterns but strength at depth > 200 cm is systematically lower than the maximum strength obtained in the first 120 cm.

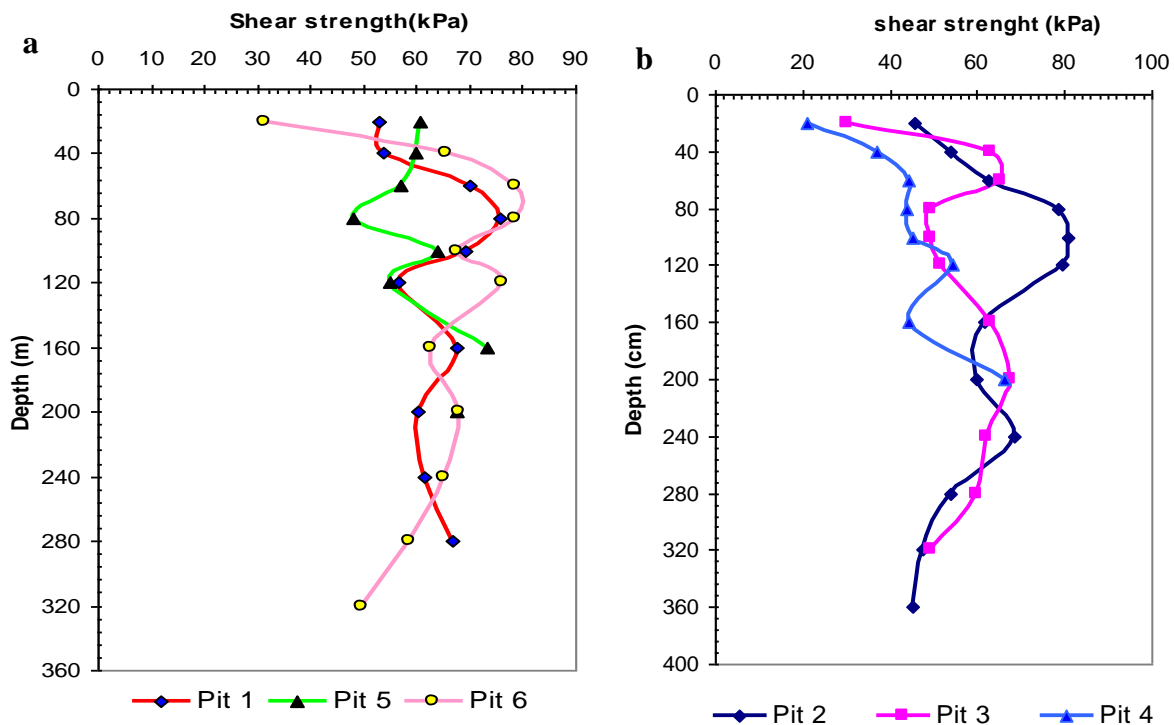


Fig. 3. 20. Relative undrained shear strength measured with a Torvane meter. Values measured on: a) soil profiles developed from weathered basaltic lava flow; b) soils developed on pyroclastic material.

From laboratory determinations, the soil samples are characterised by high effective cohesion, high effective angle of internal friction and permeability low. The static factor of safety (ratio of forces that tend to resist down slope movement and those that drive down slope movement of

slope materials) for these slopes calculated based on the standard infinite slope stability model considering that the slip surface is parallel to the ground and neglecting the effect of vegetation is

greater than 1. The following equation was used.
$$FS = \frac{C}{H\gamma \sin \beta} + \frac{\tan \phi}{\tan \beta} - \frac{m\gamma_w \tan \phi}{\gamma \tan \beta}$$

where FS is factor of safety, C the effective cohesion (kPa), γ the total unit weight of the soil (KN/m^3), H is the thickness of the sliding mass (m), β the slope gradient, γ_w unit weight of water (kN/m^3), m the height of water table, and ϕ the internal friction angle of the soil ($^\circ$).

The first term accounts for the resistance due to cohesion, and is the only one to be sensitive to variations in the thickness of the sliding layer H . The second term represents the resistance related to the internal friction angle and the third term accounts for static effect of water saturation.

Generally, all slope exist in one of the three stability stages: stable, marginally stable and unstable (Crozier, 1986) as shown on the Figure 3.21 and provide a frame work in understanding landslide causal factors. Stable slopes are those where the margin of stability is sufficiently high to withstand all destabilizing forces. Marginally stable slopes are those which will fail at some time in response to the destabilizing forces attaining a certain level of activity. Finally, actively unstable slopes are those in which destabilizing forces produce continuous or intermittent movement

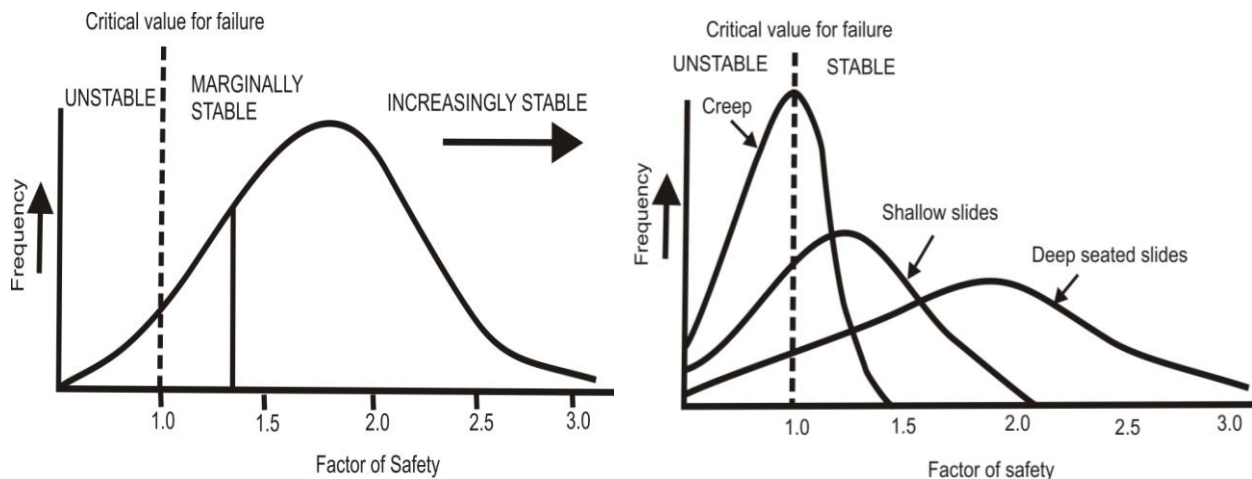


Fig. 3. 21. Probability distribution curve for the factor of safety adapted from Popescu (<http://www.geoengineer.org>)

Calculated values of the factor of safety, therefore, is a simple and clear means of distinguishing between stable and unstable slope. When $F_s < 1$ slope is unstable, $1 < F_s < 2$ slope is marginally stable and $F_s > 2$ the slope is stable.

Figure 3.22 illustrates that high FS ($\gg 1$) values are obtained from the considered slope assuming that the thickness of the sliding mass is 5 and 3 m (means soil thicknesses measured at the main scarp of landslide scars) for pyroclastics and weathered lava flows, respectively. From these graphs, and taking the worst case scenario of fully saturated soils where stability is controlled by bulk density, cohesion, angle of internal friction, slope angle, depth to solid rock and pore water pressure slopes on pyroclastic materials with gradient between 22° and 40° will be marginally stable, whereas those with gradient above 40° will be unstable. On the other hand, slope composed of weathered lava flows with gradient between 38 and 80° will be marginally stable and liable to fail in the presence of external factors while slopes greater than 80° will be unstable. These results suggest that the pyroclastic cone are more susceptible to failure than the lava flows which is in agreement with field observations.

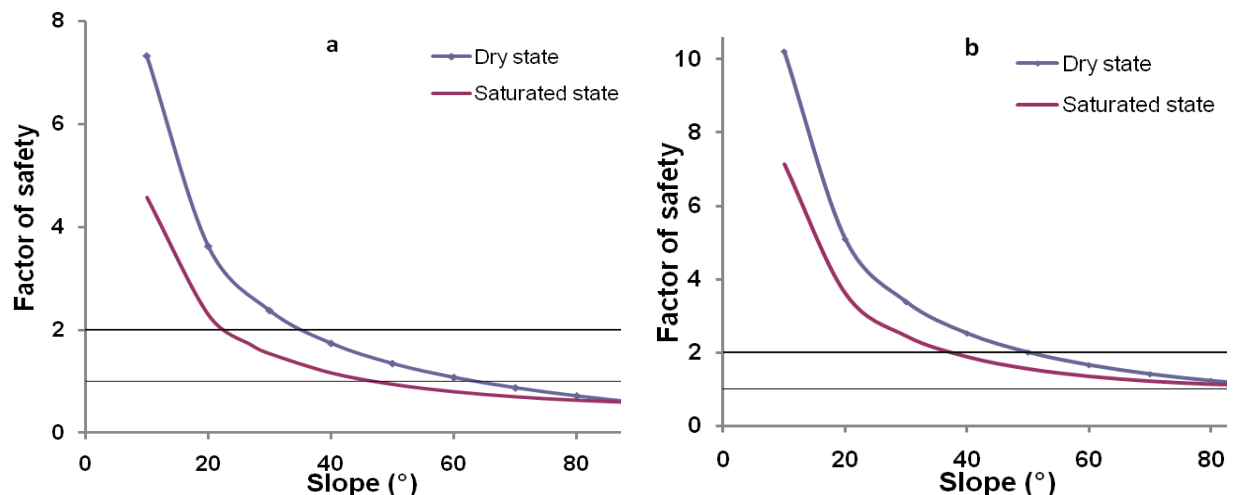


Fig. 3. 22. Variation in calculated factor of safety with slope gradient for a completely dry soil and fully saturated soil assuming a) cohesion to be 42 kPa, frictional angle 34.8° and h 5 m (pyroclastic deposits) b) cohesion 67.9 kPa, frictional angle 34.2° and h 3 m (lava flows deposits) for slope failure on the foot slopes of Mt Cameroon.

Keeping all parameters constant, i.e. cohesion 42 kPa and frictional angle 34.8° , and varying soil thickness from 1 to 10 m, it is observed that the slopes on weathered pyroclastic cones which are generally between 35° and 40° , will become quasi stable when the thickness of the sliding slab is more than 4 m and completely unstable above 6 m (Fig. 3.23). For weathered lava flows, with

cohesion 67.9 kPa and frictional angle 34.2° , slopes between 25° and 35° on which most of the slides were observed will be marginally stable when the thickness of the sliding layer is above 6 m, and become completely unstable when the soil thickness develops to more than 10 m (Fig. 3.24).

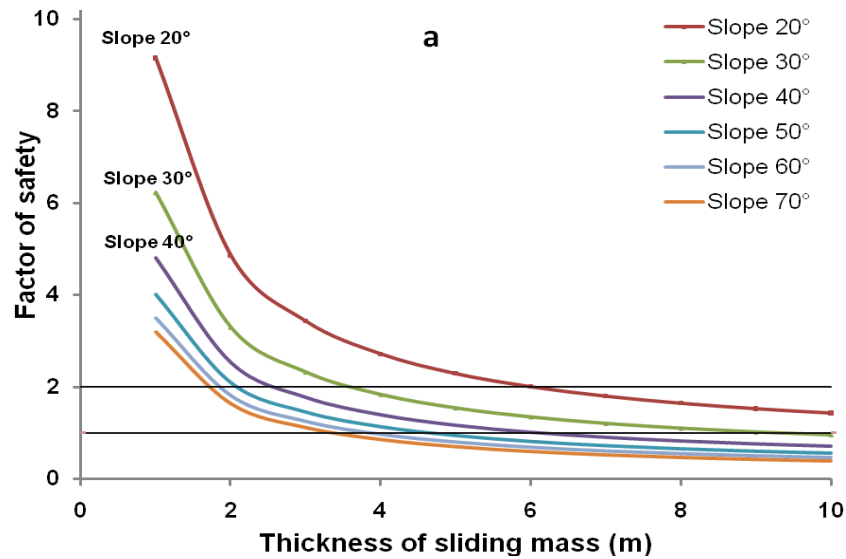


Fig. 3. 23. Calculated factor of safety assuming cohesion to be 42 kPa and effective angle of internal friction 34.8° on variable slope with variable thickness of the sliding layer.

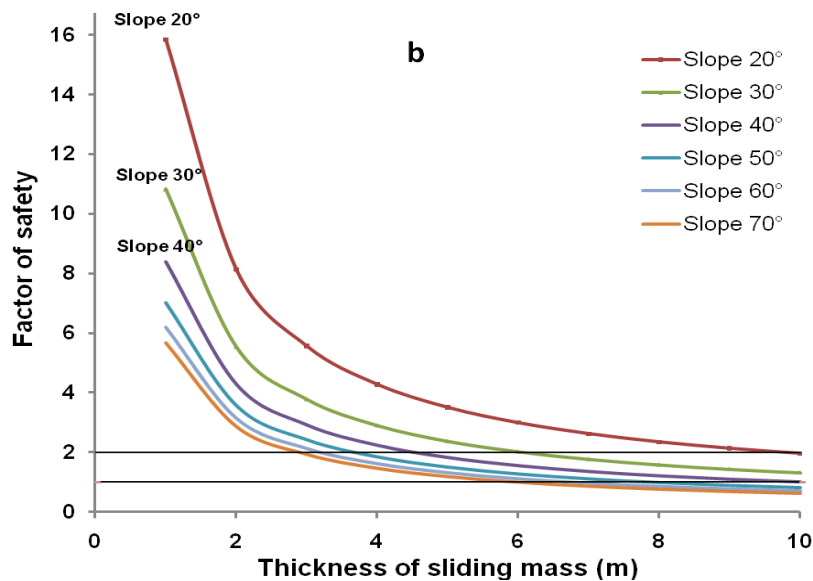


Fig. 3. 24. Calculated factor of safety assuming cohesion to be 67.9 kPa and effective angle of internal friction of 34.2° for weathered lava flow deposits on variable slope with variable thickness of the sliding layer.

Most of the slides observed in the field were recorded on slopes with gradients between 22° and 38° for natural slopes on basaltic flows and up to 40° on the pyroclastic materials. Slides on higher slopes were associated with human intervention. From the calculated factors of safety, it is evident that failure on these slopes is attributable to another mechanism than simple loading. Considering that the depth of the soil column measured at the main scarp of the Makuka slide was 3 m on a 26° slope, and 6 m on a 33° slope at Mabeta, their corresponding factor of safety are 1.2 and 4.45 respectively, which is greater larger than 1 and thus will be marginally stable and stable, respectively. However, because they failed, it is postulated that failure was caused by another mechanism than pure loading on low strength soils and thus propose that failure should be attributed to the presence of fracture permeability, which is readily explained based on field evidence that rocks in this area are highly fractured and weathering is not uniform. Through fractures located somewhere up slope, water is fed into the underlying more fractured and permeable layer (saprolite), where it results in the development of positive pore pressure, forcing the overlying clayey soils to move. This process is explained in detail hereafter.

3.7 Sliding mechanism

Rainfall is an important triggering factors for landslide occurrence. Rainwater infiltration can result in changes in the level of ground water table. It may also result in a decrease in soil matrix suction and the development of positive pore pressure, as well as raising soil unit weight and thus reducing shear strength in rocks and soils. From measured index properties, the sliding mechanisms can be determined. Based on results from the geotechnical properties of the soils, two mechanisms have been proposed to explain the sliding mechanism of different landslides on the SE foot-slope of MC: the fracture permeability model and the human induced rain triggered mechanism.

3.7.1 Fracture permeability mechanism model

Assuming that the permeability of soils, irrespective of the parent material, is driven by macropores and micropores, soil saturation during rainfall can proceed from two fronts. During rainfall events, saturation proceeds from the surface down the profile due the infiltration of rainwater through the macro- and micropore network, resulting in the propagation of a

downward wetting front. The migration of water through the macropores (fractures) is faster, particularly if the fractures are interconnected. Through these fractures, water easily penetrates into a more permeable layer overlain by a low permeability clay horizon. The lower permeability of the upper clayey soil will instead enhance the generation of surface runoff. Rapid infiltration through fractures may facilitate the development of a perched saturated zone in the underlying more permeable saprolite, particularly in areas where fracturing and weathering are not uniform. Intense and prolonged rainfall may also result in rapid changes in the ground water level creating an upward wetting front that is prevented from rising freely by the presence of the overlying impermeable layer. This will result in the development of positive pressure in the more permeable saprolite that enhances up lift and mobilizes the overlying soil column.

The lower permeability of the overlaying soils tends to retard infiltration and provide a conductive environment for the generation of positive pressure at the soil/saprolite interface because of the permeability contrast that inhibits the propagation of pressure dissipation. One can assume that this positive pressure in the silty saprolite develops hydrostatically under the level where this layer is saturated. This can cause an uplift pressure on the upper clay soil reducing the factor of safety of the slope. Notwithstanding, the amount of pressure required and the time it takes for it to build up was not quantified in this study. The downward wetting front on the other hand, causes a decrease in matrix suction to the extent that suction may reduce to zero, particularly when the two fronts meet and the soil becomes fully saturated and fails. As suction decreases, the shear strength also decreases and the soil may end up in failure. A sketch of the stages involved in this process is presented in Figure 3.25.

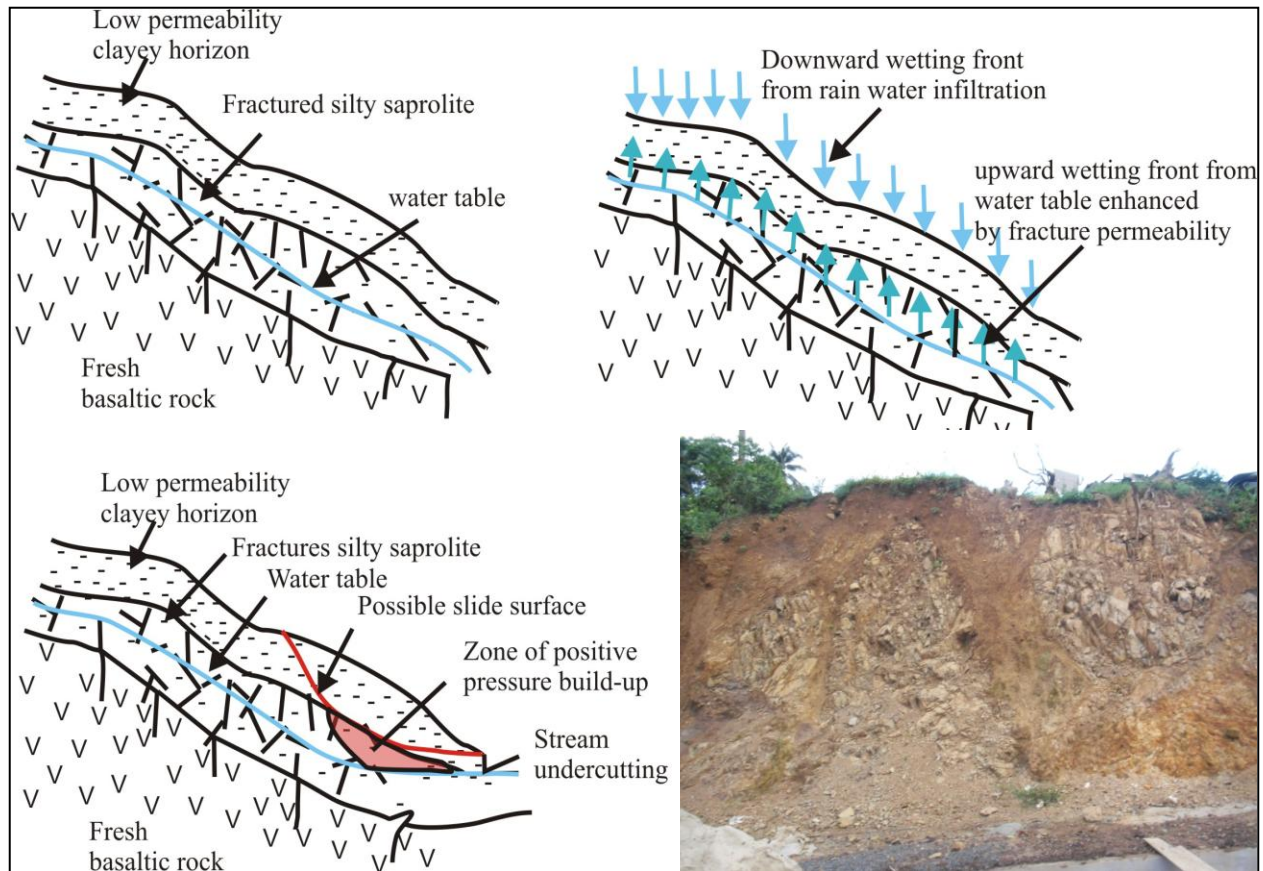


Fig. 3. 25. Sketch of the steps and processes involved in the proposed fracture permeability sliding mechanism.

3.7.2 Human induced, rain triggered mechanism

Calculated factors of safety indicate that in the absence of external forces, pyroclastic cones are always stable. As earlier mentioned, stability comes from the fact that they are formed from the deposition of volcanic ejecta such that the particles are laid down at their angle of repose (which is defined as the maximum angle to the horizontal at which rocks, soil, or loose material will remain without sliding) which is controlled by the degree of grain-grain chaining between adjacent highly irregular-shaped particles (Riedel *et al.*, 2003).

As time goes by, weathering processes set in and will change the properties of the rock. The rock may become more porous due to the dissolution of minerals, individual mineral grains are weakened and bonding between grains is lost resulting in decreasing shear strength. In addition weathering products may be leached and deposited or precipitated within pores or at grain boundaries and along fractures, thereby decreasing soil permeability but also creating a cohesion

due to cementation by clay particles. Once significantly thick soil columns are generated, plant growth also adds weight to the soil, thereby increasing the shear stress on the slopes. On the other hand, plants also play an important role in stabilizing the slope as their roots have anchoring capabilities that tend to hold the soils in place. Human interference in the form of excavation and construction either removes load at the base of the slope, or increases the load by construction. Increased load will increase shear stress on the slope and thus exacerbate failure. In the event of continuous and intense rainfall say for two to three days in a row, the soil may absorb water due to high porosity and low permeability, the soils may absorb water and become saturated or result in a change in the natural moisture content. Weight increase and the development of positive pore pressure further weaken the slopes. If the rain persists, a perched water table may develop and act as a lubricate surface on which the top soil glides in a bid to dissipate excess positive pressure and attain a new angle of repose. This mechanism is illustrated in Figure 3.25.

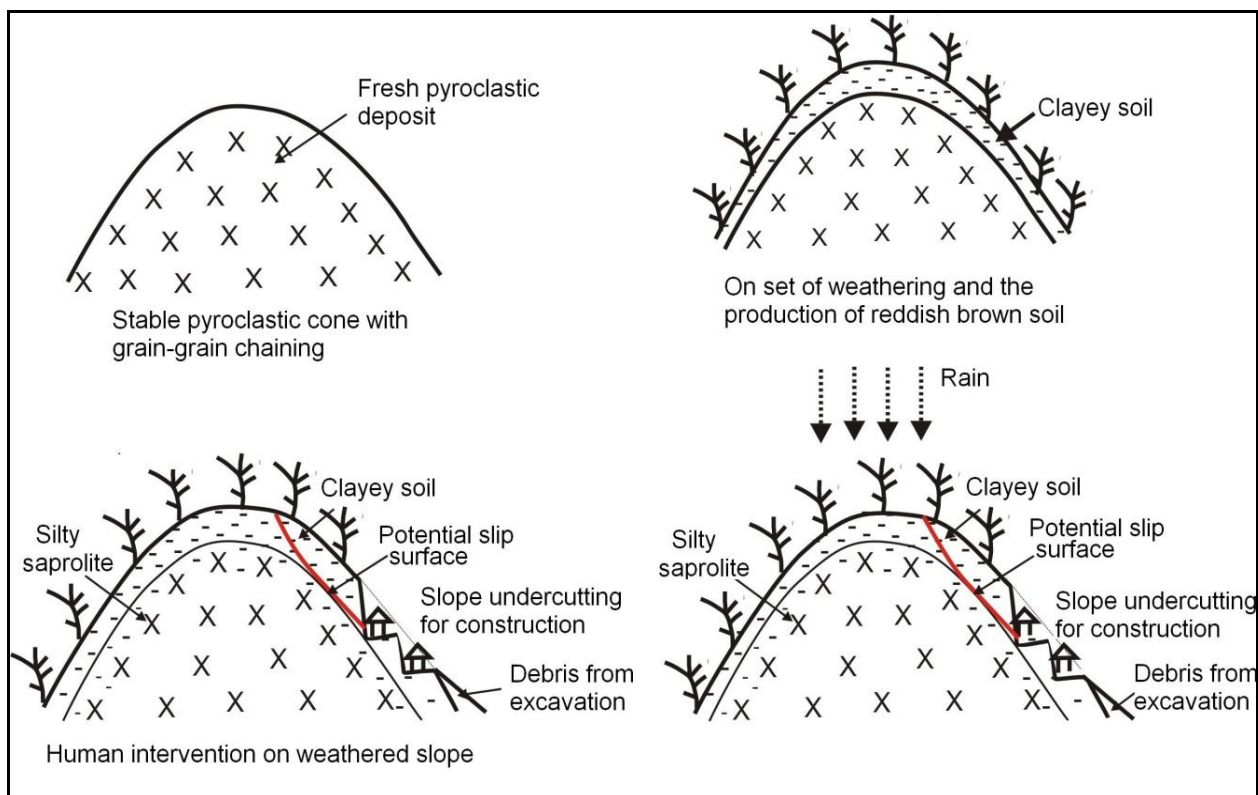


Fig. 3. 26. Sketch of the human induced, rain-triggered landslide mechanism observed in Limbe, particularly on pyroclastic cones.

In the study area, the construction of houses, roads and foot paths, particularly at Unity Quarter, Bonjo and Mabeta, involves the excavation of soil and the creation of small terraces. This soil removal changes the slope line. Above the terrace, the slope angle is much steeper than the particle's angle of repose. However, this vertical cutting may remain stable for a while due to a strong apparent cohesion. The flattened areas cause water stagnation and increased infiltration. The cutting adds stresses on the slope destabilizing the balance between forces that tend to hold the soil in place in favour of gravitational forces. In most cases, the excavated material is piled up down slope at the end of an individual land parcel. Due to changes in compaction and porosity of the excavated debris, the material has a higher potential to absorb large volumes of water. It is also worth mentioning here that moist unsaturated soils have a higher angle of repose because the surface tension between water and the soil particles tends to hold the material in place.

However, if the rate of infiltration exceeds the rate at which water flows through the debris, the liquid limit is reached and even exceeded, resulting in failure because individual particles are completely dismembered and grain-grain frictional contact is lost. This situation is further aggravated when drainage water is deviated into the excavated debris. This mechanism can be used to explain the occurrence of the 2006 slide at Bonduma, and some of the slides recorded at Bonjo.

3.8 Discussion

The study of rainfall-induced landslide mechanisms is one of the most important and difficult issues in landslide research (Hengxing *et al.*, 2003). This is because the engineering, chemical, and mineralogical properties of soils are closely related to the mechanical behaviour of soils at different moisture concentrations, the stress state and stress history. The soils analysed in this study are characterised by high natural moisture content, high particle specific gravity, high porosity, high clay and silt fractions, very high cohesion and angles of internal friction, low bulk density and low permeability. These observations imply good geotechnical performance of soil materials in this region and low susceptibility to failure. According to Sidle (1984), the dynamic conditions of pore water pressure built up during different storm events are directly related to landslide initiations. Therefore, the low permeability of the soils and fracture-enhanced

permeability of the underlying saprolite provides a conducive environment for the development of positive pore pressure and slide initiation. These parameter also suggest that the pyroclastic materials are more susceptible to failure than the lava flows. Considering that the shear strength and permeability was measured on remoulded (disturbed) samples it is possible that the values are over or underestimated as such further analysis on undisturbed samples need to be carried out for comparison and confirmation.

The granulometry curves differ significantly from the ones of sedimentary soils: they are poorly graded (no sedimentation selective classification effect) and made up of a wide range of grains, including sand, silt and clay in the same soil. This may result to a specific soil skeleton with a grain intrication favouring good mechanical properties if undisturbed. For the same reasons, the mechanical behaviour of the residual soils will completely degrade if they become over-saturated. Grain size distributions and textural classification indicate that most of the samples are inorganic silt with high plasticity probably due to the presence of allophane, halloysite and kaolinite in the soils accounting for the high liquid limits but low plasticity indices. The presence of these clay minerals may induce a strong apparent cohesion, not only due to capillarity effects in a wet but unsaturated soil, but also to cementation in relatively dry conditions.

The average particle specific gravity of soils reported in literature is ca. 2.6 g/cm^3 , with a range from 2.4 to 3.6 g/cm^3 depending on the nature of the mineral constituents (Cernica, 1995). In this study the observed G_s is generally higher than the reported mean, ranging from 2.8 to 3.0 g/cm^3 with mean values of $2.9 \pm 0.1 \text{ g/cm}^3$. These higher values can be attributed to the mafic composition of the parent rock rich in iron and magnesium silicates (olivine, pyroxenes) and the presence of magnetic minerals (e.g. haematite, magnetite, goethite, titanomagnetite, see Chapter 4) that are characterized by high specific gravity values and constitute the major opaque mineral phases in rocks of the Mount Cameroon region (Suh *et al.*, 2003; Njome *et al.*, 2008). Particle specific gravity sometimes referred to as particle density of soils gives us an idea about the relative proportion of organic matter and mineral particles present in a soil as well as the chemical composition and structure of the soil minerals.

In literature, most materials from landslide scars plot well above the A-line on a Casagrande plasticity chart (Wen *et al.*, 2007; Yalcin, 2007; Kitutu *et al.*, 2009; Azañón *et al.*, 2010), in

fields characterized by clays of high and/or medium plasticity based on the USCS classification. In this study however, all the samples plot well below the A-line in the field of silt of high and moderate plasticity and compressibility (MH and ML). They are characterised by good engineering properties, an observation that was also noted by Rouse *et al.* (1986) for volcanic soils in Dominica, West Indies. According to standard guides used in the USCS, MH soils of sedimentary origin have poor engineering properties and are considered unsuitable for various engineering purposes. On the other hand, Westly & Irfan in Blight (1997) noted that many tropical residual soils, rich in allophane, kaolinite and/or halloysite plot in the MH field and soils rich in these minerals tend to exhibit very good engineering properties. However, there has not been a clear understanding of why this is the case. Nevertheless, these properties can be attributed to the dominance of kaolinite and halloysite over 2:1 clay as observed on XRD diffraction patterns described in Chapter 4. It can therefore be suggested that another classification scheme is required for tropical residual soils or that the classification of residual soils using the USCS scheme should be treated with caution. From this study, it is noted that the soils have very good engineering properties and will be stable under normal circumstances, thus the occurrence of landslides in this area is attributable to the presence of fracture permeability or to artificial destabilization by human action.

Atterberg's plastic and liquid limits are widely used parameters for determining the consistency of cohesive soils. They provide useful information regarding soil strength, stability, mineralogy, state of consolidation of the soil, and the classification of soils into organic or inorganic clays (Yalcin, 2007). High plasticity indices in soils can be attributed to the presence of clay minerals or the abundance of organic matter content. The plasticity values observed in this study are most likely a contribution from the mineralogy of these soils though contributions from organic matter cannot be completely ruled out for the surficial layers because the area is densely vegetated and rainfall is intense. The plasticity index of the soils ranges from low to high, with a larger fraction showing values above 15 that seem to be non-liquefiable according to Gratchev *et al.* (2006). This probably account for the abundance of slide type failure and rare occurrence of debris flow type failure within the study area.

The LI of all the samples is slightly negative or slightly above zero. Other studies have shown that for remoulded samples when PI is equal to or less than zero the soil is compact, solid and

unlikely to fail by flow (Shakoor & Smithmyer, 2005). When LI is greater than 1, the soil is liquid because its natural moisture content is greater than the soils liquid limit and thus the soil is in an open and non compact state. Excavation or compaction of such slopes is subject to severe strength loss. Samples with LI greater than 1 were not observed in this study. In in situ residual soils, weathering might result in a relatively strong porous soil structure that can hold large proportions of entrapped water. When these soils are remoulded or disturbed by construction, the structure collapses and the water is realised resulting in severe weakening of the soils. The samples analysed in this study, therefore, will behave as brittle solids and are unlikely to fail by flow type movement unless large amounts of water is added (Shakoor & Smithmyer, 2005). This probably accounts for the reduced number of flow type failures observed in the study area. According to Campbell in Shakoor & Smithmyer (2005) shallow storm induced slides require three conditions to occur: a mantle of colluvial soil, a steep slope and soil moisture equal to or greater than the liquid limit of the colluvial soil. These conditions are easily attainable within the study area, particularly on the Limbe-Mabeta massif, presumed to be an older volcanic structure that is now characterised by thick soil columns due to prolonged weathering relative to the lower foot slopes of Mt Cameroon. Sliding is not very rampant because of the mineralogy of the soils. In the field, water was observed oozing out at the contact between saprolites and the soil after rainfall events, thereby confirming the existence of temporal aquifers. Eyewitness accounts of the Mabeta landslide also reported an increase in ground water discharges below foundation of some houses prior to the landslide, suggesting the emergence of pressurised ground water. This goes ahead to support the fracture permeability mechanism. Furthermore, sections observed along road cuts indicate the presence of dense fracturing and non uniform weathering in this area.

3.9 Conclusion

From the geotechnical point of view, the following conclusions may be drawn:

- Soils within the Limbe area have good geotechnical properties and will be stable under normal and/or natural circumstances but failure may be enhanced by human activities and fracture permeability.
- The good geotechnical properties of the soils in the Limbe area can be a possible explanation why large landslides are rare and why the number of landslides is not very

rampant as would be expected in other areas characterised by poorer geotechnical properties.

- Index and geotechnical properties of the soils can be used as a fingerprint or a proxy from which the sliding mechanism can be deduced.
- Based on the present results, two sliding mechanisms have been proposed to explain the occurrence of landslides within the area. Sliding can take place through the influence of fracture permeability or differential permeability with depth, and/or can be human induced and rain triggered. Other conceptual models are also possible for example the influence of vegetation change on the extent of soil saturation and sliding might also exist, but this needs to be investigated in detail to better constrain the processes involved. Like wise the fracture permeability model proposed in this study needs to be tested and to establish how much pressure and the duration required for the appropriate amount of pressure to develop.

Chapter Four

Mineralogy, chemistry and element distribution in landslide prone-soils

4.1 Introduction

Soils contain both primary minerals derived from the solidification of magma and secondary minerals produced from the weathering of primary mineral and glass phases. The primary minerals can provide insights into the origin/provenance of parent rocks and weathering rates. Secondary minerals on the other hand may strongly influence the physical and chemical properties of the soil (Harris, 2007), potentially resulting in the swelling of clays or the concentration of clays along slip surfaces and ultimately resulting in the occurrence of landslides. Weathering thus contributes significantly in the localisation of landslides because it affects the engineering properties of the rock and soil by reducing both strength and stability (Vaughan *et al.*, 1988). Many researchers have attempted to link specific clay minerals to landslide susceptibility (e.g. Shuzui, 2001; Duzgoren-Aydin *et al.*, 2002; Azañón *et al.*, 2010) while others associate the occurrence of landslides to the accumulation of clays in relict joints (e.g. Prior & Ho, 1972; Parry *et al.*, 2000). It has also been proven that clay mineralogy and chemistry provide indicators of potential sliding plane conditions (Shuzui, 2001; Zheng *et al.*, 2002; Wen *et al.*, 2004; Kitutu *et al.*, 2009). For these reasons, mineralogical and chemical characterisations of soils were incorporated in this study to enhance the understanding of the processes at work in the landslides. In addition, it offers the potential to gain insight into weathering rates and element distribution patterns of some major and trace elements during weathering.

4.2 Mineralogical characterisation

Mineralogy controls the sizes, shape and surface characteristics of soil particles. Mineralogical interaction with fluid phases determine the geotechnical properties (plasticity, swelling, compression and shear strength of soils as well as the hydraulic conductivity) and susceptibility of soils to failure. Mineralogical characterisation is thus vital in the understanding of the geotechnical performances of soils. Several techniques have been used for the mineralogical characterisation of soils such as differential thermal analysis and scanning electron microscopy, but X-ray diffraction (XRD) is the technique most heavily relied on in soil mineralogical analysis

(Harris, 2007). This technique provides information about the atomic structure of crystalline substances and is thus a powerful tool for the identification of minerals in soils particularly because clay size particles are too small to allow for the application of standard optical crystallographic techniques (Harris, 2007). In this study, 17 bulk samples (10 from the main scarp and 7 from the pits described in chapter 3) were collected from landslide scars and some of their oriented clay fractions were analysed. Table 4.1 lists the samples on which mineralogical analysis was performed.

Slide No /Locality name	Sampling site within the scar	Sample name	Colour	Description
1 Bonjo	Main scarp	SBS – 01 [#]	5Y8/2	Pale yellow
		SBA - 01 [#]	5Y7/3	Pale yellow
		BBS - 01 [#]	2.5Y8/4	Pale yellow
20 Bonjo site 2	Main scarp	BAS – 02 [#]	10YR3/6	Dark yellowish brown
		BSS – 02 [#]	2.5YR4/3	Weak red
2 Mandoli	Main scarp	MSS - 03 [#]	5Y7/2	Light gray
		MSD - 03 [#]	2.5Y7/6	Yellow
		MHB - 04 [#]	2.5YR3/6	Dark red
		MHC - 04 [#]	7.5YR3/4	Dark brown
13 Mabeta	Pit 4	MSS – 04 [#]	7.5YR4/4	Dark brown
		Assumed slip surface		
		P4S11*	7.5YR4/4	Mottled dark brown
		P4S12*		
		P4S13*		
12 Makuka	Pit 6	P6S17*		Olive brown
		P6S18*	5Y6/4	Pale olive
		P6S19*	5Y6/4	Gray
		P6S20*	10YR6/1	Gray

Table 4. 1. Description of samples used for XRD analysis: [#] both bulk sample powder and clay fraction were analysed, * samples of which only the bulk sample powder was analysed.

Most of the soils are dark red, reddish brown to light coloured pale yellow silts, clayey silts and clay overlying gray to purplish saprolite. Details on morphological descriptions and the physico-mechanical properties of the soil horizons are given in Chapter 3. Samples were collected from several horizons along a vertical channel cut into the walls of the pits or at the head scarp, placed in plastic bags for mineralogical and chemical analysis. It is worth mentioning that the humus layer was not taken into consideration in this study.

Bulk sample powders provide a general picture of the mineral species present in the sample while oriented clay fractions are used to identify the clay minerals present. These analysis were done at the Laboratory for Soil Science at the Department of Geology and Soil Science, Ghent University, Belgium using a Philips X'PERT SYSTEM with a PW 3710 based diffractometer. The diffractometer is equipped with a copper anode ($\lambda = 1.54 \text{ \AA}$), a secondary graphite beam monochromator, a xenon filled detector and a 35 position multiple sample changer. The secondary beam section of the diffractogram is made up of a 0.1 mm receiving slit, a soller slit and a 1° anti scanner slit. The tube is operated at 40 kV and 30 mA and diffractogram collected in a θ , 2θ geometry from 3° to 60° to provide enough X-ray diffraction peaks to identify most common minerals present in the soil. Irradiation time is set at 12 mm and incident beams are automatically collimated.

Sample preparation and analysis

For the bulk sample analysis, the samples are simply air-dried at room temperature, milled into fine powder to minimise the orientation preference and maximised sample representativeness. The sample powder is then bombarded with X-rays to obtain the general mineralogical composition. For the oriented fractions, samples are air dried and sieved through a stack of sieves to obtain the fraction smaller than $63\mu\text{m}$. This fraction is then saturated with 2 % sodium bicarbonate for at least 8 hours to ensure complete disaggregation of the clay fractions. After saturation and disaggregation, NaCl is added to the mixture and allowed to flocculate for another 8 hours. A small fraction of the supernatant is periodically pipetted out and clays washed by centrifugation. The clay fraction is then extracted and oriented by drying aliquots of the suspension on glass slides. Prior to XRD analysis, the clay residues are saturated with Mg^{2+} by repeated washing with normal solutions of MgCl (magnesium chloride) and $\text{Mg}(\text{OAc})_2$ (magnesium acetone). Excess of the saturation solution is washed out with acetone and alcohol until free of Cl⁻. The Mg-saturated clay slides are later solvated in a vacuum in an atmosphere of ethylene glycol.

It is observed that the diffractogram patterns for the whole samples are characterized by a lot of background diffraction. However, they display the general mineralogical characteristics of the soil whereas those from the oriented samples show smoother peaks with less background and are

used to identify some specific clay minerals present in the sample. Peak areas and d-spacings were automatically calculated by a software package attached to the diffractometer and matched with those of pure minerals from a computer database by an automatic mineral matching function to identify the mineral species present within each sample. These automatically generated results were corrected by expert interpretation of the generated peaks and confirmed by comparing the calculated d-spacing with those on the Mineral Powder Diffraction File compiled by the International Centre for Diffraction Data. The d-spacing is calculated from Bragg's equation given by

$$n\lambda = 2d \sin\theta$$

where n = is an integer number
 λ = wavelength of incident wave
 Θ = diffraction angle and
d = spacing between planes in the atomic lattice

Peaks at 14 - 15 Å in the Mg-saturated samples that expand to 17.7 - 18.0 Å after glycolation were used to identify smectites, 9.9 - 10.1 Å peaks in the Mg-saturated and glycerol solvated samples are used to identify illite, 7.1 - 7.2 Å peak in both Mg-saturated and glycolated samples represent kaolinite (Moore *et al.*, 1989). 7.3 - 7.4 Å peaks represent dehydrated halloysite, 3.51 and 1.89 Å peaks represent diffraction peaks for anatase, 4.18 and 2.45 Å represent goethite, 2.96 - 2.99 Å augite, 2.54 and 1.72 Å ilmenite, and 2.52 Å pyroxene (enstatite). The goal of these analyses was to determine the mineralogical composition of the soils from the area affected by landslides. These results are presented on Table 4.2.

4.3 Chemical characterisation

The engineering behaviour of soils does not only depend on the stress state and history but also on the state of weathering. Hence it is essential for engineering geologists to quantify the changes that take place during weathering (Ceryan, 2008) which could be expressed as changes in the chemistry of the parent material. Weathering indices (an approximation of the degree of weathering) represent one of the most widely used ways of quantifying chemical changes in rocks. These indices have been used to quantify the engineering properties of regoliths (Duzgoren-Aydin *et al.*, 2002) although they mostly provide a better understanding of element mobility during weathering. The mobilization and redistribution of elements may follow various pathways as different elements are affected differently by various pedogenic processes including dissolution of primary minerals, formation of secondary minerals, redox processes, transport of

material, and ion exchange (Middleburg *et al.*, 1988). Birkeland (1999) proposed that elements released by weathering may or may not be redistributed down-slope as a function of their mobility under constant or changing geochemical environments along the slope. Therefore, to understand the weathering patterns and the behaviour of geochemical elements during weathering within the study area, the chemical composition of 3 fresh rock and 6 soil samples was analysed and results are discussed in detail here below.

The distribution and mobility of major and some trace elements within the study area was assessed from three locations, Bonjo, Mabeta New Layout and Makuka, respectively from Pits 1, 2 and 6 described in Chapter 3. Because the pits did not reach the bedrock, fresh rock samples were collected from outcrops located at the lower reaches of the scars, along the banks of streams, or from fresh rock fragments observed within the slide debris.

Whole rock (WR) major and trace element composition was determined by Inductively Coupled Plasma - Optical Emission Spectroscopy (ICP-OES) at Ghent University, using the equipment housed at the Department of Analytical Chemistry. Soil samples were dried overnight at 40 °C while rock samples were sawed to obtain fresh pieces and crushed into finer fragments with a jaw crusher. Crushed rocks and soil samples were pulverized in an agate ball mill. About 4 g of each powder was dried at 105 °C and Loss on ignition (LOI) was determined by heating at 850 °C for two hours. After LOI determination, ~ 0.2 g of the sample was homogenised and fused with 1 g of 50/50 lithiummeta-/tetraborate flux (AccuSpec Ultrapure) with a sample/flux ratio of 1:5 in high purity graphite crucibles. The resulting glass was dissolved in 2 % HNO₃ for analysis with a Spectro Arcos ICP-OES (for Al, Ca, Fe, K, Mg, Na, P, Mn, Ti, Si and selected trace elements: Ba, Sr, Zr, V, Cr, Ni, Ce, Y, Sc and Co). Calibration lines were produced by analysis of rock standards, dissolved following the same procedure. BHVO-2, AGV-2, QLO-1, GSP-2, from the USGS (US Geological Survey), JSy-1, JB-2, from the Japanese Geological Survey, and NIM-L from Mintek, South Africa were used as standards. Calibration lines were produced by analysis of rock standards, dissolved following the same procedure. Care was taken that the rock standards bracketed the elemental composition of the unknowns. Accuracy of the analysis was monitored by the analysis of secondary rock standards, different from those used for the calibration line. Major elements are accurate within 2 % relative. The accuracy for trace elements above 10 ppm is better than 10 %.

Chemical transformation and element losses and gains that accompany physical breakdown of the parent rock into soils was quantified by parent normalisation, that is, the ratio of elemental concentration of the soils and saprolites to their concentration in the fresh rock. Parent normalisation is based on the following assumptions:

1. The system is open and all elements are mobile.
2. The fresh rock sample can be taken as a reference and
3. Relative enrichment of a certain element is calculated by normalizing the concentration of the element within the soils and saprolites to that in the parent rock. If the normalized value is greater than 1, the element is enriched, if it is less than 1 it is depleted.

The chemical mass balance model proposed by Brimhall *et al.* (1985) and Brimhall & Dietrich (1987) was not applicable in this case because all the elements analysed for in this study were mobile. Instead, the density of the samples was used as a proxy to the degree of weathering assuming that the soils formed by isovolumetric processes. Percentage changes were calculated according to the following relation (Millot & Boniface, 1955)

$$\text{Mass losses \% change} = \left[\frac{C_w \cdot \gamma_w}{C_p \cdot \gamma_p} - 1 \right] \times 100$$

where C is the concentration of any element, γ is the bulk density while w and p represent the weathered and parent rock, respectively.

The Magnesium number (Mg#), given by:

$$\text{Mg\#} = \frac{100\text{MgO}}{\text{MgO} + \text{FeO}}$$

with FeO calculated as $0.9 \times \text{Fe}_2\text{O}_3^*$ (Fe_2O_3^* total iron), was determined and used to estimate the degree of evolution of the magmas that produced the various parent rock types. It is worth noting that Mg# is calculated on a molecular basis.

Weathering indices such as the Chemical Index of Alteration CIA, the Vogt Residual Index, and the silica/alumina ratio (Ruxton ratio) given by the following equations were calculated to estimate the extent of weathering within the profiles.

$$CIA = 100 \times \left(\frac{Al_2O_3}{Al_2O_3 + CaO + Na_2O + K_2O} \right) \quad \text{Nesbitt \& Young (1982)}$$

$$V = 100 \times \left(\frac{Al_2O_3 + K_2O}{MgO + CaO + Na_2O} \right) \quad \text{Vogt (1927)}$$

$$\text{Ruxton ratio} = \left(\frac{SiO_2}{Al_2O_3} \right) \quad \text{Ruxton (1968)}$$

The calculation of these indices is done on the molecular proportion of the metal oxides based on the assumption that the distribution of chemical elements along the profile is mainly regulated by the degree of weathering (Duzgoren-Aydin *et al.*, 2006).

4.4 Results

4.4.1 X-ray diffraction

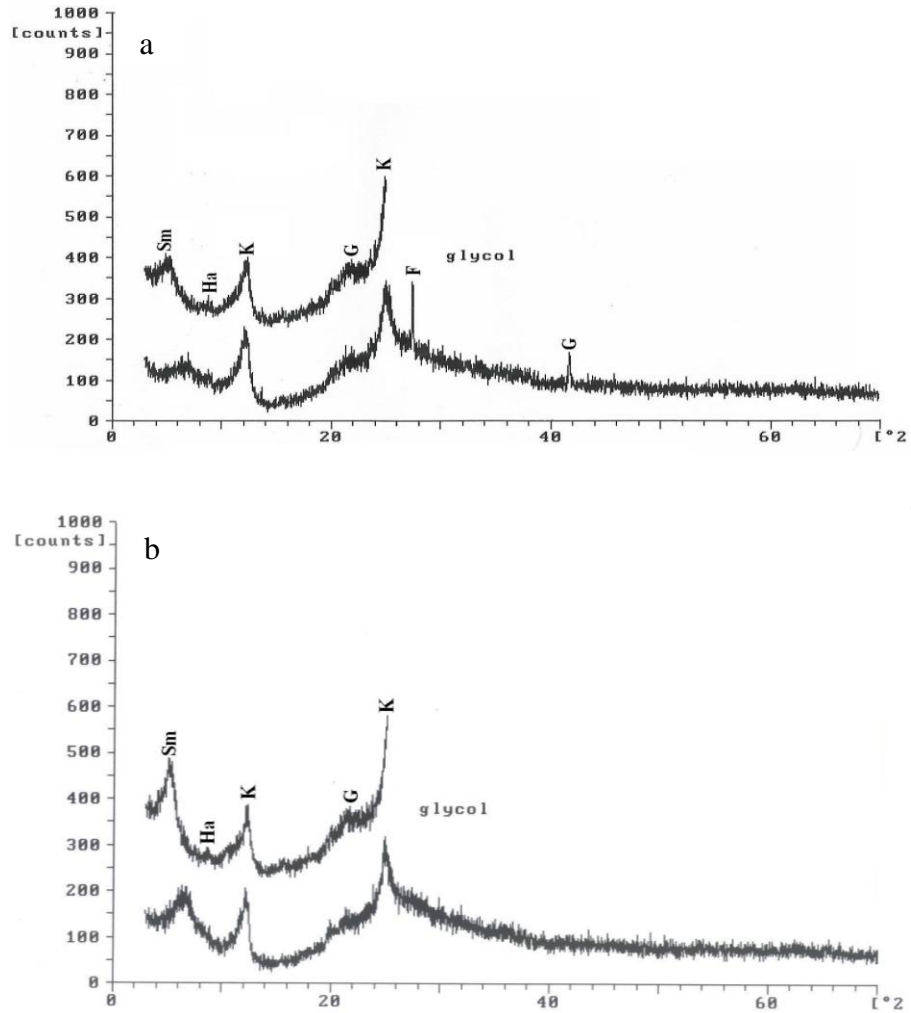
Bulk mineralogical compositions of the samples analysed in this study are given in Table 4.1. Examples of some of these diffractograms are given in Figures 4.1 to 4.6. Diffractograms from samples MSS-03 and MSD-03 from horizon B and C at Mandoli, P2S11, P2S12, and P2S13 from Mabeta New Layout are not discussed in this section due to their similarity with described diffraction patterns but are included in Appendix 5. Their mineralogy is also summarised in Table 4.1 below.

The Mg saturated clay fraction from Bonjo shows the presence of four dominant peaks: at 15 Å, 9.9 Å, 7.2 Å and 5.6 Å, with a minor peak at 3.6 Å for samples above, on and below the slip surface. Two extra peaks at 3.25 Å and 2.17 Å appear for the sample below the slide surface. After glycolation, the 15 Å peak shifts to a higher angle of ~17.2 Å indicating the presence of smectites. The 7.2 Å peak indicates the presence of kaolinite or dehydrated halloysite since the peak does not move to a higher value after glycolation. The 9.9 Å peak can be interpreted as a second order peak of smectite because it only appears after glycolation. A very low intensity goethite peak at 4.1 Å is also noted.

Sample name	SBA-01	BSS-01	BBS-03	BAS-02	BSS-02	MSS-03	MSD-03	MHB-04	MHC-04	MSS-04	P2 S11	P2 S12	P2 S13	P6 S17	P6 S18	P6 S19	P6 S20
Description	Pale yellow	Pale yellow	Pale yellow	Dark yellowish brown	Weak Red	Light gray	Yellow	Dark red	Dark brown	Dark brown	Dark brown	Dark brown	Dark brown	Olive brown	Pale olive	Gray	Gray
Moist Colour	5Y 8/2	5Y 7/3	2.5Y 8/4	10YR 3/6	2.5Y R 4/3	5Y 7/2	2.5Y 7/6	2.5Y R 3/6	7.5Y R 3/4	7.5Y R 4/4	7.5Y R 4/4	7.5Y R 4/4	7.5Y R 4/4		5Y 6/4	5Y 6/4	10Y R 6/1
Magnetite	-	-	-	-	-	X	-	X	X	X	X	X	X	X	X	X	X
Goethite	-	X	X	X	X	X	X	X	X	-	-	-	-	X	X	X	X
Ilmenite	X	-	X	-	X	X	X	X	X	-	-	-	-	X	X	X	X
Hematite	-	X	-	-	X	-	-	X	-	-	X	X	X	-	-	-	-
Plagioclase/ Feldspar	X		X	?	?	X		X	-	-	-	-	-	X	X	X	X
Olivine	-	-	-	-	-	-	-	-	X	-	-	-	-				X
Smectite	X	X	X	X	X	X	X	-	-	X	-	-	-	X	X	X	X
Halloysite/ dehydrated halloysite	X	X	X	X	X	X	X	X	-	X	X	X	X	X	X	X	X
Kaolinite	-	X	X	X	-	X	X	X	-	X	-	-	-	X	?	?	X
Sanidine	X	X	X	-	-	X	-	-	-	-	-	-	-	X	X	X	X
Anatase	X	X	-	X	X	-	-	-	?	-	-	-	-	X	X	X	X
Pyroxene		X	-	-	-	-	-	X	?	-	-	X	X	-	-	-	-
Mica	-	-	-	-	-	-	-	-	X	X	X	X	X	X	X	X	X

Table 4. 2. Mineralogical composition of bulk samples and oriented clay fractions: X = mineral present, - mineral absent, ? = presence of mineral inferred. Colour characteristics were determined from Munsell soil classification. SBA-01, BSS-02, BBS-03 represent soil samples from Pit 1 at Bonjo, BAS-02, BSS-02 are samples from the B and C horizons of an older slide at Bonjo, MSS-03, and MSD-03 from B and C horizon at Mandoli, MH-04, MHC-04, MSS-04, for samples from the B, C and presumed slide surface at Mabeta New Layout, P2S011, P2S12, P2S13 from Pit 2 at Mabeta New Layout, and P6S17, P6S18, P6S19 and P6S20 from Makuka.

The sample above the slip surface shows a slightly more intense non-swelling clay peak at 7.2 Å relative to the swelling clays while that from the slip surface show a more intense smectite peaks. Samples below the slip surface show almost an equal proportion of swelling and non-swelling clay peaks as seen in Figure 4.1



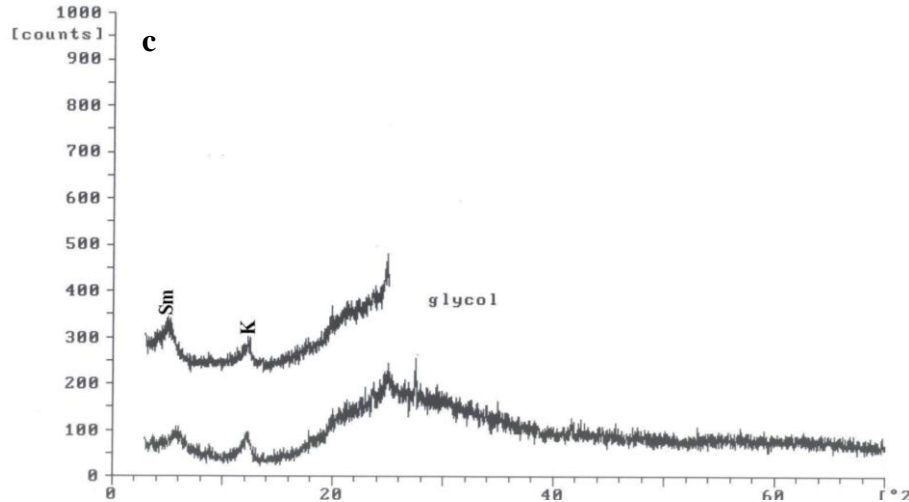


Fig. 4. 1. X-ray diffraction patterns of oriented clay fractions of the 2005 landslide at Bonjo after Mg^{2+} saturation and glycolation: a) from above the slide surface, b) on the slip surface and c) below the slip surface Sm: smectite, K: kaolinite; Ha: halloysite; G: goethite and F: feldspars

It is also observed that the intensity of these peaks decreases down the profile suggesting a decrease in the amount of clay minerals as one moves down the profile. This is contradictory to grain size data described in Chapter 3 where an observed increase in the clay size fraction with depth was observed. Whole sample powders indicate the presence of sanidine (6.50 Å, 3.7, 3.46, 3.30, 3.2 Å, 1.7 Å), anatase (3.51 - 3.53 Å, 1.89 Å), augite (3.2 Å), in addition to the above mentioned clay minerals. The abundance of the clay minerals decreases down this profile with maximum values observed in the samples above the slip surface: and minimum intensities below the slip zone diffractograms indicate that clay *mineralogy* shows no fluctuation with depth. It is observed that the intensity of the peaks of non-clay minerals increases down the profile with maximum intensities for sanidine observed in the samples below the slip surface (Fig. 4.2).

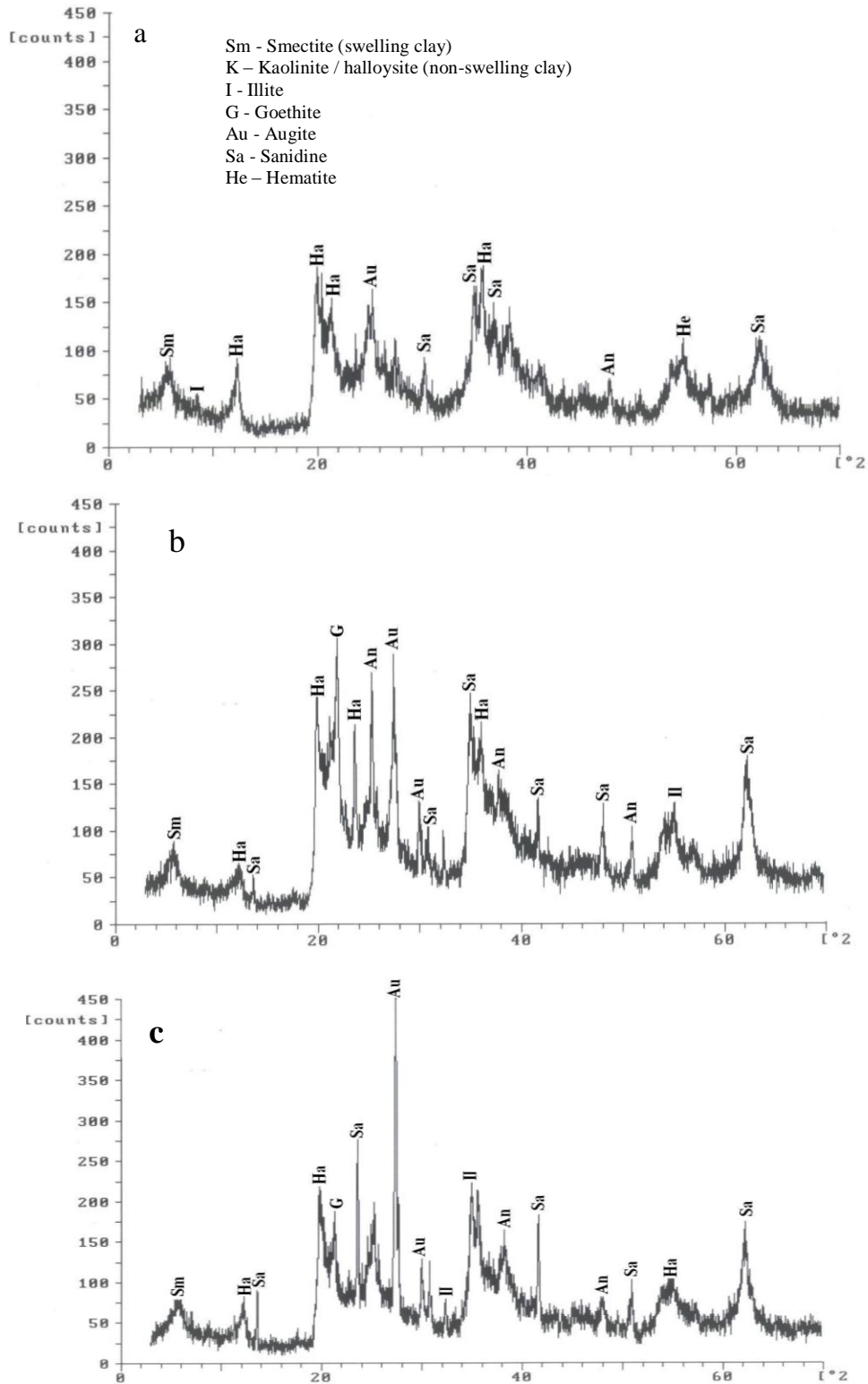


Fig. 4. 2. X-ray diffraction patterns of random soil powders of the 2005 landslide at Bonjo: a) from above the slide surface; b) on the slip surface and c) below the slip surface.

Oriented clay fractions prepared from samples BAS-02 and BSS 02 from two horizons at the head scarp of an older slide (Slide 20 in the inventory) at Bonjo suggest the dominance of smectite (swelling clays) evidenced by the presence of a very pronounced peak at 12.5 Å which expands to 16.7 Å after glycolation. Relatively lower intensity peaks occur at 7.20 Å, 4.4 Å, 4.16 Å, 3.58 Å and 3.10 Å for the magnesium treated samples, representing kaolinite, halloysite and goethite, respectively. After glycolation, the 7.2 Å peak degenerates, producing peaks at 8.45 Å (a second order reflection peak of smectite) and 7.20 Å, both with lower intensities. This implies that the peak at 7.2 Å before glycolation was a contribution from smectites and kaolinite. The peak at 5.64 Å after glycolation is the third order reflection peak of the smectite (Fig. 4.3b, c). These patterns indicate the dominance of swelling clays over non-swelling clays in this profile. There is no visible difference in the mineralogy at both horizons.

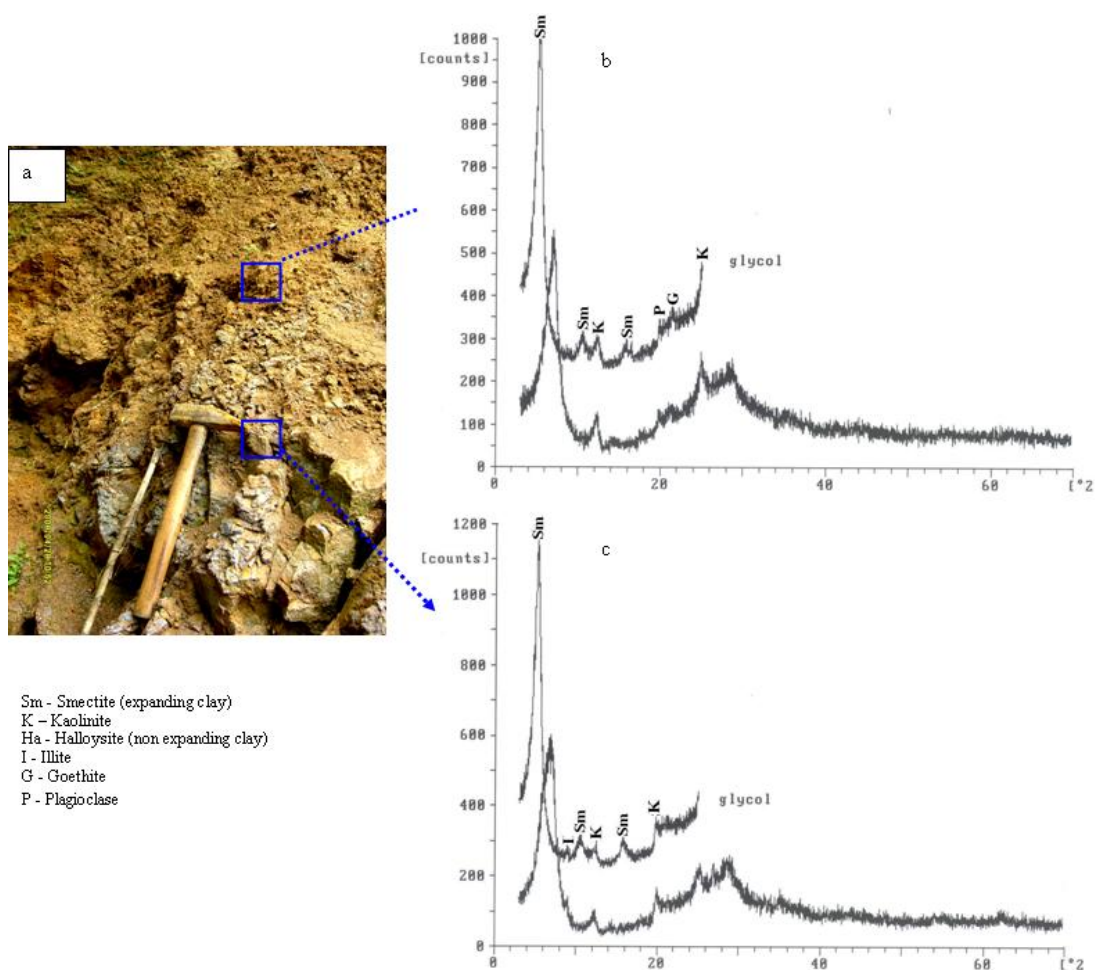


Fig. 4. 3. a) Picture of the head scarp. X-ray diffraction patterns of oriented clay fractions of slide 22 at Bonjo after Mg^{2+} saturation and glycolation: b) from B horizon and c) from the C horizon. Note the high intensity peak of the swelling clay minerals and visible colour and textural variation between the horizons.

In the Mabeta area, soils were collected from the main scarp based on observable differences in colour and texture (MHB-04, MHC-04 from the B and C horizons) and an assumed sliding plane (MSS 04). The clay fraction from this profile shows low intensity peaks at 7.3 \AA after treatment with Mg and glycolation, indicative of kaolinite and/or dehydrated halloysite. After glycolation, a low intensity peak between $16.7 - 17.0 \text{ \AA}$ is observed in all the samples suggesting the presence of minor amounts of smectites. From the diffractograms (Fig. 4.4), it is clear that the amount of clay minerals is minimal and that there are no obvious differences in the mineralogical composition of the soil in the different horizons.

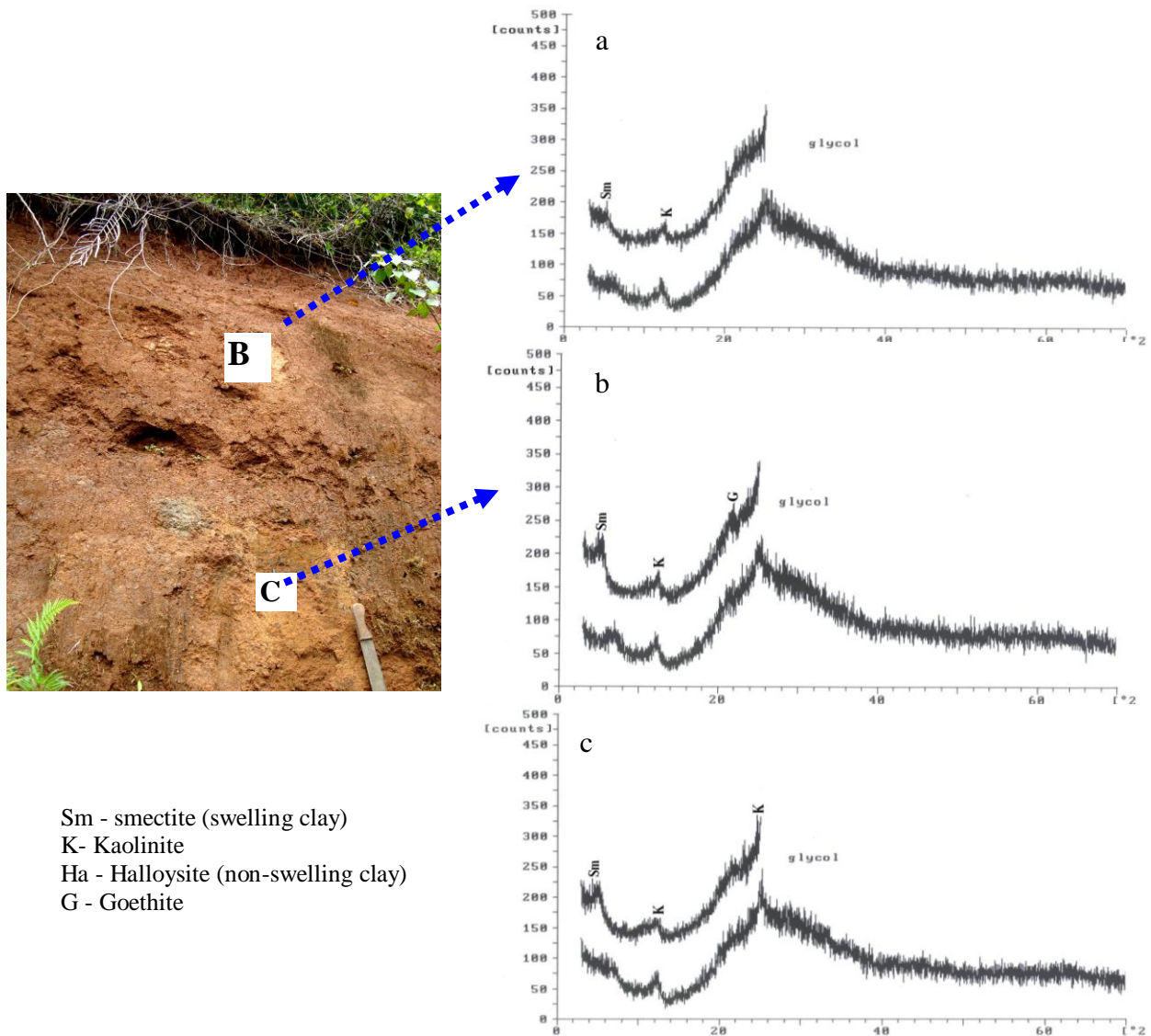


Fig. 4. 4. X-ray diffraction patterns of Mg saturated and glycolated oriented clay fractions of soils from: a) the B horizon; b) the C horizon and c) slip surface at Mabeta New Layout. No dominant clay minerals are observed except for minor kaolinite peaks.

As one descends to the B horizon an indistinct Sm peak is observed which becomes even more prominent in the sample collected from the assumed slip surface. XRD patterns for the bulk soil powders (Fig. 4.5) indicate the presence of dehydrated halloysite and/or hydrated halloysite (4.48 Å), goethite (4.15 Å), magnetite (2.96 Å), augite (2.18 Å), hematite (2.69 Å, 2.57 Å) and ilmenite (1.72 Å). Magnetite (1.61 Å, 1.48 Å) and a very low dehydrated halloysite (7.33 Å, 3.56 Å) peak are observed in the C horizon (Table 4.1, Fig. 4.5).

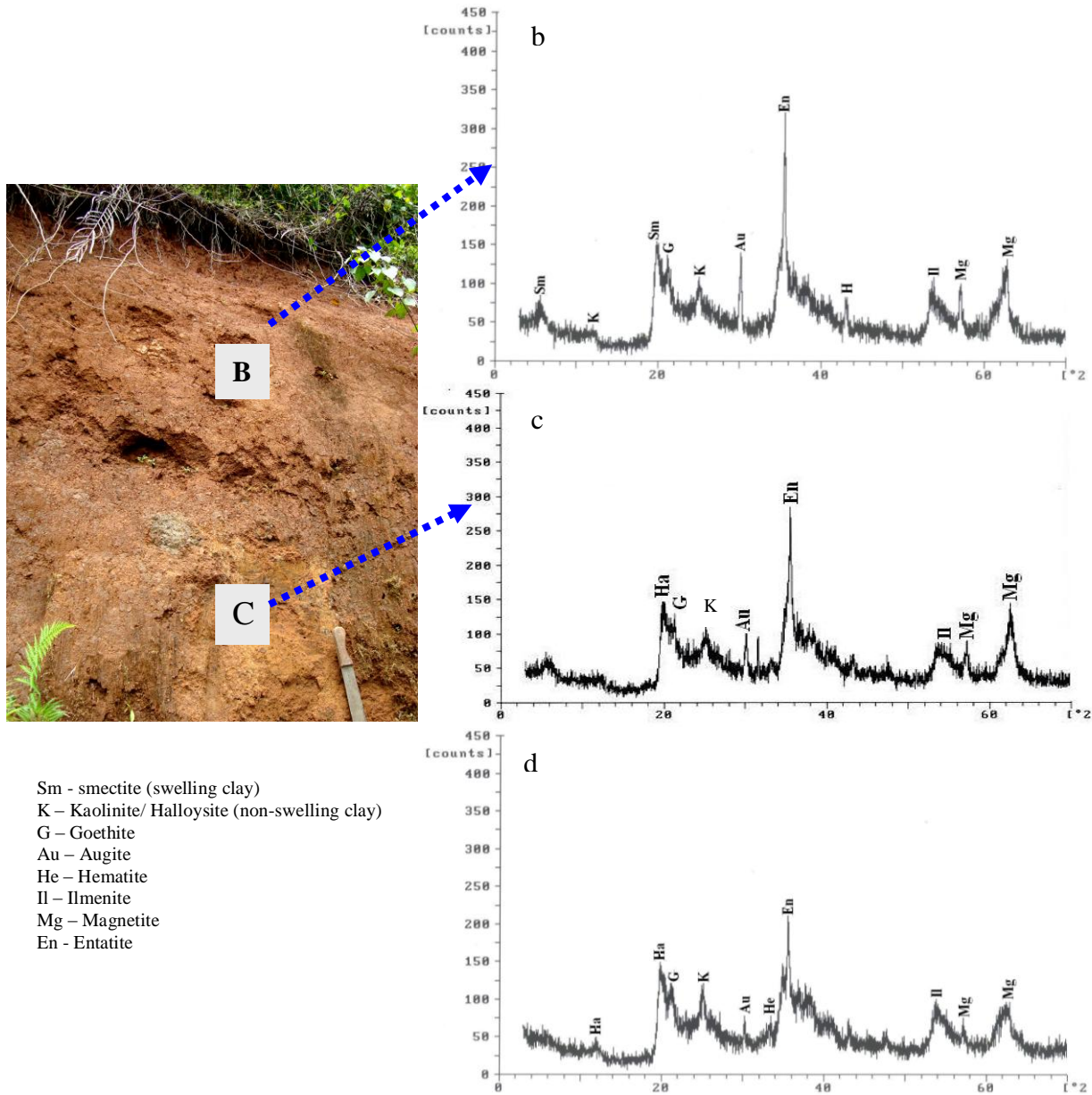
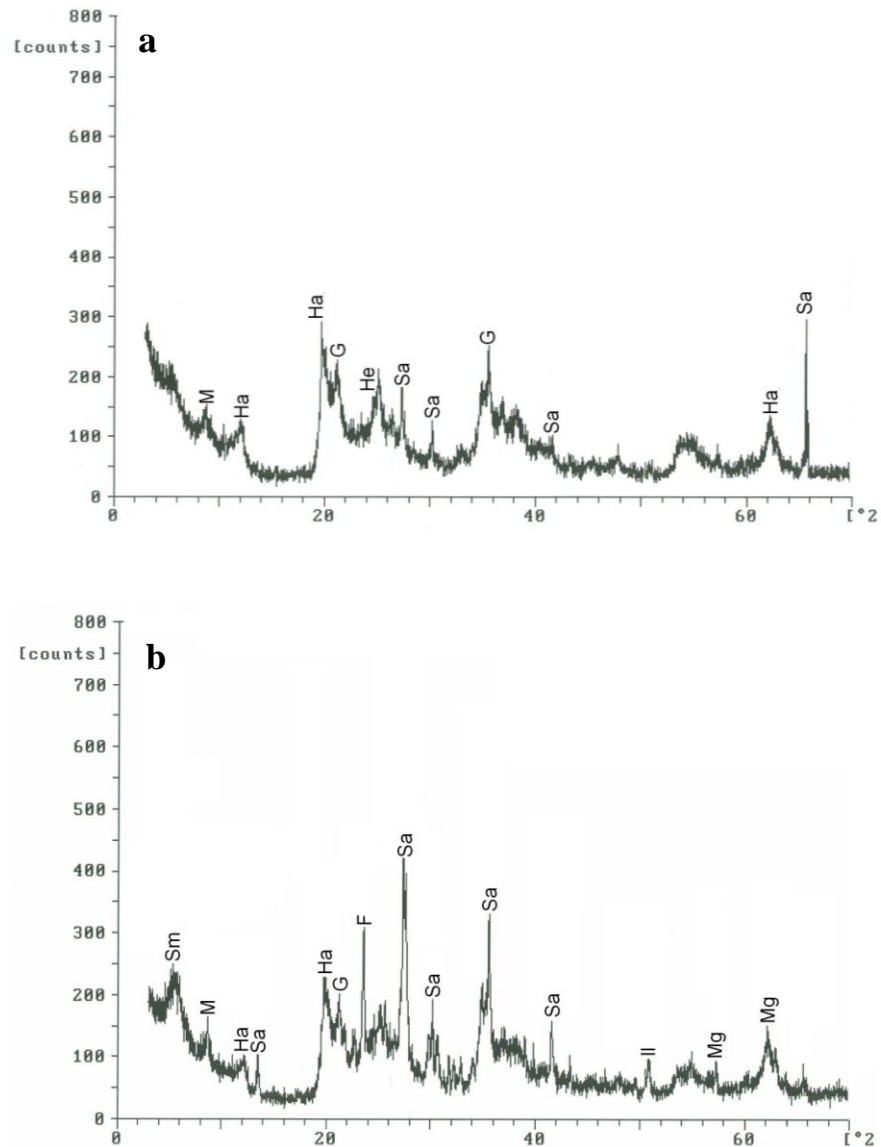


Fig. 4. 5. X-ray diffraction patterns for sample powders from a pyroclastic cone at Mabeta New Layout: a) field location of sampling point at head scarp: b) sample form B horizon: c), sample from C horizon: d) sample from assumed slip surface. Note the abundance of non-clay mineral with preference to iron bearing minerals in all samples of this profile.

Goethite and magnetite identified in this profile were also reported by Ngole *et al.* (2007). They also reported the presence of anatase which was not observed in this study. The diffraction patterns indicate that there are no obvious differences in the mineralogy of the samples down the profile. Most of the other sample analysed show similar patterns with the Bonjo and Mabeta samples. Bulk samples from Pit 2 dug into the the same scar at Mabeta show similarities in their mineralogical pattern to the clays from the C horizon; thus, the clay fraction was not analysed. Diffraction patterns from the slide at Makuka are shown in Figure 4.6. There is no significant difference in the diffraction patterns with depth. Dominant minerals include feldspars (sanidine) and halloysite with minor amounts of 2:1 clays, mica, goethite, and magnetite.



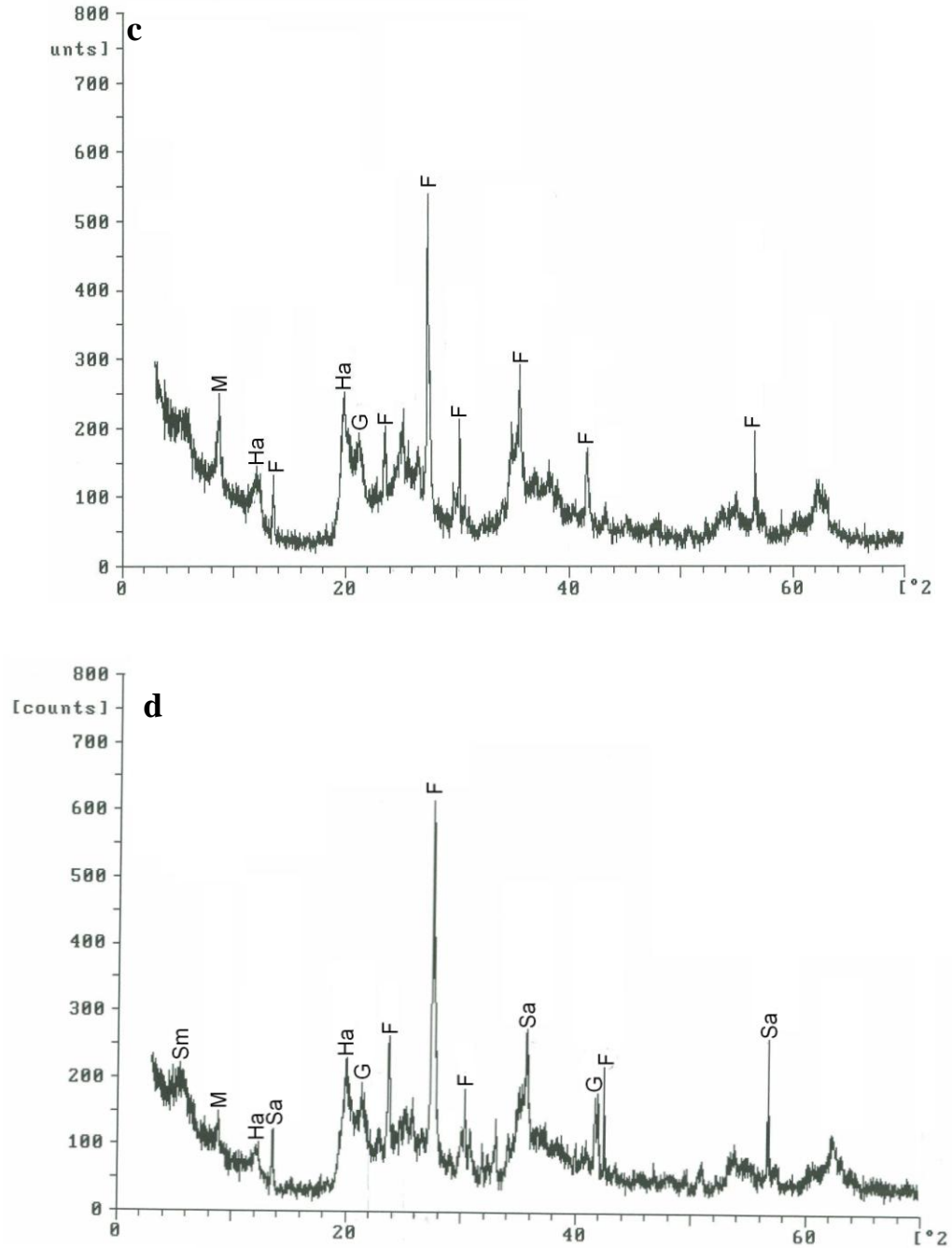


Fig. 4. 6. Diffraction patterns of bulk sample powders from Pit 6 at Makuka: a) P6S17; b) P6S18; c) P6S19 and d) P6S20. Note increasing intensity of non-clay mineral notably feldspars (sanidine) with depth. Sm: 2:1 clays; M: Mica; Ha: halloysite; G: goethite; F: feldspar; Sa: Sanidine; Mg: magnetite.

Photomicrographs of the sand fraction from the Mabeta slide (from the pits described in Chapter 3) reveal the presence of vesicular rock fragments with high amounts of shiny black magnetic minerals, dominantly magnetite and hematite, as well as visible olivine (Fig. 4.7).The

micrographs, X-ray diffraction patterns and grain-size analysis suggest that the breakdown of the pyroclastic material in the Mabeta region and in the Limbe area in general results in the formation of clay sized particles with little or no sheet-like silicates or clay minerals.

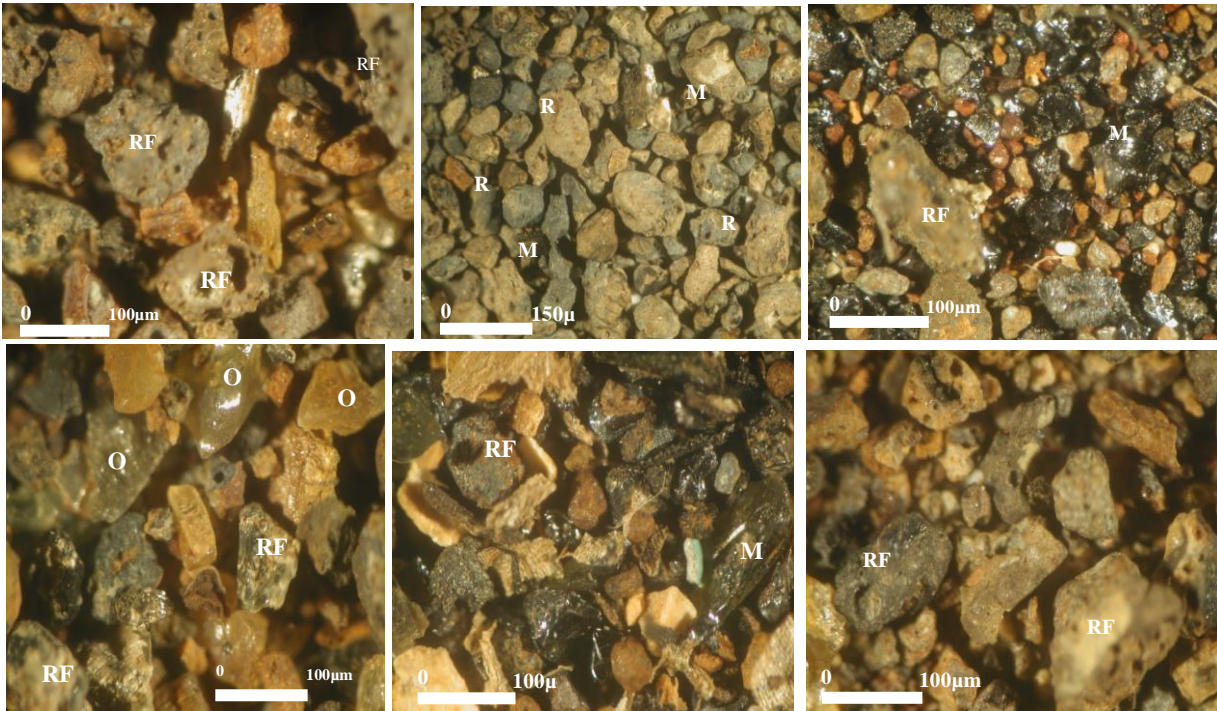


Fig. 4. 7. Photomicrographs of the sand fraction of soils derived from the weathering of pyroclastic material from the landslide scar at Mabeta. Note the abundance of opaque minerals and vesicular rock fragments with little or no feldspars. RF: rock fragment; O: olivine; M: magnetic minerals

Micrographs from the soils developed on lava flows are characterised by the presence of white, fractured sub-angular minerals (plagioclase), yellowish secondary mineral phases (goethite) and partially weathered basaltic rock fragments (Fig.4.8).

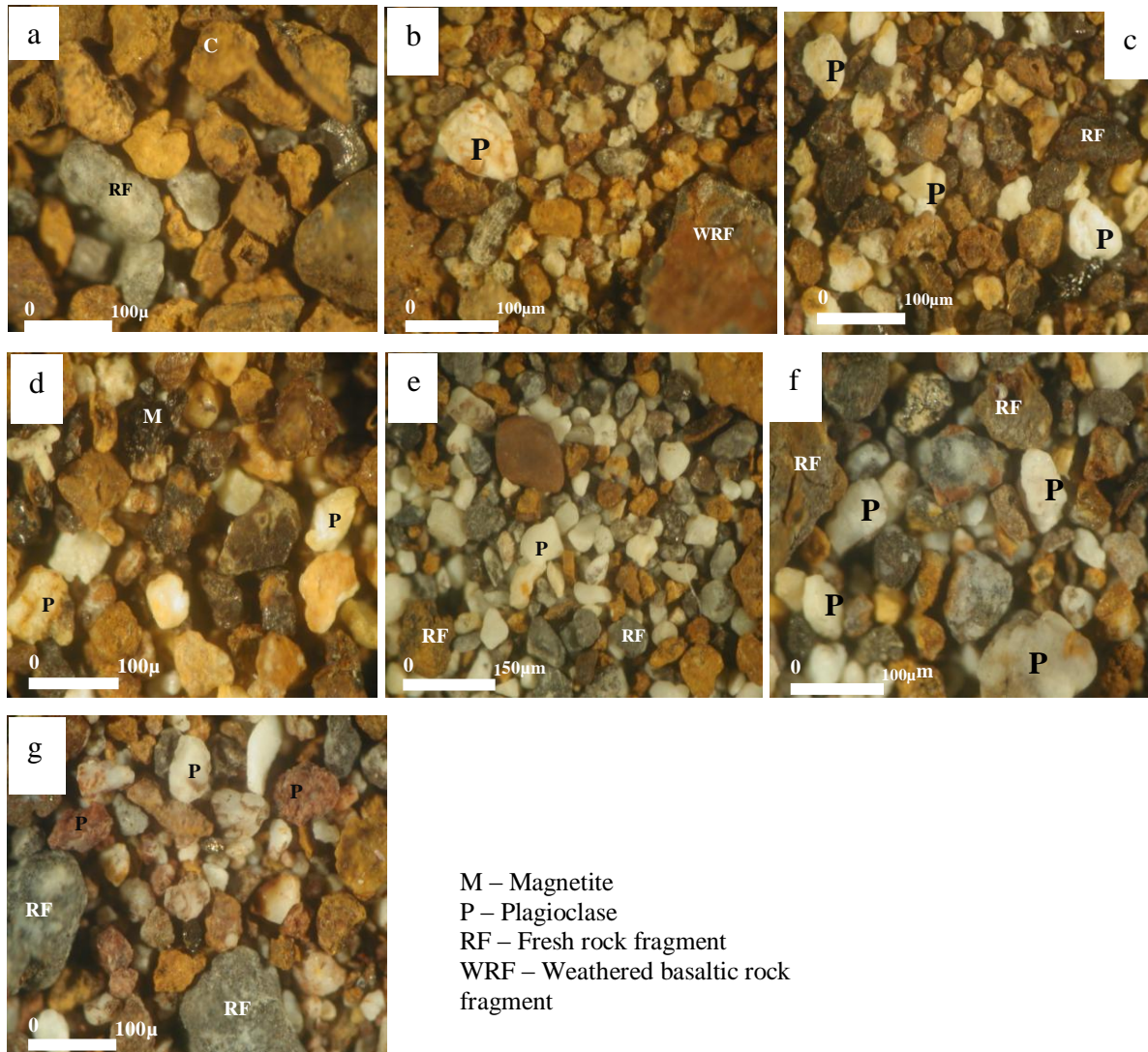


Fig. 4. 8. Photomicrographs of the sand fraction of soils developed on weathered lava flows: a, b, c and d are samples from Bonjo Pit 1; e from Pit 6, f from slide 6 in the inventory (Makuka, Fig 2.7b). Note the abundance of secondary minerals (goethite) in the Bonjo sample. Also visible are variable proportions of whitish minerals (plagioclase) within the samples. Plagioclase crystals are fractured and stained brown or pinkish. Rock fragments are devoid of vesicles relative to the samples from the pyroclastic cone.

4.4.2 Element distribution patterns

Results of WR chemistry for the rocks and soil samples are given in Table 4.2. These results are also graphically presented in Figure 4.9. HR represents fresh rock from the various profiles. The major and trace element concentrations display significant variations with depth in all three profiles. Notable values include near constant concentrations of SiO_2 and TiO_2 , systematic enrichment in Al_2O_3 and Fe_2O_3^* (Total Iron) and depletion of alkali and alkali earth metal oxides notably Ca and Sr.

Sample number	Bonjo (slide 1)			Mabeta (slide 13)			Makuka (Slide 39)			Lava from MC			
	P1S02	P1S03	HR1	P2S11	P2S12	HR2	P6S17	P6S20	HR3	MC* 1959	MC* 1982	MC* 1999	MC* 2000
Depth (cm)	80	200		160	290		50	290					
Major element concentration (wt %)													
SiO ₂	37.94	42.95	45.05	38.72	38.31	44.60	40.46	38.01	47.11	46.58	44.71	46.47	45.99
TiO ₂	3.96	5.14	3.23	4.39	3.95	2.95	5.19	4.44	3.26	3.24	3.50	3.21	3.15
Al ₂ O ₃	26.57	19.18	13.97	17.58	15.46	11.72	20.84	24.94	16.11	16.31	15.21	15.75	15.17
Fe ₂ O ₃ *	18.68	20.81	12.87	21.40	22.04	13.18	17.82	18.29	11.18	10.94	12.84	11.57	11.83
MnO	0.04	0.26	0.19	0.31	0.32	0.19	0.21	0.16	0.21	0.20	0.20	0.20	0.20
MgO	1.01	2.07	6.97	5.36	8.32	12.17	2.62	1.55	5.19	5.44	6.24	6.29	7.08
CaO	0.04	0.34	11.39	4.04	4.18	12.28	2.66	0.65	10.33	9.97	12.03	10.58	11.03
K ₂ O	0.31	0.61	1.41	0.01	0.00	0.94	1.57	0.52	1.72	4.45	3.51	4.02	3.79
Na ₂ O	0.00	0.00	3.40	0.00	0.00	1.06	0.75	0.07	3.16	1.84	1.26	1.65	1.49
P ₂ O ₅	0.48	0.53	0.63	0.06	0.05	0.40	0.89	0.61	0.75	0.84	0.54	0.73	0.67
Total	88.96	91.81	99.10	91.80	92.59	99.50	93.01	89.25	99.02	99.81	100.04	100.49	100.4
LOI	12.28	8.91	1.66	7.94	8.67	2.09	11.88	7.43	1.59				
Mg#	-	-	51.7	-	-	64.6	-	-	47.9	49.6	49.0	51.8	54.2
Trace element concentrations (ppm)													
Ba	730	375	384	537	845	361	548	613	470	516	370		
Sr	300	261	792	25	30	474	186	279	979	1140	917	1055	1063
Zr	477	387	235	328	387	244	459	469	324	386	348	404	410
V	376	466	275	349	363	314	405	412	212	246	331	266	272
Cr	90	254	183	2581	1803	800	142	85	101	44	37	106	151
Ni	57	115	82	803	479	279	100	48	44	48	65	74	88
Ce	228	146	111	116	155	102	224	160	162	163.3	143	168.4	
Y	60	47	27	53	40	27	64	45	33	36.8	31.14	33.99	33.31
Sc	28	40	27	100	86	43	37	27	16	18.1	30.8	22.3	25.1
Co	43	82	48	135	122	60	69	68	41	44	46	38	43

Table 4. 3. WR major and trace element composition of fresh rocks and soil samples from the Limbe area, SE foot-slope of MC; HR: fresh rock and S: soil samples analysed during this study. MC* are some fresh rock sample from the 1959, 1982, 1999 and 2000 lava flows of MC analysed by Suh *et al.* (2008). Note similarities in the major elements analysed in this study and variation in the trace element composition. Fe₂O₃*: total iron.

On a Total Alkali – Silica (TAS) diagram (Fig. 4.10) after Le Bas *et al.* (1986), the fresh rock samples from the lava flow (P1HR1 and P6HR3) plot within the basalt field whereas that from the pyroclastic cone (HR2) plots in the picobasalt field. The lava flow samples are mineralogically similar to lava samples analysed by Suh *et al.* (2003) and Njome *et al.* (2008) for the 1954, 1959, 1999, and 2000 lava flows of the MC area (Fig. 4.9). The pyroclastic material composition is offset from the general pattern. Calculated Mg# values are 37.56, 50.63 and 34.05 for P1HR1, P2HR2, and P6HR3, respectively. These values indicate that the pyroclastic material was produced from a more primitive magma while the lava flows were generated from more evolved magmas.

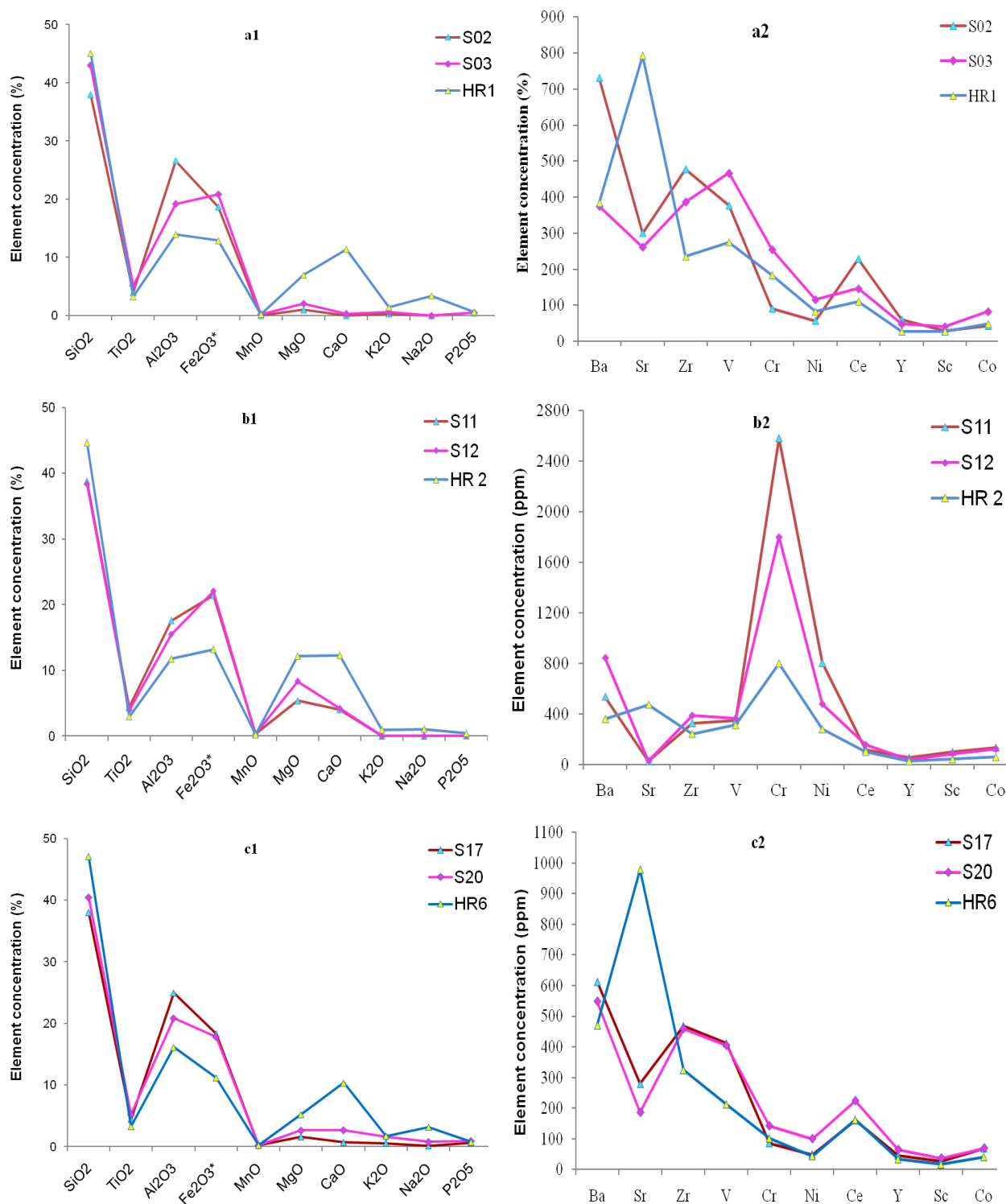


Fig. 4. 9. Element distribution patterns of: a) Pit 1 at Bonjo; b) Pit 2 at Mabeta New Layout; c) Pit 6 at Makuka. Left column represents major element patterns and right column trace element patterns. Note very high Cr and Ni concentrations in the Mabeta sample, a corresponding change in the scale of the vertical axis relative to the others, and high Sr in the Bonjo and Makuka samples.

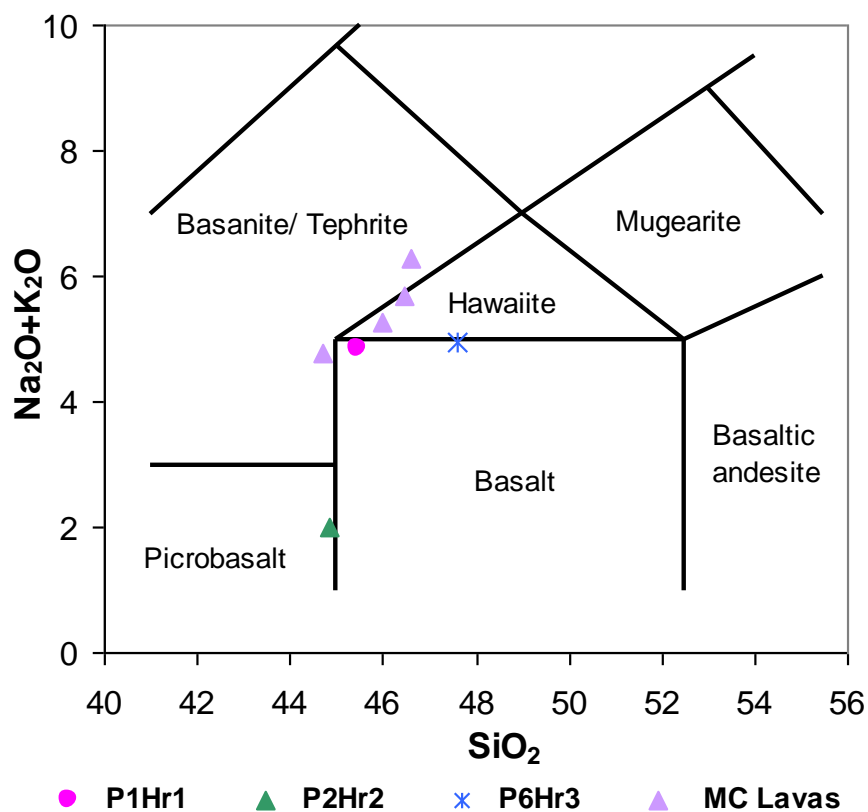


Fig. 4. 10. Total Alkali – Silica (TAS) diagram after Le Bas *et al.* (1986). Samples from other MC lavas from Suh *et al.* (2003) and Njome *et al.* (2008).

Average silica content also increases from the pyroclastic material through P1HR1 to P6HR3 with values of 44.83, 45.46 and 47.58 wt %, respectively. The chemical composition of the rocks indicates that SiO_2 , Al_2O_3 , Fe_2O_3 and CaO are the dominant oxides present, making up 83.3 % of the rock. As the rock transforms into soil, CaO , MgO , Na_2O , and K_2O are leached out, leaving behind SiO_2 , TiO_2 , Al_2O_3 , and Fe_2O_3 , which constitute ~ 91 % of the soils in the most weathered B horizon. Major element distribution patterns are similar in all the profiles whereas trace element patterns are similar for the sample from the lava flows and completely different from that of the pyroclastic material. Parent normalised element distribution patterns are presented in Figure 4.11. The most prominent feature in these plots is the significant depletion of Ca and Sr noted in all the profiles and a net increase in all the other trace elements. Similarly, there is an observed depletion in oxides of Na, K, Ca, and Mg with a corresponding enrichment in Al_2O_3 and Fe_2O_3^* (total iron).

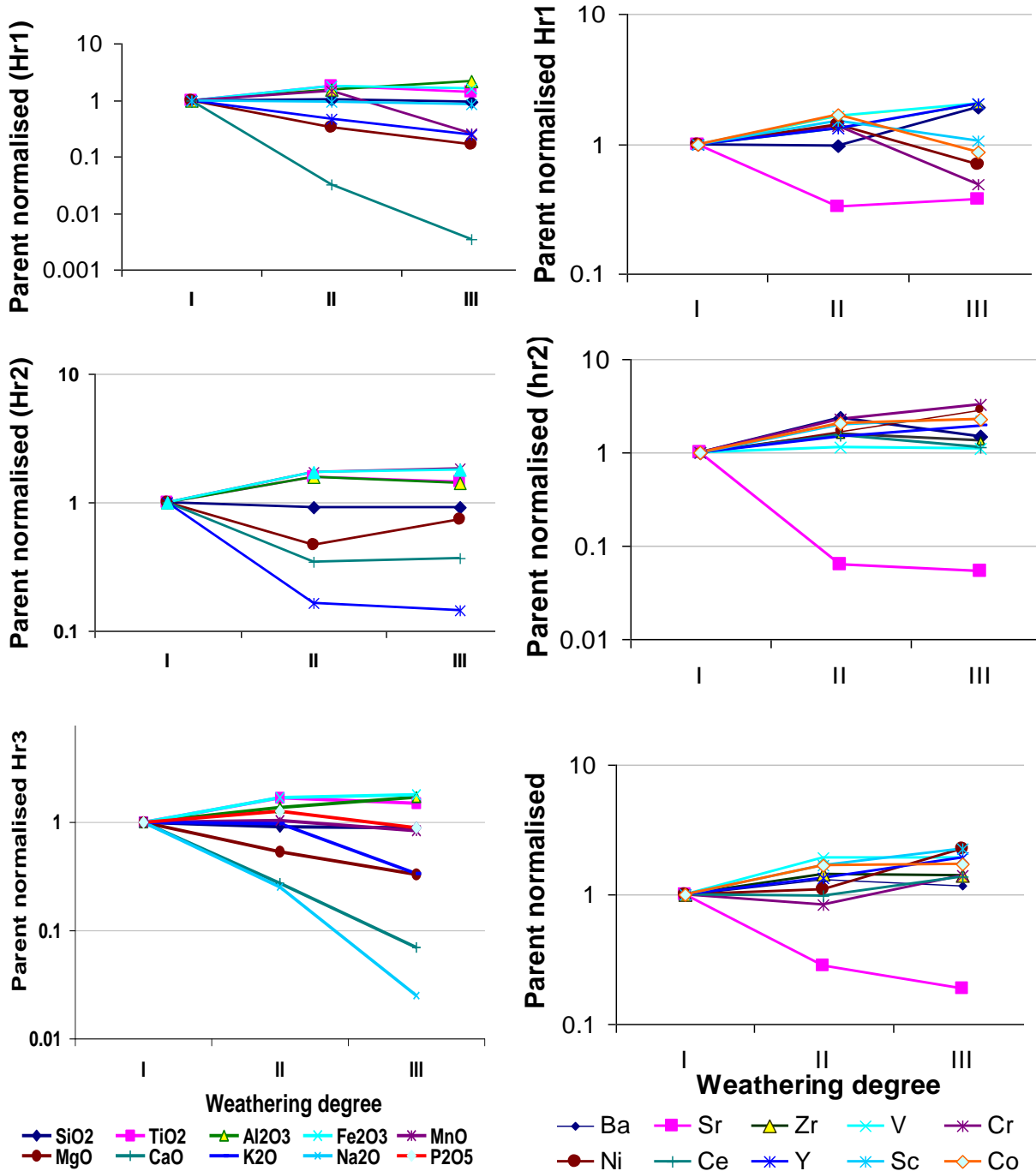


Fig. 4. 11. Parent normalised element patterns of soils and saprolites from landslide scars in Limbe. Left column represents major elements and right column trace elements. Note significant depletion in Ca, Na and Sr and a corresponding enrichment in all the other trace metals. I; parent rock; II: sample from C horizon; III: sample from horizon B.

Chemical indices are the most widely used means of measuring weathering rates. Calculated weathering indices CIA, Ruxton ratio and Vogt residual index are shown in Table 4.3.

Sample number	CIA	Ruxton ratio	Vogt ratio
P1S02	97.9	2.42	10.35
P1S03	96.5	4.11	4.17
P1HR1	34.3	5.47	0.39
P2S11	70.5	3.74	0.84
P2S12	67.0	4.20	0.54
P2HR2	31.9	6.46	0.24
P6S17	92.2	2.59	4.97
P6S20	71.6	3.29	1.91
P6HR3	39.2	4.9	0.54
Mean*	35.5 ± 0.9	5.06 ± 0.14	0.39 ± 0.03
Optimum fresh value**	< 50	> 10 (4.0-4.5 [#])	< 1
Optimum weathered value **	100	0 (2 [#])	Infinite

Table 4. 3. Weathering indices for fresh rock and soil samples from landslide scars in Limbe, SW Cameroon. Volcanic rocks on MC and world average values. * values calculated from the chemistry of fresh rock samples from the MC region by Suh *et al.* (2003) and Njome *et al.* (2008), ** values provided by Price & Velbel (2003), [#] value provided by Ruxton (1968).

Variations in these indices are compared with those of fresh rock samples from MC and optimum fresh and weathered values given by Price & Velbel (2003). The CIA and Vogt indices for the fresh rock samples are lower than the optimum fresh value reported by Price & Velbel (2003) thus representing the unaltered parent material to which the soils and saprolites are normalised. Ruxton ratio on the other hand is less than the optimum value reported by Price & Velbel (2003). P1S02, P1S03 and P6S017 show weathering indices close to the optimum weathered value suggesting almost complete weathering. P2S11, P2S12 and P6S20 show intermediate values which can be interpreted as having undergone lower weathering intensities. On the Si-Al-Fe ternary plot used by Hill *et al.* (2000), the most intense level of weathering observed in this area is the kaolinisation stage (Fig. 4.12).

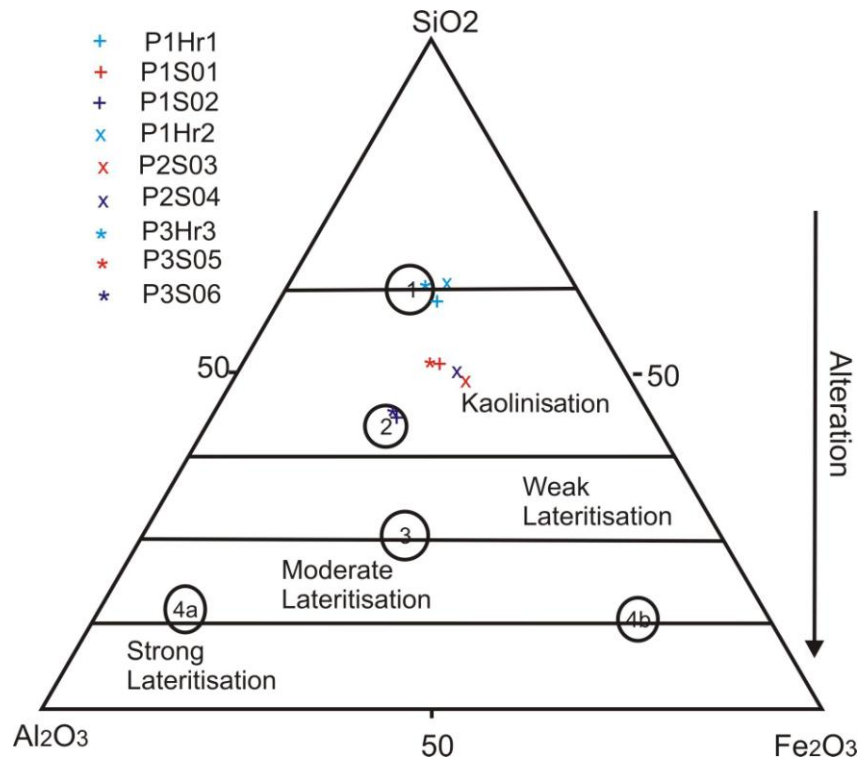


Fig. 4. 12. Si-Al-Fe ternary diagram by Hill *et al.* (2000) for the parent rocks and soil samples from landslides scars in Limbe. 1: average composition of fresh basalts; 2: Lithomarge (saprolite); 3: laterite; 4a: bauxite and 4b: Iron ore crust.

4.5 Discussion

4.5.1 Diffraction patterns

From Table 4.1 and the diffractograms described above and in Appendix 4, it is noted that the soils in this area are a mixture of non-swelling (kaolinite, dehydrated and hydrated halloysite) and swelling clays in varying proportions. Though swelling clays predominate in some samples, non-swelling clays are more wide spread particularly in material from the pyroclastic cones. The mechanical and geotechnical behaviour of the soils is thus not a function of a single clay type but rather of interplay of smectites, 1:1 clays and other non-clay minerals such as goethite, hematite, anatase, olivine, sanidine and magnetite, all present in the coarse fraction. Vingiani *et al.* (2010) working on the Ischia landslides in Italy, noted that the volcanic soils on which the slide occurred were characterised by the presence of poorly ordered kaolinite in all horizons and expandable clay minerals only in the deepest horizons. The low concentrations of smectite in the profiles may be a result of the decomposition of smectite to amorphous oxides and 1:1 or non-swelling clays due to the high rainfall and good drainage conditions that exist in this area.

Limited concentrations of swelling clays, high clay fraction in the soils and the presence of non-swelling clays may be indicative that these slopes will be stable under normal conditions as has been noted by Vaughan *et al.* (1988).

In literature, there has been much research linking the occurrence of landslides to the presence of swelling clays (Matsuura, 1985; Shuzui, 2001; Zheng *et al.*, 2002). However, this study shows that sliding is also possible in soils characterised by non-expansive clays as has been noted by Vingiani *et al.* (2010). The presence of the non-swelling clays may highlight the fact that soils in the Limbe area are characterised by good geotechnical properties and failure in this case can be associated with other factors such as fracture permeability described in Chapter 3. Dixon & Robertson (1970), Blight (1996), and Queiroz & Simmons (1997) explained that soils with large amount of halloysite are characterised by high plasticity, low permeability and display sensitivity to drying and manipulation. This might be a possible explanation for the observed high moisture content and liquid limits observed in the samples.

Diffraction patterns do not show clear variations within profiles but there are significant variations in the mineralogy from one profile to another indicating the uniqueness of each failure site. Mineralogical heterogeneities within profiles were not identified in this study. Instead, index properties and geotechnical characterisation discussed in Chapter 3 make the presence of geotechnical heterogeneities within the profiles evident. Based on results from this study, clay mineralogy, cannot be used in this case as an index in identifying areas or horizons that are susceptible to failure. However, more analysis and further research involving clay mineralogical analysis in this area is recommended to better constrain this assertion. Site specific characterisation is thus an invaluable tool for local and regional engineering applications since results from one site are not directly transferable to another area due to non uniform distribution of geotechnical properties.

The mineralogy of soils derived from basaltic flows is different from those derived from pyroclastic material. Duzugoren-Aydin *et al.* (2006) also noted variations in weathering products from pyroclastic material and those from granitic profiles in Hong Kong. They noted higher halloysite-to-kaolinite ratios for granitic profiles than for pyroclastic profiles at the same degree of weathering and attributed this to better leaching conditions in the granite relative to the

pyroclastics. In this study, pyroclastic material is weathered to clay sized particles with very little clay minerals mainly non-swelling clays, whereas a mixture of swelling and non-swelling clays are present in the profiles from weathered basaltic flows. This is probably due to poorer drainage in the basaltic flows than in the pyroclastic material. Higher porosity enhances rapid and more intense weathering in the pyroclastic materials. Deep weathering coupled with steeper slopes that characterise pyroclastic material make them more susceptible to failure. This may account for the variation in failure susceptibility of these materials. In addition, the high clay fraction, low plasticity index and low concentration of clay minerals in the pits on the pyroclastic material suggest that the plasticity of the soil is dependent on the type of clays and not only the amount of clays fraction present.

Halloysitic soils are known to display high natural moisture content, high liquid limit, and relatively low plasticity indices (Dixon & Robertson, 1970; Queiroz & Simmons, 1997). Because of the high liquid limits, high moisture contents, low plasticity indices and the peaks observed on the X-ray diffractograms, hydrated and dehydrated halloysite could be coexistent with kaolinite in these samples. Further analysis such as the formamide test, heat treatment at 300 and 500 °C of K-saturated samples would need to be conducted to actually confirm which of these two species (kaolinite or halloysite) are more abundant because the peaks at 7.1 -7.35 Å in the glycolated samples could signify the presence of any of these two minerals. Prominent peak at 3.5 Å may be interpreted as a second order reflection of the halloysite and kaolinite peaks or as indicative of the presence of short range order clays such as allophane (Sieffermann *et al.*, 1968). Sieffermann *et al.* (1968) identified allophane, ferrihydrite, and imogolite in soils from the MC areas. Tests for the presence of allophane and other short range order clays (for example oxalate extraction) is therefore recommended as soils dominated by these minerals exhibit very good geotechnical properties. Goethite and sanidine were also observed in some profiles identified by the presence of peaks at 4.18 and 2.70 Å, and 3.51 and 1.89Å, respectively. These peaks could still be reflection peaks of the aforementioned minerals, hence further analysis would be required for complete characterisation.

4.5.2 Variations in element distribution

Variations in major element concentrations within the basaltic saprolites strongly indicate the unstable nature of their primary minerals (olivine, pyroxene, amphibole and plagioclase), the formation of secondary minerals, and mobility of each element during weathering. Strong depletion in the alkali and alkali earth metals (K_2O , Na_2O , and CaO) reflects intense and even complete decomposition of plagioclase and high mobility of these elements. Weaker depletion in MgO could be related to the decomposition of olivine and other ferromagnesian minerals whereas SiO_2 , Al_2O_3 , $Fe_2O_3^*$, TiO_2 , and MnO remain constant or show slight enrichment. This enrichment might be associated with the formation of secondary minerals (Wen *et al.*, 2004), particularly clays and sesquioxides (Duzugoren-Aydin *et al.*, 2002).

Comparing the trace element concentration in the rock samples measured in this study with those of fresh rock samples from MC (Suh *et al.*, 2003; Chauvel *et al.*, 2005; Njome *et al.*, 2008) it is observed that their concentrations in P1HR1 and P6HR3 are similar while P2HR2 shows wide differences with exceptional high Ni and Cr concentrations. Deurelle *et al.* (1987) and Sato *et al.* (1990) have measured similar concentration in some rock samples from the MC region. Generally, fresh rocks from MC are characterised by high Ba (400 to 609 ppm) and Sr (927 to 1216 ppm) values.

Looking at the trace elements concentrations in the soils and the parent rocks, it is observed that they all show significant enrichment to the noticeable exception of Sr that is significantly depleted in the soils. High Ba concentrations in the soils result from a high initial concentration in the parent material that becomes enriched as weathering proceeds. The soils are also characterised by a high Sr concentration. Similar results have also been noted by Dia *et al.* (2006) who measured Ba concentrations between 200 and 619, and Sr between 374 -1021 ppm in multiple soil samples from MC and by Nchia (2010) who measured Ba concentrations between 136 and 1117 ppm, and 906 – 1196 ppm Sr in top soils within the Limbe area.

Significant Sr depletion might be related to the decomposition of plagioclase in which Sr replaces Ca. This relationship is confirmed by a strong negative correlation between Sr and Ca with an r (Pearson's correlation coefficient) value of -8.2. Sr is a highly mobile element with

similar chemical behaviour to Ca and K, implying that soils will generally have lower concentrations of Sr than the parent rocks. Studies have shown that Mn easily scavenges Ba, showing a high affinity for Mn in diverse redox-active environments (Wen *et al.*, 2004). Thus Ba accumulation may also be associated with both abundance and mineralogy of clays (Wen *et al.*, 2004). However, there is no correlation between Ba and MnO ($r = -0.15$) within these profiles. Other studies have shown that Ba partitions in sanidine, which is still present in profiles 1 and 3.

The pyroclastic rock and soils derived from it are characterised by the presence of high Ni and Cr concentrations ranging from 800 ppm in the parent rock to 2581 ppm in the soil for Cr and 279 ppm in the parent to 803 ppm in the soil for Ni. Other rocks from MC measured by Suh *et al.* (2003, 2008), Chauvel *et al.* (2005), and Njome *et al.* (2008) have values that range between 48 - 213 and 40 - 99 ppm, for Cr and Ni, respectively. The pyroclastic rock is also characterized by a higher magnesium oxide, lower Al₂O₃ and K₂O content than other rocks of the MC region. Liu *et al.* (1996) found that soils developed on basalts normally have higher concentrations of elements that belong to the Fe family, such as Ti, V, Co, Cr, and Ni relative to soils developed on more evolved rocks such as granite and rhyolite. These trace elements become relatively enriched in the soils formed from basaltic rocks due to preferential loss of the other major elements during weathering. Observed r values between these elements are also high (Table 4.4.) These observations were also noted in this study as metals of the iron family all show relative positive enrichment with intense weathering. Significant enrichment in Cr and Ni noted for Profile 2 can be accounted for by the fact that the parent rock in this area is characterised by pyroxene, amphibole and olivine which are the principal hosts of Cr and Ni. The weathering of these minerals would liberate these elements, which are enriched in the soil because of their low mobility.

From the parent normalized patterns, it is noted that all elements are mobile as some are relatively depleted and others enriched. This observation is contrary to the common assumption that Ti and Zr are nearly always immobile as assumed in many mass balance calculations within the tropics (Beyala *et al.*, 2009). A wider suite of trace and rare earth element analyses is recommended to further constrain the most appropriate inert element that can be used in isovolumetric mass balance evaluations in this region.

	SiO ₂	TiO ₂	Al ₂ O ₃	Fe ₂ O ₃ *	MnO	MgO	CaO	K ₂ O	Na ₂ O	P ₂ O ₅	LOI	Ba	Sr	Zr	V	Cr	Ni	Ce	Y	Sc	Co	
SiO ₂	1																					
TiO ₂	0.78	1																				
Al ₂ O ₃	0.49	0.01	1																			
Fe ₂ O ₃ *	-0.02	-0.43	-0.66	1																		
MnO	-0.04	0.05	-.96**	0.64	1																	
MgO	-0.51	-0.50	-.85*	0.69	0.79	1																
CaO	-0.58	-0.33	-0.82	0.39	0.77	.89*	1															
K ₂ O	0.41	0.78	0.22	-.80*	-0.25	-0.50	-0.24	1														
Na ₂ O	0.07	0.56	0.01	-0.74	-0.07	-0.19	0.14	.91*	1													
P ₂ O ₅	0.47	0.71	0.58	-.88*	-0.56	-0.78	-0.60	.91*	0.70	1												
LOI	-0.10	-.31	0.88*	-0.26	-0.80	-0.62	-0.73	-0.25	-0.45	0.16	1											
Ba	-0.72	-0.50	0.11	-0.12	-0.17	0.10	0.36	-0.27	0.00	-0.32	0.14	1										
Sr	0.61	0.56	0.70	-0.68	-0.75	-.88*	-.82*	0.68	0.40	.87*	0.36	-0.28	1									
Zr	0.06	0.29	.87*	-.92*	-.86*	-.86*	-0.62	0.59	0.46	0.79	0.56	0.23	0.77	1								
V	.94**	.90*	0.18	-0.25	-0.10	-0.62	-0.63	0.56	0.20	0.65	-0.15	-0.68	0.65	0.25	1							
Cr	-0.54	-0.62	-0.79	0.78	0.74	.98**	.85*	-0.67	-0.37	-.90*	0.48	0.21	-.93**	-.86*	-0.69	1						
Ni	-0.52	-0.62	-0.77	0.80	0.73	.98**	0.81	-0.66	-0.38	-.88*	-0.46	0.12	-.91*	-.86*	-0.67	.99**	1					
Ce	-0.11	-0.10	.97**	-0.61	-.89*	-0.78	-0.71	0.10	-0.07	0.45	0.91*	0.26	0.53	.84*	0.05	-0.69	-0.69	1				
Y	-0.14	-0.35	0.72	-0.24	-0.65	-0.36	-0.60	-0.14	-0.30	0.22	0.81*	-0.21	0.28	0.38	-0.07	-0.33	-0.25	0.69	1			
Sc	-0.49	-0.57	-0.78	.85*	0.79	.95**	.82*	-0.71	-0.44	-.92**	-0.45	0.20	-.96**	-.88*	-0.63	.99**	.98**	-0.68	-0.35	1		
Co	-0.33	-0.32	-.90*	0.80	.93**	.94**	.85*	-0.53	-0.28	-0.81	-0.63	0.05	-.93**	-.91*	-0.44	.94**	.93**	-0.81	-0.49	.96**	1	

Table 4. 4. Pearson's correlation matrix for major and trace element analysed in this study. ** Correlation is significant at the 0.01 level (2-tailed). * Correlation is significant at the 0.05 level (2-tailed).

Y in this case is more conservative and can be used as an inert element though Hill *et al.* (2000) note that Y is mobile at the very early stages of the weathering of basaltic rocks.

4.5.3 Weathering indices

Changes in weathering indices with depth in all profiles correlate with their degree of weathering. Each change corresponds to a horizon where soil has developed at the expense of the initial parent rock and with the development of alteration gradients. Irregular or anomalous patterns might be a result of the mixing of soil material by slope forming processes such as landslides and other colluvial processes. Ruxton (1968) proposed a weathering index based on the $\text{SiO}_2/\text{Al}_2\text{O}_3$ ratio of the bulk soil. He found that fresh Si-Al rocks commonly have a value of 4.0-4.5, which decreases progressively until it reaches a value of 2 in pure kaolinite. Ruxton ratios for fresh rock samples from MC calculated from data generated in this study and data reported by Suh *et al.* (2003) and Njome *et al.* (2008) range from 4.9 to 5.47 with a mean value of 5.06. The ratio decreases progressively with increasing weathering intensity to values of 2.4, 3.74 and 2.59 for Pits 1, 2 and 6, respectively, indicating intensive weathering resulting in the enrichment of Al_2O_3 and slight depletion of SiO_2 . Furthermore, calculated CIA is close to 100 suggesting that there has been an almost complete removal of feldspars within the system relative to the fresh rock. Vogt residual indices range from 0.54 in the pyroclastic material at Mabeta New Layout to 10.35 in the weathered lava flow suggesting that the lava flows are more intensely weathered than the pyroclastic materials.

4.5.4 Mass Balance Evaluations

There are no universal methods used in estimating changes in the concentration of individual elements during weathering (Duzugoren-Aydin *et al.*, 2002). In this study, chemical transformation and elemental losses and gains accompanying the physical breakdown of the parent rock into soils is done by parent normalisation. Relative depletion patterns follow the order $\text{Na} = \text{Ca} = \text{Sr} > \text{Mg} > \text{K} > \text{P} > \text{Si}$. The observed patterns tally with the overall bulk chemistry of the parent rock. The rocks are enriched in Ca relative to Mg due to the presence of Ca-rich plagioclase, and smaller proportions of Mg- and K-rich minerals. Sr patterns follow those of Ca because it replaces the latter element in the lattice structure of plagioclase. Silica is

relatively immobile. Generally, dramatic differences exist in the physical properties of soils and parent rocks. Soil bulk densities are generally less than half those of the parent rock with the lowest values measured in the most weathered soils. This decline in density results from a progressive increase in porosity with weathering due to the loss of elements accompanied by volume increase and/or decrease. Similar results were reported by Jersak *et al.* (1995) and Anderson *et al.* (2002) in the USA.

4.6 Conclusion

From the mineralogical and chemical characterisation of soils from landslide scars on the SE foot slope of MC the following conclusions can be drawn:

- Clay mineralogy is composed of a mixture of swelling and non-swelling clays.
- The dominant clay types are the 1:1 or non-swelling clays (kaolinite, hydrated and dehydrated halloysite).
- The sand and silt fraction is characterised by rock fragments, anatase, goethite, hematite, magnetite and ilmenite.
- Significant differences exist in the trace mineral patterns of soils from different parent materials, in this case basalt flows and pyroclastic material.
- Significant depletion in Sr, alkali and alkali earth metals is remarkable in weathering profiles within this area.
- Significant mineralogical heterogeneities exist between profiles with minimal heterogeneity within the same profile.
- The most advanced stage of weathering in this area is the kaolinisation stage. The soils developed on the lava flows have undergone greater intensity of weathering than those on the pyroclastic material.
- Based on the results presented in this thesis, neither mineralogy nor chemistry of the profiles can be used as a fingerprint to identify slip zones for sliding in the study area. Hence further research in this area is recommended.

Chapter Five

Landslide susceptibility mapping (modelling)

5.1 Introduction

Considering that every location on a slope is continuously experiencing a tug-of-war between forces that tend to resist down-slope movement of material and gravitational forces that tend to move material down slope, we observe that slides only occur in those areas where the gravitational forces exceed the strength of the resisting forces. Usually, these forces are at a state of equilibrium. However, natural and human forces tend to destabilize this state of equilibrium in favour of gravitational forces (Ahmad & McCalpin, 1999). Although some slope failures are abrupt, in most circumstances landslides usually progress gradually until a trigger sets in and accelerates the movement. Triggers refer to single events that actually initiate failure whereas the cause of a slide may be defined as the reason why a slope failed at a particular location and at a particular time. The cause could also be considered as the (combination of) factor(s) that make a slope vulnerable or more susceptible to failure and may include geological, anthropogenic, climatic and geomorphologic aspects.

Landslide susceptibility modelling basically involves landslide cartography aimed at producing a landslide inventory map and a map of all potential triggering and conditioning factors. Maps are the tools earth scientists fancy in order to portray geological information and convey it to other scientists, decision-makers and the public (Guzzetti, 2005). Landslide maps are prepared to show where landslides have happened (inventory) or where they are expected to occur in the future (susceptibility), and can be used to divide land areas into zones of different hazard and risk levels (zonation).

During the past 5 decades, research, environmental and government organizations over the world have invested huge resources in forecasting the spatio-temporal occurrence probability and intensity of all types of slope movements (Aleotti & Chowdhury, 1999; Bonnard *et al.*, 2003; Guzzetti, 2005) with the goal of minimizing damage and fatalities linked to landslide phenomena. Mitigation of landslide related hazards can only be successful when detailed information about the frequency, magnitude and character of slope failures within a particular area is known (Vijith *et al.*, 2009). For this reason, the identification of landslide prone areas

represents a cheap and fast method in understanding this hazard. Mitigation could begin with landslide susceptibility assessment. **Landslide susceptibility** involves predicting where a potentially damaging landslide may occur without any reference to the time or the intensity of associated damage (Ahmad & McCalpin, 1999; Ohlmacher, 2000; Sorriso Valvo, 2002; Van Western *et al.*, 2006) and ranks the degree to which parts of the slope are prone to future failure, based on the factors that produced past landslides.

Landslide intensity on the other hand is a measure of the destructive potential of a landslide, based on a set of physical parameters, such as velocity, thickness of the displaced debris, volume, energy and impact forces. Susceptibility and intensity can be expressed in qualitative and/or quantitative terms. Intensity varies with location along and across the travel path of the material and therefore should ideally be described using a spatial distribution for adequate mitigation measures to be implemented.

Landslide risk is defined as the potential degree of damage losses due to landslides and the expected number of lives lost, people injured, damage to property and disruption of economic activities (Varnes *et al.*, 1984). It is expressed as a simple overlay between elements at risk and landslide susceptibility categories. Elements located in the high and very high landslide susceptibility zones are very vulnerable. Landslide risk assessment therefore requires the construction of an inventory of objects at risk. Objects at risk could vary immensely from whole villages through specific houses, walls and individuals based on the scale of the assessment.

5.1 Methods of landslide susceptibility assessments

Various studies have been performed in different areas around the world, using diverse methods to generate susceptibility maps that can help in the reduction of landslide related damage. Miller *et al.* (2007) used aerial photo interpretation, geomorphological mapping and field surveys (direct methods) to produce a landslide inventory map. They applied Bayesian conditioning probability for weighing factors conditioning sliding and integrated these into a Geographic Information System (GIS) package to produce a landslide susceptibility model for St Thomas, Jamaica. Bivariate statistical methods (matrix, seed cell, weight of evidence method, weighed factor, information value) have been applied in landslide susceptibility assessment in other areas (e.g. Cross, 1998; Donati & Turrini, 2002; Suzen & Doruyan, 2004; Ayelew *et al.*, 2005; Thiery *et al.*, 2007; Conoscenti *et al.*, 2008; Ruff & Czurda, 2008; Yalcin, 2008; Jiménez-Peràlvarez *et*

al., 2009, Vijith *et al.*, 2009). Discriminant analysis and logistic logic regression have also been used in landslide hazard modelling and spatial prediction of landslides (Gorservski *et al.*, 2000; Santacana *et al.*, 2003; Ayalew *et al.*, 2005; Lei & Jing-Feng, 2006). On a local scale, deterministic methods involving geotechnical characterisation of soil properties and liquid equilibrium methods have been applied. The factors conditioning slope failure in most of these studies include elevation, slope, slope orientation, profile curvature, plan curvature, tangent curvature, flow path and upslope gradient.

From the above methods, it is observed that most landslide susceptibility assessment approaches blend into each other and are based on the principle of uniformitarianism which states that the past and present are keys to the future. That is, under conditions of environmental similarity future slides will occur in similar areas and under the same conditions as past and present failures (Varnes *et al.*, 1984; Carrara *et al.*, 1991, 2003; Hutchinson, 1995; Guzzetti *et al.*, 2003). Despite their operational differences, the above assessment methods involve 3 steps:

- Landslide inventory
- Mapping of factors conditioning slope failure
- Estimating the relative contributions of each factor.

The above methods can be regrouped into three: deterministic, heuristic and statistical methods. The deterministic model involves site specific characterisation of the geotechnical properties of the sliding material and is thus capital intensive and can only be applied on a limited or restricted area. The heuristic approach, based on expert knowledge, is very subjective and affected by limited reproducibility. The statistical approach can either be bivariate or multivariate depending on the analysis method (Soeters & van Western, 1996). In multivariate statistical analysis, factors are assumed to be related and are treated together whereas bivariate methods assume factor independence and treat the influence of each factor on landslides independently and sum them up. The fate of the final susceptibility map is often decided by the theoretical basis and assumptions made in the model (Carrara *et al.*, 1999).

According to Jiménez-Perálvarez *et al.* (2009), landslide inventory is of prime importance in any susceptibility assessment project and determines the quality of the final results. Landslide mapping and the identification of conditioning factors is either done by intensive field surveys and/or from the interpretation of aerial photographs and other remote sensing data such as

LANDSAT, ASTER, SPOT and IKONOS images. The contribution of each factor can be evaluated based on expert's knowledge about the relation between the occurrence of landslides and their hypothetical predisposing factors (Thiery *et al.*, 2007) or statistically by calculating landslide densities per factor class (Carrara *et al.*, 1991; Soeters & van Western, 1996; Ruff & Czurda, 2008; Yalcin, 2008). From these calculations, assessments are made on those sites where failures are likely to occur in the future (Carrara *et al.*, 1999). Reviews outlining the methods used in landslide susceptibility are given by Brabb (1984), Hutchinson (1995), Soeters & Van Westen (1996), Aleotti & Chowdhury (1999) and Guzzetti *et al.* (1999).

There are no universal guidelines regarding the selection of factors in susceptibility mapping (Ayalew *et al.*, 2005). Although any parameter may be important with respect to landslide occurrence in a certain area, the same parameter may not be important for another area. A very wide number of factors have been identified as landslide conditioning and triggering factors, including geological, hydrological, geomorphological and geotechnical properties of the sliding material. From detailed hydrological analysis, Fiorillo & Guadagno (2000) suggested that historical reactivations of Adriatic landslides are connected to long rainy periods with high cumulative rainfall of low intensity. High pore pressure due to saturation has also been reported to be one of the major causes of landslides (Montgomery & Dietrich, 1994; Davies *et al.*, 2005). Esu & Grisolia (1991) ascribe episodic reactivation of landslides along the Adriatic coast to changes in pore pressure. Trefois *et al.* (2007) suggest that increasing hydrostatic pressure and human mismanagement are the major causes of large landsliding while deforestation and large population increase are indirect causes of slide reactivation around Bukavu. Yalcin (2007) reported the importance of soil geotechnical parameters as causal factors. Though qualitative answers to landslide controlling factors can be made using engineering or geomorphologic judgment, human reasoning alone is inadequate to synthesize the mass of factors involved in complex slope stability problems (van Westen *et al.*, 2006).

In this study we implement a data driven bivariate landslide susceptibility model to build a susceptibility zonation map for the Limbe area. The seed cell method proposed by Süzen & Doyuran (2004) is modified and combined with the Infoval (Information value) method used by Vijith *et al.* (2009). This model is based on:

1. Systematic documentation of the location and characteristics of past landslides in the area (Che *et al.*, 2011) and converting them into seed cells
2. Identification of key factors that control slope stability, systematic mapping of these factors and transferring them into grids.
3. Calculation of zonal statistics between the seed cells and factor maps to obtain the number of seed cells per factor class, which is later used to create weighed factor maps.

This model was adopted because it is flexible, robust and has the ability to minimise expert subjectivity. It also does not require intensive computer resources or extensive computer modelling experience.

5.1.1 Raw data

Four data sets were used to generate the predisposing factor maps necessary for the evaluation of landslide susceptibility. Table 5.1 shows a list of available data sets, corresponding factors derived from them and associated factor classes. A 1:50000 scale topographic map (with 20 m contour lines) of the study area published by the French National Institute of Cartography in 1963, was scanned and geo-referenced for use in a GIS (ERSI ArcGIS 9.1). Elevation contour lines, the road network and drainage pattern of the area were digitized from this map.

Three sets of satellite images namely 1 TM and 2 ETM+ acquired on December 12, 1986, December 10, 2000, and January 31, 2008, respectively were down loaded from the University of Maryland Global Land Cover Facility (GLCF <http://glcfapp.glc.f.umd.edu:8080/esdi/index.jsp>). These satellite images were used together in with 1 Advanced Space Transmission and Reflection Radiometer (ASTER) image acquired in 2007 bought from the United States Geological Survey (USGS) Global Visualisation Viewer (GLOVIS). Direct landslide mapping on these images was not possible because of the small sizes of the observed slides and a relatively coarse pixel size of the image. The depletion zone of the slides in this study hardly exceeds 25 m suggesting that the typical landslide area will only occupy a single pixel in a Landsat image and is unrecognisable. Hence Landsat images were only used to digitize land cover types. A brief description of the characteristics of the Landsat and ASTER images is given in Tables 5.2, 5.3 and 5.4. Detailed descriptions of these images are provided by Lillesand & Kiefer (2000).

Data	Source of data	Data type	Derived map	Factor class
Landslide inventory	Field observations	Point	Seed cells	Pyroclastic Porphyritic basaltic lava flow Porphyritic vesicular basalt Mud flow deposit Alluvial deposits Beach sand, shingle and pillow lava Massive basalts
Geology/parent rock type	Field survey, literature	Polygon	Rock type	
Soil type	Hasselo 1961	Polygon	Soil type	Ash soil Litho sol Old volcanic soil Valley clay soil Rocky soil Fragipan Lava soils
Land cover type	2000 ETM+ and field observations	Polygon	Land use raster	Built-up areas Plantation Forest Mangrove forest
DEM	1/50000 Topographic map	Digitised contour lines (line vector)	Slope (in degree)	0 – 5° 5 – 10° 10 – 15° 15 – 20° 20 – 25° 25 – 30° 30 -35° >35°
			Slope orientation	N NE E SE S SW W NW
River	1/50000 topographic map	Lines	Distance from rivers and stream density values	0 – 50 m 50 – 100 m 100 – 150 m 150 - 200 m 200 – 250 m 250 – 300 m > 300 m
		Euclidean distance interpolation of stream network	Stream density	Extremely low Very low Low Moderate High Very high Extremely high
Road net work	1/50000 topographic map and field survey	Line	Distance from road	0 – 50 m 50 -100 m 100 – 150 m >150 m
Faults and fractures	1/200000 geologic map from the GRINP Project	Line	Distance from faults	<100 m 100 - 200 m 200 – 300 m 300 - 400 m 400 – 500 m 500 – 600 m > 600 m
Mean Annual precipitation	20 - 34 years monthly rainfall from 12 stations operated by the CDC		Rainfall (mm)	< 2400 mm 2400 – 2800 mm 2800 – 3200 mm 3200 – 3600 mm 3600 – 4000 mm >4000 mm

Table 5. 1. Raw data, associated list of parameters (factors) observed to control landslide activities and factor classes used in landslide susceptibility assessment on the SE foot slopes of Mt Cameroon.

Landsat TM metadata

Bands	Resolution (m)	Spectral range
1	30	Blue
2	30	Red
3	30	Green
4	30	Near infra red
5	30	Short wave infra red
6	120	Thermal infra red
7	30	Shortwave infra red

Table 5. 2. Properties of Landsat TM images.

Landsat ETM+ metadata

Bands	Resolution (m)	Spectral range
1	30	Blue
2	30	Red
3	30	Green
4	30	Near infra red
5	30	Mid infra red
6	30	Thermal infra red
62	60	
7	30	Shortwave infra red
8	15	Panchromatic

Table 5. 3. Properties of Landsat ETM+ images.

ASTER metadata

Bands	Resolution (m)	Spectral range
1	15	Blue
2	15	Red
3N	15	Visible near infra red
3B	15	Visible near infra red
4	30	Shortwave infra red
5	30	Shortwave infra red
6	30	Shortwave infra red
7	30	Shortwave infra red
8	30	Shortwave infra red
9	30	Thermal infra red
10	90	Thermal infra red
11	90	Thermal infra red
12	90	Thermal infra red
13	90	Thermal infra red

Table 5. 4. Properties of ASTER images

The third data set is a soil map produced by Hasselo (1961). Faults and fractures were extracted from the geologic map produced by the GRINP Project that was carried out in 2005 to evaluate geohazards around the Mt Cameroon region.

5.1.2 Landslide mapping and generation of seed cells

From February 2008 to June 2010 intensive field surveys were undertaken to determine the spatial distribution of landslide scars (landslide inventory map) described in Chapter 2. A total of 63 landslides recorded between 2001 and 2010 were described. The inventory map was prepared at a scale of 1:50000 based on field surveys due to the unavailability of aerial photographs. Landslide locations were obtained at the centre of the main scarp. As slide scars are of relatively small size, they were recorded as point data in the Geographic Information System (GIS) database. The landslide data set was divided into a training set (75 %) used to calibrate the model and a validation set (25 %) used to validate the model in ArcGIS 9.1. Considering that the best undisturbed morphological conditions (conditions before failure) can be extracted from the vicinity of the landslide itself, seed cells were selected using a 25 m buffer zone around each landslide point. This buffer interval was chosen as the width and length of the landslide depletion zone rarely exceeded 25 m. Hence this buffer zone includes the entire failed area and its direct surrounding and thus provides the best representation of the properties of unstable areas. As the factor raster maps were produced at 20 m spatial resolution, a 25 m buffer resulted in at least 4 seed cells per landslide scar. This technique produced 222 seed cells from the training dataset and 84 seed cells from the validation data set, from which the contribution of the different determinant factor to landslide occurrence was calculated.

5.1.3 Data processing and generation of factor maps

All images and maps were first registered in Universal Transverse Mercator (UTM) Zone 32 N with WGS 84 as datum. However, because multi-temporal satellite images are acquired on different dates with different resolution, acquisition angles, sun angle and atmospheric influence, the coordinates of ground cells usually do not correspond between different images. Hence, the registered images could not be perfectly overlain on each other. For this reason, all the images were co-registered using ground control points and then wrapped onto a master image (ETM+ 2000) using the image and image polynomial warping algorithm in ENVI 3.6.

The study area is located in the hot humid tropical area: thus the images are strongly influenced by climatic perturbations and are frequently cloud covered. Correction for climatic influence on

the quality of the images was necessary to improve on its quality. In the absence of field data for calibration, the darkest pixel method was used. This involves subtracting the digital number (DN) of the darkest pixel in each band from the DNs of all the other pixels in that band. Enhancement and supervised classification were performed on all the images to reveal subtle differences and reduce data redundancy. Due to abundant cloud coverage in the 2000 image (Fig. 5.1), classification results were not good and were modified by manual digitisation.

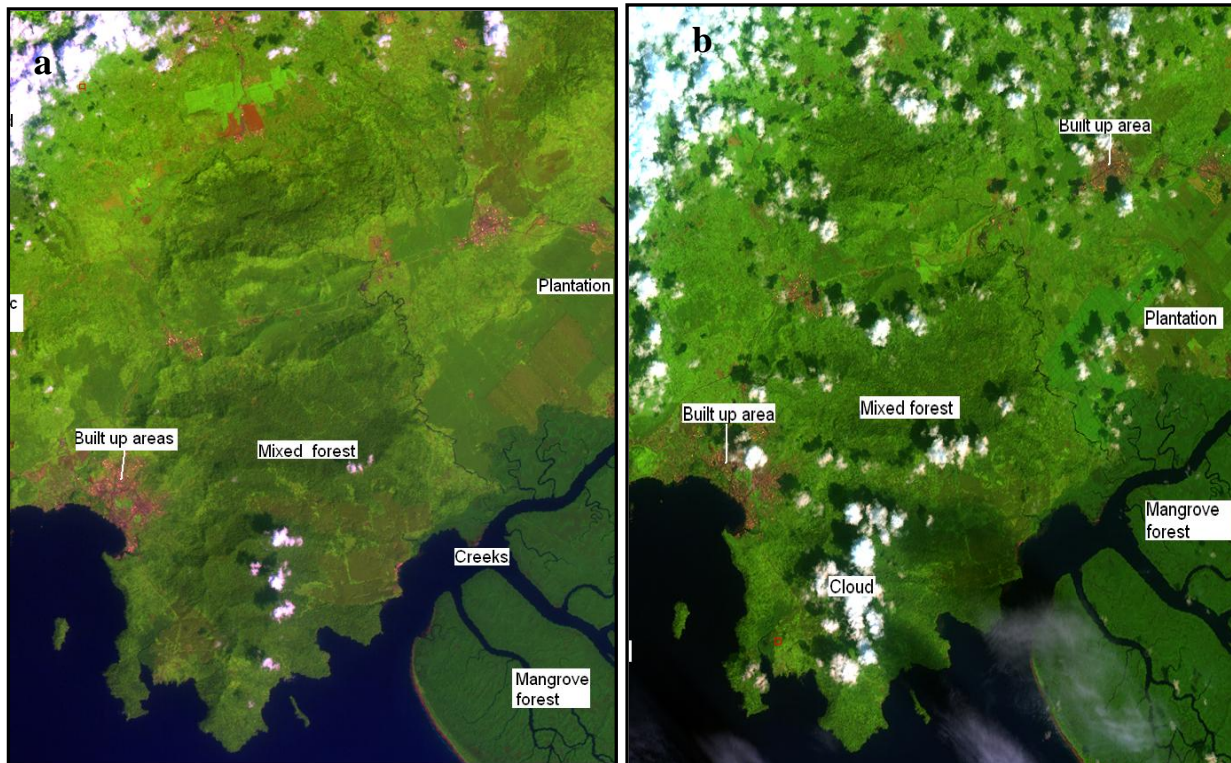


Fig. 5. 1. False colour composite of: a) band 532 of 1986 image and b) band 542b of 2000 image. Note the presence of clouds particularly on the 2000 and the distribution of land use patterns.

As mentioned above, no universal guidelines exist regarding the selection of factors in susceptibility mapping. However, the selection of the causal factors must take the nature of the study area and data availability into account. In a GIS based study, the factors selected must be operational, represented over the entire area, non-uniform, non-redundant and measurable (Ayalew *et al.*, 2005). Based on the above criteria, field observations, enquiries from inhabitants of affected areas, literature and available data, a total of 10 predisposing factors were considered in this study: rock type, soil type, land use, type slope gradient, slope direction, distance from streams, stream density, distance from roads, distance from faults and major fractures, and mean

annual precipitation (MAP). After selecting a causal factor, thematic maps were prepared for each of these factors following the methods and data described hereafter. Figure 5.2 shows a flow chart of the steps involved in the production of factor maps and associated factor weights.

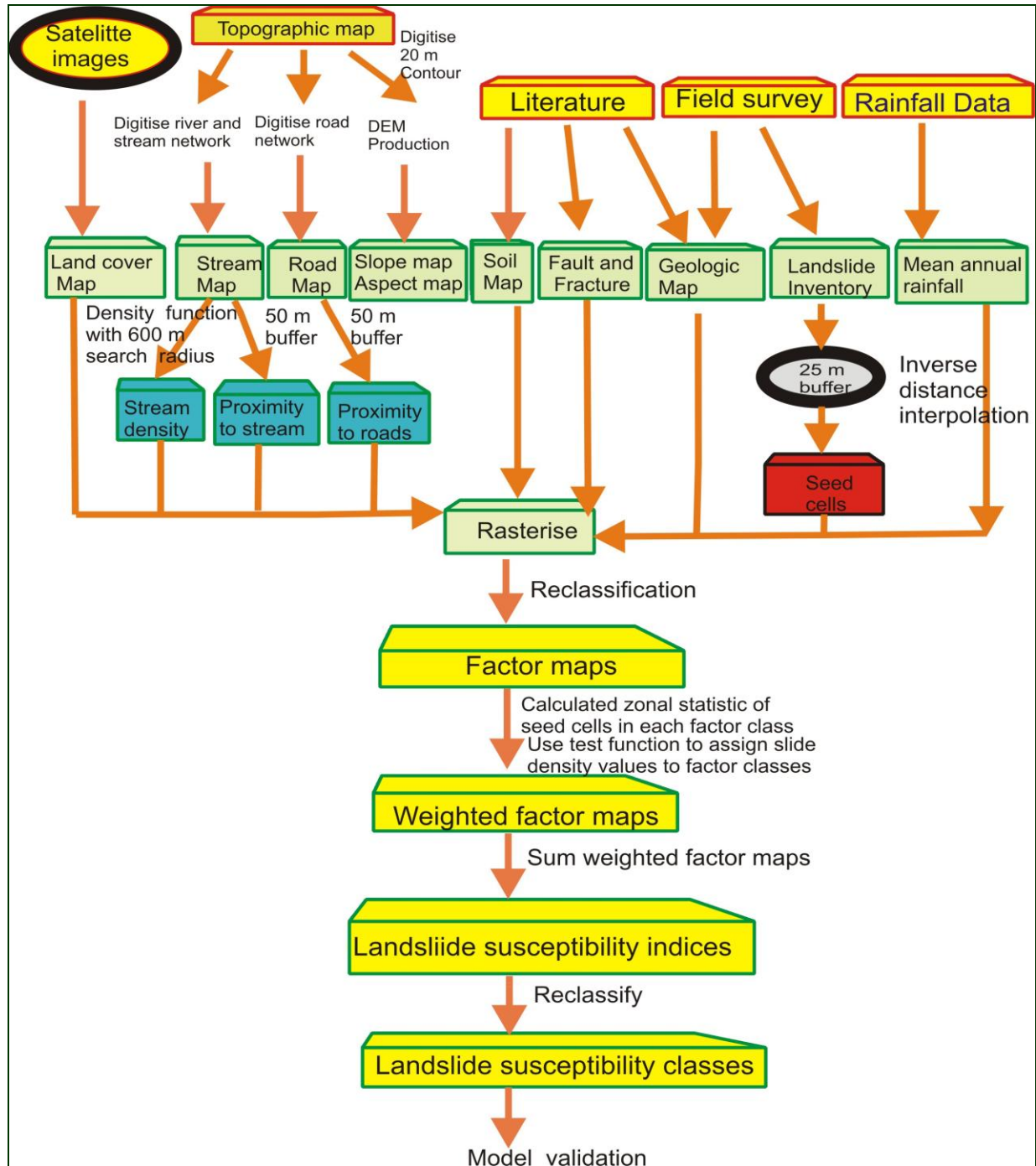


Fig. 5. 2. Schematic illustration of the steps involved in the creation of factor maps and in the susceptibility evaluation procedure used in this study.

Rock type

Though gravity is the main driving force in the occurrence of landslides, it does not act alone but in conjunction with other factors such as rock type (geology), soil type, slope gradient and so on. Many researchers agree that rock type has a major impact on the occurrence of landslides (Dia *et al.*, 2001, Yalcin, 2007). Parent rock type (lithology) determines to a great extent the rate of weathering and plays an important role in conditioning the development of drainage lines. Parent rock may also determine the shear strength and permeability of soils and rock and hence controls the rate of water infiltration. It also influences the properties of the residual soils derived from it, hence soil type was considered as one of the conditioning factors as well. The lithologic map was constructed by compiling field observations, geologic maps from existing literature (Endeley *et al.*, 2001; Njome, 2008; Thierry *et al.*, 2008), topographic maps and interpretation of satellite images. Figure 5.3 shows the lithologic map containing 7 rock types: porphyritic basalt, pyroclastic deposits, lahar (mudflow deposits), alluvial deposits, massive and vesicular porphyritic basalts, beach sand, shingle and pillow lava. Porphyritic basalts occupy about 74 % of the study area followed by lahar deposits that make up 17 % whereas the other classes each cover less than 5 % of the study area. Due to the limited amount of outcrops and the various data sources used, the position of the lithological boundaries has limited accuracy. Some slides are located on weathered pyroclastic cones, particularly those that have been modified by human interference in the form of excavation for construction without the application of any formal stabilization measure. Rock fall was observed within lahar deposits along the banks of the Ombe and Ndongo Rivers and on cliffs along the rocky coast of the Atlantic Ocean. A correlation between the rock type and the seed cells indicates that the pyroclastic material is more susceptible to failure than the lava flows and mudflow deposits.

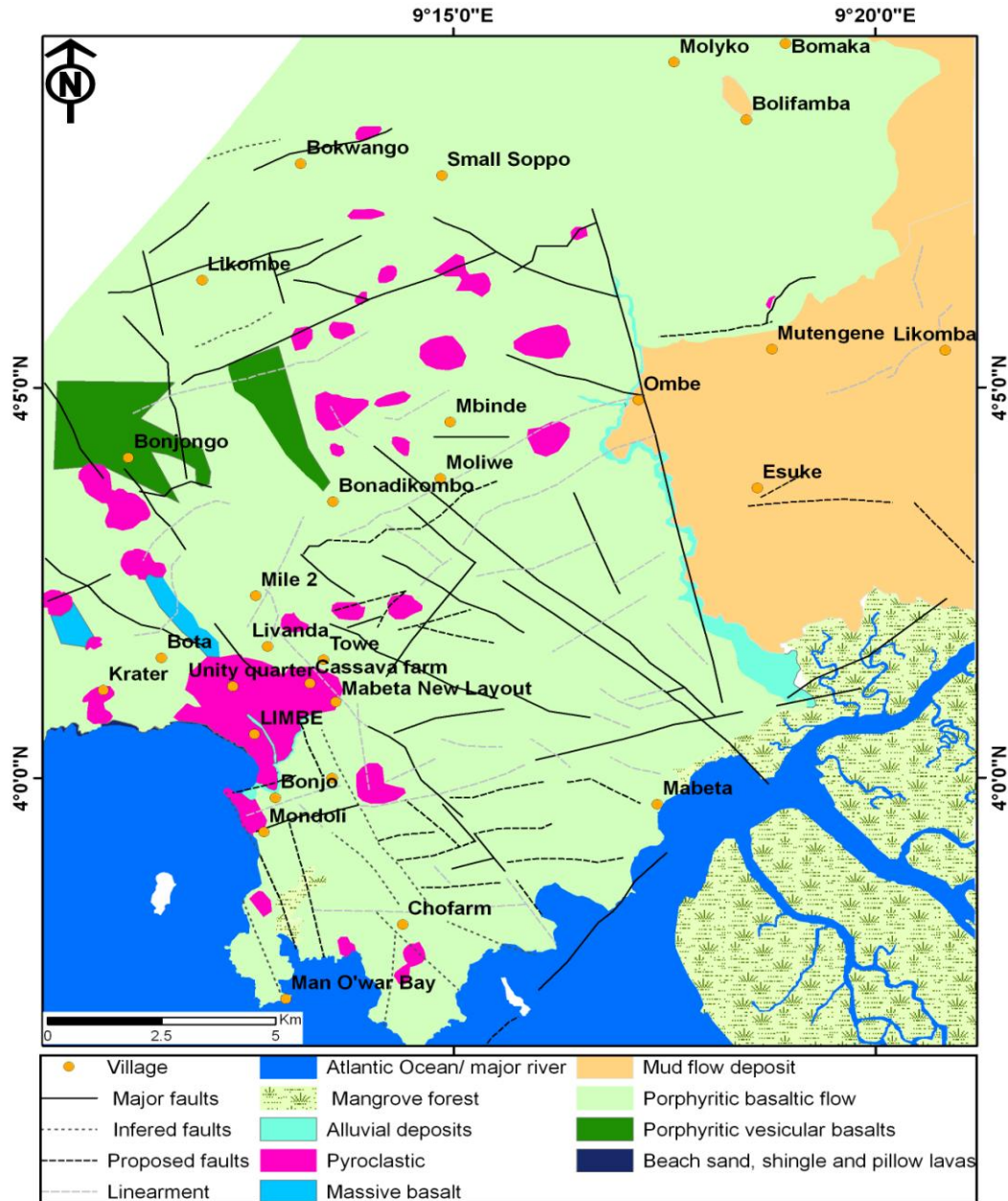


Fig. 5. 3. Geological map of the study area modified from Endeley *et al.* (2000), Njome *et al.* (2008) with field check. The limit of the lahar deposits was adjusted and pyroclastic deposits included. Faults, fractures and lineament were extract from the geological map of MC produced by the GRINP Project, Thierry *et al.* (2008).

Soil type

Soil type influences the occurrence of landslides within a particular area. Different soil types can be derived from the weathering of the same parent rock. The resulting product depends on the degree of weathering and the drainage condition operating during the weathering process. Soils within the study area are mottled, reddish brown, yellowish brown and pale yellow clayey silts,

silts and clays with diverse physical and chemical properties. They are characterized in detail in Chapter 3. However, due to limited aerial coverage of the soils analysed during this research, the soil map produced by Hasselo (1961) was digitised and used in this study. According to Hasselo's classification, there are seven soil types: old volcanic soil, ash soil, lava soil, lithosol, valley clay soil, stony soil and fragipan. Old volcanic soil refers to soils developed on basalts of the first volcanic phase of activity along the Cameroon Volcanic Line in the Mio-Pliocene. They are moderately deep soils characteristic for the Mabeta massif. The second volcanic phase is characterised by more evolved lava (trachyte, Awah, http://cameroun-foret.com/system/files/11_01_62.pdf) and these products are not found on MC. Ash soils, lava soils and lithosols are developed from lava of the third volcanic phase (Quaternary to Recent). Ash soils are soils on lava flows washed down slope by lahars, lithosols refer to shallow soils developed on hard rock such as basalts. Valley clay soils, fragipans, and rocky soils are young soils with volcanic parent material. Valley clay soils form in the valleys separating the ridges of the Mabeta massif. Stony soils are less than 60 cm thick, characterised by undulating broken surfaces and correspond to gravelly and stony soils developed on "young lava flows". The distribution of the soil groups is presented in Figure 1.4. In this study, the seven major soil groups were adopted and make up 28, 36, 18, 2, 11, 2 and 3 % of the study area, respectively.

Land use

Landslides are natural occurring phenomena and will occur whether people are present or not. However, human land use practice may accelerate the occurrence or play a vital role in the occurrence of landslides. A land use map (Fig. 5.4) was produced by supervised classification of an orthorectified Landsat image of the Mount Cameroon region, on the 10th of December 2000. This classification was based on observed variations in colour, texture and tone of objects on the image, calibrated using field observations or ground truthing. Because of significant cloud coverage, results of the classification were edited and simplified by manual digitalisation. Four main land use types were considered, namely forest, plantations, built-up areas and mangrove forest. These classes make up ~58, 36, 6, and <1 % of the study area, respectively.

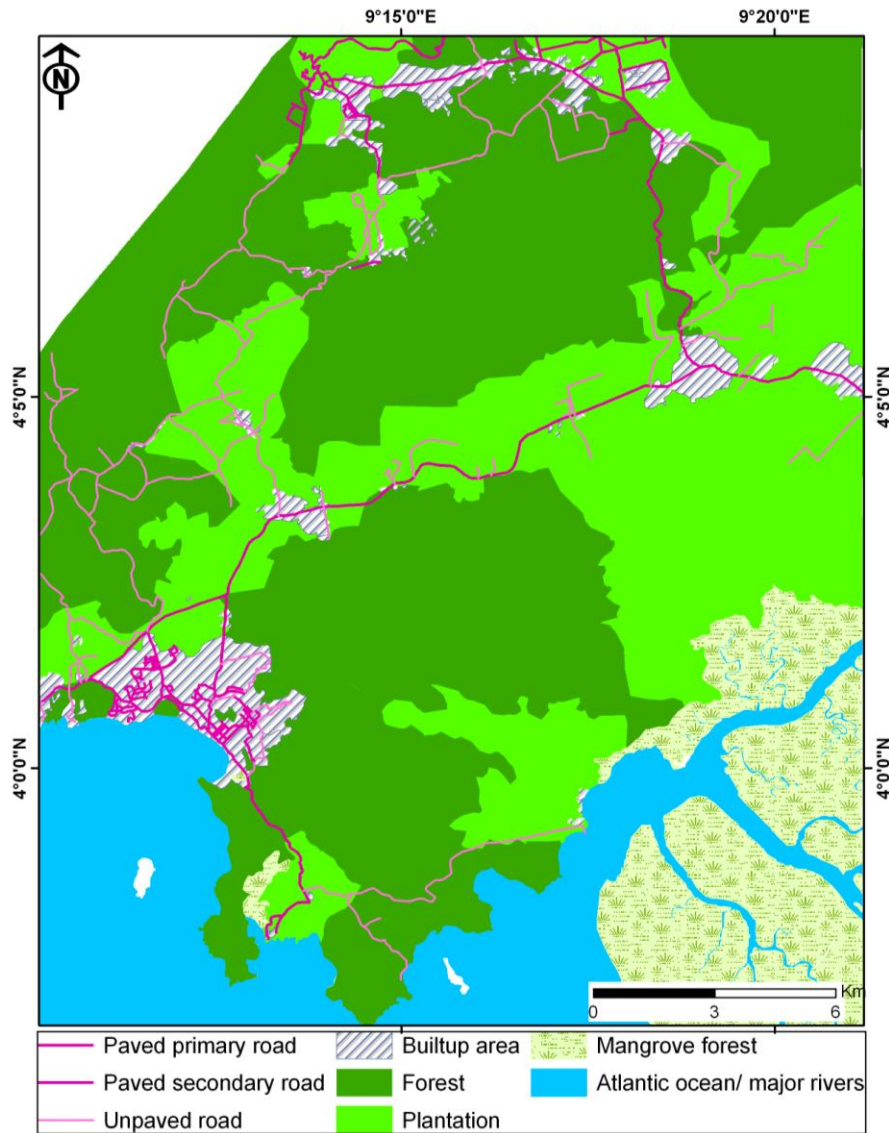


Fig. 5. 4. Land use map of Limbe and its environment, manually digitised from a 2000 Landsat image.

Slope gradient and slope orientation

It has been observed that slope failure is more common on steep slopes than on gentle slopes. Thematic maps of slope gradient (Fig. 5.5), and slope orientation were generated using 20 m grids from the Digital Elevation Model (DEM). The DEM was obtained by interpolating 20 m contour lines digitised from a geo-referenced 1:50000 topographic map using the “Topo to Raster” function in ERSI ArcGIS 9.1.

The Topo to Raster algorithm is an interpolation method specifically designed for the creation of hydrologically corrected DEMs. It is based on the ANUDEM program developed by Hutchinson (ArcGIS desktop help). ANUDEM calculates ridges and streams from points of maximum local curvature on contour lines and incorporates a drainage enforcement algorithm that automatically removes spurious sinks in the fitted elevation surface (Hutchison, 1988).

Slope gradient derived from the DEM ranges from 0 to 43° and was regrouped into 8 classes of 5° intervals to cover the entire range of values, all the pixels with slope above 35° being grouped into one single class. Tests were made to assess the influence of the class ranges on the derived factor class weight, but an equal interval was found to be the most rational choice.

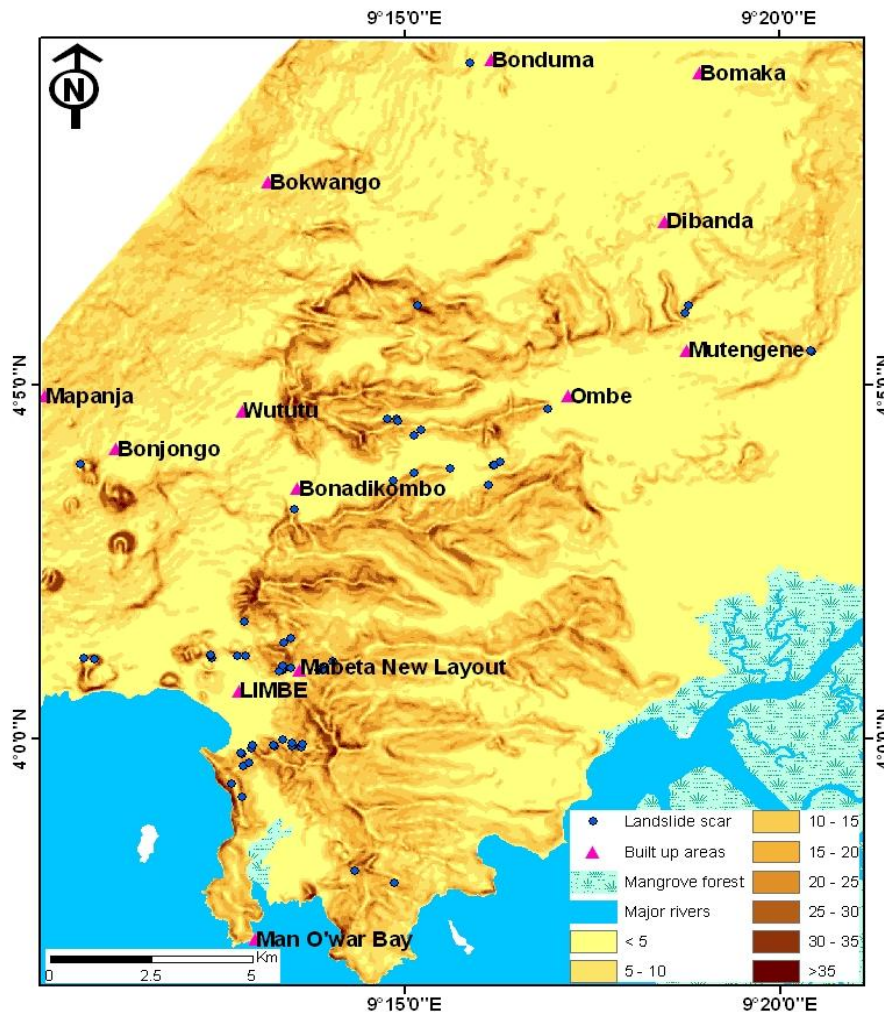


Fig. 5. 5. Slope map of the study area generated from a 20 m DEM showing the location of observed landslide scars. The DEM was derived from Topo to Raster interpolation of 20 m contour lines. Slope angles are given in degrees.

Slope orientation, which represents the direction of maximum slope, was categorised into 8 classes of 45° interval, i.e. into N, NE, E, SE, S, SW, W and NW facing slopes (Fig. 5.6).

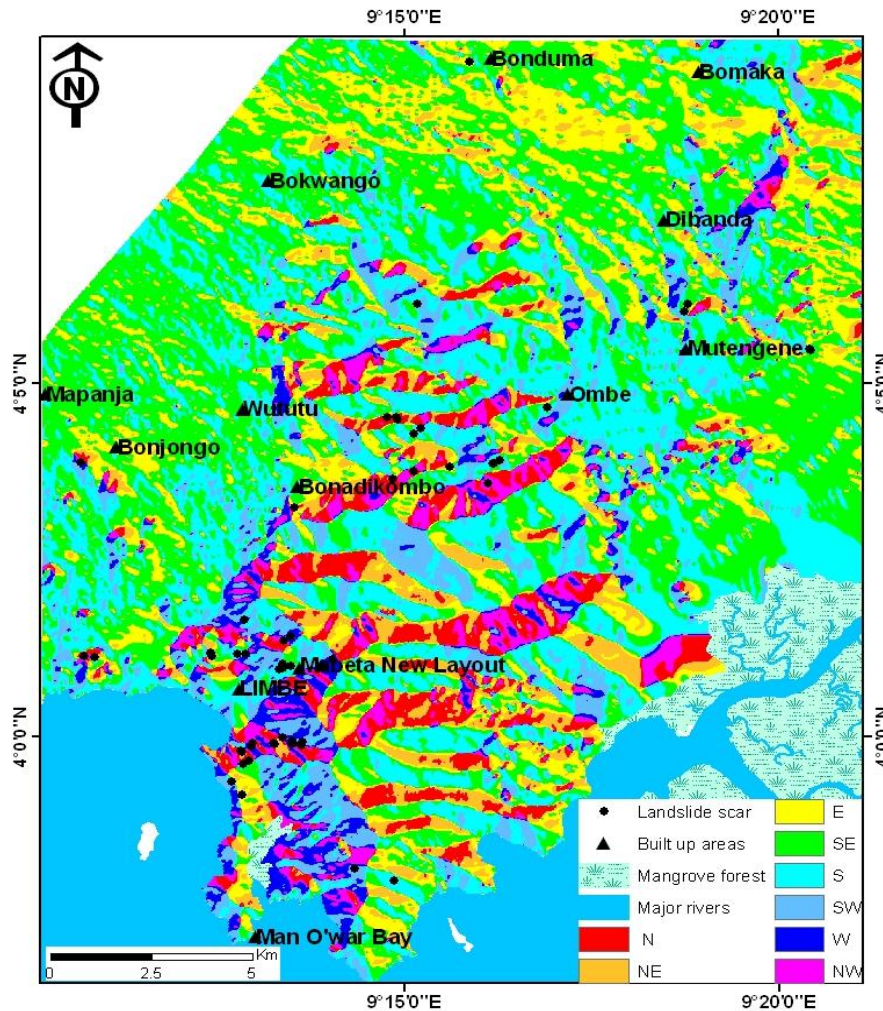


Fig. 5. 6. Slope orientation map of the study area generated from a 20 m DEM showing the location of observed landslide scars.

Proximity to streams and stream density

The proximity to streams is considered as a potential controlling factor as stream undercutting of slope base has been recognized to be the cause of several landslides in the region (Che *et al.*, 2011). The potential effect of proximity to stream is implemented by applying the Euclidean distance function in ArcGIS along the streams and rivers digitised from the topographic map. The distance is then reclassified into 7 classes of 50 m intervals, all pixels further than 300 m from rivers were grouped into one single class as it is assumed that the influence of the stream would be negligible beyond such a distance.

To approximate the regional distribution of ground water conditions, a drainage density map (Fig 5. 7), which defines the number of line elements of fixed length in a fixed area (Süzen & Doyuran, 2004), was obtained by a non-interpolative mean using the density function in ArcGIS and used as a factor. The stream drainage density map was computed with a search radius of 600 m and classified into 7 classes of equal interval of density values.

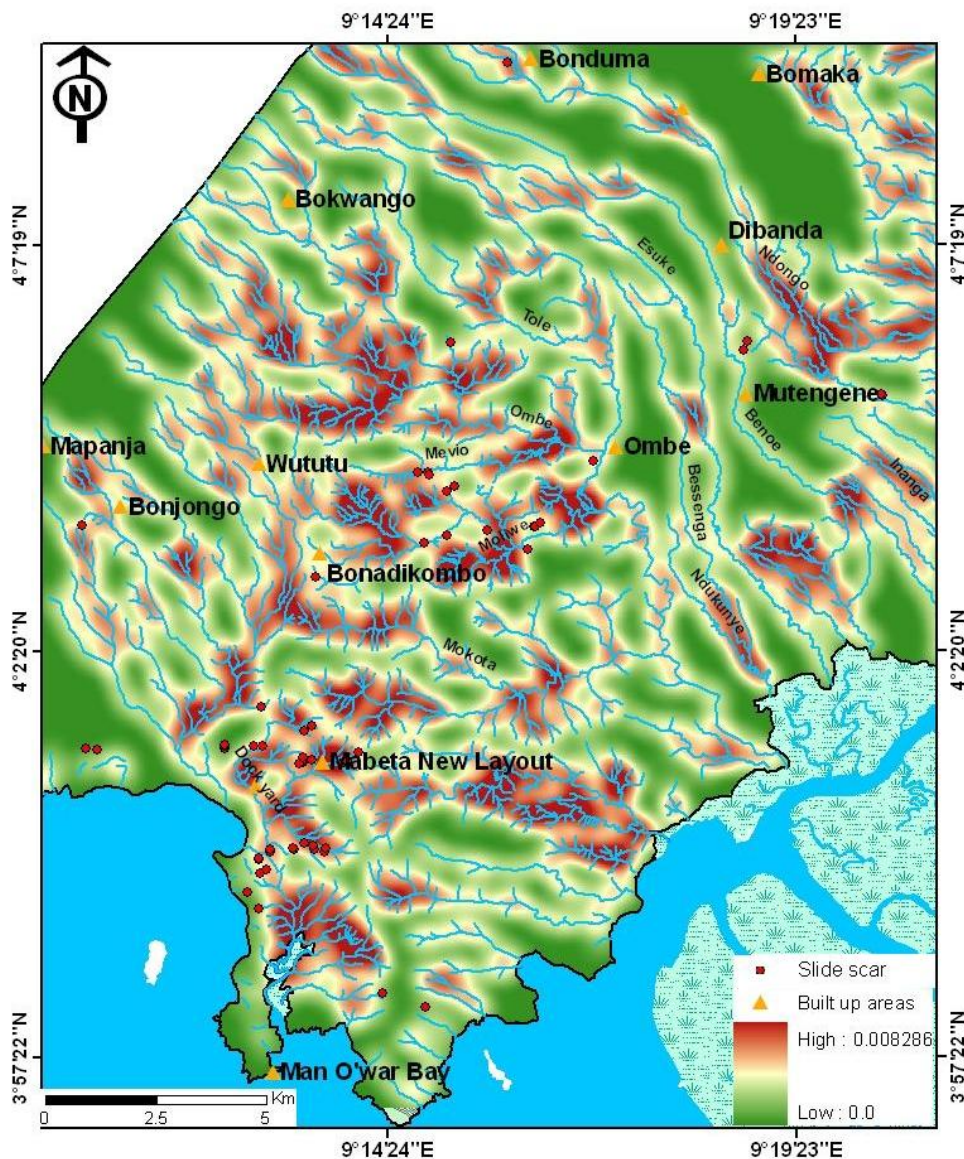


Fig. 5. 7. Stream density map (search radius 600 m) of streams identified in the Limbe area. Density values are in number of line elements/km². Streams are superimposed on the density map and landslide scars represented as red dots.

Proximity to roads

Proximity to roads is considered as a potentially important factor because road construction is usually accompanied by excavation in some areas and the addition of material to the slope. This might result in changes in the slope line or may be accompanied by the creation of artificial slope or road cuts that might be affected by landslide activities (Che *et al.*, 2011). The role of these processes on the occurrence of landslides is evaluated by applying multiple buffers (50 m increments) around roads digitised from the topographic map and corrected by tracking new roads with a Garmin GPS 60CSX receiver (Fig. 5. 4). The 50 m buffer was chosen as a trade-off between the 20 m resolution of the factor map and the accuracy of the road mapping from the initial topographic map. Areas located at a distance greater than 150 m from a road were considered as not affected by road-related instability and grouped into a single class.

Proximity to major fractures and lineaments

Faulting results in fracturing and destabilization of rock and soils and thus was considered as one of the main factors. Field observations indicate that rocks within the study areas are highly fractured and weathering is not uniform. Faults and major fractures were extracted from the geological map produced by the GRINP (Management of Natural Risks and Civil Protection) project (Thierry *et al.*, 2008) and multiple buffers of 100 m incremental distance were used to generate a 'proximity to fault' map (Fig. 5.8). The area is characterised by low magnitude earthquakes and faults that are not very active. Hence, their destabilizing potential will tend to decrease with increasing distance from the fault line. A 100 m interval is thus appropriate to mimic the influence of faults on the occurrence of landslides.

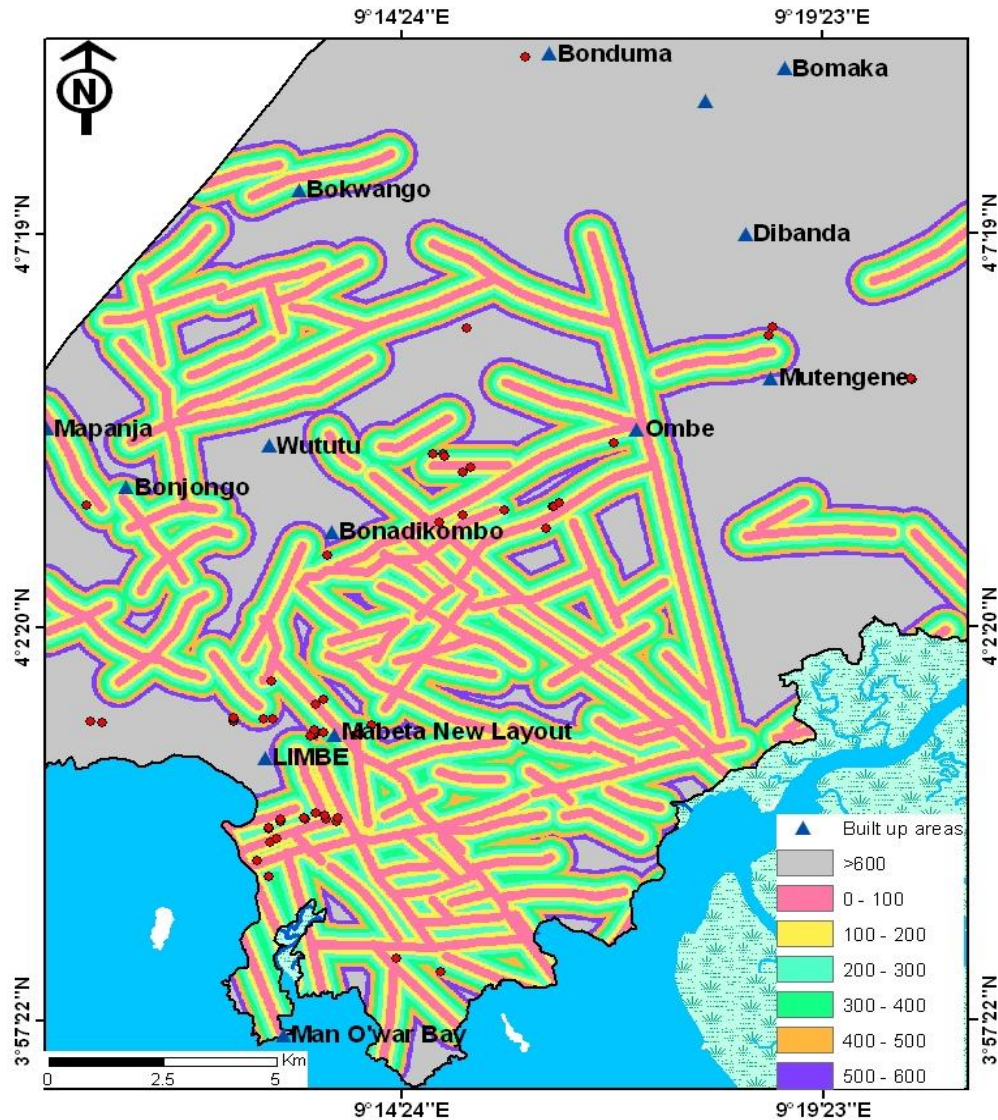


Fig. 5. 8. Proximity to faults and major fractures digitised from the geological map of Mt Cameroon modified after Thierry *et al.* (2008), obtained by applying the Euclidian distance function in ArcGIS 9.1. Categories are defined by 100 m incremental distance. Distance values are in m.

Mean annual precipitation (MAP)

MAP is considered as a factor potentially contributing to slope instability as rainfall is the principal source of groundwater recharge coupled with the fact that the area is characterised by a long rainy season that lasts at least 8 months per year. The spatio-temporal distribution of rain is highly variable within this region. Mean annual rainfall distribution therefore provides a general picture of groundwater distribution within the study area and can better explain the long term effect of soil water on slope destabilization. The lack of long term daily rainfall data prevents

using rainfall to assess the triggering factor controlling the timing of landslides. MAP is obtained by interpolating 20 - 34 years of mean annual rainfall data from 12 stations (Fig. 5.9), 10 located within and 2 outside the study area (to the NE and SW). The Inverse Distance Weighted Interpolation method used here does not enable to account for topographic control on rainfall distribution, but constraints are lacking to calibrate a more realistic interpolation. Minimum MAPs is ~2000 mm and maximum ~4400 mm/ year. This range was sub-divided into 6 classes of 400 mm interval to cover the entire range of values.

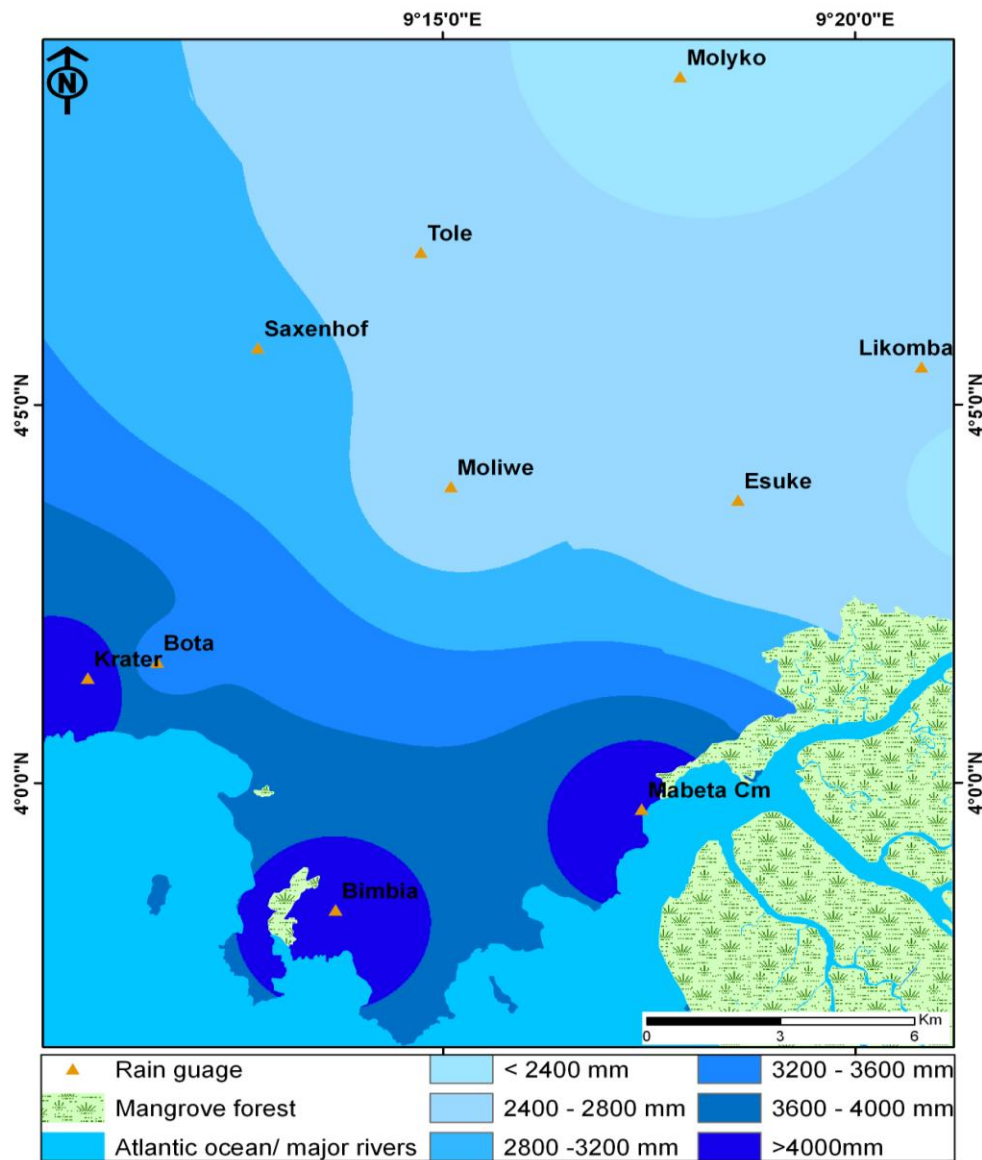


Fig. 5. 9. MAP of the study area obtained by the inverse distance interpolation technique of 20 to 35 years of monthly rainfall data from 12 rain stations managed by the CDC.

5.2 Landslide susceptibility evaluation

Bivariate statistical analysis involves determining the abundance of landslides within each factor class. To evaluate the influence of each factor class on landslide susceptibility, zonal statistics from factor maps for all the seed cells of the training dataset were calculated and the frequency of seed cells per factor class used to calculate landslide density values per factor class based on the following formula:

$$D_j = 10000 \times \frac{Npix(Sc)_j}{Npix(F_j)}$$

where D_j = slide density for the factor class j
 $Npix(Sc)_j$ = number of seed cells within a factor class j
 $Npix(F_j)$ = number of cells within the factor class.

To determine the influence of each factor on the entire area, weighting values were introduced, which, following Süzen & Doyuran (2004) enable the comparison of the slide density per factor class to the slide density in the entire study area. This is done by subtracting the landslide density of the entire area from the landslide density of each factor class.

$$W_j = D_j - 10000 \frac{\sum Npix(Sc)}{\sum Npix(F)}$$

where W_j = weighted factor for class j
 $\sum N_{pix}(Sc)$ = total number of seed cells within the study area
 $\sum N_{pix}(F)$ = total number of pixels within the study area

To avoid negative weighting values, normalization (rescaling) is implemented by adding the absolute value of the largest negative value to the weight of each factor class. Negative values indicate a low tendency for landslides to occur within that factor class. Normalized weights (Information value (Infoval)) are assigned to each factor class to obtain weighted factor maps. These factor maps are then summed up on a 20 m grid basis using the raster calculator tool to obtain a landslide susceptibility index value for each pixel.

Resulting susceptibility indices, which are continuous variables, are then reclassified into five susceptibility classes (very low, low, moderate, high and very high). It should be noted that there are no universally acceptable norms with regards to the division of continuous data into discrete parameters (Ayalew *et al.*, 2005). In this study, the susceptibility indices were reclassified into

five classes with the mean susceptibility index as the lower boundary of the moderate susceptibility class. Other classes were then defined using the standard deviation as the class interval. Susceptibility indices above the mean plus twice the standard deviation were considered to be in the very high susceptibility category. This idea is borrowed from mineral exploration, where element concentrations less than the mean plus two standard deviations are considered as normal background values whereas values above the mean plus two standard deviations are considered as enrichment zones or ores. Although this classification is based on a subjective choice, it was shown to generate acceptable results and as it is based on the statistical distribution of susceptibility values, it can be reproduced in a comparable manner for different factor combinations. The model was evaluated with the training data set to obtain the accuracy and then validated with the validation seed cells that were not used for model calibration. Success rate curves are drawn to test the prediction potential of the factor maps.

5.3 Landslide risk assessment

In this study, risk is perceived as the number of people, roads and specific structures that are likely to be affected by future landslides, and can be expressed as a simple overlay of element at risk on the susceptibility map. The outline of built-up areas was used, including an inventory of 133 individual structures that could be occupied by a large number of persons, such as schools, hospitals, churches, markets and financial institutions, as well as 20 road junctions and 12 bridges on the SE foot slopes of MC (Table 5.5).

Structure	Number
Schools	46
Bridges	12
Clerical institutions	15
Health facilities	8
Financial institutions	13
Government administrative structures	49
Water Tanks	1
Markets	2
Road junctions	20
Total	166

Table 5. 5. Summarised inventory of objects at risk.

The outline of built-up areas (Fig. 5.10) acts as a surrogate to the total population, whereas the road network acts as a fingerprint to the disruption of economic activities. Limits of built-up areas were extracted by digitising from 3 LANDSAT ETM+ images acquired on December 12,

1986, December 10, 2000 and on January 31, 2008. These shape files were converted to raster files and zonal statistics between the susceptibility map and objects at risk evaluated to identify the proportion of the objects at risk within each SC.

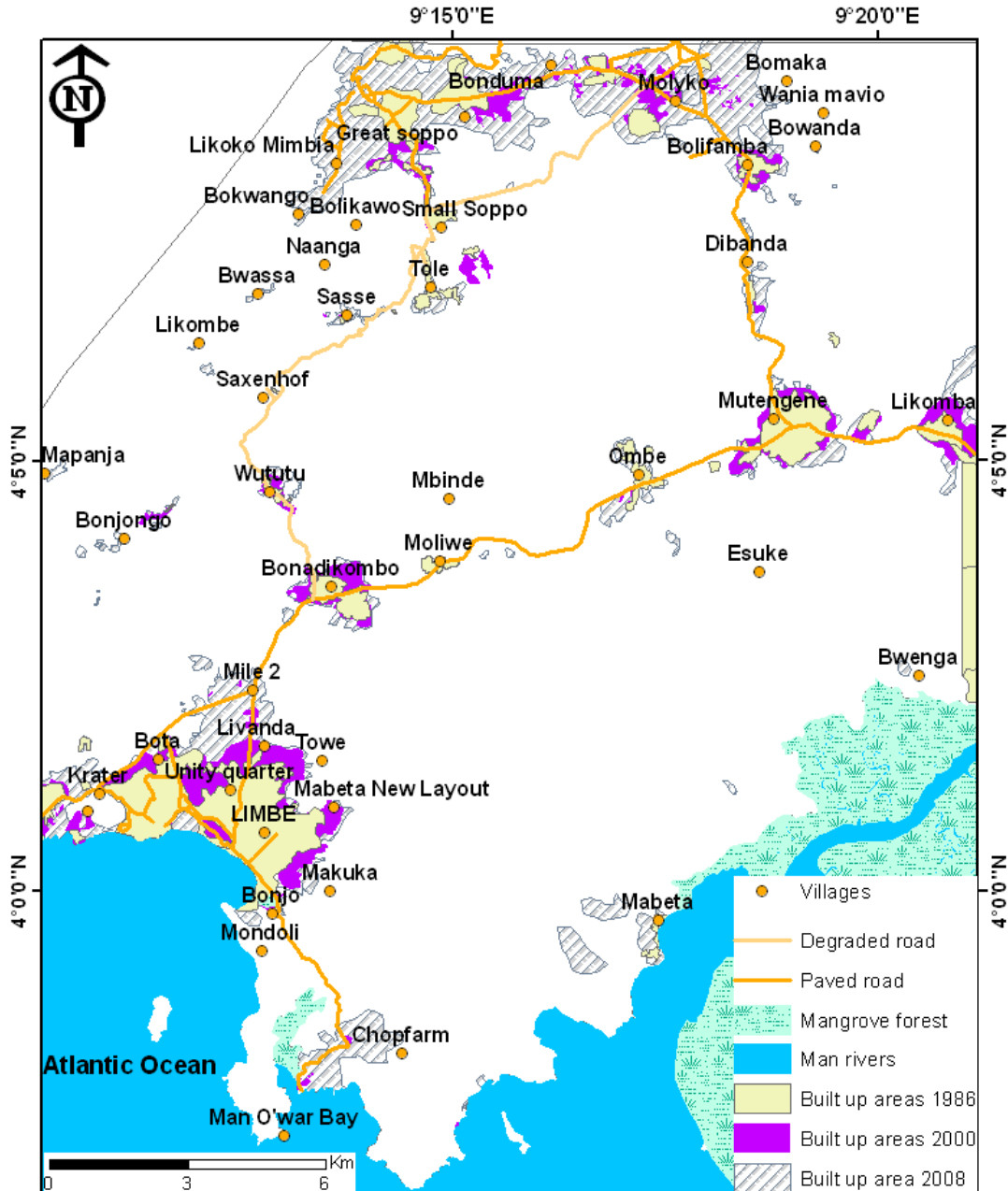


Fig. 5. 10. Time series changes in the outline of built-up areas on the SE foot slope of MC digitized from 3 Landsat images acquired in 1986, 2000 and 2008. Note gradual expansion of the outline of built-up areas with time.

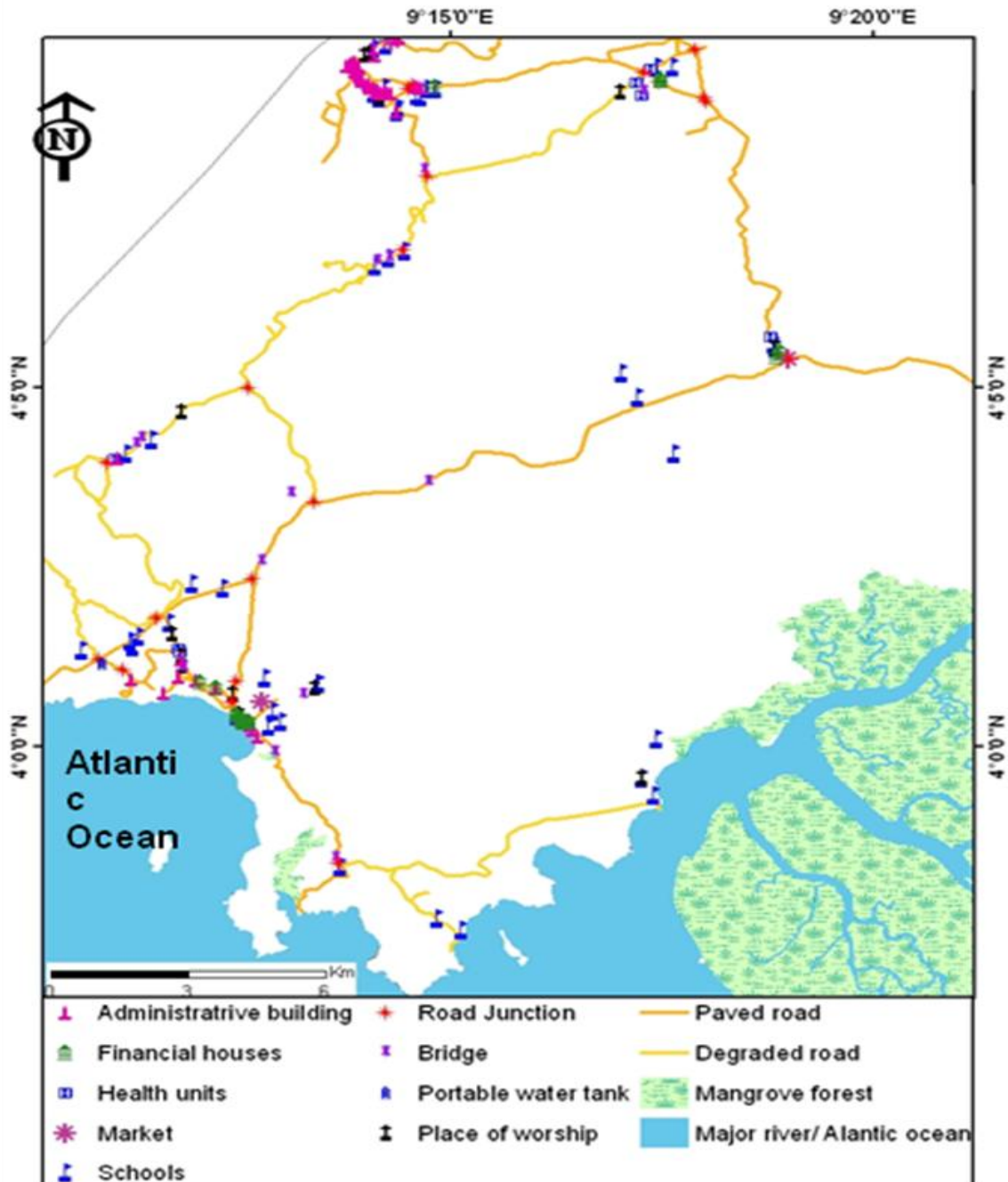


Fig. 5. 11. Spatial distribution of important facilities within the study area.

5.3.1 Relationship between factors and seed cells.

Histograms of the proportion of seed cells within each factor class and the distribution of factor classes within the study area are shown below. Based on calculated Information value (Infoval), rock type and slope gradient seem to be the most influential parameters in the study area with

values of 15.56 and 12.04, respectively recorded on pyroclastic materials and on slopes with a gradient between 25 - 30°.

Considering the factor rock type, 68 % of the training seed cells fall in porphyritic basaltic lava flows, 28 % on pyroclastic material and 3 % on mudflow deposits. None of the training seed cells were observed on porphyritic vesicular basalt or on massive basalt. Figure 5.12 shows the distribution of rock types and associated seed cells. Looking at the relatively high proportion of seed cells on the pyroclastic material relative to its aerial extend in the study area, it can be concluded that pyroclastic materials are more susceptible to failure than lava flows and mudflow deposits. Maximum Infoval in this factor is linked to the pyroclastic material indicating a high susceptibility to failure. All the other classes show rather low susceptibility. Table 5.6 shows the proportion of pixels in each factor class, associated number of pixels and calculated Infoval from which the histograms in Figure 5.12 were derived. Similar tables for all the 9 other factors are included in appendix 6.

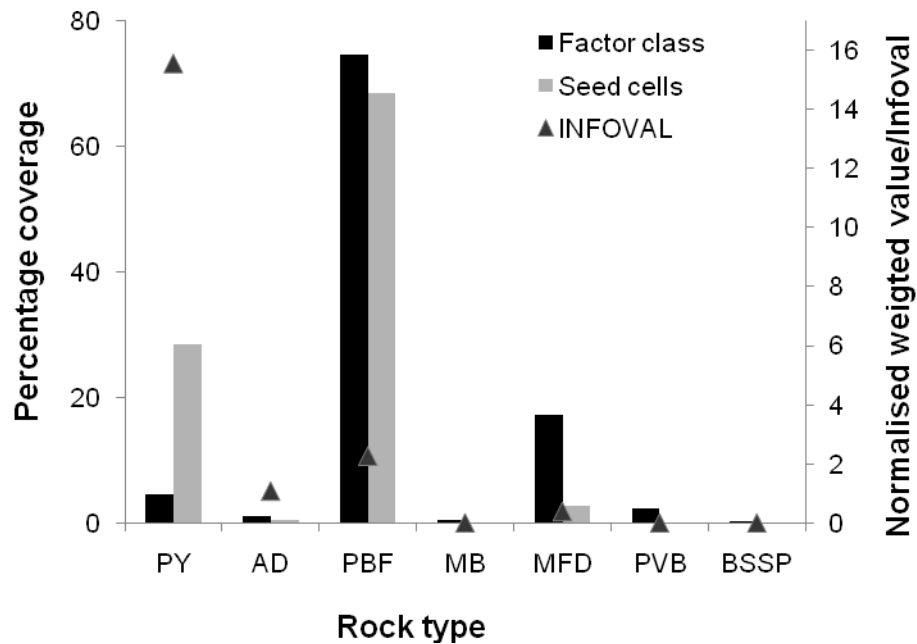


Fig. 5. 12. Distribution of the various rock types, proportion of seed cells they contain and associated normalized weighted values (Infoval) for the factor layer. PY: pyroclastics; AD: alluvial deposit; PBF: porphyritic basaltic lava flow deposit; MB: massive basalt; MFD: mudflow deposit; PVB: porphyritic vesicular basalt; BSSP: beach sand, shingle and pillow lava.

Rock type	Total number of pixels	Number of seed cells	% of total area covered	% of seed cells	Seed cell density per factor class	Weighted density	Normalized values
Pyroclastics	40483	63	4.49	28.38	15.6	13.10	15.56
Alluvial deposits	9275	1	1.03	0.45	1.1	-1.38	1.08
Porphyritic basaltic flow	671636	152	74.50	68.47	2.3	-0.20	2.26
Massive basalt	3690	0	0.41	0.00	0.00	-2.46	0.00
Mudflow	155174	6	17.21	2.70	0.39	-2.08	0.39
Porphyritic vesicular basalt	20628	0	2.29	0.00	0.00	-2.46	0.00
Beach sand , shingle and pillow lava	630	0	0.07	0.00	0.00	-2.46	0.00
	901516	222					

Table 5. 6. Distribution of the various rock types, proportion of seed cells they contain and associated normalized values (Infoval) for the factor layer.

Based on soil type, 77 % of the training seed cells occur within old volcanic soil, 11.7 % in valley clay soils, 8.1 % in ash soil, whereas the other soil types contain very low or no training seed cells. Figure 5.13 shows the distribution of soil types and the proportion of associated seed cells. It is worth noting that old volcanic soils which make up 28.4 % of the study area host 77 % of the seed cells. Maximum Infoval in this factor is linked to the old volcanic soil with a rating value of 6.69. Lower but significant weights are assigned to rocky and valley clay soils. All other classes show extremely low weights suggesting lower susceptibility to failure. The full table is included in Appendix 6, Table A 6.

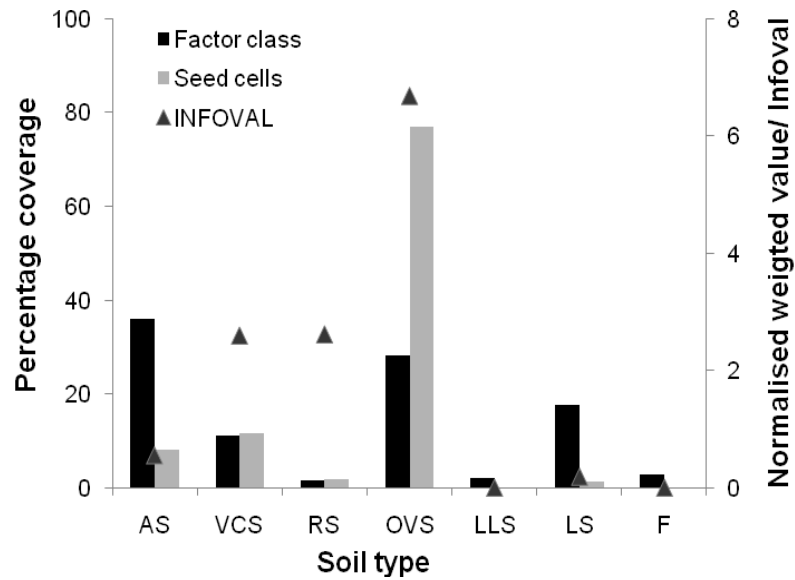


Fig. 5.13. Distribution of the various soil types, proportion of seed cells they contain and associated normalized values (Infoval) for the factor layer. AS: ash soil; VCS: valley clay soil; RS: rocky soil; OVS: old volcanic soil; LLS: lithosol; LS: lava soil; F: fragipan.

Of the four land use patterns noted in the area, forest covers 58 %, plantations 36 % and built-up areas 6 % of the study area (Fig. 5.14). These land use types are associated with 70, 15 and 15 % of the seed cells, respectively. Maximum Infoval is observed in built-up areas. In addition, built-up areas have the highest weighted value followed by forest/mixed land (Table available in Appendix 6, Table A 7). It was observed that some of the slides within palm plantations occurred after older palms were cut down for replanting (Che *et al.*, 2011).

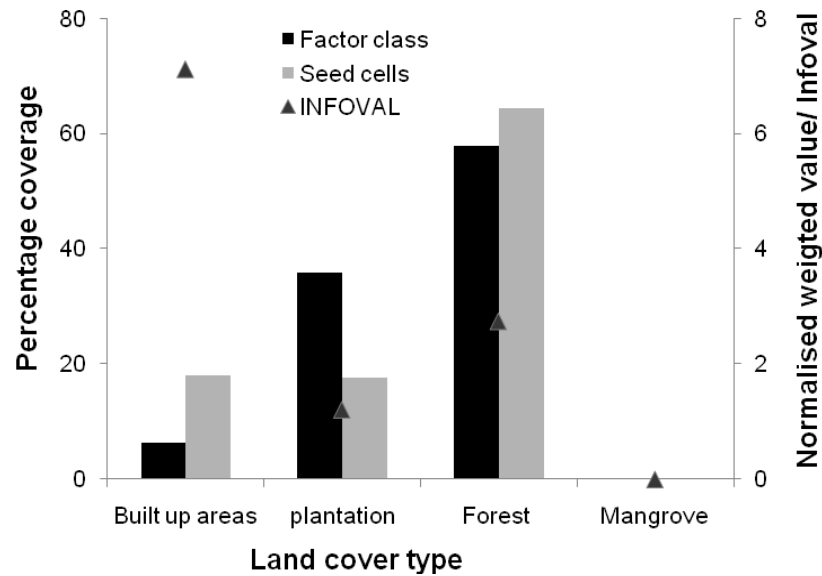


Fig. 5. 14. Summary of land use factor class distribution, proportion of seed cells they contain and associated normalized values for the land cover type.

Slopes with gradients $< 10^\circ$ make up 69 % of the study area and contain less than 15 % of the seed cells (Fig. 5.15), whereas slopes with a gradient between 10° and 30° represent 31 % of the area and contain 85 % of the seed cells. Maximum Infoval for the slope factor (Table available in Appendix 6, Table A 8) is associated with slope gradients between 25° and 30° , followed by gradients between 20° and 25° and 15° and 20° indicating a high probability of failure for these slope categories. It is worth noting that slope gradients measured in the field are slightly different and generally higher than those obtained from the DEM. This is probably due to the limited DEM resolution and effect of the interpolation method used for obtaining slope gradients. In the field slides occurred only on slopes above 15° but were dominant on slopes between 26° and 40° .

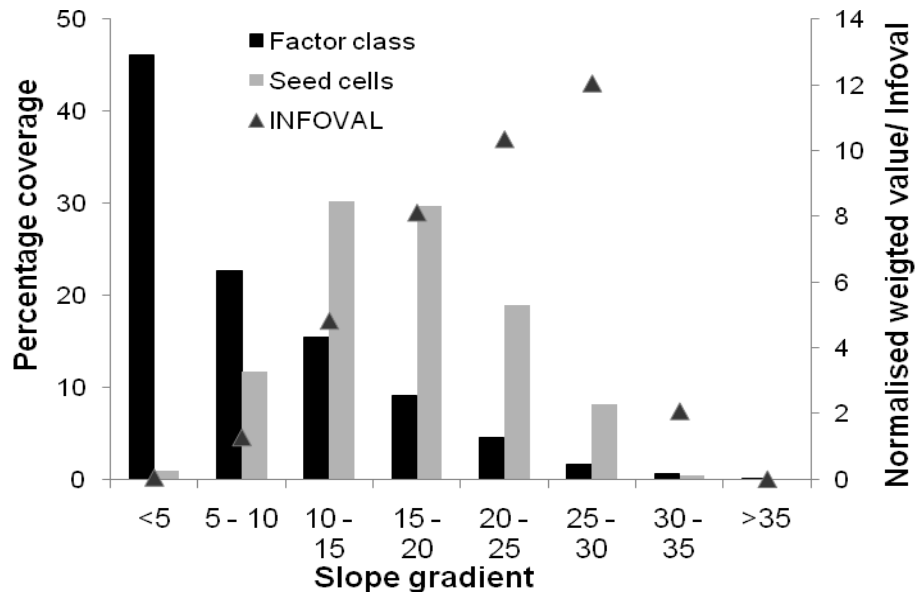


Fig. 5. 15. Distribution of slope gradient factor classes associated seed cells and associated Infoval.

The dominant slope orientations are SE, S and E facing, making up 32 %, 24 % and 15 % of the study area, respectively (Fig. 5.16). All other directions each make up less than 9 % of the study area. The number of seed cells is highest on S facing slopes whereas SE, SW, NW, W and N slopes have almost the same percentage of seed cells. High Infoval is associated with N, NW and W facing slopes whereas moderate values appear on NE and SW facing slopes (Appendix 6, Table A 9). This is probably due to the fact that the dominant rift zone follows a NE-SW orientation, and hence major failure directions should be oriented perpendicularly to the rift zone, i.e. NW and SE. All other classes represent low to very low probability of failure.

From the relationship existing between the training seed cells and the factor proximity to stream, it is noted that the distribution of seed cells do not vary significantly with various factor classes. However, minimum values are recorded for the class interval 250 - 300 m. Similarly, calculated Infoval does not vary greatly and ranges from 0 - 3.5 (Fig. 5.17). These values are small when compared to Infoval calculated for other factor classes, thus suggesting that proximity to stream does not play a major role in the localisation of landslide scars within the study area. Figure 5.17 shows that there is no clear pattern for occurrence of landslides in relation to the distance to streams. The complete table presenting the distribution of seed cells within the study area and their relationship to the proximity to stream is included in Appendix 6, Table A 10.

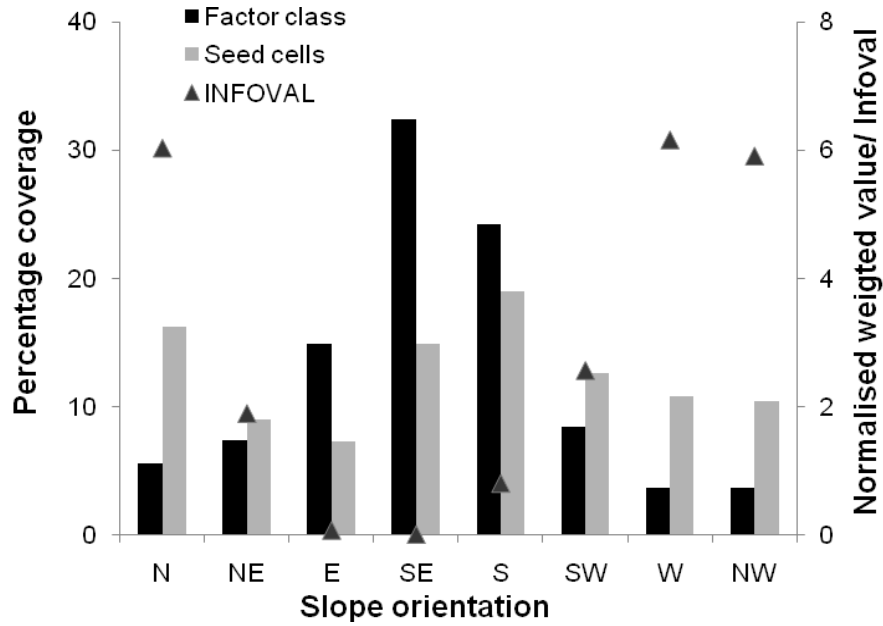


Fig. 5. 16. Distribution of slope orientation factor classes, associated seed cells and Infoval.

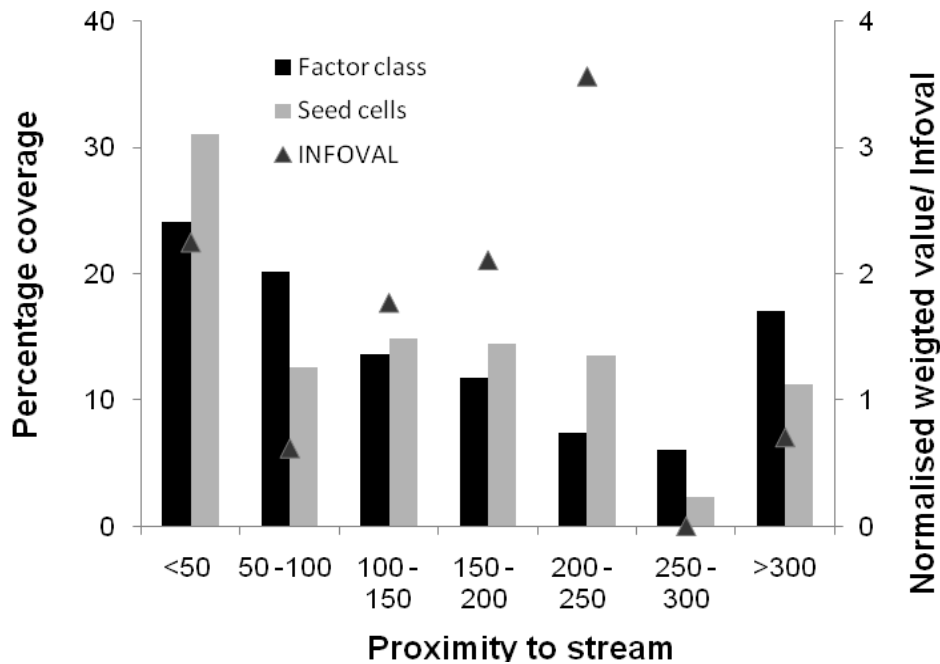


Fig. 5. 17. Distribution of proximity to stream factor classes, associated seed cells and Infoval.

The stream density evaluation indicates that 68 % of the training seed cells occur in the moderate and high stream density categories. Areas with high and moderate stream density show higher Infoval (Fig. 5.18) than those with low or very high density values. The full table is included in Appendix 6, Table A 11. Considering that stream density provides an idea about regional

groundwater distribution, regions with very high and extremely high stream density correspond to low lying, marshy and swampy areas, flood plains and stream channels where slope failure is less likely to occur. Areas with high and moderate stream densities are more likely to fail because of high ground water concentration and a net negative influence on soil stability due to increasing shear stresses. Lower stream densities indicate drier soils and it has been proven that drier soils tend to be more stable than wet soils.

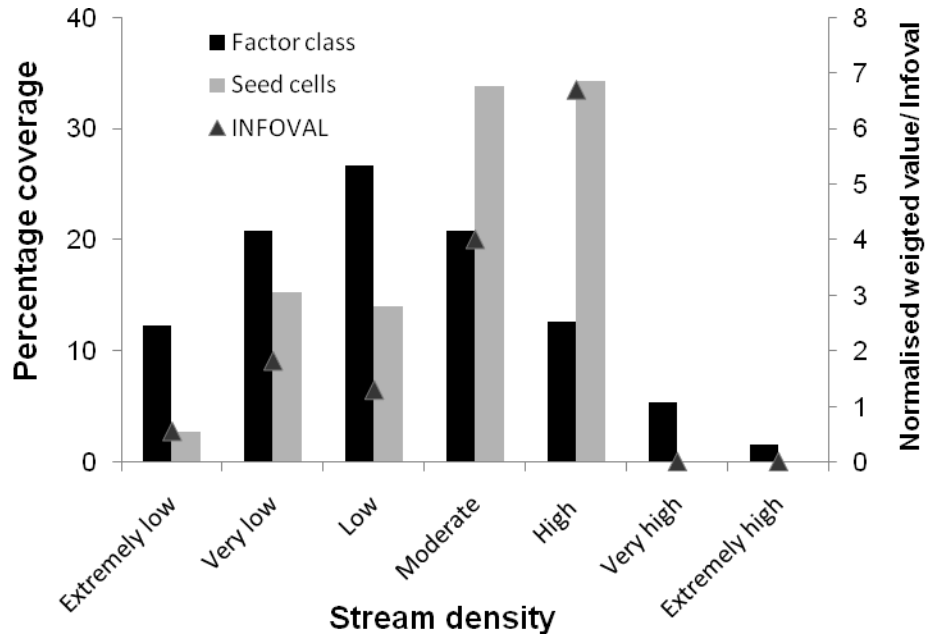


Fig. 5. 18. Distribution of stream density factor classes, associated seed cells and associated Infoval for the factor stream density used in landslide susceptibility assessment in the Limbe area.

The factor proximity to roads shows a bimodal distribution for the seed cells within the various classes; 21 % of the seed cells are located within < 50 m from roads. This percentage drops to 8 in the interval 50 – 100 and then increases progressively towards a maximum value at a distance above 150 m, suggesting that there are two types of slides in this area: road related and non-road related slides. Calculated Infoval indicate that the maximum values are recorded in the 0 - 50 m category, followed by the 100-150 categories (Fig. 5.19). This suggests that the presence of roads affect the occurrence of some of these slides while others occur in areas where roads do not have an impact on their occurrence. The complete table illustrating the distribution of pixels in relation to the factor proximity to roads is given in Appendix 6, Table A 12.

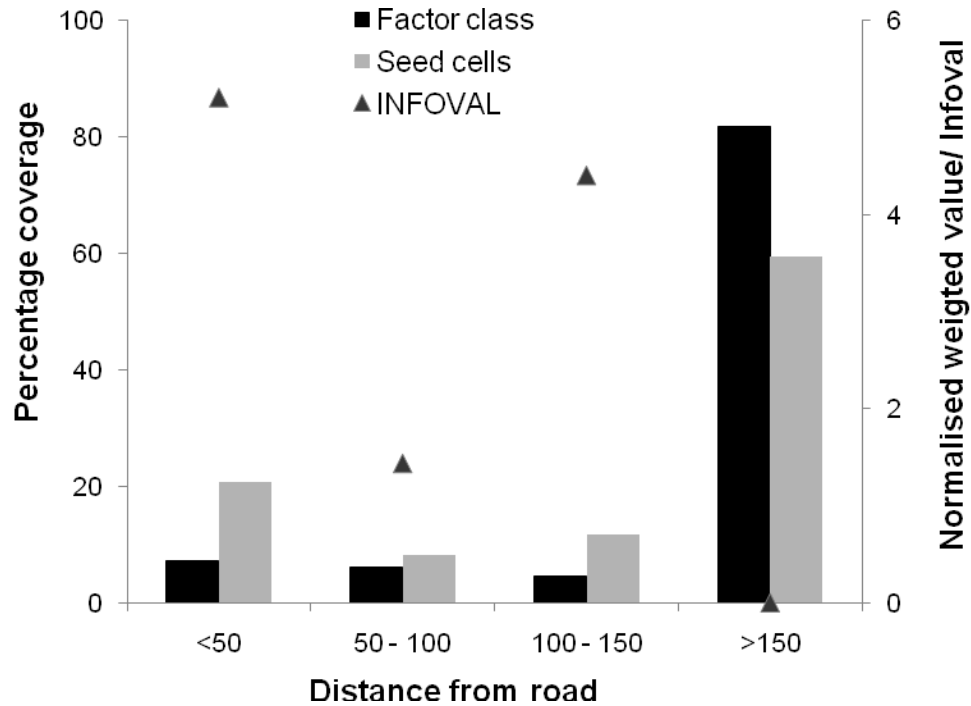


Fig. 5. 19. Distribution of factor classes for factor distance to road, associated seed cells and associated Infoval.

For the factor proximity to major fractures and lineaments, the total number of pixels and seed cells per class decreases progressively with increasing distance from lineaments (Fig 5.20). However, the maximum number of seed cell occur in the < 100 m class interval. Similarly, Infoval decreases gradually with increasing distance. There thus exist a relative negative correlation between distance to faults and distribution of seed cells. However, maximum Infoval values (4.79) are relatively low when compared to other factors. In addition, the variation in Infoval for various classes is not significantly different as most of the values range between 2 and 4.8 with only the class > 600 m having Infoval less than 2. This means that the presence of fractures in this area contributes positively to failure though the contribution is not significant. Fractures probably enhance infiltration of ground water resulting in positive pore pressure build-up particularly in areas characterized by non-uniform weathering. Field observation makes it evident that the main rock types are highly fractured and weathering is not uniform. Furthermore, seismic activity in this area is characterised by low magnitude earthquakes (Ateba *et al.*, 1997) and do not contribute in the occurrence of landslides in this area (Buh, 2009). The complete table describing the distribution of pixels in relation to the factor proximity to lineaments is given in Appendix 6, Table A 13.

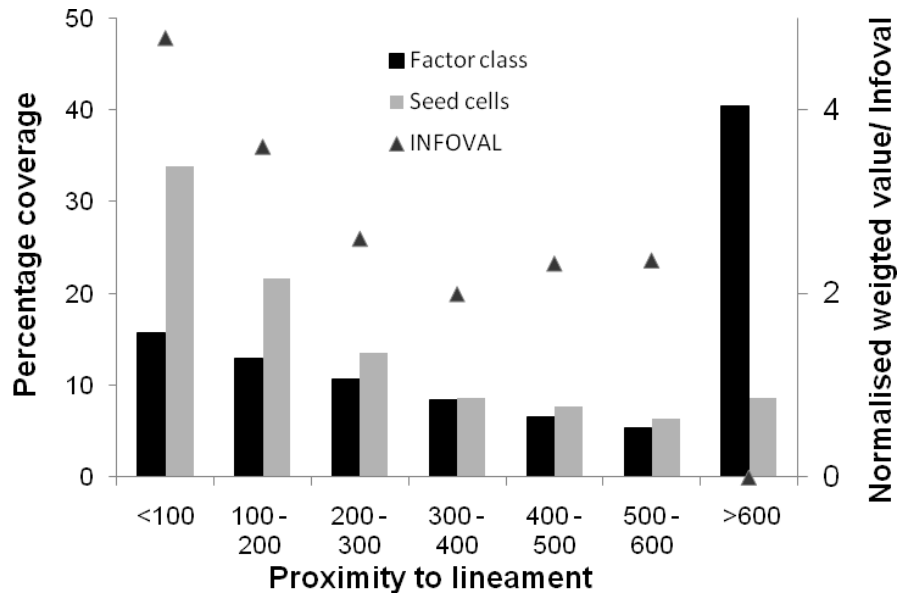


Fig. 5. 20. Distribution of proximity to lineament factor classes, associated seed cells, and associated Infoval.

Looking at the factor MAPs, it is observed that high Infoval is associated with areas that receive between 3600 and 4000 mm of rain annually, followed by those that receive between 3200 and 3600 mm (Fig 5. 20). Lower values are obtained for areas that receive less rain. Detailed values are presented in Appendix 6, Table A 14. As mentioned before, MAP provides a general picture of the groundwater condition within the study area and can better explain the long-term effect of soil water on slope destabilization.

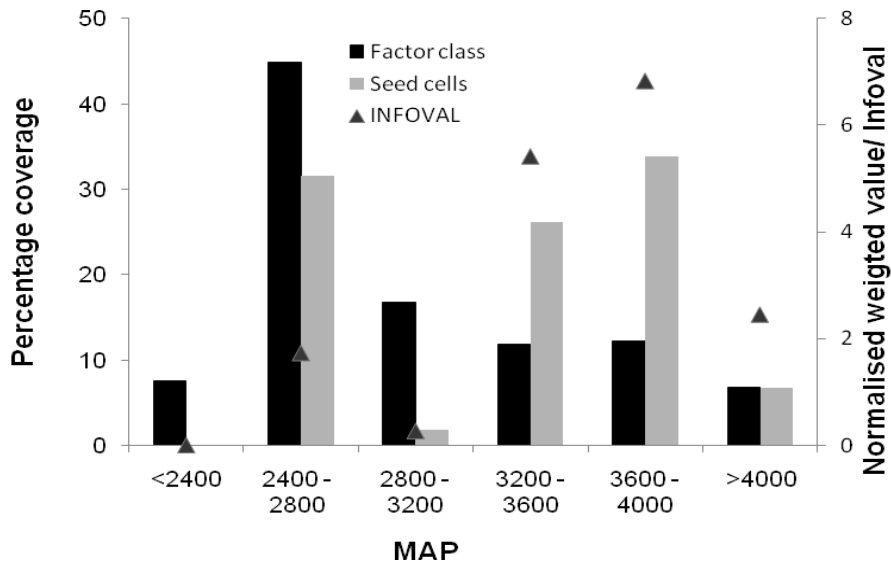


Fig. 5. 21. Distribution of MAP factor classes associated seed cells and Infoval.

5.3.2 Selection of suitable factor combinations

The way in which important independent variables that condition failure are selected for landslide susceptibility analysis and how these variables are adequately combined is a subject of debate (Chau *et al.*, 2004). Although all factors considered in this study were observed to be operational in the study area (Che *et al.*, in press), calculated Infoval show that some of the factors do not enable the discrimination of zones with higher landslide frequency. It was therefore necessary to investigate the most meaningful factor combination that would account for most of the landslides observed in the study area. As the bivariate approach also assumes independence between the controlling factors, correlation between the factors was considered for this selection and prediction performance of several factor combinations was assessed.

Firstly, a model where all the factors are added cumulatively in decreasing order of maximum Infoval was assessed. Generated susceptibility indices were evaluated and success rate curves constructed. These curves are plots of the cumulative percentages of training seed cells in each of the susceptibility classes against the cumulative sum of pixels in each susceptibility class arranged in decreasing susceptibility ranking (Fig. 21; Chung & Fabri, 1999; Conoscenti *et al.*, 2008). The success rate curves allow us to estimate the goodness of fit of the predictive model by representing the proportion of training seed cells that are correctly categorised into the high and very high categories, respectively.

In the second case, a series of models with an increasing number of controlling factors was assessed. Each successive model introduced one additional factor, with factors being introduced in decreasing order of recorded maximum Infoval. The accuracy of each model was evaluated by the construction of success rate curves. If the added factor did not increase the slope of the first portion of the curve, it was considered redundant and eliminated from the set of factors because its impact is already accounted for by the other factors. In this way, the factors proximity to streams and proximity to major fractures and lineaments were excluded. For two models with a comparable success rate curve, the one with the lowest number of controlling factors would be favoured. It is worth noting that a factor combination that shows the highest true positive value with the training seed cells does not necessarily mean the best factor combination: it just indicates an accurate estimate of the quality of analysis.

A third set of models similar to the second was assessed: here the factor lithology was eliminated from the set of factors due to uncertainties in the boundaries of the geological map. This elimination was required despite the high Infoval value of 15 for pyroclastic rock as it resulted in high to very susceptibility classes in the centre of Limbe, notwithstanding a low angle to flat topography. This highlights the need to reassess the exact position of lithological boundaries in the study area.

All the susceptibility maps generated were validated with the validation dataset and sensitivity ratio (i.e. the ratio between true positives values observed with the validation dataset and the proportion of the study area categorised into the H and VH SC) was calculated. The factor combination with the highest sensitivity ratio, which categorises a minimal portion of the study area into the H and VH SC, and has a high prediction value for the validation data, is considered as the best prediction combination.

Table 5.7 presents the proportions of test and validation seed cells categorised into the high and very high susceptibility classes, and the sensitivity ratio of the factor combinations used in this study. Some factor combinations have a good accuracy but lower prediction capability, evidenced by high proportions of training seed cells in the H and VH SCs and by a corresponding lower proportion of test seed cells in the H and VH categories. Furthermore, the proportion of the study area categorized into the VH SC is also quite variable when these factor combinations are considered. Based on the selection criteria mentioned above, the best factor grouping was a six factor combination: slope gradient, land use, MAP, stream density, slope orientation and distance from roads (Table 5.7).

From Table 5.7 it is noted that various factor combinations have diverse contributions to shallow landslide occurrences. Success rate curves for the above factor combinations are shown on Figure 5.21.

	Rock type	Slope gradient	Land use	Mean annual precipitation	Stream density	Soil type	Proximity to roads	Slope orientation	Proximity to lineament	Proximity to streams	% of TSC in H+ VH SC	% TSS H +VH SC (Sensitivity)	% of TP in H +VH SC	% TP in VH SC	Sensitivity Ratio
	x	x	x	x	x	x	x	x	x	x	83.0	78.6	17.1	4.6	4.6
	x	x	-	-	-	-	-	-	-	-	63.0	65.5	17.3	4.5	3.8
	x	x	x	-	-	-	-	-	-	-	61.0	65.5	16.4	4.4	4.0
	x	x	x	x	-	-	-	-	-	-	66.7	66.7	14.5	4.3	4.6
	x	x	x	x	x	-	-	-	-	-	70.0	61.9	13.6	4.7	4.6
	x	x	x	x	x	x	-	-	-	-	71.5	72.6	17.7	4.6	4.1
	x	x	x	x	x	x	x	-	-	-	75.5	75.0	21.7	3.4	3.5
	x	x	x	x	x	x	x	x	-	-	77.5	77.4	16.4	4.7	4.7
	x	x	x	x	-	x	x	x	x	-	77.0	77.4	17.3	4.9	4.5
	x	x	x	x	x	x	x	x	x	-	78.5	79.8	17.1	4.6	4.7
	x	x	x	x	x	x	-	x	x	x	80.5	72.6	17.6	4.6	4.1
	x	x		x	-	x	-	-	-	-	71.5	72.6	17.4	4.6	4.1
	-	x	x	-	-	-	-	-	-	-	61.0	54.8	19.4	4.4	2.8
	-	x	x	x	-	-	-	-	-	-	70.0	77.4	19.4	4.4	3.9
	-	x	x	-	x	-	-	-	-	-	75.0	67.9	16.5	4.6	4.1
	-	x	x	x	x	-	-	-	-	-	73.0	84.5	17.6	4.6	4.8
	-	-	-	-	-	x	-	x	x	x	81.5	64.3	18.7	4.7	3.4
	-	x	x	x	x	x	-	-	-	-	73.0	72.6	18.7	4.1	3.9
	-	x	x	x	x	x	x	-	-	-	81.5	79.8	18.8	3.7	4.2
	-	x	x	x	x	x	-	x	-	-	77.5	72.6	18.8	4.6	3.86
	-	x	x	x	x	-	x	x	-	-	82.0	78.6	16.9	4.9	4.7
	-	x	x	x	x	x	-	x	x	-	78.5	72.6	18.8	4.3	3.9
	-	x	x	x	x	x	-	x	x	x	76.5	76.2	18.7	4.1	4.1

Table 5. 7. Factor grouping, associated proportion of pixels in the high and very high susceptibility classes, percentage of training and test seed cells in the high and very high susceptibility class, and the sensitivity: percentage of pixels in the high and very high susceptibility class, used to determine the best factor combination for landslide susceptibility assessment in the Limbe area. H+VH SC: high and very high susceptibility classes; TSC: training seed cells; TSS: test seed cells. TP: proportion of total area.

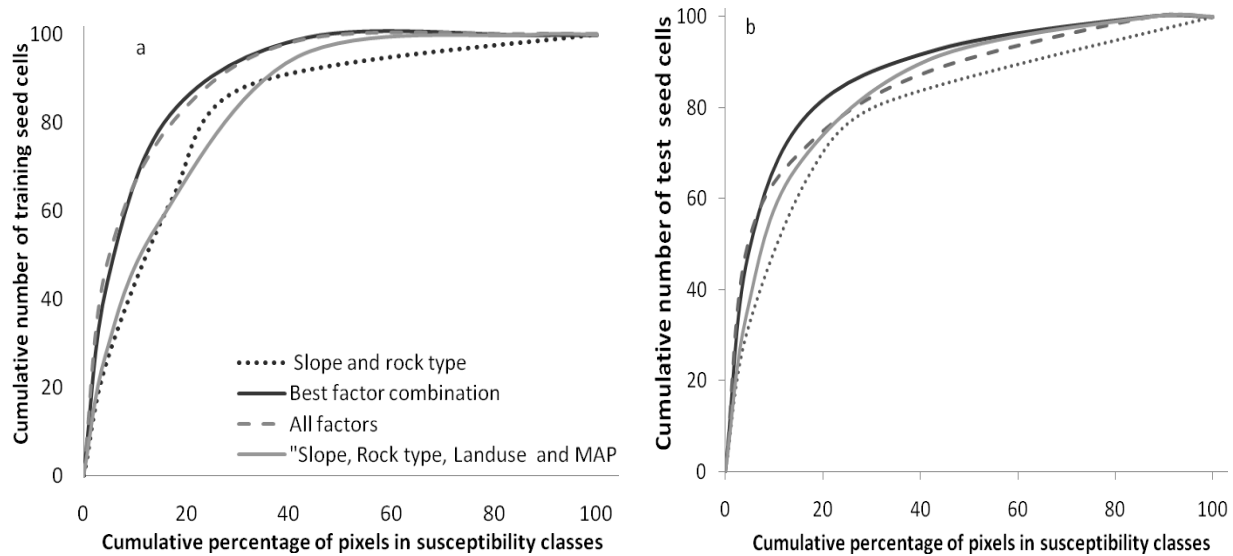


Fig. 5. 22. Prediction performance (success rate curve) of grouping of multiple factor combinations: a) from the training data set and b) for the validation data set for 4 different factor combinations.

The susceptibility map generated using all the factors (10) considered in this study correctly classifies 83 % of the training seed cells and shows a lower prediction performance of 78.6 % for the validation seed cells. With this combination, 17.1 % of the total area is categorized in the high and very high susceptibility classes.

Eliminating the factors proximity to streams and proximity to major fractures and lineaments, the accuracy decreases to 77.5 % for the training seed cells and to 77.4 % for the test cells while 16.3 % of the study area is categorised into the H and VH SCs.

In the third case where rock type is removed, the best trade off between the model accuracy and the number of factors was obtained using only six parameters: slope gradient, land cover, mean annual precipitation, stream density, soil type and proximity to roads. This model enables to categorizes 82 % of training seed cells and 78.6 % of validation seed cells in the high and very high susceptibility classes. Based on this factor combination, 16.9 % of the study area falls in the high and very high susceptibility categories. These results are similar to the ones of the first model that made use of 10 factors. Validating this model with the validation seed cells, it is observed that 47.6 % of the seed cells occur in the very high susceptibility class, and 31 % in the high category. Only 7 % of the validation seed cells is attributed to the low susceptibility class and none to the very low susceptibility class (Table 5.8). This is an indication that the model has a high predictive power.

Scenario	Susceptibility ranking	Susceptibility index	Pixel % in study area	Proportion of training seed cells	Proportion of validation seed cells
All factors considered (10 factors)	Very low	2.5 – 9.8	13.8	0	0
	Low	9.8 – 20.1	43.6	0.5	10.7
	Moderate	20.1 – 30.5	25.5	16.5	10.7
	High	30.5 – 40.4	12.5	36.5	25.0
	Very High	40.4 – 69.2	4.6	46.5	53.6
All factors except distance to streams and distance to lineaments (8 factors)	Very low	2.5 – 7.2	12.2	0	0
	Low	7.2 – 16.7	46.9	0.5	11.9
	Moderate	16.7 – 26.1	24.5	22.0	10.7
	High	26.1 – 35.6	11.6	31.5	22.6
	Very High	35.6 – 65.5	4.7	46.0	54.8
Best factor combination (slope, land use, MAP, stream density, slope orientation and distance from roads) 6 factors without mask	Very low	1.5 – 5.6	14.8	0	0
	Low	5.6 – 11.8	41.8	0.5	7.1
	Moderate	11.8 – 18.0	26.5	17.5	14.3
	High	18.0 – 24.2	12.2	38.0	31.0
	Very High	24.2 – 42.5	4.7	44.0	47.6
Best factor combination (slope, land use, MAP, stream density, slope orientation and distance from roads) 6 factors with mask	Very low	1.5 – 5.6	27.0	0	3.6
	Low	5.6 – 11.8	33.5	0.5	3.6
	Moderate	11.8 – 18.0	23.8	17.5	14.3
	High	18.0 – 24.2	11.4	38.0	31.0
	Very High	24.2 – 42.5	4.4	44.0	47.6

Table 5. 8. Training and validation results for landslide susceptibility in Limbe for three scenarios analysed in this study. Note the proportion of the study area in the high and very high susceptibility categories. The proportion of seed cells in the very low susceptibility category is minimal for the 6-factor scenario.

Figure 5. 23a shows the susceptibility map of the Limbe area obtained from the best factor combination. Despite the good prediction performance of the model, some areas observed to have slopes less than 2° in the field appear in the high and very high categories, particularly in the town of Limbe. These areas are characterized by a combination of parameters with high Infoval such as, built-up areas for the land cover factor, a close proximity to roads and high mean annual rainfall, resulting in a high susceptibility despite the low slope gradient. To correct for this, a mask was applied that attributes very low susceptibility to areas with slope gradient less than 2° irrespective of all other factor combinations. The applied mask however did not change the success rate of the model but reduced the total amount of pixels classified in the high and very high susceptibility classes by 0.8 and 0.2 %, respectively as seen on Table 5.8. Fig. 5. 23b is the susceptibility map obtained after the application of the mask.

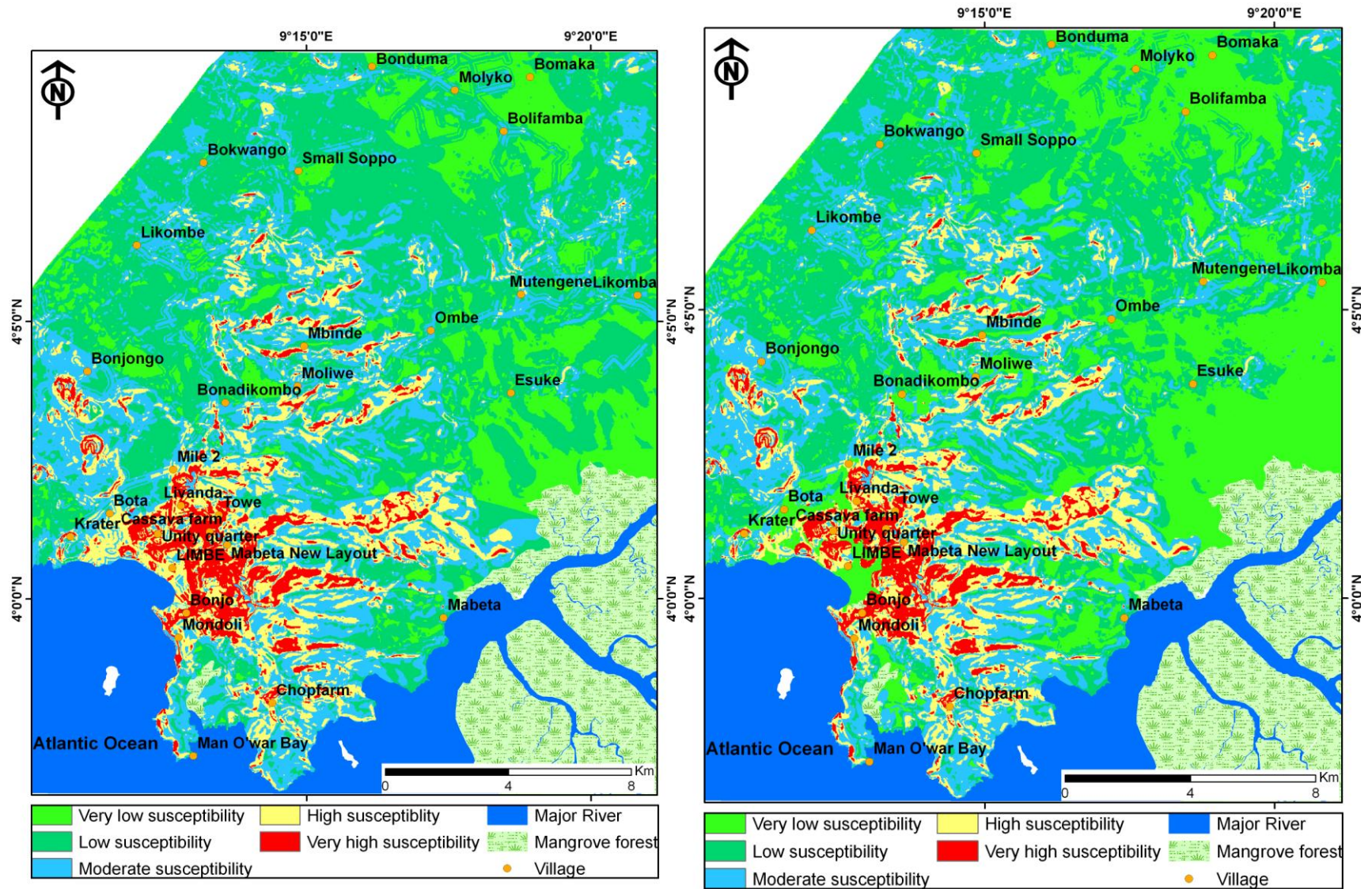


Fig. 5. 23. Landslide susceptibility map of Limbe, using the six-factor combination: a) susceptibility before the application of a mask and b) susceptibility after application of a mask. Note that there is no significant difference in the distribution of the high and very high susceptibility classes.

5.4 Limitation of the model

Despite its high predictive power, the proposed model has some limitations.

- First, it assumes that landslides will happen under the same combination of factors (principle of uniformitarianism) whereas field observations indicate that some slides are caused by a specific set of factors (e.g. proximity to rivers in conjunction with other factors like land use and slope gradient; Che *et al.*, 2011).
- Secondly, this susceptibility analysis requires a continuous update of the input factors: a change in the land cover might, for example, significantly increase the landslide susceptibility of an area.
- Third, this model tends to oversimplify factors that condition sliding by considering only those factors that are easily mappable or can be derived from the DEM. It neglects geotechnical characteristics of the soil which vary enormously in space.
- Finally, this bivariate takes into account the independent relationships of individual factors with landslide occurrence, without accounting for the possible combination of factors that might act together in increasing the slope instability.

5.5 Risk assessment

As mentioned earlier, landslide risk is a measure of the potential degree of damage to a given element or sets of elements at risk. In this study we used the outline of built-up areas, the road network and the distribution of some strategic objects to evaluate their vulnerability to future landslide occurrences. Built-up areas as at December 2000 covered 22 km², i.e. about 6 % of the study area. About 6 km² of this area lies in the high to very high susceptibility category. By 2008, the total built-up area had doubled to 45.6 km², i.e. 12.6 % of the study area. Of the 24.2 km² increase in built-up areas between 2000 and 2008, 9 % (2.2 km²) of it lies in the high and very high susceptibility classes (Table 5.9). These values suggest a tremendous increase in urbanisation and a corresponding extension of lifeline into hazardous and safe areas. Approximately 253 km of both paved and unpaved roads exist in this region. Of this length, 69.3 km, i.e. 23 % of the road network is likely to be affected by future failures. Of the 166 individual structures recorded, 24.6 % of them are located in the high and very high susceptibility categories and thus are highly vulnerable. Individually, there are 10 schools, 8 bridges, 3 health facilities and 14 government administrative structures in the high and very high susceptibility categories (Table 5.10).

Susceptibility class	Proportion of built-up area in 2000 (%)	Proportion of built-up areas between 2000 and 2008 (%)	Road net work at risk (%)
Very low	33	36	23
Low	16	40	21
Moderate	24	15	33
High	13	06	16
Very high	13	03	07
Total	22.6 km ²	24.2 km ²	261 km

Table 5. 9. Proportion of built-up areas in various landslide susceptibility categories on the SE foot slope of MC. Totals given in square kilometers.

Structure	Number	Number in the VH SC	Number in the H SC
Schools	46	3	7
Bridges	12	2	6
Clerical institutions	15	3	1
Health facilities	8	1	2
Financial institutions	13	1	1
Government administrative structures	49	2	12
Water tanks	1	1	0
Markets	2	0	0
Road junctions	20	1	7
Total	166	14	36

Table 5. 10. Distribution of individual objects at risk, objects are located in the high and very high susceptibility classes of the susceptibility map. VH SC: very high susceptibility class; H SC: high susceptibility class.

Figure 5.24 shows the spatial distribution of objects at risk in this area and the different susceptibility categories. Amongst these structures, the water tank at Kie, Saker Baptist College, Government Nursery School Mabeta, the delegation of Town Planning and Housing, and FIFA Limbe were observed to be at high risk during field surveys. These structures also fall in the very high susceptibility category of the susceptibility map. Figure 5. 25 displays the distribution of the outline of built up areas superimposed on the susceptibility map.

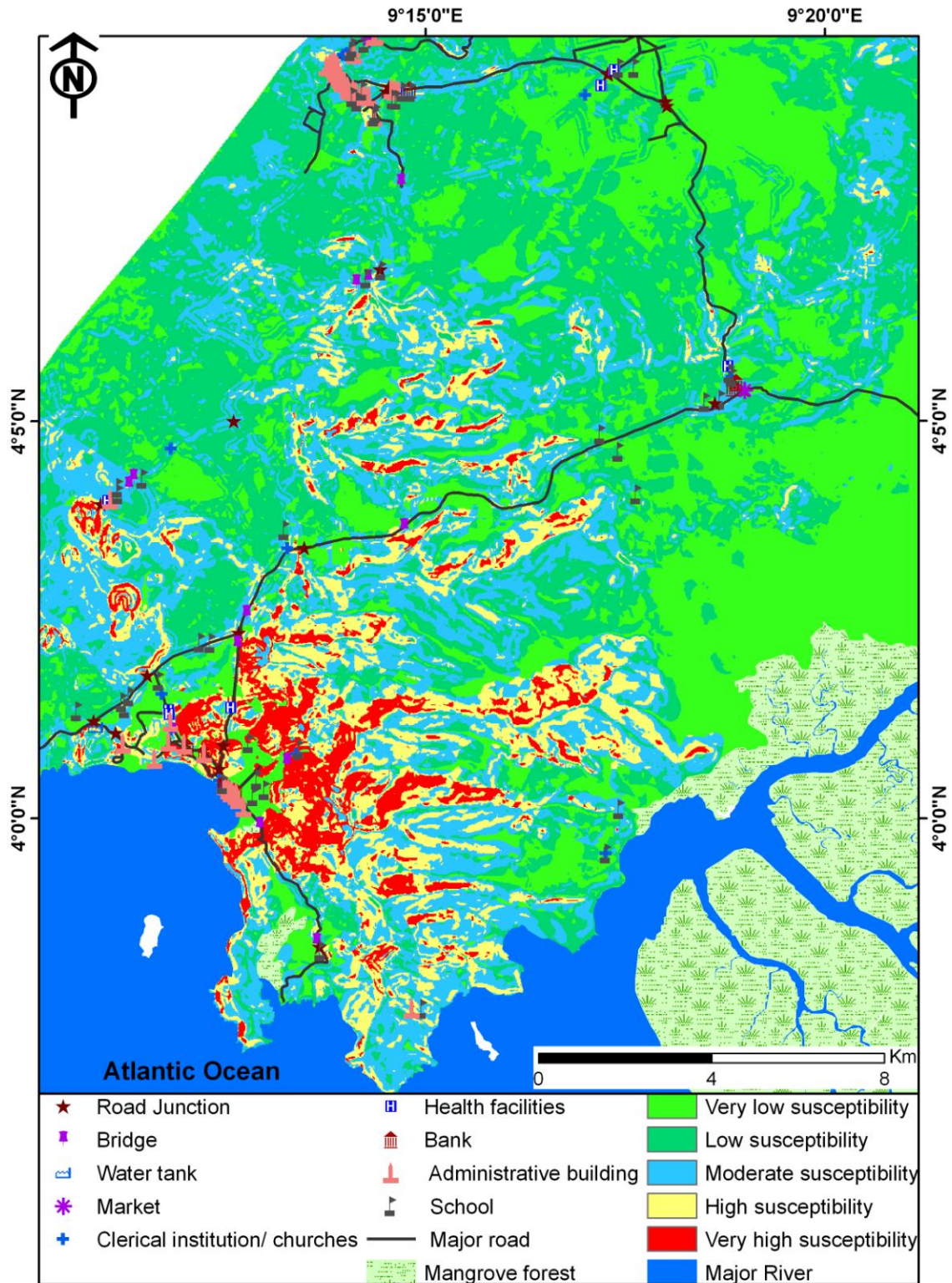


Fig. 5. 24. Specific objects at risk superimposed on the susceptibility map.

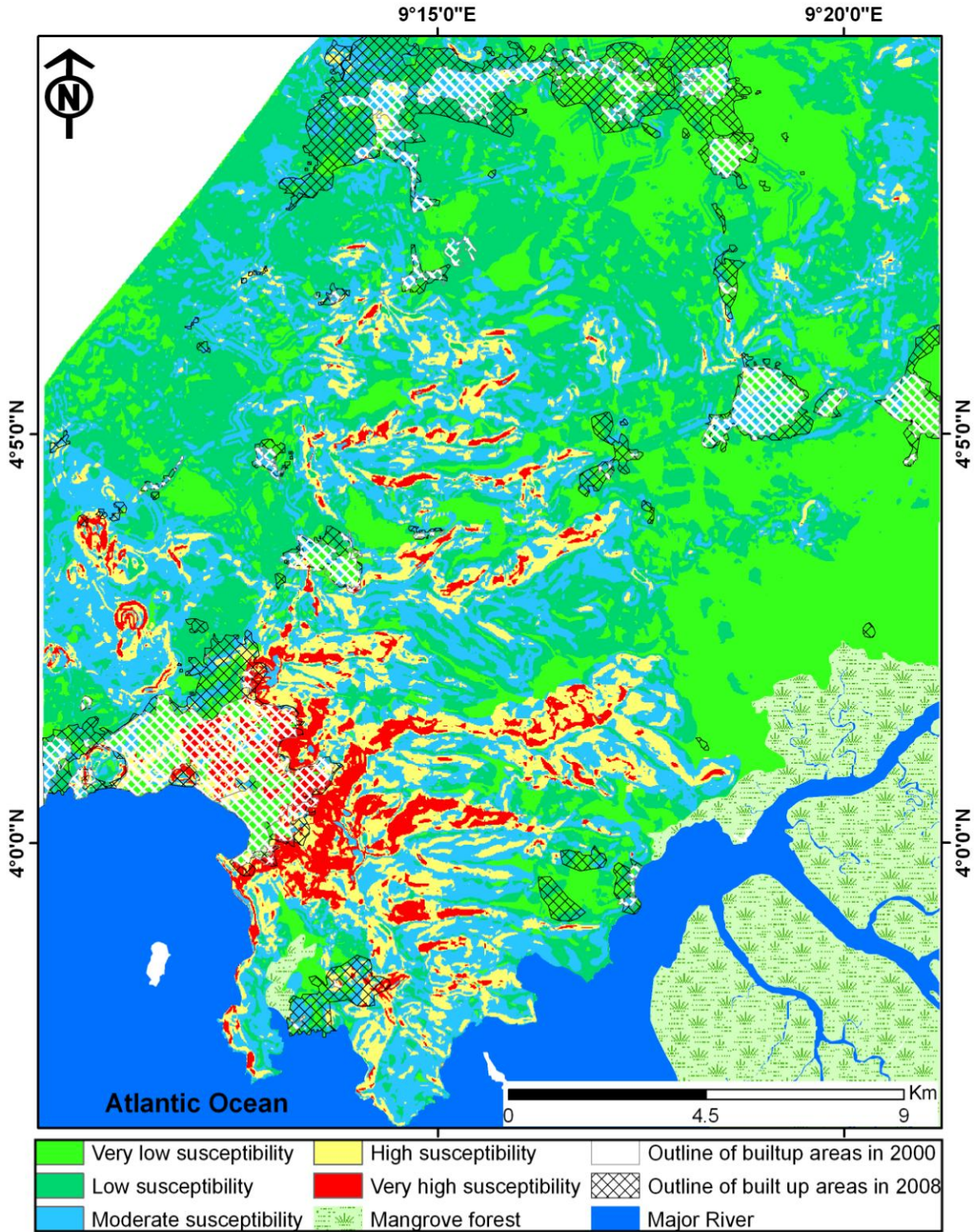


Fig. 5. 25. Spatial distribution of the outline of built-up areas superimposed on the susceptibility map of Limbe expressing the spatial distribution of human population and infrastructure vulnerability to the impact of future landslides.

5.6 Discussion

Understanding the factors and processes that lead to the occurrence of landslides is crucial in managing hazards and in understanding landscape evolution. Based on this fundamental principle, this study presents the results of a comprehensive landslide susceptibility evaluation for the Limbe area. The susceptibility map describes the zoning of relative probability of future landslide occurrence based on field identification of possible contributing factors. Landslide densities for each contributing factor and Infoval are computed and used to rank the importance of each factor in landslide processes. It is important to emphasize the fact that the quality of this output depends on the quality of the input parameters. In this case the geological map was flawed with uncertainties that result in miscalculation of susceptibility zones and thus had to be eliminated from the model, despite the fact that the bivariate analysis highlighted the concentration of landslides on pyroclastic rocks.

In this study, the seed cell method is combined with the Infoval method, which is a bivariate statistical method applied in landslide susceptibility assessment to model rain induced shallow translational slides in the Limbe area. This method was adopted because the dominant failure type within the study area were rain induced shallow translation slides which, according to Sützen & Doyuran (2004), are most suitable for the application of the seed cell method since the slope form does not change significantly after failure. Moreover the method reduces the impact of expert opinion in susceptibility determination since no special ranking measures are introduced but for those that result from data-driven factor weight calculation. This implies that the combined seed cell and Infoval method is an objective method when compared to other bivariate statistical methods although their operation principles are basically the same.

Generally, the model has a good predictive power as it categorizes 78.6 % of test seed cells into the high and very high landslide susceptibility classes. It is possible that the seed cells in the moderate and low susceptibility classes result from the fact that the observed slides are rather small when compared to the dimensions of the buffer used in generating the seed cells. They may also result from errors in mapping the boundaries of some parameter classes. In addition, to correct for areas where landslides are not expected but appear in the high and very high susceptibility class, a mask is used that attributes low susceptibility to slopes with a gradient less than 2° irrespective of the factor combination. Susceptibility mapping with the seed cell methods

mostly consider the depletion zone and does not take into account the size and potential run-out of the slides nor the assessment of the areas down slope from the unstable slope thereby resulting in the underestimation of risk.

Thierry *et al.* (2008) used slope as the principal factor in landslide susceptibility zoning and categorized about 80 % of the Mabeta massif in the high and very high susceptibility classes, which probably overestimates the susceptibility of this area. In the present study based on field observations it is noted that several factors contribute to slope instability in the study area. Slope alone would not be a good predicting factor. After several trials and eliminations, the best factor combination that accounts for landslides in the study region includes slope gradient, land use, mean annual precipitation, slope orientation, distance to roads and stream density, predicting 79.8 % of the test seed cells and categorizing 16.9 % of the study area into the high and very high susceptibility categories. Proximity to streams and faults have minimal influence on the occurrence of landslides in this area though field observations indicated a significant influence of streams on the occurrence of some slides. This indicates that factors that are the actual causes of specific landslide cannot always be used to account for the spatial distribution of all landslides in the whole region, as the specific controlling factors differ from one slide to another. This is probably because some of the streams present in the field are not visible on the topographic map and thus were not digitised or accounted for in the model. Instead, MAP and stream density, which acts as a surrogate to groundwater distribution (Vijith *et al.*, 2009) or provides clues for the regional hydrogeological properties of the rock (Süzen & Doyuran, 2004), are more significant contributors. Furthermore, uncertainties in the quality and the scale of the geologic map used in this study might have a neutralising effect on the contribution of distance to faults. Decreasing Infoval with increasing distance from the major faults and fractures is understandable, considering that the area is characterised by low intensity earthquakes. A decreasing influence of seismic acceleration with increasing distance from the fault line could play a role in landslide distribution but a more detailed study of the distribution and characteristics of active geological structures is required to constrain this potential control.

From field surveys it was noted that construction works, particularly on weathered pyroclastic cones, are abundant and not accompanied by any stabilization measures, thereby enhancing susceptibility particularly in steep areas covered by pyroclastic materials. Excavation for any

form of construction changes the slope line creating terraces and sub-vertical slopes, whereas addition of material results in extra load on the slope and reduction in infiltration, particularly when impermeable materials are used, thus locally concentrating runoff and changing ground water flow paths. This might account for the high weighted values observed for areas very close to roads and in built-up areas.

From the susceptibility map, it is observed that significant portions of the study area especially around Limbe and in the Limbe-Mabeta massif are highly susceptible to failure. Any new development project should therefore be directed away from these hazard-prone areas. Safer areas characterised by low susceptibility indices are identified to the north of Limbe (Bojongo, Wututu, and Tole) or to the east of the Limbe-Mabeta massif (Ombe and Mutengene). W of Limbe there exist low susceptibility areas that could be used, instead of building on very steep slopes of weathered pyroclastic cones. However, if unavoidable, adequate stabilization and remediation measures are essential to decrease the risk of loss of life and to minimize other adverse impacts. Field observations indicate that most of the occupants of houses constructed on steep slopes are less-well-off citizen who, because of poverty and destitution, cannot afford to pay for land in safer areas due to the exorbitant costs involved in the acquisition of land titles in safe areas relative to those in unsafe areas. Ancestral attachment also represents one of the major reasons why some of them are reluctant to leave.

Low-cost bio-engineering applications could also be implemented to stabilise slopes. For example, vetiver grass (*Vetiveria zizanioides*) barriers have been successfully used to stabilise landslide areas on the Befang-Wum road (Abia, 2003); it has also been applied in other areas such as Vietnam and Australia. This method could easily be applied in the Limbe area as well. Buttressing slopes and constructing retaining walls is currently being practised on a limited scale but could be extended particularly along road cuts and embankments generated by excavation for construction. Surface and subsurface drain pipes and drainage corridors can also be constructed and maintained, particularly in areas characterized by loose soils so as to divert runoff and decrease the rate of infiltration. Respect of building codes and building licenses is also imperative. Continuous sensitisation of the local populace is also a very important component and has been initiated by the use of radio programs and the installation of billboards to make the population aware of impending risk and its consequences.

The landslide susceptibility map can be used by local authorities to raise the awareness and preparedness of future landslide impact. However, for detailed urban planning and enforcement of exclusion zones in high hazard areas, detailed site specific investigations are strongly recommended.

5.7 Conclusions

From the above susceptibility assessment, the following conclusions can be drawn:

1. Landslides in the Limbe area are caused by a number of factors that interplay to make slopes susceptible to failure although their contribution varies from one slide to the other. Notwithstanding this variability, the best factor combination that accounts for most of the failures includes slope gradient between 10 and 35°, land use type, mean annual rainfall, stream density, slope orientation and distance from roads.
2. The parent rock type also contributes significantly to landslide occurrence with pyroclastic cones showing a higher susceptibility to failure than lava flow deposits. More detailed geological mapping is recommended to better constrain the control of lithology upon landslide susceptibility.
3. The combined seed cell and Infoval susceptibility modelling method is appropriate for this area. Validation results expressed as success rate curves indicate that the model's predictive abilities are good.
4. Areas on the Mabeta massif are more likely to fail than those located on the foot slopes of MC.
5. The susceptibility map can be used by local authorities in urban planning and development. However, detail on-site geotechnical characterisation is required for on-site specific development projects.

Conclusions and perspectives

This thesis provides a detailed analysis of small-scale landslide processes that affect the livelihood of inhabitants on the SE foot slopes of MC, based on field observations and laboratory measurements. It focuses on the description of the geometric parameters of landslide scars, the physico-mechanical properties, mineralogy and chemistry of landslide-prone soils and on landslide susceptibility assessment as a method to reduce the impact of future devastating landslides based on experiences in the Limbe area. It provides direct answers to the scientific questions raised at the onset of the research project, including: 1. where have landslides occurred and what are their geometric properties; 2. what are the causal and triggering factors 3. where are the zones with the highest probability of future landslides and finally, what are the elements at risks. It also makes an attempt to identify rainfall thresholds that might trigger failure.

Apart for providing information about landslides, it is also a major contribution in the analysis of the geotechnical properties of tropical residual soils which has not been extensively treated in the literature.

The thesis provides a post-sliding evaluation of landslides within the Limbe municipality, and has resulted in a better understanding of the factors that cause movement and the mechanisms that result in sliding. It also brings to light the importance of a multidisciplinary approach in the understanding of landslide processes as it integrates aspects of geology, soil mechanics and engineering in the evaluation of landslide processes. The fact that some devastating landslides were recorded during the course of this research emphasises the significance of this problem on the SE foot slope of MC. Based on the results obtained from this study, the following conclusions are made.

First, typical landslides on the SE foot slopes of MC are rain-triggered very small to small earth and debris slides with individual volumes less than 50000 m³. In addition, landslides with volumes > 10⁴ m³ are rare. The slip surfaces of most of these slides lay within saprolites or at the soil/saprolite interface. Observations from this study highlight the fact that there is no direct correlation between landslide volume and their impact. Instead, the impact of landslides is controlled by its proximity to population and human infrastructural elements. Although several factors contribute to the occurrence of landslides within the study area, this study makes it

evident that the combination of factors operating at each landslide site is unique to that particular location. Hence, the factors taken into account in subsequent modelling needs to consider the various factor combinations at different sites.

Furthermore, the occurrence of landslides in the Limbe area is enhanced by anthropogenic factors such as anarchical construction and the excavation of material on steep weathered slopes. Some anthropogenic instability factors might be reduced by well-thought out and enforced regulations, engineering stabilization techniques (retention walls, construction and maintenance of drainage network, and the use of vertiver grass barriers), but landslides controlled by natural factors can be expected to continue occurring in the study area.

The landslide inventory used in this study was generated by the traditional field-based approach that allows the extraction of first-hand information about causal factors by systematically documenting observed landslide scars. The dataset is presented as point data on a map in a GIS environment to acquire a picture of the spatial distribution of landslides within the study area. From the map, it is noted that landslide scars are not uniformly distributed throughout the study area but is observed to be concentrated within specific zones characterised by steep slopes, and weathered pyroclastic cones. The field method has some major setbacks in that some of the landslide scars might not have been mapped out particularly in the densely forested areas which are difficult to access. Moreover, this method is time consuming but it remains the only way through which first hand information about landslide processes can be obtained and used to constrain subsequent modelling in absence of frequently acquired very high resolution imagery.

Secondly, this thesis highlights the value of a field-based landslide inventory in tropical regions affected by landslides. Most landslide research nowadays relay on the interpretation of remote sensing data, traditional aerial photo interpretation, newspaper reports and other published articles with minimal field checks to confirm the interpretation of the images. These large-scale images have for example been used by Barlow *et al.* (2003) and Cheng *et al.* (2003) in locating landslides. During this research project, it was noted that small-scale landslides, which characterise the Limbe area, cannot be identified on Landsat and ASTER images. Thus, the applicability of these techniques in identifying individual slide scars is limited and only applicable to large-scale sliding. Only landslide scars with dimensions larger than 200 x 200 m

and clear land cover contrast would be identifiable on Landsat images but slides of this dimension were not observed in the study area. Remote sensing data are also valuable for time series evaluation but at the scale of landslides observed in the study area, coupled with persistent cloud coverage, dense vegetation and rapid vegetation recovery rates, they prove not to be useful. Thus, the applicability of large scale satellite images in the study of extremely small to medium slides in the humid tropical environment characterised by dense forest is questionable. Repetitive air photos acquisition is also lacking in Cameroon. This therefore means that higher resolution images such as Quickbird or Ikonos images would be required. These images are relatively expensive thus limiting their applicability in large scale research areas. The Landsat and ASTER images however proved valuable in mapping out spatio-temporal land use changes.

Thirdly, to effectively monitor, model and manage landslide processes, it is essential to understand the fundamental causes of their occurrence and the failure mechanisms involved. This is achieved through systematic field surveys and mapping of the geometric properties of the visible landslide scars and through the characterisation of landslide-prone soils. From this study, it can be concluded that geotechnical characterisation of slide prone soils is invaluable in any landslide research as the geotechnical characteristics provide insights into the sliding mechanism. From six pits dug into three slide scars it is concluded that soils within the Limbe area have good geotechnical properties and will not favour the occurrence of landslides (i.e. in the absence of external forces). The soils are characterized by high cohesion and effective angle of internal friction, and a low permeability. Most of the soils have PI values greater than 15 and are thus not liquefiable. This accounts for the dominance of slide type failure over flow within the study area.

From mineralogical analysis obtained so far, clay mineralogy cannot be used to identify horizons that are more susceptible to failure. As described in Chapter 4, the soils in the study area are made up of a mixture of swelling and non-swelling clays. Identified clay minerals present in these soils include smectite, kaolinite, halloysite and some mica. However, clay mineralogy shows significant heterogeneity between the various profiles but demonstrate minimal variation down the profile. In addition, the weathering of pyroclastic material result in the production of clay-sized particles but with little amount of clay, principally kaolinite and illite. The silt and clay fraction of the soils in the study area are characterized by the presence of anatase, sanidine, ilmenite and goethite for profiles developed on weathered lava flows whereas the above

mentioned minerals together with hematite and magnetite were recorded in samples from weathered pyroclastics materials.

From a chemical point of view, major element and trace element composition of the lava flows analysed in this study are similar to those of other MC lavaflores; however, there exist significant differences in major and trace element composition between the soils and rock from the pyroclastic cone analysed in this study and those of other Mt Cameroon rocks. The pyroclastic rock and its soils are characterised by the presence of extremely high Ni and Cr concentrations ranging from 800 ppm in the parent rock to 2581 ppm in the soil for Cr and 279 ppm in the parent rock to 803 ppm in the soil for Ni while other rocks from MC have values that range between 48-213ppm and 40-99 ppm, for Cr and Ni, respectively. The pyroclastic rock is also characterised by a higher magnesium oxide, lower Al_2O_3 and K_2O content than other rocks of the MC region. Sr is the most mobile of all the trace elements and is significantly depleted from the weathering profile while all the other trace elements particularly Ba are relatively enriched as weathering advances.

Based on the geotechnical measurements and the mineralogical characterisation, two conceptual models are proposed to explain landslide occurrence mechanisms for the area. Sliding will occur where infiltrating water results in the development of positive pore pressure within a lower more permeable horizon underlying a less permeable soil horizon. The less permeable horizon impedes the free rise of pore water and enhances the development of positive pore pressure in the underlying horizon. This positive pressure will result in uplift and mobilization of the overlying soil. Some sliding can also be explained by the human induced rain-triggered model. In this case, human activities increase shear stresses on the slope or rework slope material resulting in loose soil particles that can enhance rapid water absorption and saturation. The saturated loose soils are more easily eroded and transported during intense rainstorms resulting in failure.

Susceptibility mapping as conducted here is a key step in identifying zones that should not be developed or that require mitigation measures to limit the impact of naturally-occurring landslides. Based on this map, vast areas on the Limbe –Mabeta massif are susceptible to failure. Safer areas exist to the E, W, and N portions of Limbe and these could be exploited to minimise losses due to sliding. The produced map has limited applicability on a local scale and requires

on-site geotechnical characterisation of individual sites to take knowledge-based decisions with regards the best stabilization method required for each site. Notwithstanding, the produced susceptibility map will already enable the implementation of future practices aimed at reducing landslide occurrence or impact via remediation, land-use and urban planning efforts. These efforts can be implemented at several scales ranging from individual through regional to a nation level.

1. Individuals can act through the use of low-cost bioengineering approaches used in slope stabilization such as the planting of vertiver grass barriers which have been documented to be effective in other areas.
2. In addition, individuals could be sensitized to produce gently sloping talus when cutting terraces and terracing could be done in a more organised and uniform manner instead of the disorganised terracing system currently in place.
3. The implementation of standard stabilization methods such as the construction of retaining walls after cutting steep slopes for construction should be encouraged. The local Council too can engage in the construction of retaining walls along road cuts as has been implemented in some parts of Limbe. Furthermore, organised construction and maintenance of drainage corridors should be encouraged by the City Council.
4. Strict rules prohibiting construction on steep slopes can be implemented by the Ministry of Town Planning and Housing. Demolition of structures existing in very susceptible areas should only be considered if no other feasible stabilization or mitigation measures can be applied.
5. Furthermore, a denser network of rain stations capable of measuring real-time rainfall intensity and transmitting this information to scientists would be vital to be able to identify actual rainfall amounts and duration that may trigger landslides. With this approach, a well-constrained early-warning system could be developed so as to minimise the rate of false alarms.
6. In situations of very intense rainfall, individuals might consider leaving their homes for a while until the storm is over. However, they need to be sensitized on when this should be done and where they should go to by state agents and other groups of authorised persons or organisations interested in natural disaster reduction programs.

7. Improving and making safe transport infrastructures around landslide-prone zones, both for evacuating the population and for bringing in relief should also be considered.

From field expeditions and interviews with the local population, it is noted that people are less aware of the causes and consequences of slope instability than of hazards related to volcanic activities. Even for those that are aware of these hazards, poverty will force individuals to settle in slide-prone areas because the cost of lands in the safer areas is high and their income will not permit the establishment of standard remediation measures. Continuous sensitization campaigns can be organised to educate the local population about the processes and the areas at risk, about the measures that can be implemented to ensure stabilization of some of these slopes, and about some of the regulations that will help reduce their exposure to this natural hazards. These campaigns have been initiated in the course of this project through the use of media interviews, the installation of billboards, seminar presentations and interaction with some administrative bodies and with the local population and through lessons given in some schools to inform the local population about the damage with which they live. These sensibilisation campaigns need to be sustained as individuals tend to forget fast in the absence of immediate danger.

Moreover, from the literature, no standard method of assessing the magnitude or severity of landslides, although some studies have used landslide size (i.e. area and volume) or frequency/area statistics as a proxy for landslide magnitude. Magnitude/severity in this study refers to the amount of physical, emotional, material impact and human casualties induced by a landslide. In this study, it is noted that the impact of a landslide is not dependent on the size of the slide nor on the volume of debris produced but is rather linked to the location of the landslide in relation to human infrastructure. It is therefore necessary to be able to document all landslide types rather than only focusing on the large debris generating slides, which might in effect be of less consequence than small-scale failures in densely populated areas. Standardising the way landslide magnitude is reported will make it easier to report and communicate amongst researchers involved in landslide analysis in different parts of the world.

The findings from the present study also have generic value and can be used to tackle small-scale slope instability problems elsewhere in the subtropics. Besides providing insights into small-scale devastating landslides affecting vulnerable people, it provides first hand field-measured

geometric characteristics of landslide scars and systematically documents and quantifies for the first time the overall features, and geometric parameters of volume-limited devastating slides in Limbe. It thus provides constraints for modelling, monitoring and remediation efforts that might be applied in other areas affected by similar small-scale failures.

Future perspectives

Since this area is characterised by a dense vegetation cover, frequently cloud-coverage and has rapid vegetation recovery rates, periodic aerial photographic surveys would be vital to document temporal changes. This would enable to document the approximate timing and spatial characteristics of new landslide events. It would put further constraints on the temporal relationship of land cover changes or new road infrastructure and the destabilization of specific slopes. The aerial photographs will also allow to make knowledge-based decisions with regards to the direction in which urban development projects could be expanded. Interaction and active participation of the local inhabitants is vital so that the exact date and time of landslide occurrence can be reported.

Future studies can be developed to test the validity of the proposed models. This would involve the installation of piezometers at well-defined points on some of these slopes from which changes in pore pressure in relation to rainfall can be monitored. In addition, monitoring groundwater level changes in response to rainfall is also necessary to be able to document quantify the amount of pore pressure that is required to initiate sliding. In addition, systematic soil coring and site geotechnical analysis should be encouraged to ensure that appropriate remediation measures are put in place before any construction project is carried out.

Furthermore, a dense network of rain gauges capable of recording, storing and making data available to scientists in real time would be necessary together with information regarding the time and date of occurrence of landslides such that an effective early-warning system can be designed and implemented for the Limbe area. This is required to reduce the number of false alarms that might result from the system and create unnecessary panic in the local population. From such a system, the local population may be sensitised to leave their homes for a while when specific rainfall thresholds are reached. This will help minimise the damage or casualties that could result in case a slide occurs. The rainfall record also have implications for other

natural hazards such as floods which are also frequent in this area and can be taken into consideration in future research projects.

The government should consider possibilities of developing rescue centres where individuals could run to for shelter in case of danger.

Susceptibility assessment indicates that rock and soil type play a fundamental role in the occurrence of landslides. However, detailed geologic and pedologic maps do not exist for the Limbe study area. Future research dedicated to the production of reliable and high-resolution geological maps for this region is of prime importance for future susceptibility assessment. Extensive soil testing to generate geotechnical maps is also deemed necessary. Geotechnical tests for new constructions in any area and particularly in landslide-proned zones should be a rule as this would aid in the implementation of appropriate stabilization measures.

References

- Abia, H.A., 2003. Landslide reduction along the Bamenda-Wum road in Cameroon. Hydra Project International, Cameroon. pp 324 - 325.
- Ahmad, R. and McCalpin, J.P., 1999. Landslide susceptibility maps for the Kingston metropolitan area, Jamaica with notes on their use. USD publication no. 5.
- Alexander, E.D., 1989. Urban landslides. *Progress in Physical Geography*, 13, 157–191.
- Alexander, E.D., 2008. A brief survey of GIS in mass-movement studies, with reflection on theory and methods. *Geomorphology*, 94, 261- 267.
- Aleotti, P. and Chowdhury, R. 1999. Landslide hazard assessment: summary review and new perspectives. *Bulletin of Engineering Geology and the Environment*, 58, 21- 44.
- Anderson, S.P, Dietrich W.E, and Brimhall Jr. G.H., 2002. Weathering profiles, mass balance analysis, rates of solute loss; linkages between weathering and erosion in a small, steep catchment. *Geological society of America Bulletin* 114, 1143-1158.
- Annan, K., 2002. Disaster reduction and sustainable development: Understanding the link between vulnerability and risk related to development and environment. Open file report. International strategy for disaster reduction United Nation, UN/ISDR.
- Ateba, B. and Ntepe, N., 1997. Post eruptive seismic activity of Mount Cameroon (Cameroon), West Africa: a statistical analysis. *Journal of Volcanology and Geothermal Research*, 79, 199-219.
- Ateba, B., Dorbath, C., Dorbath, L., Ntepe, N., Frogneux, M., Aka, F.T., Hell, J.V., Delmond, J.C. and Manguelle, D., 2009. Eruptive and earthquake activities related to the 2000 eruption of Mount Cameroon volcano (West Africa). *Journal of Volcanology and Geothermal Research*, 179, 206 - 216.
- Awah, Soil map of Mount Cameroon project area, explanatory report. http://cameroun-foret.com/system/files/11_01_62.pdf.
- Ajani, E.N 2004. A critical assessment of the natural disaster risk management framework in Cameroon. End of course training report CEFAM, Buea. unpublished.
- Ayalew, L., Yamagishi, H., Marui, H. and Kanno, T., 2005. Landslides in Sado Island of Japan: part II. GIS-based susceptibility mapping with comparison of results from two methods and verifications. *Engineering Geology*, 81, 432 – 445.
- Ayonghe, S.N., Mafany, G.T., Ntasin, E. and Samalang, P., 1999. Seismically activated swarms of landslides, tension cracks and rockfall after heavy rainfall in Bafaka, Cameroon. *Natural Hazards* 19, 13-27.
- Ayonghe, S.N., Suh, C.E., Ntasin, E.B., Samalang, P. and Fantong, W., 2002. Hydrologically, seismically and tectonically triggered landslides along the Cameroon volcanic line. *Cameroon Geoscience Review*, 19, 4, 325-335.
- Ayonghe, S.N., Ntasin, E.B., Samalang, P. and Suh, C. E., 2004. The June 27, 2001 landslide on volcanic cones in Limbe, Mount Cameroon, West Africa, *Journal of African Earth Science*, 39, 435- 439.
- Ayonghe S.N. and Ntasin, E.B., 2008. The geological control and triggering mechanisms of landslides of the 20th July 2003 within the Bamboutos Caldera, Cameroon. *Journal of the Cameroon Academy of Science* 7, 3, 191-204.
- Azañón, J.M, Azor, A., Yesares, J., Tsige, M., Mateos, R.M., Nieto, F., Delgado, J., López-Chicano, M., Martin, W. and Rodriguez-Fernandez, J., 2010. Regional-scale high-plasticity clay-bearing formation as controlling factors on landslide in Southeast Spain. *Geomorphology*, 120, 26-37.
- Barlow, J., Martin, Y., and Franklin, S.E., 2003. Detecting translational landslide scars using segmentation of Landsat ETM+ and DEM data in the northern Cascade Mountains, British Columbia. *Canadian Journal of Remote Sensing*, 29, 4, 510-517.
- Barton, M.E., 1973. The Degradation of the Barton Clay cliffs of Hampshire. *Quarterly Journal of Engineering Geology*, 6, 423 – 440.
- Beyala, V.K.K., Onana, V.L., Priso, E.N.E., Parisot, J.C. and Ekodeck, G.E., 2009. Behaviour of REE and mass balance calculations in a lateritic profile over chlorite schist in South Cameroon. *Chemie der Erde*, 69, 61-73.

References

- Bhasin, R., Grimstad, E., Larsen, J.O., Dhawan, A.S., Singh, R., Verma, S.K., and Venkatachalam, K., 2001. Landslide hazards and mitigation measures at Gangtok, Sikkim, Himalaya. *Engineering Geology*, 64, 4, 351-368.
- Bonnard, C., Forlati F. and Scavia C. 2003. Identification and mitigation of larges landslide risks in Europe. *Advances in risk assessment*. Balkema, Leiden, 317 p.
- Bonne, K., Kervyn, M., Cascones, L., Njome, M.S., Van Ranst, E., Suh, C.E., Ayonghe, S., Jacobs, P., and Ernst, G.G.J., 2008. A new approach to assess long term lava flow hazard and risk using GIS and low cost remote sensing: the Case of Mount Cameroon, West, Africa. *International Journal of Remote sensing*, 29, 6537-6562.
- Bonne, K., 2006. Assessment of hazardous volcanological phenomena on Mount Cameroon using remote sensing and field observations. MSc thesis, University of Ghent, 123p.
- Brabb, E.E., 1984. Innovative approaches to landslide hazard mapping. *Proceedings 4th International symposium on landslides*, Toronto, Ont., 16-21 September 1984. BiTech Publishers, Vancouver, B.C. 1, 307-324.
- Brabb, E.E., 1991. The world landslide problem. *Episodes*, 14, 1, 52-61.
- Brand, E.W., Premchitt, J. and Phillipson, H.B. 1984. Relationship between rainfall and landslides. *In Proceedings of the 4th International Symposium on Landslides*, Toronto, Ont., 16-21 September 1984. BiTech Publishers, Vancouver, B.C., 1, 377-384.
- Brikeland, P.W., 1999. *Soil and Geomorphology*. Oxford University Press, New York, 377-384.
- Brimhall, G.H, Alpers, C.N. and Cunningham, A.B., 1985. Analysis of supergene ore-forming processes and ground water solute transport using mass balance principles: *Economic Geology*, 80, 1227-1256.
- Brimhall, G.H. and Dietrich, W.E., 1987. Constitutive mass balance relations between chemical composition, volume, density, porosity, and strain in metasomatic hydrochemical systems: Results on weathering and pedogenesis: *Geochimica et Cosmochimica Acta*, 51, 567-587.
- Brunetti M.T, Guzzetti F. and Rossi M. 2009. Probability distribution of landslide volume. *Non linear Processes*, 16, 179-188.
- Buea, Carte provisoire de l'Afrique centrale au 1/50,000 Republique Fédérale du Cameroun feuille NB-32-IV-IB dessiné et publié par l'Institut Géographique National – Paris (Annexe de Yaoundé) en 1963.
- Buh, W.G., 2009. Geographic information systems based demarcation of risk zones: the case of the Limbe Sub-Division-Cameroon. *Journal of Disaster Risk Studies*, 2, 1, 54-70.
- Bureau Central des Recensements et des Etudes de Population, 2010. Rapport de présentation des résultats définitifs, 68 p.
- Campbell, R.H., 1975. Soil slips debris flow, and rainstorms in Santa Monica Mountains and vicinity, South California. In *US Geological Survey Professional paper 851*, US Government Printing Office Washington D.C, 51 p.
- Carrara, A., Cardinali, M., Detti, R., Guzzetti, F., Pasqui, V. and Reichenbach, P., 1991. GIS techniques and statistical models in evaluation landslide hazards, *Earth Surface Processes and Landforms*, 16, 427- 445.
- Carrara, A., Guzzetti, F., Cardinali, M., and Reichenbach, P., 1999. Use of GIS technique in the prediction and monitoring of landslide hazard. *Natural Hazards* 20, 117-135.
- Carrara, A., Crosta, G., and Frattini, P., 2003. Geomorphological and historical data in assessing landslide hazards. *Earth Surface Processes and Landforms* 28, 1125 – 1142.
- Caine, N., 1980.the rainfall intensity duration control of shallow landslide and debris flows. *Geografiska Annaler*, 62, A 1-2, 23-27.
- Casagrande, A., 1948. Classification and identification of soils, *Transactions, ASCE*, 113, 901-930.
- Casadei, M, Dietrich, W.E., and Miller, N.L., 2003. Testing a model for predicting the timing and location of shallow landslide initiation in soil-mantled landscapes. *Earth Surface Processes and landforms*, 28, 925-950.
- Cengiz, O., Sener, E., and Yagmurlu, F., 2006. A satellite image approach to the study of lineaments, circular structures and regional geology in the Golcuk Crater district and its environs (Isparta, SW Turkey). *Journal of Asian Earth Sciences*, 27, 155-163.
- Cernica, J. N., 1995. *Geotechnical engineering: soil mechanics*, John Wiley & Sons, Inc., USA

References

- Ceryan, S., 2008. New chemical indices for estimating the mechanical properties of rock a case study from the Kürtün Granodiorite, NE Turkey Trukish Journal of Earth Science, 17, 187-207.
- Chadwick, O.A, Gavenda, R.T., Kelly, E.F., Ziegler, K, Olson, C.G., Elliott, W.C., Hendricks, D.M., 2003. The impact of climate on the biogeochemical functioning of volcanic soils. Chemical Geology, 202, 195 – 223.
- Cheng, K.S., Wei, C., Chang, S.C., 2003. Locating landslides using multi-temporal satellite images. Advances in Space Research, 33, 296-301.
- Chau, K.T., Sze, Y.L., Fung, M.K., Wong, W.Y., Fong, E.L., Chan, L.C.P., 2004. Landslide hazards analysis for Hong Kong using landslide inventory and GIS, Computer Geoscience 30, 429 – 443.
- Chauvel, C., Dia, A.N., Bulourde, M., Chabaux, F., Durand, S., Ildefonse, P., Gerard, M., Deruelle, B., and Ngounouno, I., 2005. Do decades of tropical rainfall affect the chemical composition of basaltic lava flows in Mount Cameroon? Journal of Volcanology and Geothermal Research, 141, 195-223.
- Che, V.B, Kervyn, M, Ernst G.G.J, Trefois P, Ayonghe S, Jacobs P, Van Ranst, E., Suh C.E. Systematic documentation of landslide events in Limbe area (Mt Cameroon Volcano, SW Cameroon): Geometry, controlling and triggering factors. Natural Hazards. DOI 10.1007/s11069-011-9738-3
- Che V.B., Kervyn M., Suh C.E., Ernst G.G.J., del Marmol M-A., Trefois P., Jacobs P. Landslide susceptibility assessment in Limbe region (SW Cameroon), through a field calibrated seed cell and information value method (Catena, in revision).
- Chung, C.F. and Fabbri, A.G., 1999. Probabilistic prediction model for landslide hazards mapping. Photogrammetric Engineering and Remote Sensing 65, 12, 1389-1399.
- Chung, C.F. and Fabbri, A.G., 2003. Validation of spatial prediction models as landslide hazards mapping. Natural Hazards, 30, 451-472.
- Claessens, L., Knapen, A. Kitutu, M.G., Poesen, J. and Deckers, J.A., 2007. Modelling landslide hazards, soil redistribution and sediment yield of landslide on the Ugandan foot slopes of Mount Elgon. Geomorphology, 90, 23 – 35.
- Clerici, A., Perego, S., Tellini, C. and Vescovi, P., 2002. A procedure for landslide susceptibility zonation by the conditional analysis method. Geomorphology 48, 349-364.
- Coe, J.A., Godt, J.W., Parise, M. and Moscariello, A., 2003. Estimating debris flow probability using fan stratigraphy, historical records and drainage-basin morphology, interstate 70 highway corridor, central Colorado, USA, <http://landslides.usgs.gov/docs/coe/DFHM2003.pdf>
- Conoscenti, C., Di Maggio, C., Rotigliano, E., 2008. GIS analysis to assess landslide susceptibility in a fluvial basin of NW Sicily (Italy). Geomorphology 94. 325-339.
- Corominas J., 1996. The angle of reach as mobility index for small and large landslides. Canadian Geotechnical Journal, 33, 206-271.
- Croney P and Croney D, 1997. the design and performance of road pavement 3rd ed, McGraw-Hill, 502 p.
- Cross, M., 1998. Landslide susceptibility mapping using the Matrix Assessment Approach: a Derbyshire case study. In: Maund, J.G., and Eddleston, M. (eds) Geohazards in Engineering Geology. Geological Society, London, Engineering Geology Special Publication. 15, 247 – 261.
- Crovelli, R.A., 2000. Probability model for estimation of the number and cost of landslide, US Geological Survey Open File Report, 00-249, 23p. <http://pubs.usgs.gov/of/2000/ofr-00-249>
- Crozier, M.J., 1986. Landslides causes, consequences, and environment. Croom Helm, London, 252p.
- Cruden, D.M., 1991. A simple definition of landslides. Bulletin International Association for Engineering Geologist, 43, 27-29.
- Cruden, D.M., and Varnes, D.J., 1996. Landslide types and processes, Chapter 3 in Landslides: Investigations and Mitigation, Turner, A.K., and Schuster, R.L. eds., Transportation Research Board, Special Report 247, 36-75.
- Dahl, M.P.J., Mortensen, L.E., Veihe, A. and Jensen, N.H., 2010. A simple qualitative approach for mapping regional landslide susceptibility in the Faroe Islands. Natural Hazards and Earth Systems Sciences, 10, 159–170.
- Dai, F.C., Lee, C.F., Li, J., Xu, Z.W., 2001. Assessment of landslide susceptibility on the natural terrain of Lantau Island, Hong Kong. Environmental Geology 43 3, 381–391.

References

- Dai, F.C. and Lee, C.F., 2002. Landslide characteristics and slope instability modelling using GIS, Lantau Island, Hong Kong. *Geomorphology* 42, 213-228.
- Davies, M.R., Paulen, R.C. and Hickin, A.S., 2005. Inventory of Holocene landslides, Peace River Area, Alberta (NTS 84C): Alberta Energy and Utilities Board, EUB/AGS Geo-Note 2003-43.
- Déruelle, B., Ngounouno, I. and Demaiffé, D., 2007. The 'Cameroon Hot Line' (CHL): a unique example of active alkaline intraplate structure in both oceanic and continental lithospheres. *Geoscience* 339, 589-600.
- Deruelle, B., N'ni, J. and Kambou, R., 1987. Mount Cameroon: an active volcano of the Cameroon Line. *Journal of African Earth Science*, 6, 2, 197-214.
- Dia, A., Chauvel C., Bulourde M., and Gerard M., 2006. Eolian contribution to soils on Mount Cameroon: Isotopic and trace element records. *Chemical Geology*, 226, 232–252.
- Dikau, R., Brunsten, D., Schrott, L. and Ibsen, M-L., (ed) 1996. *Landslide recognition: identification, movement and courses*. John Wiley and sons Ltd, 251 p.
- Dixon, H. H., and Robertson, R.H.S, 1970. Some engineering experiences in tropical soils, *Quarterly journal of Engineering Geology and Hydrogeology*, 3,3, 137-150.
- Donati, L. and Turrini, M.C., 2002. An objective method to rank the importance of the factors predisposing to landslide with the GIS methodology: application to an area of the Apennines (Valnerina, Perugia, Italy). *Engineering Geology*, 63, 277-289.
- Duman, T.Y., Can, T., Gokceoglu, C. and Nefeslioglu, H.A., 2005. Landslide susceptibility mapping of Cekmece area (Istanbul, Turkey) by conditional probability. *Hydrology and Earth Systems Sciences Discussions* 2, 155-208. SRef-ID:1812-2116/hessd/2006-2-155.
- Dumort, J.C., 1968. Notice Explicative de la Feuille Douala Ouest avec carte géologique au 1/500000. Direction des mines, Géologie, Cameroon, scale 1/500000.
- Duzgoren-Aydin, N.S., Aydin, A., and Malpas, J. 2002. Re-assessment of chemical weathering indices: case study from pyroclastic rocks of Hong Kong. *Engineering Geology* 63, 99–119,
- Duzgoren-Aydin, N.S., Aydin, A., and Malpas, J. 2002. Distribution of clay minerals along a weathered pyroclastic rock profile, Hong Kong, *Catena*, 50, 17–41.
- Duzgoren-Aydin, N.S., and Aydin, A., 2006. Chemical and mineralogical heterogeneities of weathered igneous profiles: implications for landslide investigations. *Natural Hazards and Earth System Science*, 6, 315-322.
- Endeley, R.E., Ayonghe S.N., and Tchuenteu, F., 2001. A preliminary hydrogeochemical baseline study of water sources around Mount Cameroon. *Journal of the Cameroon Academy of Science*, 1, 3, 161-168.
- Esu and Grissolia 1991 In Fiorillo, F., 2003. Geological features and landslide mechanisms of an unstable coastal slope (Petacciato, Italy). *Engineering Geology*, 67, 255-267.
- Fell, R., 1994. Landslide risk assessment and acceptable risk. *Canadian Geotechnical Journal*, 31, 261– 272.
- Fernadas, N.F., Guimarães, R.F., Gomes, R.A.T., Vieira, B.C., Montgomery, D.R. and Greenberg, H., 2004. Topographic controls of landslides in Rio de Janeiro field evidence and modeling. *Catena*, 55, 163-181.
- Fernandez Merodo, J.A, Pastor, M., Mira, P., Tonni, L., Herreros, M.I., Gonzalez, E. and Tamagnini, R., 2004. Modelling of diffuse failure mechanisms of catastrophic landslides. *Computer methods in applied mechanics and engineering*, 193, 2911-2939.
- Fitton, J.G., Kilburn, C.R.J., Thirlwall M.F. and Hughes, D.J., 1983. 1982 eruption of Mount Cameroon, West Africa. *Nature*, 306, 327 – 332.
- Fiorillo, F., 2003. Geological features and landslide mechanisms of an unstable coastal slope (Petacciato, Italy). *Engineering Geology*, 67, 255-267.
- Fiorillo, F. and Guadagno, F.M., 2000. Analysis of rainfall patterns triggering reactivation of a large landslide in Pleistocene clays in Molise (Italy). 8th International Symposium on landslides, v 2. Thomas Telford, London; 553-557.
- Gali, M., Bell, R., Cardinali, M., Glade, T. and Guzzetti, F., 2007. Combined use of aerial photographs and LIDAR elevation data to obtain large scale landslide inventory maps. *Geophysical Research Abstracts* 9, 03227.
- Geertsema, M. and Pojar, J.J., 2007. Influence of landslides on biophysical diversity- A perspective from British Columbia. *Geomorphology*, 89, 55-69.

References

- Geological Society Engineering Group working party report. 1990. Tropical residual soils. *Quarterly Journal of Engineering Geology*, 23, 1. 101p.
- Glade, T., 1998. Establishing the frequency and magnitude of landslide triggering rainstorm events in New Zealand. *Environmental Geology*, 35, 2-3, 160-174.
- Glade, T. and Crozier, M.J., 2005. A review of scale dependency in landslide hazard and risk analysis. In Glade, T., Anderson, M., Crozier, M.J., (eds), *Landslide hazard and risk*. John Wiley and sons, Chichester, 75-138.
- Gorsevski, P.V., Foltz, R.B., Gessler, P.E. and Elliot, W.J., 2006. Spatial prediction of landslide hazards using logistic regression and ROC analysis. *Transactions in GIS*, 10, 3, 395-415.
- Görög, P., and Török, Á., 2007. Slope stability assessment of weathered clay by using field data and computer modeling: a case study from Budapest. *Natural Hazards and Earth System Sciences*, 7, 417-422.
- Gratchev, I.B., Sassa, K., Fukuoaka, H., 2006. How reliable is the plasticity index for estimating the liquefaction potential of clayey sands? *Journal of Geotechnical and Geoenvironmental Engineering ASCE*, 132, 124-127.
- Guthrie, R.H., Evans, S.G., 2004a. Analysis of landslide frequencies and characteristics in a natural system, coastal British Columbia. *Earth Surface Processes and Landforms* 29, 1321-1339.
- Guzzetti, F. Review and selection of optimal geological models related to spatial information available action no 1.14, IRPI CNR, Perugia, Italy.
- Guzzetti, F., Carrara A., Cardinali M. and Reichenbach, P., 1999. Landslide hazard evaluation: a review of current techniques and their application in a multi-scale study, Central Italy, *Geomorphology*, 31, 181-216.
- Guzzetti, F., Reichenbach, P., Cardinali, F.A. and Galli, M., 2003. The impact of landslides in the Umbria region, Central Italy. *Natural Hazards and Earth System Sciences*, 3, 469-486.
- Guzzetti, F., Reichenbach, P., Cardinali, M., Galli, M. and Ardizzone, F., 2005. Landslide hazard assessment in the Staffora basin, Northern Italian Apennines. *Geomorphology*, 72, 272-299.
- Guzzetti, F., Peruccacci, S., Rossi, M. and Stark, C.P., 2007. The rainfall intensity- duration control of shallow landslides and debris flows: an update. *Landslides*
- Guzzetti, F., Peruccacci, S., Rossi, M. and Stark, C.P., 2007. Rainfall threshold for the initiation of landslides in Central and Southern Europe. *Meteorology and Atmospheric Physics*, 98, 239-267.
- Guzzetti, F., Ardizzone, F., Cardinalli, M., Rossi, M. and Valigi, D. 2009. Landslide volume and landslide mobilization rates in Umbria, central Italy.
- Hansen, A., 1984. Landslide hazards analysis. In Brunsten, D., Prior, D.B (Eds), *Slope instability*, Wiley, New York, pp. 523-602.
- Harris, W., 2007. *Methods of soil analysis Part 5. Mineralogical Methods*, SSSA book Series, No5. Soil science society of America, 667 Segoe road, Madison, USA.
- Hasselo H.N., 1961. The soils of the lower eastern slopes of the Cameroon Mountain and their suitability for various perennial crops. Wageningen, 69 p.
- Havenith, H.B., Strom, A., Jongmans, K., Abdrakhmatov, K., Delvaux, D., and Tréfois, P., 2003. Seismic triggering of landslides, Part A: field evidence field evidence from the Northern Tien Shen. *Natural Hazards and Earth System Sciences*, 3, 135-149.
- Hengxing, L., Chebghu, Z., Lee, C.F., Sijing, W. and Faquan, W., 2003. Rainfall -induced landslide stability analysis in response to transient pore pressure. A case of natural terrain landslide in Hong Kong. *Science in China Ser. E Technological Sciences*, 46, 52-68.
- Hill, I.G., Worden R.H. and Meighan I.G., 2000. Yttrium: The immobility-mobility transition during basaltic weathering, *Geology* 28, 10; 923-926
- Hoek, E., and Bray, J.W., 1977. *Rock Slope Engineering*. The Institution of Mining and Metallurgy, London: 358 p.
- Hovius, N., Stark, C.P. and Allen, P.A., 1997. Sediment flux from a mountain belt derived by landslide mapping. *Geology*, 25, 231-234.
- Hong, Y., Adler, R. and Huffman, G., 2006. Evaluation of the potential of NASA multi-satellite precipitation analysis in global landslide hazard assessment. *Geophysical Research Letters*, 33, L22402.

References

- Hurlimann, M., Ledesma, A. and Maarti, J., 2001. Characterisation of volcanic residual soils and its implication for large landslide phenomena: application to Tenerife, Canary Islands. *Engineering Geology*, 59, 115-132.
- Hutchinson, J.N., 1988. General report: morphological and geotechnical parameters of landslides in relation to geology and hydrology. 5th International Symposium on Landslides, Balkema, Rotterdam, 1: 3-35.
- Hutchinson, J.N. 1995. Keynote paper: Landslide hazard assessment. In *Landslides, Proceeding from the Sixth International Symposium on Landslides, February*, (Ed. D.H. Bell), Christchurch, New Zealand. A.A. Balkema, Rotterdam, the Netherlands, 3, 1805-1841
- Ietto, F., Donato, F.F. and Ietto, A. 2007. Recent reverse faults and landslide in granitoid weathered profiles Serre Mountains (Southern Colombia, Italy), *Geomorphology*, 87, 196 – 206.
- Inganga, SF., Ucakwun, E.K. and Some D.K., 2001. Rate of swelling of expansive soils: a critical factor in the triggering of landslides and damage to structures. *Documenta naturae*, 136, 93-98.
- Islam, M.R., Peuraniemi, V., Aario, R., Rojstaczer, S., 2002. Geochemistry and minerology of saprolite in Finnish Lapland. *Applied Geochemistry*, 17, 885 - 902.
- Jaiswal, P. and van Westen C.J., 2009. Estimating temporal probability for landslide initiation along transportation routes based on rainfall thresholds. *Geomorphology*, 112, 96-105.
- Jakob, M. and Weatherly, H., 2003. A hydroclimatic threshold for landslide initiation on the North Shore Mountains of Vancouver, British Columbia. *Geomorphology*, 54,137-156.
- Jennings, P.J. and Siddle, H.J., 1998. Use of landslide inventory data to define the spatial location of landslide sites, South Wales, UK. In Maund, J. G., and Eddleston, M (eds) *Geohazards in Engineering Geology*. Geological society, London, Engineering Geology Special Publications 15, 199-211.
- Jersak, J., Amundson, R. and Brimhall J.G., 1995. A mass balance analysis of podzolization: Examples from North Eastern United States. *Geoderma*, 66, 15-42.
- Jiménez-Perálvarez, J.D., Irigaray, C. and El Hamdouni, R., 2009. Building models for automatic landslide susceptibility analysis, mapping and validation in ArcGIS. *Natural hazards*, 50, 571-590.DOI 10.1007/s11069-008-9305-8.
- Kitutu, M.G, Muwanga, A., Poesen, J. and Deckers J.A 2009. Influence of soil properties on landslide occurrences in Bududa district, Eastern Uganda. *African Journal of Agricultural research*, 4, 7, 611-620
- Knapen, A., Kitutu, M.G., Poesen, J., Breugelmans, W., Deckers, J. and Muwanga, A., 2006. Landslides in a densely populated county at the foot slopes of Mount Elgon (Uganda): Characteristic and causal factors. *Geomorphology*, 73, 149-165.
- Lambe, T.W. and Whitman, R.V., 1979. *Soil Mechanics*, SI Version John Wiley and Sons, New York.
- Lambi, C.M., 1989. The dynamic landscape around Akum and Santa (Bamenda Highland Region): Landslide. *Cameroon Geographic Review* VIII, 65-78.
- Lambi, C.M. and Ngwana, B.S., 1991. Human interference and environmental instability. The case of the Limbe landslide. *Cameroon Geographic Review*, 44-52.
- Lambi, C.M., Kometa, S.S. and Fombe, L.F., 2002. Environmental hazards and land use planning for sustainable development: the Limbe unstable coastal region Cameroon. In Telford T (ed) *Instability planning and management*, London. Pp 151-159.
- Lambi, C.M., 2004. A revisit of the recurrent landslides on the Bamenda escarpment (North West Province of Cameroon). *Journal of Applied Social Sciences*, 4, 1, 4-26
- Larsen , M.C. and Simon, A., 1993. Rainfall-threshold conditions for landslide in a humid –tropical system, Puerto Rico. *Geografiska Annaler*, 75 a 1-2, 13 -23.
- Le Bas M.J, Le Maitre R.W., Streckheisen, A. and Zanettin B., 1986. Chemical classification of volcanic rocks based on the total alkali–silica diagram. *Journal of Petrology*, 27, 745 – 750.
- Lee, S., Ryu, J., Won, J., and Park, H., 2004. Determination and application of weights for landslide susceptibility mapping using artificial neural network. *Engineering Geology*, 71, 3-4, 289-302.
- Lei Z., Jing-feng H., 2006. GIS–based logistic regression method for landslide susceptibility mapping in regional scale. *Journal of Zhejiang University Science A*, 7, 12, 2007-2017

References

- Leroueil, S., Vaunat, J., Picarelli, L., Locat, J., Faure, R., & Lee H., 1996. A geotechnical characterisation of slope movements. Proceeding of the 7 international Symposium on Landslide, Trondheim, 1, pp 53-74, Balkema, Rotterdam;
- Lillesand, T.M., and Kiefer, R.W., 2000. Remote sensing and image interpretation, John Wiley and Sons, New York, 784 p.
- Liu, Z., Cai, Z.C. and Wang, J.F., 1996, Microelements of Soils in China: Nanjing, Jiangsu Science and Technology Press, 329 p.
- Lohnes, R.A, Fish, R.O, and Demirel, T., 1971. Geotechnical properties of selected Puerti Rican soils in relation to climate and parent rock. , Geological society of American Bulletin, 82, 2617-2624
- Lumb, P. 1975. Slope failures in Hong Kong. Quarterly Journal of Engineering Geology, 8: 31–65.
- MahdaviFar, M.R., Solaymani, S. and Jafari, M.K., 2002. Landslide triggered by the Avaj, Iran earthquake of June 22, 2002. Engineering Geology 86, 2-3, 166-182.
- Malamud B.D., Turcotte D.L., Guzzetti F., Reichenbach P., 2004. Landslides, earthquakes, and erosion, Earth and Planetary Science Letters 229, 45 – 59.
- Malamud B.D., Turcotte D.L., Guzzetti F., Reichenbach P., 2004. Landslide inventories and their statistical properties, Earth Surface Processes and Landforms 29, 687–711
- Mateos, R.M., Azanon, J.M., Morales, R., Lopez-chicano, M., 2007.Regional prediction of landslide in the Tramuntana range (Majorca) using probability analysis of intense rainfall. Z.Geomorph. N. F 51, 3, 287-306.
- Martel S.J., 2004. Mechanics of landslide initiation as a shear fracture phenomenon. Marine Geology, 203, 319-339.
- Marzoli, A., Piccirillo, E.M., Renne, P.R., Bellient, G., Iacumin, M., Nyobe, J.B., and Tongwa, A.T., 2000. The Cameroon Volcanic Line revisited: Petrogenesis of continental basaltic magmas from lithospheric and asthenospheric mantle sources: Journal of Petrology 41, 87-109.
- Masson, D.G., Watts, A. G., Gee, M.J.R., Mitchel, N.C., Le Bas, T.P., and Canals, N.C., 2002. Slope failures on the flanks of the western Canary Islands. Earth-Science Reviews 57, 1-35.
- McCalpin, J., 1984. Preliminary age classification of landslides for inventory mapping, In Proceedings 21 Annual Symposium on Engineering Geology and Soils Engineering, Pochtello, Idaho
- Meisina, C., and Scarabelli, S., 2007. A comparative analysis of terrain stability model for predicting shallow landslides in colluvial soil. Geomorphology, 87, 207-223.
- Meusbürger, K. and Alewell, C. 2008. Impact of anthropogenic and environmental factors on the occurrence of shallow landslides in an alpine catchment (Urseren Valley, Switzerland) Natural hazards and earth system sciences, 8, 509–520,
- Middelburg, J.J, and van der Weijden, C., and Woittiez, J.R.W., 1988. Chemical processes affecting the mobility of major, minor and trace elements during weathering of granitic rocks. Chemical Geology, 68, 253-278.
- Miller, S., Harris, N., Williams, L. and Bhalai, S., 2007. Landslide susceptibility assessment for St. Thomas, Jamaica, using geographic information system and remote sensing methods. In Teeuw, R.M. (ed) Mapping Hazardous terrain using Remote Sensing. Geological Society, London, Special Publication, 283, 77 – 91.
- Moeyersons, J., Trefois, P., Lavreau, J., Alimasi, D., Badriyo, I., Mitima, B., Mundala, M., Munganga, D.O. and Nahimana, L., 2004. A geomorphological assessment of landslide origin at Bukavu, Democratic Republic of the Congo. Engineering Geology, 72, 73-87.
- Montgomery, D.R., and Dietrich, W.E., 1994. A physically based model for the topographic control on shallow landsliding. Water Resources Research, 30, 4, 1153 - 1171.
- Nchia P.N., 2010. Trace metal content and spatial distribution in urban top soils of Limbe Cameroon. Unpublished MSc thesis
- Nesbitt, W.W. and Young, G.M., 1982. Early Proterozoic climates and plate motions inferred from major element chemistry and lutites. Nature, 299, 715-717.
- Ngwa C.N., Suh C.E., Devey C.W. 2010, Phreatomagmatic deposits and stratigraphic reconstruction at Debunsha Maar (Mt Cameroon volcano) Journal of Volcanology and Geothermal Research 192: 201-211.

References

- Ngole, V.M; Ekosse G.E., Ayonghe, S.N., 2007, Physico-chemical, mineralogical and chemical considerations in understanding the 2001 Mabeta New Layout landslide, Cameroon , *J. Appl. Sci. Environ. Manage* 11, 2, 201 – 208
- Njome, M.S., Suh, C.E., Sparks, R.S.J., Ayonghe, S.N., and Fitton, J.G., 2008. The Mount Cameroon 1959 compound lava flow field: morphology petrology and geochemistry. *Swiss Journal of Geoscience* 101, 85-98.
- Ohlmacher, G.C., 2000. The Relationship between geology and landslide hazards of Atchison, Kansas, and vicinity. *Current Research in Earth Sciences*, 244, 3, 1–16.
- Ortigao, J. A. R., and Sayao, A. S. F. J., 2004. *Handbook of slope stabilization*. Springer, 478p.
- Parry, S., Campbell, S.D.C., and Churchman, C.J., 2000. Kaolin-rich zones in Hong Kong saprolites- their interpretation and engineering significance. *Proceeding of Geological Engineering*, 2000. Melbourne, Australia. 6 pp.
- Popescu, M. E. Landslide causal factors and landslide remedial options, <http://www.geoengineer.org/Lanslides-Popescu.pdf>.
- Price, R. J and Velbel, A.M., 2003. Chemical weathering indices applied to weathered profiles developed on heterogeneous felsic metamorphic parent rock, *Chemical Geology*, 202, 379-416.
- Prior, D.B., and Ho, C., 1972. Coastal and mountain slope instability on the islands of St. Lucia and Barbados. *Engineering Geology*, 6, 1-18.
- Rao, S.M., 1997. Mechanistic approach to the shear strength behaviour of allophonic soils; *Engineering Geology*, 40, 215-221.
- Rahman, Z.A., Hamzah, U, Taha, R, Ithnain N.S., and Almad, N., 2010. Influence of oil contamination on geotechnical properties of basaltic residual soil. *American Journal of Applied Science* 7, 7, 954-961.
- Rankenburg, K., Lassitter, J.C., and Brey, G., 2005. The role of continental crust and lithospheric mantle in the genesis of Cameroon volcanic line lavas. Constraints from isotopic variations in lavas and megacryst from the Bui and Jos Plateaux, *Journal of Petrology* 46, 169-190.
- Revellino, P., Guadagno, F.M., and Hungr, O. 2008. Morphological methods and dynamic modeling in landslide hazards assessment of the Campania Apennine carbonate slope. *Landslides*, 5, 59-70.
- Riedel, C., Ernst G.G.J, Riley M, 2003. Control on the growth and geometry of pyroclastic constructs. *Journal of Volcanology and Geothermal Research*, 127, 121-152.
- Rosenfeld, C.L., 1994. The geomorphological dimensions of natural disasters. *Geomorphology* 10, 27–36.
- Rosenak, S., 1963. *Soil Mechanics*, Bedford, London, 196 p.
- Rouse, W.C., Reading, A.J. and Walsh, R.P.D., 1986. Volcanic soil properties in Dominica , West Indies. *Engineering Geology*, 23, 1-28.
- Ruff, M. and Czurda, K., 2008. Landslide susceptibility analysis with heuristic approach in the Eastern Alps (Vorarlberg, Austria). *Geomorphology*, 94, 314-324.
- Ruxton, B.P., 1968. Measure of the degree of chemical weathering of rocks. *Journal of Geology*, 76, 518–527.
- Santacana, N., Baeza, B., Corominas, J., De Paz, A. and Marturia, J. 2003. A GIS-based multivariate statistical analysis for shallow landslide susceptibility mapping in La Pobla de Lillet area (Eastern Pyrenees, Spain), *Natural Hazards and Earth System Sciences*, 30, 281–295.
- Sato, H., Aramaki, S., Kusakabe, M., Hirabayashi, J., Sano, Y., Nojiri, Y. and Tchoua, F., 1990. Geochemical difference of basalts between polygenetic and monogenetic volcanoes in the central part of the Cameroon Volcanic line. *Geochemical Journal*, 24, 357-370.
- Schuster, R.L. and Fleming, R.W., 1986. Economic losses and fatalities due to landslides. *Bulletin American Association Engineering Geologists*, 23, 1, 11–28.
- Schuster, R.L., 1995a. Socioeconomic significance of landslides. In: Turner, A.K., Schuster, R.L. Eds., *Landslides, Investigation and Mitigation*. Transportation Research Board Special Report 247. National Academy Press, WA, 12–35.
- Schuster R.L. and Highland L.M. 2001 – Socioeconomic and environmental impacts of landslides in the western hemisphere. – USGS Open-File Report, 2001-01, 276p.

References

- Sengupta, A., Gupta, S. and Anbarasu, K., 2010. Rainfall thresholds for the initiation of landslide at Lanta Kholra in North Sikkim, India. *Natural hazards*, 52, 31-42.
- Shakoor, A. and Smithmyer A.J., 2005. An analysis of storm-induced landslides in colluvial soils overlying mudrock sequences, south eastern Ohio, USA. *Engineering Geology*, 78, 257-274.
- Shuzui, H., 2001. Process of slip-surface development and formation of slip-surface clay in landslides in Tertiary volcanic rocks, Japan. *Engineering Geology*, 61, 199-219.
- Sieffermann, G, Jehl, G. and Millot, G., 1968, Allophanes et minéraux argileux des alterations récentes des basaltes du Mount Cameroun, *Bulletin groupe française argiles*, t. XX, pp 109-129
- Sidle, R.C., 1984. Shallow groundwater fluctuations in unstable hill slopes of coastal Alaska. *Zeitschrift für Gletscherkunde und Glazialgeologie*, 20, 79-95.
- Sidle, R.C., Pearce, A, J. and O'loughlin, C.L., 1985. Hill slope stability and land use. American Geophysical Union, Washington DC, USA. 125 p.
- Skempton, A. W., 1953. Soil mechanics in relation to geology, *Proceeding of the Yorkshire Geological Society*, 29, Part 1, 3, 33-62.
- Soeters, R. and van Westen, C.J., 1996. Slope stability recognition, analysis and zonation. In turner, A.K., Schuster, R.L., (eds). *Landslide investigation and mitigation*. Transport Research Board, special Report 247. National research Council Washington, pp 129-177.
- Sorriso Valvo, M., 2002. Landslides from inventory to risk In Rybar, J., Stemberk, J., Wagner, P.,(eds)*Landslides proceedings of the International Conference on Landslides*, Balkema, Rotterdam, 79-93.
- Suh, C.E., Ayonghe, S.N. and Njumbe E.S., 2001. Neotectonic earth movement related to the 1999 eruption of Cameroon Mountain, West Africa. *Episode*, 24, 1, 9 - 12
- Suh, C. E., Sparks, R. S. J., Fitton, J. G., Ayonghe, S. N., Annen, C., Nana, R. and Luckman, A. 2003. The 1999 and 2000 eruptions of Mount Cameroon: eruption behaviour and petrochemistry of lava. *Bulletin of Volcanology*, 65, 267-281.
- Suh C.E., Luhr J.F. and Njome, M.S., 2008. Olivine-hosted glass inclusions from Scoriae erupted in 1954–2000 at Mount Cameroon volcano, West Africa. *Journal of Volcanology and Geothermal Research*, 169, 1–33.
- Suh C.E., Stansfield S.A., Sparks R.S.J., Njome M.S., Wantim M.N. and Ernst G.G.J 2010. Morphology and structure of the 1999 lava flows at Mount Cameroon Volcano (West Africa) and their bearing on the emplacement dynamics of volume-limited flows. *Geological Magazine*, 148, 22-34.
- Süzen. M.L. and Doyuran, V., 2004. Data driven bivariate landslide susceptibility assessment using geographical information systems: method and application to the Asarasuyu catchment, Turkey. *Engineering Geology*. 71, 303-321.
- Tarolli, P., Borga, M. and Fontana, G.D., 2007. Analysing the effect of upslope bedrock outcrop on shallow landsliding. *Geomorphology*, 93, 3 - 4, 186 - 200.
- Terzaghi, K., Peck, R.B., Mesri, G. 1996. *Soil mechanics in engineering practice*. 3rd ed, John Wiley and sons, 549p.
- Thiery, Y., Malet, J.P., Sterlacchini, S., Puissant, A. and Maquaire, O., 2007. Landslide susceptibility assessment by bivariate methods at large scale: Application to a complex mountainous environment. *Geomorphology*, 92, 1-2, 38 - 59.
- Thierry, P., Stieltjes, L., Kouokam, E., Ngueya, P. and Salley, P., 2008. Multi-hazard risk mapping and assessment on an active volcano: the GRINP project at Mount Cameroon. *Natural hazards*, 45, no3, 429 - 456
- Trefois, P., Moeyersons, J., Lavreau, J., Alimasi, D., Badriyo, I., Mitima, B., Mundala, M., Munganga, D.O. and Nahimana, L., 2007. Geomorphology and urban geology of Bukavu (R. D. Congo): interaction between slope instability and human settlement. In Teeuw, R. M., (ed) *Mapping hazardous terrain using remote sensing*. Geological Society London, Special Publication; 283, 65 - 75.
- Tytgat Nele J.L. 2008. *Susceptibility Analysis of the Risk of Small Landslides on the Southern Slope of Mount Cameroon Volcano*, Unpublished MSC thesis , Ghent University, 132 p
- Ubangoh, R.U., Pacca, I. G. and Nyobe, J. B. 1998. Palaeomagnetism of the continental sector of the Cameroon Volcanic Line, West Africa, *Geophysical Journal International*, 135, 362-374.

References

- Valadão, P., Gaspar, J.L., Queiroz, G. and Ferreira, T., 2002. Landslide density map of S. Miguel Island, Azores archipelago. *Natural hazards and Earth System Sciences*, 2, 51-56.
- Van Ranst, E., Awah, E.T., and Hof, J., 1990. Volcanic soils patterns as related to the geomorphology of the lower slopes of Mount Cameroon, (West Africa). *Pedologie*, XL-1, 65 - 78.
- Van Reeuwijk, L. P. 1993. Procedures for soil analysis, International Soil reference and Information Centre, Wageningen, the Netherlands
- Van Westen, C.J., Van Asch, Th W.J. and Soeters, R., 2006. Landslide hazards and risk zonation: why is it still so difficult? UNESCO, Paris 63p.
- Varnes, D.J., 1978. Slope movement types and processes. In Schuster, R.L and Kriezek R. J (eds) *Landslide analysis and control*. Transportation Research Board, Special Report No 176, National Academy of Science, 11- 33.
- Varnes, D.J. and IAEG Commission on landslide and other mass movements, 1984. *Landslide hazard zonation: a review of principles and practice*. UNESCO Press, Paris, 63 p.
- Vaughan, P. R., Maccarinit, M. and Mokhtar, K. 1988. Indexing the engineering properties of residual soil. *Quarterly Journal of Engineering Geology*, 21, 69-84.
- Vingiani, S., De Mascellis, R., Mele, G., Orefice, N., Minieri, L. and Terribile, F., 2010. Ischia landslides (Italy): A multidisciplinary approach aimed to increase knowledge of soil properties. 19th World Congress of Soil Science, Soil Solutions for a Changing World 1 – 6 August 2010, Brisbane, Australia.
- Vijith, H., Rejith P.G., and Madhu, G., 2009. Using InfoVal Method and GIS techniques for the spatial modelling of landslides susceptibility in the Upper catchment of River Meenachil in Kerala. *Indian Society of Remote Sensing* 37, 241-250.
- Vogt, T., 1927. Sulitjelmefeltets geologiog petrografi. *Norsk Geologisk Tidsskrift*, 121 1-560.
- Wen, B. P., Ayin, A., Duzgoren-Aydin, Aydin, A., 2004. Geochemical characteristics of the slip zones of a landslide in granitic saprolite, Hong Kong: implications for their development and microenvironments. *Environmental Geology*, 47, 140-154.
- Wen, B. P., Ayin, A., Duzgoren-Aydin, N.S., Li, Y.R., Chen, H.Y., and Xiao, S.D., 2007. Residual strength of slip zones of large landslides in the three gorge area, China. *Engineering Geology*, 93, 82-98.
- Westly, L.D and Irfan T.Y., Classification of residual soils in Blight, G.E., (ed), 1997, AA Balkema Mechanics of residual soils
- White ID, Mottershead DN, Harrison J.J. 1996. *Environmental Systems*, 2nd Edition. London: Chapman & Hall, 616 p.
- Wieczorek, G.F., Matthias, J., Roman, J.M., Sandra L.Z., and Patricia, C., Preliminary assessment of landslide-induced wave hazards: Tidal Inlet, Glacier Bay National Park Alaska U. S. Geological Survey Open-File Report 03-100.
- Williams, A.B. and Donaldson, G.W., 1980. Development relating to building on expansive soils in South Africa: 1973 – 1980 Proceeding of the 4th international conference on Expansive soils, Denver, 2, 834 – 844.
- Woldearegay, K., Schubert, W., Klima, K. and Mogessie, A., 2006. Landslide hazards mitigation strategies in the northern highlands of Ethiopia. In: Nyssen, J., Poesen, J., Nurhussen Taha, Deckers., J. (Eds.), *Highland 2006 International Conference, Mekelle. Mid-Symposium Excursion Guide*, 16–29.
- Yalcin, A., 2007. The effect of clay on landslides. *Applied Clay Science*, 38, 1-2, 77-85.
- Yalcin, A., 2008. GIS-based landslide susceptibility mapping using analytical hierarchy process and bivariate statistics in Ardesen (Turkey): comparison of results and confirmations. *Catena*, 72, 1-12.
- Zezere, J.L., 2002. Landslide susceptibility assessment considering landslide typology, A case study in the area north of Lisbon (Portugal) *Natural Hazards and Earth System Sciences*, 2, 73-82.SRef-ID:1684-9981/nhess/2002-2-73.
- Zhang, G-L, Pan, J-H, Huang, C-M, Gong, Z-T., 2007. Geochemical features of a soil chronosequence developed on basalt in Hainan Island, China. *Revista Mexicana de Ciencias Geológicas* 24, 2 261-269.
- Zheng, G., Lang, Y., Takano, B., Matsuo, M., Kuno, A., and Tsushima, H., 2002. Iron speciation of sliding mud in Toyama Prefecture, Japan. *Journal of Asian Earth Science*, 20: 955-963.

References

- Zhu L., Huang J., 2007. GIS –based logistic regression method for landslide susceptibility mapping in regional scale. *University Science A* 7, 12, 2007-2017.
- Zogning, A., Ngouanet, C., and Tiafack, O., 2007. The catastrophic geomorphological processes in humid tropical Africa: A case study of the recent landslide disasters in Cameroon. *Sedimentary Geology* 199, 1-2, 13-17.

Summary

Limbe town and surrounding areas on the SE foot slopes of the active Mt Cameroon Volcano, have experienced numerous small-scale shallow landslides within the last 20 years. These resulted in the loss of ca. 30 lives and significant damage to farmland and properties. In the first section of this thesis, landslides and their scars are identified in the field and their geometry systematically measured to construct a landslide inventory map for the study area. Typical slides within the study area are small-scale, shallow, translational earth and debris slides although some rotational earth slides were also documented. In total 63 landslide scars were identified. The depletion zones have mean widths of $22 \text{ m} \pm 17 \text{ m}$ and lengths of $25 \pm 23 \text{ m}$. The estimated aerial extent of landslide scars and the volume of generated debris range from 10 to 10^4 m^2 and from 2×10^0 to $5 \times 10^4 \text{ m}^3$, respectively. By plotting these scars in a GIS environment, it is observed that landslides are not uniformly distributed within the study area but are spatially clustered. Specific landslides are investigated in detail to identify site-specific controlling and triggering factors. This is aimed at constraining key input parameters and their variability for subsequent susceptibility and risk modelling for immediate local and regional applications in land-use planning. A key finding is that most slope instabilities within the study area are associated with and appear to be exacerbated by man-made factors such as excavation, anarchical construction and deforestation of steep slopes. Prolonged, high-intensity rainfall notably during localized storms is the principal triggering factor identified so far. The findings from this case study have relevance to understand some key aspects of locally devastating slope instabilities that commonly occur on intensely weathered steep terrains across subtropical Africa and in the subtropics worldwide and affecting an ever denser and most vulnerable population.

Previous studies suggest that the occurrence of landslides in any area may be attributed to the geotechnical, mineralogical and chemical properties of the soils as well as forces acting on these materials. Thus after identifying the spatial distribution of landslides in the Limbe area, it was necessary to characterise the nature of the landslide-prone soils. In the third and fourth chapters of this thesis, geotechnical, mineralogical and chemical characterisation of some selected landslide scars is performed to obtain insights into the role the soil characteristics play

in the occurrence of shallow translational landslides. This involve digging six, 2.5 to 4 m deep pits into three landslide scars. From these pits, the soil profile was described, in-situ shear tests performed on the walls of the pit and samples collected for laboratory analysis. Laboratory results show that the soils are dominantly inorganic silts of high plasticity according to the Unified Soil Classification System. Bulk density varies from 1.11 to 1.60 g/cm³, specific gravity from 2.76 to 2.98 g/cm³, porosity from 43 to 62 %, and natural moisture content from 38.2 to 56.3 %. The plasticity index range for most of the samples is greater than 15 and the soils are thus not liquefiable. Permeability values range from 3.62×10^{-10} to 6.90×10^{-10} m/s. Undrained triaxial tests performed on reconstructed samples yield cohesion and effective angle of internal friction values of 42 to 67.9 kPa and 34.2 to 34.8°, respectively. These values are high, thus the calculated factor of safety using a standard infinite slope model for these slopes is greater than 1.

X-ray diffraction analysis indicate that the clay fraction of the soils is made up of both swelling and non-swelling clays. Bulk soil samples contain sanidine, anatase, goethite, magnetite and ilmenite, all accounting for the high specific gravity values recorded in this study. The mineralogical composition varies from one profile to another with 1:1 clays being abundant in some profiles and 2:1 clays more significant in others. Clay mineralogy however, does not change significantly with depth in the same profile. It is concluded that the soils, from a geotechnical point of view, are highly stable. Slope instability is thus attributed to other factors than pure loading on the soils. Field observations suggest that the presence of fracture permeability may play a major role in the sliding mechanism. This is most likely because the rocks in this area are highly fractured and weathering is not uniform. Through fractures, water easily penetrates into a more permeable layer overlain by a low-permeability clay horizon. This results in an upward wetting front that is prevented from freely rising by the presence of a low permeability horizon above, resulting in the development of excessive positive pore pressures lifting up and mobilizing the overlying soil column. Furthermore, chemical analysis was made to determine the degree of weathering that the rock has experienced and the behaviour of some major and some trace elements during weathering. It is noted that all alkali and alkali earth metals are depleted while SiO₂, Al₂O₃, Fe₂O₃ and TiO₂ become enriched. All trace elements

analysed in this study (Ba, Sr, Zr, V, Cr, Ni, Ce, Y, Sc and Co) are relatively enriched to varying degrees with the notable exception of Sr that is significantly depleted.

From field and laboratory investigations together with data from previous studies, ten potential causal factors are identified and used in landslide susceptibility modelling. In Chapter 5 of this thesis, a raster-based data driven method involving seed cells is used to construct a landslide susceptibility map for the Limbe area. Factors considered to be potential controls on the occurrence of slope failure within this area include slope gradient and direction, rock type, distance from roads, mean annual precipitation, soil type, land use type, stream density, distance from streams and from geological structures. Landslide data is randomly divided into a training (75 %) and validation dataset (25 %) and seed cells are generated by creating 25 m buffer zones around the head scarp of each scar. This method is advantageous because the buffer takes into account the characteristics of the immediate vicinity of the slide and provides the best representation of the pre-failure properties of the considered slope. Though all factors used in this study were operational from field observations, normalised factor weighting (information values) were not significant for two factors, thus several factor groupings were evaluated to identify the best predictive factor combination. Our preferred model combines the weights of 6 factors (i.e. slope gradient, land use, mean annual precipitation, stream density, proximity to roads and slope orientation). Based on this model, 14.8, 41.8, 26.5, 12.2 and 4.6 % of the study area are classified into the very low, low, moderate, high and very high susceptibility categories, respectively. Using the validation dataset, 7.1 % of the seed cells are categories into the low susceptibility class, 14.3 in the moderate, 31.0 and 47.6 % of the validation seed cells in the high and very high susceptibility category respectively.

To estimate the degree to which humans and infrastructure in the study area are at risk of being affected by future landslides, an inventory of roads, key individual structures frequently occupied by a large number of persons (e.g. churches, markets, hospitals, schools, financial institutions), and the outline of built-up areas in 2000 and its extension as at 2008 was used. The outline of built-up areas act as a proxy for the total population, while the road network acts as a fingerprint to the disruption of economic activities. Of the 24.2 km² of urban extension from 2000 to 2008, 9 % was located in the high and very high susceptibility categories. In total

14 administrative buildings, 10 schools, 4 clerical institutions, 8 bridges, 3 health facilities, 2 financial institutions, and 1 portable water supply tank and ~23 km of roads are located within the high to very high susceptibility classes. From the susceptibility map, it is observed that vast areas on the Mabetta massif are susceptible to failure with more stable areas occurring to the E (Ombe, Mutengene and Esuke areas), N (Wututu and Tole areas) and W (Bota Ngeme area) of Limbe city that could be used for human habitation or the expansion of urban developmental projects. If construction on the Mabetta massif is however unavoidable, low-cost bioengineering and other stabilization techniques should be put in place using the expertise of civil and geotechnical engineers.

In an attempt to evaluate rainfall thresholds required to trigger landslides, it is observed that high intensity rain generally above 110 mm per day following dry periods of 2-3 days would result in the occurrence of landslides. Also, lower intensity and long duration of 60 mm for 3 to 4 days rolling (> 210 mm, 3 days cumulative rainfall) may also result in slope failure within the Limbe area.

Overall, this thesis provides a description based on first-hand field observations of the geometric properties of landslides on the SE foot slopes of Mt Cameroon and proposes two conceptual models of landslide mechanisms. It also provides a better understanding of the causes of landslide problems that can be extended to other areas suffering from small-scale but devastating landslide issues in subtropical areas where high temperatures and heavy rainfall dominate. In addition to the benefit of this work to assist in civil protection and urban planning efforts in SW Cameroon, the low-cost readily applicable landslide susceptibility approach does not require intensive computer resources or extensive computer modelling experience and has the potential to support geohazard risk scientists in developing countries where modelling skills are limited.

Samenvatting

De stad Limbe en haar omgeving, gelegen op de zuidoostelijke lage flanken van de actieve vulkaan Mount Cameroon, werden in de voorbije 20 jaar getroffen door talrijke kleinschalige aardverschuivingen. Deze hebben ongeveer 30 dodelijke slachtoffers geëist en belangrijke schade toegebracht aan landbouw en infrastructuur. In het eerste deel van deze thesis worden aardverschuivingen en hun littekens geïdentificeerd in het veld en wordt hun geometrie systematisch opgemeten om op deze manier een inventarisatiekaart te kunnen maken van aardverschuivingen voor het studiegebied. De typische aardverschuivingen die in het studiegebied voorkomen, zijn kleinschalige, ondiepe, translationele aard- en puinlawines hoewel enkele rotationele aardverschuivingen ook werden opgetekend. In totaal werden 63 littekens van aardverschuivingen geïdentificeerd. De aardverschuivingszones hebben een gemiddelde breedte van 22 ± 17 m en een gemiddelde lengte van 25 ± 23 m. De totale oppervlakte van de littekens van de aardverschuivingen en het volume van verplaatst puin worden geschat op respectievelijk $10 - 10^4$ m² en $20 - 5 \times 10^4$ m³. Door deze littekens in een GIS op te nemen, valt het op dat de aardverschuivingen niet uniform verdeeld voorkomen in het studiegebied, maar ruimtelijk geclusterd zijn. Specifieke aardverschuivingen worden in detail onderzocht om de specifieke factoren te bepalen die bijdroegen tot de onderliggende oorzaak en de uiteindelijke aanleiding van de verschuiving. De bedoeling hiervan is om de determinerende inputparameters en hun variabiliteit vast te leggen voor latere susceptibiliteit- en risicomodelleren voor zowel lokale als regionale toepassingen in ruimtelijke ordening. Een belangrijke conclusie is dat de meeste hellingsinstabiliteiten in het studiegebied geassocieerd zijn aan en lijken te worden verergerd door factoren die door de mens geïnduceerd worden zoals uitgraving, ongeordende bouwwerken en ontbossing van steile hellingen. Aanhoudende hevige regenval, vooral tijdens lokale stormen, is de voornaamste aanleidingsfactor die totnogtoe geïdentificeerd is. De resultaten van deze studie zijn relevant om de lokale verwoestende hellingsinstabiliteiten te begrijpen die vaak voorkomen op intens verweerd en steil terrein in subtropische gebieden, zowel in Afrika als elders in de wereld, en die een effect hebben op een steeds grotere en kwetsbaardere bevolking.

Eerdere studies hebben aangetoond dat het voorkomen van aardverschuivingen in eender welk gebied kan worden toegeschreven aan de geotechnische, mineralogische en chemische eigenschappen van de bodems, alsook aan de krachten die inwerken op het materiaal. Daarom

was het, na de identificatie van de ruimtelijke verdeling van de aardverschuivingen in het gebied rond Limbe, nodig om de aard te karakteriseren van de bodems die eventueel onderhevig kunnen zijn aan aardverschuivingen. In het derde en vierde hoofdstuk van deze thesis wordt een selectie van littekens van aardverschuivingen geotechnisch, mineralogisch en chemisch gekarakteriseerd om inzicht te verschaffen in de rol die deze bodemkenmerken spelen in het voorkomen van ondiepe, translationele aardverschuivingen. Hiervoor werden zes 2.5 tot 4 m diepe putten gegraven in drie littekens van aardverschuivingen. In elk van deze putten werd het bodemprofiel beschreven, een *in situ* schuifproef uitgevoerd op de wanden van de put, en monsters genomen voor laboratoriumanalyses. Testresultaten tonen aan dat volgens het *Unified Soil Classification System* (bodemclassificatiesysteem, *USCS*) de bodems voornamelijk bestaan uit anorganische silt met een hoge plasticiteit. De bulk dichtheid varieert van 1.11 tot 1.60 g/cm³, de materiaaldichtheid van 2.76 tot 2.98 g/cm³, de porositeit van 43 tot 62 %, en het natuurlijke vochtgehalte van 38.2 tot 56.3 %. Voor de meeste stalen is de plasticiteitsindex groter dan 15. De bodems zijn dus niet vloeibaar. De permeabiliteit varieert tussen 3.62×10^{-1} en 6.90×10^{-10} m/s. Niet-gedraineerde triaxiale tests op gereconstrueerde monsters geven waarden voor de cohesie en effectieve hoek van interne wrijving van respectievelijk 42 – 67.9 kPa en 35.2 – 34.8°. Dit zijn hoge waarden waardoor de factor van veiligheid berekend aan de hand van een standaard onbeperkt hellingsmodel voor de bestudeerde hellingen meer dan 1 bedraagt.

X-stralendiffractie onderzoek toont aan dat de kleifraction van de bodems bestaat uit zowel zwellende als niet-zwellende kleimineralen. Bulkmonsters bevatten sanidien, anataas, goethiet, magnetiet en ilmeniet die bijdragen aan de hoge materiaaldichtheid van de bestudeerde bodems. De mineralogische samenstelling varieert tussen de verschillende profielen, waarbij 1:1 kleimineralen meer voorkomen in bepaalde profielen, en 2:1 kleimineralen dan weer belangrijker zijn in andere. De kleimineralogie verandert echter niet significant met de diepte in hetzelfde profiel, en kan dus in dit studiegebied niet gebruikt worden om de meest waarschijnlijke diepte van een mogelijk toekomstig glijvlak in te schatten. Vanuit een geotechnisch standpunt bekeken zijn de bodems zeer stabiel. Hellingsinstabiliteit wordt dus toegeschreven aan andere factoren dan zuivere lading op de bodems. Veldwaarnemingen suggereren dat de aanwezigheid van breukgerelateerde permeabiliteit een belangrijke rol zou kunnen spelen in het verschuivingsmechanisme. Dit is zeer waarschijnlijk omdat de gesteenten in dit gebied sterk gebroken zijn en hun vertering niet uniform gebeurt. Water kan gemakkelijk langs breuken in

een meer permeabele laag terechtkomen die bedekt wordt door een weinig permeabele kleilaag. Dit leidt tot een opwaarts stijgend waterfront dat wordt verhinderd om vrij te stijgen door de aanwezigheid van een bovenliggende weinig permeabele laag. Dit resulteert in de ontwikkeling van een excessieve opwaartse druk in de poriën die de bovenliggende bodemmassa optilt en mobiliseert. Verder werden chemische analyses uitgevoerd om de graad van verwerking die het gesteente heeft ondergaan en het gedrag van bepaalde hoofd- en spoorelementen tijdens verwerking te bepalen. De bodems zijn verarmd in alkali- en aardalkalimetalen, en aangerijkt aan SiO_2 , Al_2O_3 , Fe_2O_3 en TiO_2 . Alle spoorelementen geanalyseerd in deze studie (Ba, Sr, Zr, V, Cr, Ni, Ce, Y, Sc en Co) zijn in verschillende mate aangerijkt, met uitzondering van Sr dat duidelijk uitgelooft is.

Uit veld- en laboratoriumanalyses, aangevuld met data uit eerdere studies, werden tien mogelijke oorzaakfactoren geïdentificeerd, die gebruikt werden in de modellering van susceptibiliteit voor aardverschuivingen. In Hoofdstuk 5 worden de data geplaatst in een raster om een susceptibiliteitskaart te construeren voor aardverschuivingen in het Limbe gebied. De factoren die een mogelijke invloed hebben op het al dan niet voorkomen van een afglijding in het studiegebied zijn: hellingsgradiënt en –richting, gesteentetype, afstand tot wegen, gemiddelde jaarlijkse neerslag, bodemtype, landgebruik, dichtheid van riviernetwerk, afstand tot rivieren, en afstand tot geologische structuren (bv. breuken). De gegevens van de aardverschuivingen werden willekeurig ingedeeld in een oefendataset (75 %) en een validatiedataset (25 %). Invoercellen worden gegenereerd door bufferzones van 25 m te creëren rond de aflijning van elke aardverschuiving. Deze methode is voordelig omdat de bufferzone de kenmerken van de onmiddellijke omgeving rond de verschuiving in rekening brengt en de kenmerken van de betrokken helling vóór de verschuiving het best weergeeft. Hoewel alle factoren die in deze studie gebruikt werden duidelijk van belang waren zoals bleek uit de veldwaarnemingen, werden voor twee factoren de genormaliseerde gewogen waarden niet significant bevonden. Daarom werden verschillende factorgroeperingen geëvalueerd om de best voorspellende combinatie te identificeren. Het model dat de voorkeur geniet, combineert het gewicht van zes factoren: hellingsgradiënt en –richting, landgebruik, gemiddelde jaarlijkse neerslag, dichtheid van riviernetwerk, afstand tot wegen. Op basis van dit model wordt 14.8, 41.8, 26.5, 12.5 en 4.6 % van het studiegebied respectievelijk ingedeeld in de categorieën zeer lage, lage, matige, hoge en zeer hoge susceptibiliteit. In het studiegebied wordt 16.9 % dus gecategoriseerd in de klassen van

hoge tot zeer hoge susceptibiliteit. Met de validatiedataset wordt 7.1 % van de invoercellen ingedeeld in de klasse van lage susceptibiliteit, en 14.3% in de matige, 31 % in de hoge en 47.6 % in de zeer hoge susceptibiliteit.

Om in te schatten in welke mate mens en infrastructuur in het studiegebied risico lopen om geaffecteerd te worden door een aardverschuiving, werd een inventaris gemaakt van wegen, belangrijke infrastructuurelementen die regelmatig door een grote hoeveelheid mensen tegelijk bezocht worden (bv. kerken, markten, ziekenhuizen, scholen, financiële instellingen), en de bebouwde oppervlakte in 2000 in vergelijking met haar uitbreiding in 2008. De bebouwde oppervlakte is een indicatie voor de totale bevolking, terwijl het wegennetwerk van vitaal belang is voor economische activiteiten. De bebouwde oppervlakte is tussen 2000 en 2008 toegenomen met 24 km², waarvan 9 % gelokaliseerd is in de categorieën van hoge tot zeer hoge susceptibiliteit. Tien administratieve gebouwen, elf scholen, drie kerken, drie gezondheidsinstellingen, drie financiële instellingen, één voorraadtank voor drinkbaar water, zeven bruggen en ongeveer 23 km wegen zijn gelokaliseerd in de zones van hoge tot zeer hoge susceptibiliteit. Op de susceptibiliteitskaart is het duidelijk dat aanzienlijke delen van het Mabeta massief potentieel onderhevig zijn aan afglijdingen. De meer stabiele gebieden komen voor ten oosten (Ombe, Mutengene en Esuke), ten noorden (Wututu en Tole) en ten westen (Bota Ngeme) van de stad Limbe, en zouden preferentieel kunnen aangewend worden voor bewoning of de uitbreiding van (ontwikkelings)projecten. Indien bebouwing op het Mabeta massief echter onvermijdelijk is, zouden goedkope landbouwkundige en andere stabilisatietechnieken moeten toegepast worden gebruik makende van de expertise van burgerlijke, landbouwkundige en geotechnische ingenieurs.

Uit de evaluatie van de hoeveelheid neerslag die nodig is om een aardverschuiving in gang te zetten, wordt geconcludeerd dat hevig intense neerslag van meer dan 110 mm per dag na periodes van 2 à 3 dagen, aanleiding kan geven tot het voorkomen van aardverschuivingen. Daarnaast kunnen minder intense regens gedurende een langere periode, meer bepaald 60 mm per dag gedurende 3 à 4 dagen na elkaar, ook leiden tot hellingsinstabiliteiten in het Limbe gebied.

Deze thesis bevat een beschrijving van veldwaarnemingen van de geometrische eigenschappen van aardverschuivingen op de zuidoostelijke lage flanken van Mount Cameroon en stelt daarbij twee conceptuele modellen van aardverschuivingsmechanismen voor. Zij draagt ook bij tot een beter begrip van de oorzaken van aardverschuivingen, die kunnen worden uitgebreid naar andere gebieden met kleinschalige, maar verwoestende aardverschuivingen in de subtropen die gedomineerd worden door hoge temperaturen en hevige neerslag. De resultaten van dit werk kunnen gebruikt worden voor ontwikkelingen in civiele bescherming en stedelijke planning in ZW Kameroen. Daarnaast biedt de goedkope en gemakkelijk toepasbare methode voor het bepalen van de aardverschuivingsgevoeligheid het voordeel dat ze geen intensieve computerberekeningen of uitgebreide ervaring in numerieke modellering vereist. De methode heeft daarom het potentieel om aangewend te kunnen worden door wetenschappers betrokken bij studies naar natuurlijke gevaren en gerelateerde risico's in ontwikkelingslanden waar ervaring in modellering vaak beperkt is.

Appendix

Appendix

slide ID	Longitude in UTM	Latitude in UTM	Elevation (m)	Width of scarp(m)	Height of scarp (m)	Length (m)	Initial slope	Volume (m ³)	Area (m ²)	Type
1	523900	441613	58	31.6	2.8	23.7	22	1098	749	Complex
2	523720	440616	114	85.0	10.0	110.0	30	48976	9350	Translational
3	527485	438384	157	30.0	5.0	47.9	N/A	3764	1437	Translational
4	526511	438697	194	39.0	3.0	27.6	46	1691	1076	Translational
5	524517	441942	124	24.5	3.0	108.0	26	4158	2646	Translational
6	524980	441957	110	17.9	3.5	20.0	32	656	358	Translational
7	524967	441942	105	40.0	4.0	40.0	27	3352	1600	Translational
8	524962	442031	81	37.0	5.0	29.0	28	2810	1073	Translational
9	523737	441716	36	12.5	5.0	13.0	32	426	163	Translational
10	523710	441747	33	21.2	2.0	27.0	28	600	572	Translational
11	524741	442101	43	9.5	2.5	22.6	32	281	215	Translational
12	524724	443904	78	11.5	3.5	14.5	28	306	167	Translational
13	524712	443952	104	22.5	6.0	57.6	32	4073	1296	Translational
14	524706	443902	76	16.5	2.0	10.0	28	173	165	Translational
15	524637	443881	86	17.0	2.5	6.0	32	134	102	Translational
16	527967	450028	186	8.4	1.1	6.3	28	30	53	Translational
17	528141	450164	213	20.3	1.5	6.2	28	99	126	Rotational
18	525626	443912	112	12.7	8.3	5.0	45	276	64	Translational
19	525683	443932	129	9.0	2.5	15.0	28	177	135	Translational
20	523765	441418	103	18.2	5.3	34.3	22	1733	624	Translational
21	523903	441501	96	20.9	2.0	39.8	36	871	832	Translational
22	523907	441491	84	30.0	1.5	15.1	22	356	453	Translational
23	529936	449242	184	3.0	3.0	0.5	70	2	2	Rock fall
24	529951	449253	182	39.4	2.0	0.5	70	21	20	Translational
25	530086	449339	184	79.0	5.6	12.0	30	2781	948	Translational
26	528870	449164	179	15.0	1.2	3.1	46	29	47	Translational
27	529801	448735	196	30.0	8.0	-	-	-	-	Translational
28	525200	441895	124	55.1	5.0	52.1	26	7519	2871	Translational
29	524507	441968	121	15.0	3.5	3.0	60	83	45	Translational
30	523968	441888	14	15.0	10.0	1.0	70	79	15	Translational
31	534675	453220	289	8.0	1.0	12.0	0	50	96	Translational
31	534675	453220	289	8.0	1.0	12.0	0	50	96	Translational
32	534740	453428	322	25.0	3.0	13.0	0	511	325	Translational
33	534753	453427	320	12.0	2.0	12.0	0	151	144	Translational
34	537788	452214	110	34.0	1.0	10.0	40	178	340	Translational
35	523619	444280	33	8.0	0.9	-	-	-	-	Translational
36	523804	444280	34	7.0	5.0	-	-	-	-	Translational
37	531282	450718	174	-	-	-	-	-	-	Translational
38	519728	449274	628	-	-	-	-	-	-	Translational
39	525017	448109	246	0.0	0.0	0.0	-	-	-	Translational
41	523466	440966	140	19.2	2.8	32.0	29.8	901	614	Translational
40	524928	443980	103	8.0	1.0	0.0	-	-	-	Translational
42	527551	450455	221	8.0	1.5	0.0	-	-	-	Translational
43	527579	450403	242	13.6	5.2	0.0	-	-	-	Translational
44	525724	443941	133	30.0	7.0	0.0	-	-	-	Translational
45	525976	444147	223	43.1	2.0	42.1	32	1901	1815	Translational
47	524754	444622	164	31.1	4.0	45.0	30	2932	1400	Translational
48	524934	444748	162	15.0	2.5	30.0	40	589	450	Translational
49	527319	450454	228	16.0	2.5	31.7	20	664	507	Translational
50	524725	444033	147	8.8	2.0	13.2	58	122	116	Translational
51	525228	441975	97	8.0	1.0	10.0	-	42	80	Translational
52	529349	459734	716	9.0	1.0	20.0	30	94	180	Translational
53	528052	453405	461	10.0	1.0	50.0	36	262	500	Translational
54	522967	444229	65	4.0	1.0	10.0	65	21	40	Translational
55	522952	444282	83	9.5	1.0	9.0	64	45	86	Translational
56	522947	444309	86	10.0	1.0	7.0	64	37	70	Translational
57	523785	445174	106	17.7	3.0	6.0	40	167	106	Translational
58	527458	448862	187	6.0	1.0	6.0	30	19	36	Translational
59	527974	449037	204	20.8	2.3	61.6	26	1539	1277	Translational
61	520080	444212	138	52.5	6	36.0	34	5940	1890	Rotational
62	519827	444235	80	46.2	6	45.0	36	6534	2079	Translational

Table A. 1. Location of individual slides and their characteristics identified during this study.

Appendix 2

slide ID	Location name	Year of occurrence	Farm land	Culvert	Building destroyed	Road block	Casualties /injury	Other damage
1	Bonjo	21-Jul-05	X	-	-	X	-	-
2	Mondoli	27-Jun-01	X	-	-	-	-	-
3	Chop farm	27-Jun-01	-	X	-	X	-	-
4	Chop farm	27-Jun-01	-	-	-	X	-	-
5	Makuka	27-Jun-01	X	-	X	-	-	-
6	Makuka	27-Jun-01	-	-	-	-	-	-
7	Makuka	27-Jun-01	X	-	-	-	-	-
8	Makuka	unknown	-	-	-	-	-	-
9	Bonjo	2004	-	-	X	-	-	-
10	Bonjo	1999	-	-	X	-	-	-
11	Makuka	08-Aug	-	-	-	-	-	-
12	Mabeta New Layout	27-Jun-01	X	-	X	-	-	-
13	Mabeta New Layout	27-Jun-01	X	-	X	-	-	-
14	Mabeta New Layout	27-Jun-01	-	-	-	-	-	-
15	Mabeta New Layout	27-Jun-01	X	-	-	-	-	-
16	Mt Mbinde	unknown	X	-	-	-	-	-
17	Mt Mbinde	unknown	X	-	-	-	-	-
18	Mabeta New Layout	unknown	-	-	-	-	-	-
19	Mabeta New Layout	unknown	-	-	-	-	-	-
20	Bonjo	unknown	X	-	-	-	-	-
21	Bonjo	unknown	X	-	-	-	-	-
22	Bonjo	unknown	-	-	-	-	-	-
23	Ombe1	unknown	X	-	-	-	-	-
24	Ombe 2	unknown	X	-	-	-	-	-
25	Ombe 3	unknown	X	-	-	-	-	-
26	Tomatel 1	unknown	X	-	-	-	-	-
27	Tomatel 2	unknown	X	-	-	-	-	-
28	Makuka	27-Jun-01	X	-	-	-	-	-
29	Makuka	unknown	-	-	-	-	-	-
30	Bonjo	unknown	-	-	-	-	-	-
31	Mutengene	2007	-	-	-	-	-	-
32	Mutengene	2007	-	-	-	-	-	-
33	Mutengene	2007	-	-	-	-	-	-
34	Likomba	unknown	-	-	-	-	-	-
35	Cassava farm	27-Jun-01	-	-	-	-	-	-
36	Cassava farm	27-Jun-01	-	-	-	-	-	-
37	Mevio	unknown	-	-	-	-	-	-
38	Engel Mount	unknown	-	X	-	-	-	-
39	Mile 4	unknown	-	-	-	-	-	-
40	Mabeta New Layout	27-Jun-01	-	-	-	-	-	-
41	Mondoli	unknown	X	-	-	-	-	-
42	Mt Mbinde	unknown	X	-	-	-	-	-
43	Mt Mbinde	unknown	X	-	-	-	-	-
44	Mabeta New Layout	27-Jun-01	-	-	-	-	-	-
45	Mabeta New Layout	27-Jun-01	X	-	6	-	14	X
46	Mabeta New Layout	unknown	-	-	-	-	-	-
47	Towe slide 1	27-Jun-01	X	-	X	-	-	-
48	Towe slide 2	27-Jun-01	X	-	X	-	-	-
49	Mt Mbinde	unknown	X	-	-	-	-	-
50	Mabeta New Layout	unknown	-	-	-	-	-	-
51	Makuka	unknown	-	-	-	-	-	-
52	Bonduma	18-Jul-06	X	-	1	-	4	-
53	Balondo hill	unknown	X	-	-	-	-	-
54	Unity quarter	29-Jun-09	-	-	1	-	-	-
55	Unity quarter	29-Jun-09	-	-	1	-	2	-
56	Unity quarter	29-Jun-09	-	-	1	-	-	-
57	Lifanda South	Jun-09	-	-	1	-	-	-
58	Moliwe	29-Jun-09	X	-	-	-	-	-
59	Moliwe	29-Jun-09	-	-	-	-	-	-
60	Mile one Limbe	Jun-09	X	-	-	-	-	-
61	Kie Village	06-Aug-09	X	X	X	1	1	-
62	Kie Village	Aug -09	-	-	-	-	-	-

Table A. 2. Year during which landslides were recorded with associated damage involved at each site. ‘Unknown’ means the actual date of occurrence is not known but morphologic properties show that they took place within the last 2 decades. X: damage observed; - damage category not observed

Appendix 3

	Particle specific gravity (kN/m ³)	γ_s	27.85					
Physical parameters	Confining pressure (kPa)	σ_3	49	98	196	392	CS	CS
	Dry unit weight (kN/m ³)	γ	12.74	13.02	12.97	12.94	12.88	12.60
	Porosity	n	0.55	0.54	0.54	0.55	0.55	0.56
	Void ratio	e	1.23	1.18	1.19	1.20	1.21	1.26
Moisture properties	Initial moisture content (%)		41.60	41.48	42.03	42.47	41.23	43.03
	Initial degree of saturation (%)		98.63	99.80	98.95	98.77	98.93	99.29
	Final moisture content (%)	wf	48.11	48.14	47.23	45.89	41.23	43.51
	Final degree of saturation (%)	Sf	100.00	100.00	100.00	100.00	98.93	100.00
Condition at failure	Cell pressure (kPa)	σ_3	49.0	98.0	196.0	392.0	0.0	0.0
	Effective normal stress (kPa)	σ'_1	321.32	470.36	539.24	797.36	808.79	362.86
	Effective lateral pressure (kPa)	σ'_3	27.29	49.23	78.78	153.57	0.00	0.00
	Effective stress ratio	σ'_1/σ'_3 *100	1177.32	955.51	684.53	519.23	808.79	362.86
	Pore pressure (kPa)	u	21.71	48.77	117.22	238.43	0.00	0.00
	Relative deformation (%)	ε	1.31	2.56	1.86	2.32	2.47	2.53
Pore pressure is deducted from the values given in the table								
	Pore pressure (KPa)	u_0	196.00					

Table A. 3. Parameters and components used and derived from the triaxial cell test for samples from the pyroclastic cones

	Particle specific gravity kN/m ³	γ_s	27.86					
Physical parameters	Confining pressure (kPa)	σ_3	49	98	196	392	CS	CS bis
	Dry unit weight (kN/m ³)	γ	14.28	14.20	14.59	14.82	13.88	14.18
	Porosity	n	0.49	0.49	0.48	0.47	0.50	0.49
	Void ratio	e	0.95	0.96	0.91	0.8789	1.01	0.96
Moisture properties	Initial moisture content (%)	w ₀	33.61	33.46	32.72	34.35	35.10	32.58
	Degree of saturation (%)	S ₀	95.51	95.16	95.50	94.30	99.06	95.94
	Final moisture content (%)	wf	35.88	36.05	35.90	34.92	35.58	33.02
	Final degree of saturation (%)	Sf	100.00	100.00	100.00	100.00	100.00	97.23
Failure conditions	Total stress (kPa)	σ_3	49.0	98.0	196.0	392.0	0.0	0.0
	Effective normal stress (kPa)	σ'_1	273.60	410.79	589.29	858.57	105.95	171.57
	Effective lateral pressure (kPa)	σ'_3	40.14	58.25	116.53	192.40	0.00	0.00
	Effective stress ratio	σ'_1/σ'_3 *100	681.63	705.23	505.69	446.24	105.95	171.57
	Pore pressure (kPa)	u	8.86	39.75	79.47	199.60	0.00	0.00
	Relative deformation (%)	ε	1.41	2.43	2.52	5.45	14.71	2.35
Pore pressure is deducted from the values given in the table								
	Pore pressure (KPa)	u_0	196.00					

Table A. 4. Parameters and components used and derived from the triaxial cell test for samples from lava flows.

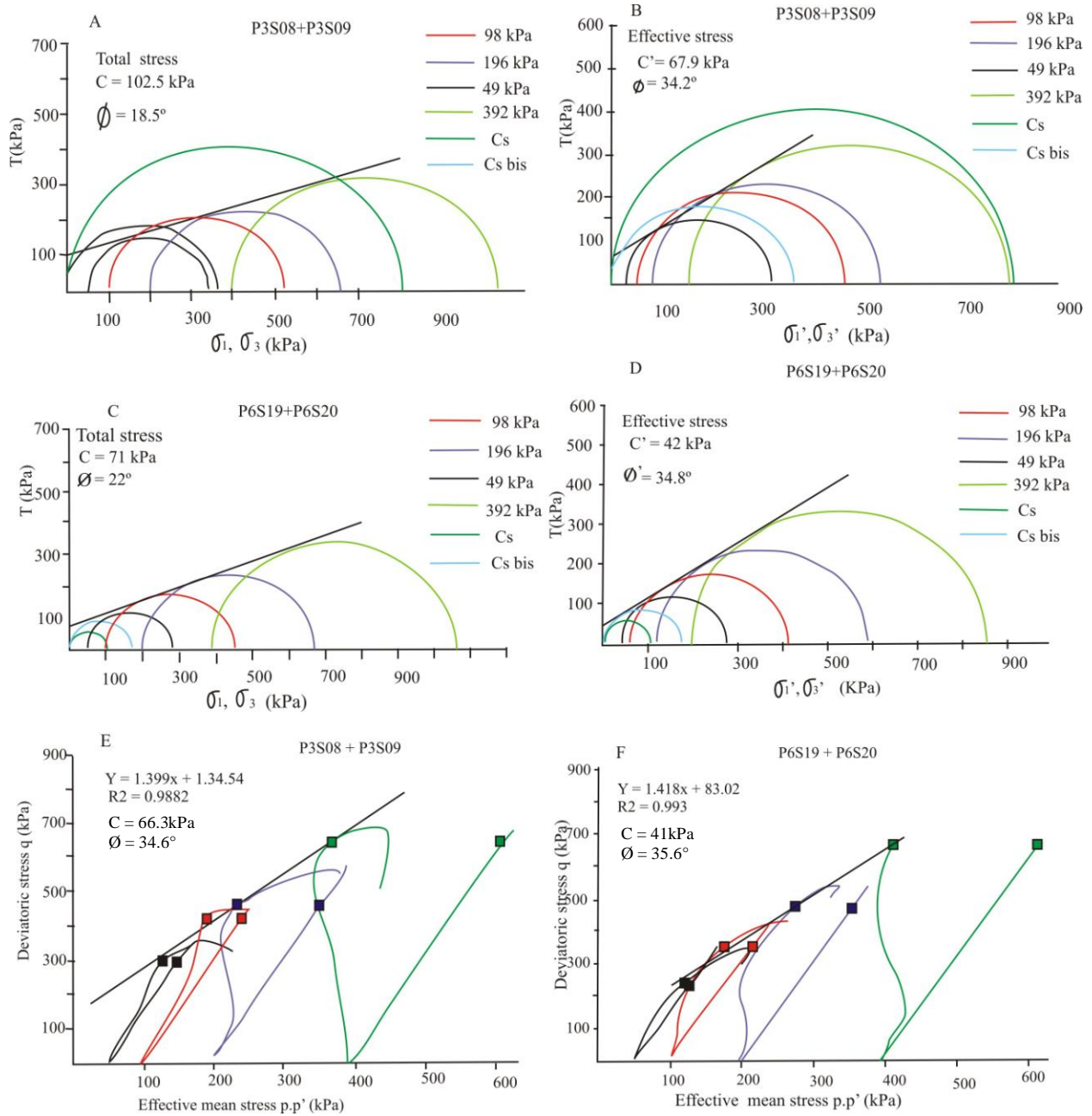


Fig. A. 1. Test results of consolidated undrained triaxial tests on reconstructed samples from landslide scars in Limbe, SW Cameroon. Stress envelopes and Mohr circles of: a) total; b) effective stress envelope for samples from the pyroclastic cone; c) total; d) Effective stress envelope stress for samples from weathered lavaflow; e) plot of deviatoric stress against effective stress for samples from the pyroclastic cone; and f) plot of deviatoric stress against effective stress for samples from the weathered lavaflow. σ_1 : normal stress; σ_3 : axial stress; C: total cohesion; ϕ : total angle of internal friction; σ_1' : effective normal stress; σ_3' : axial stress; C' : effective cohesion; ϕ' : effective angle of internal friction.

Appendix

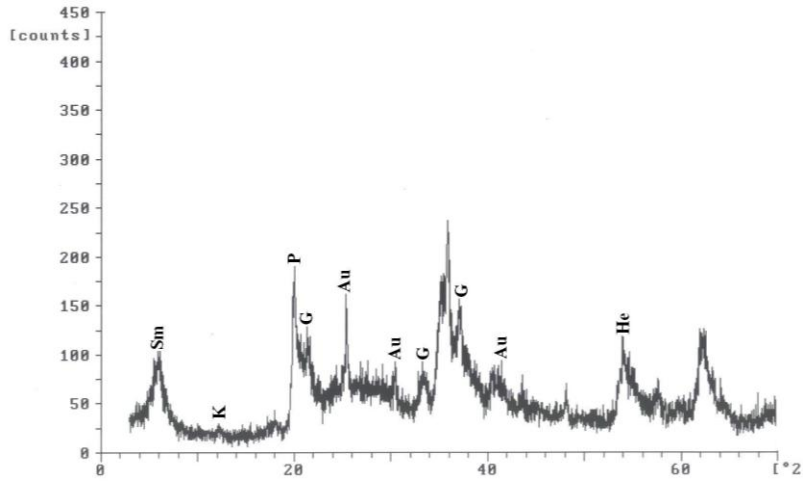
Appendix 4

Depth (cm)	50-70	100-120	190-210	50-70	100-130	200-230	40-60	150-170	260-280	40-60	160-180	280-300	30-50	100-120	50-70	160-180	220-240	290-310	
Sample number	P1 S01	P1 S02	P1 S03	P4 S05	P4 S06	P4 S07	P3 S08	P3 S09	P3 S10	P2 S11	P2 S12	P2 S13	P5 S14	P5 S15	P6 S17	P6 S18	P6 S19	P6 S20	
Particle diameter	Percentage less than																		
2380	0.0	0.0	0.0	0.0	0.0	0.0	0.0	0.0	0.0	0.0	0.0	0.0	0.0	0.0	0.0	0.0	0.0	0.0	0.0
1680	0.0	0.0	0.0	0.0	0.0	0.0	0.0	0.0	0.0	0.0	0.1	0.5	0.2	0.0	0.1	0.2	0.2	0.2	0.1
840	1.2	0.2	1.1	4.6	0.1	0.1	0.1	0.1	0.1	2.0	10.0	19.3	2.4	2.8	1.6	3.6	3.6	1.6	1.6
420	2.2	1.0	6.8	21.2	0.3	0.7	0.4	0.3	0.3	10.1	28.8	51.1	8.4	11.8	6.3	12.1	12.1	7.1	7.1
210	3.4	1.8	12.6	29.8	0.6	1.5	0.7	0.6	0.5	18.5	36.5	61.4	14.9	20.4	10.4	18.3	18.3	12.3	12.3
105	5.0	3.0	18.9	32.4	1.0	2.0	0.9	0.9	0.7	26.3	42.1	65.2	23.8	29.5	15.0	24.8	24.8	20.2	20.2
74	5.8	3.8	20.3	32.5	1.2	2.0	1.0	1.0	0.8	29.2	44.7	66.6	26.9	33.4	16.9	28.0	28.0	22.5	22.5
45	43.7	41.6	25.9	37.6	9.1	9.7	7.1	10.3	9.4	34.3	48.6	73.5	38.7	49.1	24.8	32.6	35.7	34.2	34.2
32	49.6	42.2	28.9	43.5	10.6	14.2	8.6	10.3	12.3	37.5	51.6	76.4	40.2	55.1	32.3	39.4	41.3	40.6	40.6
23	52.6	43.1	34.8	46.5	13.5	18.7	10.1	11.8	15.3	42.8	54.6	79.4	46.3	61.1	36.9	46.9	49.2	48.6	48.6
15	55.5	49.1	39.3	49.5	16.4	24.7	11.6	13.3	22.6	49.1	57.7	83.3	50.9	67.0	42.9	55.4	56.0	54.9	54.9
8	61.5	52.1	43.7	55.4	20.8	32.3	14.5	13.3	29.9	56.5	60.7	87.2	58.6	73.0	51.9	66.9	65.6	69.8	69.8
6	64.4	55.1	46.7	58.4	25.2	36.8	17.5	14.8	34.3	61.8	63.7	89.2	63.2	77.5	54.9	74.9	71.8	76.1	76.1
4	67.4	58.1	51.1	61.3	28.1	41.3	20.4	16.3	40.1	64.5	66.7	90.2	66.3	82.0	57.9	79.4	78.6	80.4	80.4
2	74.8	64.1	55.6	67.3	32.5	51.8	26.3	26.7	47.4	70.3	71.3	92.1	72.4	88.0	63.9	85.7	85.9	87.8	87.8
0.9	79.2	71.5	65.9	70.3	39.9	54.8	32.2	32.7	54.7	72.4	75.8	94.1	77.0	91.0	69.9	88.0	91.0	92.6	92.6

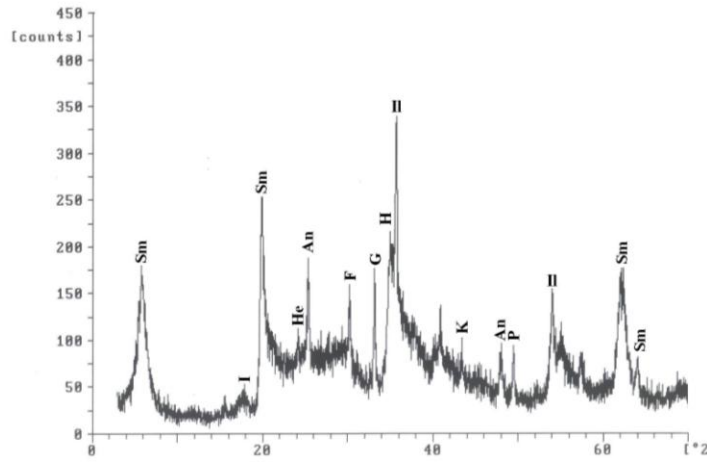
Table A. 5. Percentage retained fraction from dry sieving and sedimentation analysis (granulometric analysis of soil samples from landslide scars in Limbe). Data set used in plotting grain size distribution curves in Chapter 3.

Appendix 5.

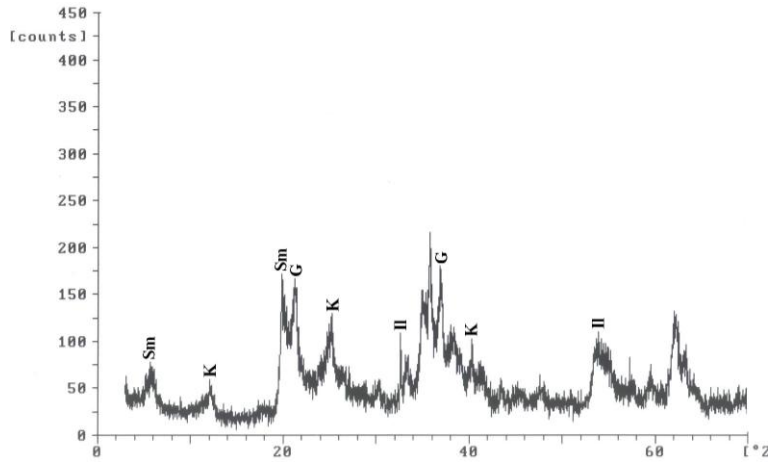
X-ray diffractograms for samples collected from landslide scars in the Limbe area.



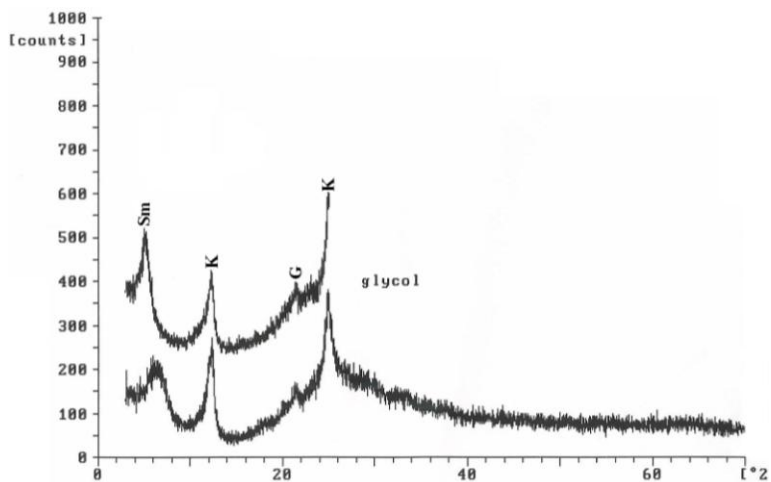
Bulk powder sample diffractogram for BAS 02 from horizon B of slide 20 at Bonjo.



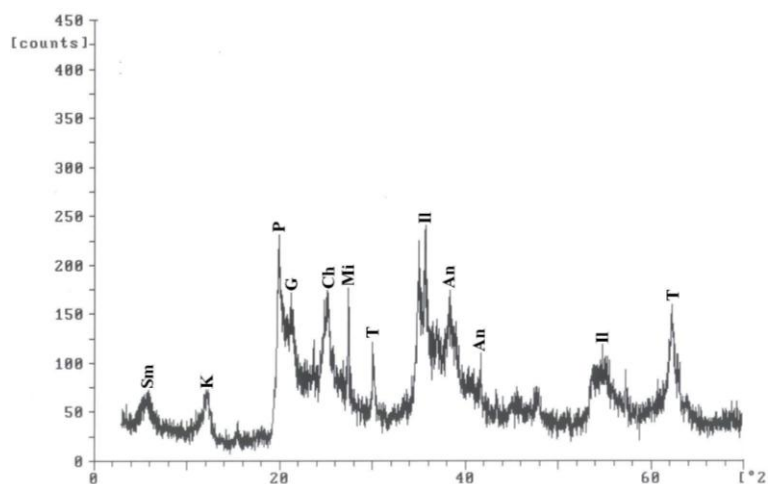
Bulk powder sample diffractogram for sample BBS 02 from horizon C of slide 20 at Bonjo.



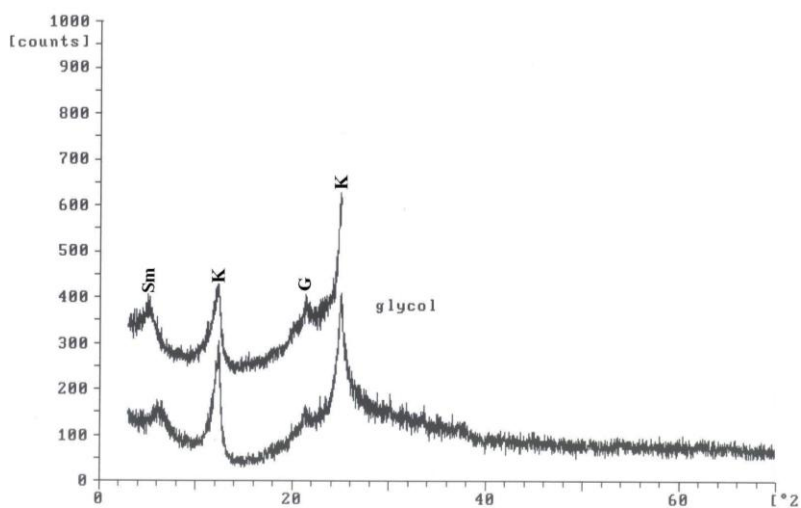
Bulk powder sample diffractogram for MSD-03 from horizon B Slide 2 at Mandoli.



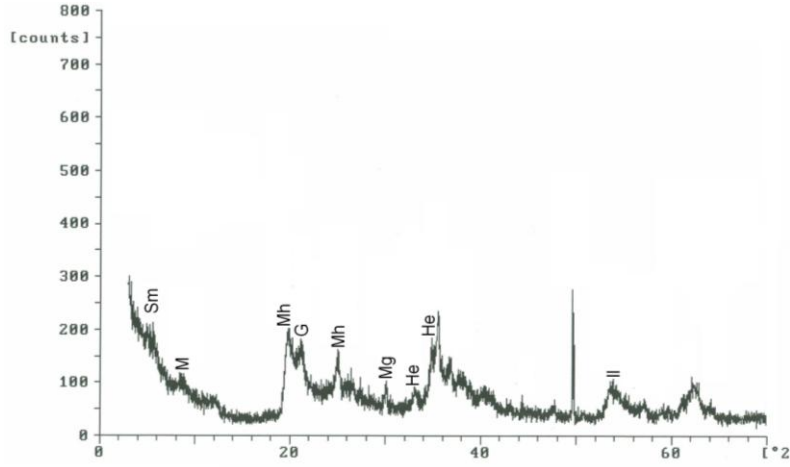
Diffractogram of oriented clay fraction of sample MSD-03 from horizon B Slide 2 at Mandoli.



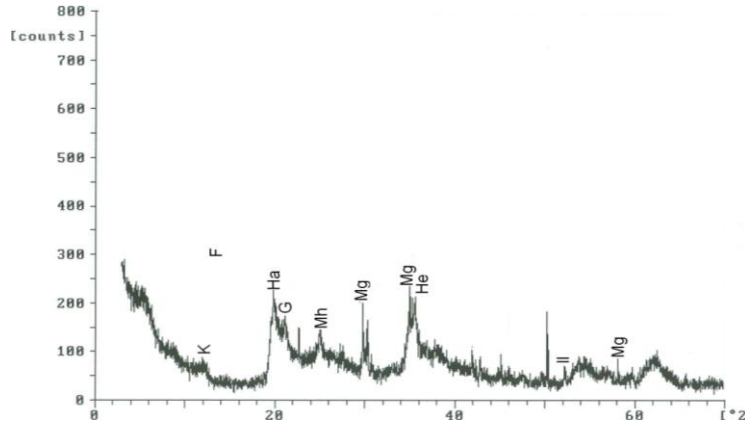
Bulk powder sample diffractogram for MSS-03 from horizon C Slide 2 at Mandoli.



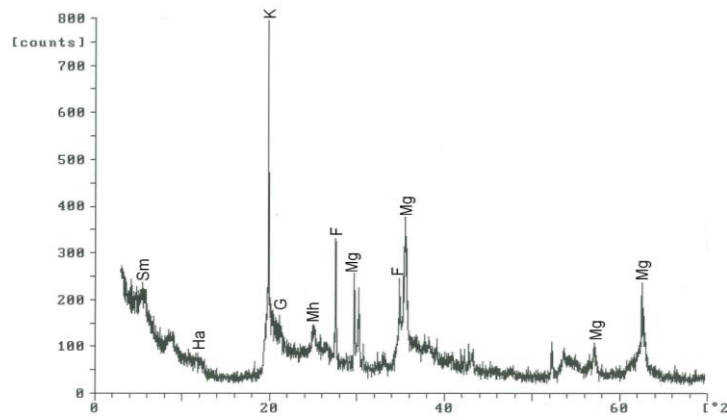
Diffractogram of oriented clay fraction of sample MSS-03 from horizon C Slide 2 at Mandoli.



Bulk powder sample diffractogram for sample P2S10 from Mabeta New Layout.



Bulk powder sample diffractogram for sample P2S12 from Pit 2 at Mabeta New Layout.



Bulk powder sample diffractogram for sample P2S13 from Pit 2 Mabeta New Layout.

Appendix 6

Soil type	Total number of pixels	Number of seed cells	% of total area covered	% of seed cells	Seed cell density factor class	Weighted density	Normalised values
Ash soil	325142	18	36.07	8.11	0.55	-1.91	0.55
Valley clay soil	100100	26	11.10	11.71	2.60	0.13	2.0
Rocky soil	15272	4	1.69	1.80	2.62	0.16	2.62
Old volcanic soil	255785	171	28.37	77.03	6.69	4.22	6.69
Lithosol	19980	0	2.22	0.00	0.00	-2.46	0.00
Lava soil	158647	3	17.60	1.35	0.19	-2.27	0.19
Fragipan	26590	0	2.95	0.00	0.00	-2.46	0.00
	901516	222					

Table A. 6. Proportion of pixels within the study area, seed cells, landslide density and Infoval for the factor soil type.

Land cover	Total number of pixel	Number of seed cells	% of total area covered	% of seed cells	Seed cell density factor class	Weighted density	Normalized values
Built-up area	56294	40	6.24	18.02	7.11	4.64	7.11
Plantation	323090	39	35.84	17.57	1.21	-1.26	1.21
Forest	521981	143	57.90	64.41	2.74	0.28	2.74
Mangrove	150	0	0.02	0.0	0.00	-2.46	0.00
	901515	222					

Table A. 7. Proportion of pixel within the study area, seed cell, landslide density and Infoval for the factor land use.

Slope	Total number of pixels	Number of seed cells	% of total area covered	% of seed cells	Seed cell density factor class	Weighted density	Normalised values
0 – 5	415690	2	46.11	0.90	0.05	-2.41	0.05
5 – 10	204142	26	22.64	11.71	1.27	-1.19	1.27
10 – 15	139003	67	15.42	30.18	4.82	2.36	4.82
15 – 20	81374	66	9.03	29.73	8.11	5.65	8.11
20 – 25	40607	42	4.50	18.92	10.34	7.88	10.34
25 – 30	14949	18	1.66	8.11	12.04	9.58	12.04
30 – 35	4836	1	0.54	0.45	2.07	-0.39	2.07
>35	914	0	0.10	0.00	0.00	-2.46	0.00
	901515	222					

Table A. 8. Proportion of pixels within the study area, seed cells, landslide density and Infoval for the factor slope gradient.

Slope orientation	Total number of pixels	Number of seed cells	% of total area covered	% of seed cells	Seed cell density per factor class	Weighted density	Normalised values
N	50319	36	5.58	16.22	7.15	4.69	6.02
NE	66278	20	7.35	9.01	3.02	0.56	1.89
E	133797	16	14.84	7.21	1.20	-1.27	0.06
SE	291615	33	32.35	14.84	1.13	-1.33	0.00
S	217941	42	24.17	18.92	1.93	-0.54	0.80
SW	75901	28	8.42	12.61	3.69	1.23	2.56
W	32955	24	3.66	10.81	7.28	4.82	6.15
NW	32709	23	3.63	10.36	7.03	4.57	5.90
	901515	222					

Table A. 9. Proportion of pixels within the study area, seed cells, landslide density and Infoval for the factor slope orientation.

Appendix

Distance from rivers	Total number of pixels	Number of seed cells	% of total area covered	% of seed cells	Seed cell density factor class	Weighted density	Normalized values
<50	217419	69	24.12	31.08	3.17	0.71	2.25
50 - 100	181669	28	20.15	12.61	1.54	-0.92	0.62
100 - 150	122467	33	13.58	14.86	2.69	0.23	1.77
150 -200	105523	32	11.71	11.71	3.03	0.57	2.11
200 - 250	66818	30	7.41	7.41	4.49	2.03	3.57
250 - 300	54115	5	6.00	6.00	0.92	-1.54	0.00
>300	153504	25	17.03	17.03	1.63	-0.83	0.70
	901515	222					

Table A. 10. Proportion of pixels within the study area, seed cells, landslide density and Infoval for the factor proximity to stream/river.

Stream density	Total number of pixel	Number of seed cells	% of total area covered	% of seed cells	Seed cell density factor class	Weighted density	Normalized values
Extremely low	110467	6	12.25	2.70	0.54	-1.92	0.54
Very low	187594	34	20.81	15.32	1.84	-0.65	1.84
Low	240413	31	26.67	13.96	1.29	-1.17	1.29
Moderate	187561	75	20.81	33.78	4.00	1.54	4.00
High	113635	76	12.60	34.23	6.69	4.23	6.69
Very high	48043	0	5.33	0.00	0.00	-2.46	0.00
Extremely high	313802	0	1.53	0.00	0.00	-2.46	0.00
	901486	222					

Table A. 11. Proportion of pixels within the study area, seed cells, landslide density, and Infoval for the factor stream density.

Distance from road	Total number of pixels	Number of seed cells	% of total area covered	% of seed cells	Seed cell density factor class	Weighted density	Normalised values
0 – 50	65753	46	7.29	20.72	7.00	4.53	5.21
50 – 100	55820	18	6.19	8.11	3.22	0.76	1.44
100 – 150	41974	26	4.66	11.71	6.19	3.73	4.41
>150	737968	132	81.86	59.46	1.79	-0.67	0.00
Total	901515	222					

Table A. 12. Proportion of pixels within the study area, seed cells, landslide density and Infoval for the factor proximity to roads.

Distance from Fault	Total number of pixels	Number of seed cells	% of total area covered	% of seed cells	Seed cell density factor class	Weighted density	Normalised values
<100	141248	75	15.67	33.78	5.31	2.85	4.79
100-200	116355	48	12.91	21.62	4.13	1.66	3.60
200-300	96038	30	10.65	13.51	3.12	0.66	2.60
300-400	75365	19	8.36	8.56	2.52	0.06	2.00
400-500	59567	17	6.61	7.66	2.85	0.39	2.33
500-600	48487	14	5.38	6.31	2.89	0.43	2.37
>600	364455	19	40.43	8.56	0.521	-1.94	0.00
Total	901515	222					

Table A. 13. Proportion of pixel within the study area, seed cell, landslide density and Infoval for the factor proximity to fault and major lineament.

Appendix

MAP	Total number of pixels	Number of seed cells	% of total area covered	% of seed cells	Seed cell density factor class	Weighted density	Normalized values
<2400	67749	0	7.52	0.00	0.00	-2.46	0.00
2400 - 2800	404360	70	44.85	31.53	1.73	-0.73	1.73
2800 - 3200	151509	4	16.81	1.80	0.26	-2.20	0.26
3200 - 3600	107001	58	11.87	26.13	5.42	2.96	5.42
3600- 4000	109695	75	12.17	33.78	6.84	4.37	6.84
>4000	61201	15	6.79	6.79	2.45	-0.01	2.45
	901515	222					

Table A. 14. Proportion of pixels within the study area, seed cells, landslide density and Infoval for the factor MAP.

Curriculum Vitae

Personal details

Date of Birth: 17th April 1982
Place of birth: Bafut-Mezam, Cameroon
Nationality: Cameroonian
Contact address: Tel +237 75 03 08 02
Tel +32 483 06 93 58

Institutional address

Ghent University
Department of Geology and Soil Science
Krijgslaan 281/S8, B-9000, Ghent, Belgium

University of Buea
Department of Geology and Environmental Science
Faculty of Science
P.O Box, 63, SW Region, Cameroon

Email:

chevivanbih@yahoo.com
chevivanbih@gmail.com

Academic profile

2008 - Present PhD in Geology
2004 - 2006 Masters of Science in Applied Geology
2003 - 2004 University of Yaoundé 1 Maitrise en Géologie Appliqué
1999 - 2003 Bachelor of Science in Geology with a minor in Environmental Science

Extra courses

2007 - 2008 Royal Museum for Central Africa, Tervuren, Belgium. Diplôme en traitement de données et analyse géologique
April- Sept 2003. Tele business computing College Bamenda

Teaching experience

2007 – 2008 Graduate teaching assistant at the University of Buea: practical course on Precambrian geology of Cameroon

International peer reviewed articles

- Che, V.B.**, Kervyn, M., Ernst G.G.J, Trefois, P., Ayonghe S, Jacobs P, Van Ranst, E., Suh C.E. Systematic documentation of landslide events in Limbe area (Mt Cameroon Volcano, SW Cameroon): Geometry, controlling and triggering factors. *Natural Hazards*. DOI 10.1007/s11069-011-9738-3
- Che, V.B.**, Kervyn M., Suh C.E., Ernst, G.G.J., del Marmol M-A., Trefois P., Jacobs P. Landslide susceptibility assessment in Limbe region (SW Cameroon), through a field calibrated seed cell and information value method (Catena, in revision).
- Che, V.B.**, Fontijn, K., Gerald G.J Ernst., Kervyn M., Elburg, M., Van Ranst, E., Suh C.E., Evaluating the degree of weathering in landslide-prone soils in the humid tropics: The Case of Limbe, SW Cameroon (submitted Geoderma)

Conference abstract

Tening, A.S., Hornibrook, E., Chuyong, G.B., Asongwe. G.A., Fonge, B.A., Lifongo, L.L., Mvondo-Ze, D.A., **Che V.B.**, Suh. C.E., The effects of nutrient loading on the Douala-Edea mangrove ecosystem, Cameroon

Climate Change Symposium for the World Environment and Water Resources Conference, Palm Spring California , 22-26 May 2011

Che V.B., Trefois P., Kervyn M., Ernst G.G.J., Van Ranst E., Verbrugge J-C, Schroeder C., Jacobs P., and Suh C. E. Geotechnical and mineralogical characterisation of soils from landslide scars, inferred sliding mechanism, case of Limbe, SW Cameroon. The Second World Landslide Forum Rome, 3-9 October 2011.

Posters

Che V.B., Wantim M.N., Kervyn M., Tening A.S., Fonge B.A., Trefois P., Mih A.M., Nkwatoh A., Ernst G.G.J., Ayonghe S., Egbe A.E., del Marmol M.-A., Ntasin E., Njome M.S., Chuyong G.B., Van Ranst E., Jacobs P., Suh C.E. Spatial display of data for natural resources management and disaster prevention: case of Mount Cameroon Region. Poster presentation, University of Buea, Inter-science symposium 2010.

Che V.B., Trefois P, Suh C.E., Kervyn M., Ayonghe S.N., Jacobs P., Morphological characteristics of typical landslide scars around Limbe, South West Cameroon. University of Buea Faculty of Science Exposition, Science EXPO, March 2009.

Che V.B., Landslide hazards and risk susceptibility assessment: Case of Limbe, South eastern foot slopes of Mount Cameroon Train the trainer Course on Computer Tools for the Management of Natural Resource & Environment., Yaoundé Cameroon, **2009** United Nations University - Institute for Natural Resources in Africa

Che V.B., Trefois P., Kervyn M., Karen F., Ernst G.G.J., Van Ranst E., Verbrugge J, Schroeder C, Jacobs P., and Suh E.C. Shallow translational sliding mechanism in residual soils on the SE foot slopes of Mt Cameroon.

Media communications

Che V. B. Landslide as one of the major geohazards affecting areas along the Cameroon volcanic line. (Focus on Mount Cameroon). Cameroon Radio-Television, Environment Half-Hour show, Buea, September 2008

Che V.B. Are we prepared to face future landslide activities, Cameroon Radio-Television, Environment Half-Hour show, Buea, September 2008